1992

Hydrothermal alteration and fluid inclusion geochemistry of auriferous deformation zones and vein systems, S.W. Michipicoten greenstone belt, Ontario.

Bulent. Bas
University of Windsor

NOTICE

The quality of this microform is heavily dependent upon the quality of the original thesis submitted for microfilming. Every effort has been made to ensure the highest quality of reproduction possible.

If pages are missing, contact the university which granted the degree.

Some pages may have indistinct print especially if the original pages were typed with a poor typewriter ribbon or if the university sent us an inferior photocopy.

Reproduction in full or in part of this microform is governed by the Canadian Copyright Act, R.S.C. 1970, c. C-30, and subsequent amendments.

AVIS

La qualité de cette microforme dépend grandement de la qualité de la thèse soumise au microfilmage. Nous avons tout fait pour assurer une qualité supérieure de reproduction.

S'il manque des pages, veuillez communiquer avec l'université qui a conféré le grade.

La qualité d'impression de certaines pages peut laisser à désirer, surtout si les pages originales ont été dactylographiées à l'aide d'un ruban usé ou si l'université nous a fait parvenir une photocopie de qualité inférieure.

La reproduction, même partielle, de cette microforme est soumise à la Loi canadienne sur le droit d'auteur, SRC 1970, c. C-30, et ses amendements subséquents.

HYDROTHERMAL ALTERATION AND FLUID INCLUSION GEOCHEMISTRY OF AURIFEROUS DEFORMATION ZONES AND VEIN SYSTEMS, S.W. MICHIPICOTEN GREENSTONE BELT, ONTARIO

by
Bulent Bas

A Thesis
Submitted to the Faculty of Graduate Studies and Research
through the Department of Geology in
Partial Fulfillment of the Requirements for the
Degree of Master of Science at the
University of Windsor

Windsor, Ontario, Canada
1992

ISBN 0-315-72785-3

ABSTRACT

HYDROTHERMAL ALTERATION AND FLUID INCLUSION GEOCHEMISTRY OF AURIFEROUS DEFORMATION ZONES AND VEIN SYSTEMS, S.W. MICHIPICOTEN GREENSTONE BELT, WAWA, ONTARIO

by

Bulent Bas

The southwestern part of the Archean Michipicoten Greenstone Belt, southeast of Wawa, Ontario, contains several auriferous deformation zones. Gold mineralization occurs in and around the Jubilee Shear, but there are also several, mineralized, smaller, northeast- and northwest-trending deformation zones, all of which are located in the hanging wall of the Jubilee shear zone.

Three vein sets occur at wawa: 1) early, deformed, auriferous, quartz-Fe-dolomite ± alkali feldspar ± sulphide veins; 2) barren quartz-calcite-chlorite-tourmaline veins (Pinto Veins), which cross-cut the first vein set; and 3) quartz-ankerite veins and breccias (Jubilee Breccia) which post-date all of the earlier veins.

Three stages of hydrothermal alteration have been identified at Wawa: 1) an early, pre- to syn-deformation alteration, represented by quartz-chlorite-Fe-dolomite-muscovite schists and chlorite-Fe-dolomite ± biotite schists (developed in felsic and mafic protoliths, respectively); 2) fenitization (biotite and riebeckite alteration) related to carbonatite-lamprophyre intrusives; and 3) late, fracture-related ankeritic and hematitic alteration. Events 1 and 3 are related to vein sets 1 and 3, respectively.

Three generations of fluids have been recognized from fluid inclusion studies. The first fluid is an immiscible mixture of 1) high-salinity (18-23 wt. % NaCl), aqueous fluids, 2) low-salinity (4 to 7 wt. % NaCl), aqueous-carbonic fluids ($XCO_2 \leq 20$), and 3) CO_2-CH_4-N_2 fluids. This fluid is restricted to vein set 1 in the Surluga Mine and may have caused the early alteration in the Jubilee shear zone. Gold and sulphides were deposited in fractures at a late stage in the formation of vein set 1 as a result of fluid immiscibility. The second fluid is a low- to moderate-salinity (5 to 16 Wt. % NaCl), aqueous fluid which may contain up to 10 mole % CO_2. This fluid contains elevated concentrations of HCO_3^{2-}, as the inclusions contain nahcolite as a daughter mineral. This fluid post-dates the Pinto Veins and may be related to fenitization. The third fluid is a low-salinity (2 to 10 equiv. Wt. % NaCl) aqueous-carbonic fluid with significant amounts of CO_2 ($XCO_2 = 0.23$-0.35). This fluid deposited the Jubilee veins (vein set 3) and breccias, and caused the related ankeritic and hematitic alteration.

To my mother, whose love, patience and longing
made this work worthy, and to my father for his great
inspiration and encouragement for education

ACKNOWLEDGEMENTS

I would like to acknowledge Citadel Gold Mines Inc., who provided access to the examined properties, drill-core records and company reports. Mr. R. Rupert is kindly thanked for his time in discussing various aspects of mineralization at Wawa.

I would like to thank my supervisor Dr. Iain Samson of the Department of Geology, University of Windsor, for his invaluable support, patience and direction in the process of preparation of this thesis.

Dr. Paul Holm, also of the Department of Geology, University of Windsor, provided insights into the structural aspects of the mineralized deformation zones in Wawa.

Dr. T.E. Smith of the Department of Geology and Dr. J. Morrissey of the Department of Computer Science, both at University of Windsor, are sincerely thanked for their constructive comments on the first submission of this thesis.

Finally, I would like to express my gratitude towards Mr. Antun Knitl for sharing his experience with me in the preparation of the doubly-polished fluid inclusion wafers which I had previously no clue about how to prepare them.

TABLE OF CONTENTS

PAGE

PAGE

LIST OF TABLES

LIST OF FIGURES

FIGURE PAGE

FIGURE PAGE

LIST OF APPENDICES

CHAPTER I
INTRODUCTION

The southwestern part of the Archean Michipicoten Greenstone Belt, centred on McMurray Township, southeast of Wawa, Ontario, contains a number of shear zones which host gold-bearing quartz vein systems (Rupert, 1975, 1979; Sage, 1979).

The major gold-hosting structure in the area is the Jubilee shear (JSZ), a north-northeast-trending brittle-ductile shear zone that cuts both the Jubilee stock, a subvolcanic intrusion of dioritic to granodioritic composition, and its host metavolcanic sequence, composed dominantly of felsic to intermediate flows and pyroclastic rocks (Sage, 1979, 1981).

Several smaller, northeast- and northwest-trending shear zones and vein systems, all of which are located in the hanging wall of the Jubilee shear, are also mineralized (Rupert, 1975, 1979). These have yielded small amounts of gold in the past. As pointed out by Rupert (1975), most of the gold mineralization in the area occurs in and around quartz veins that are localized in the shear zones that cut both the Jubilee stock and the volcanic sequence. Gold production from these vein systems is given in Table 1. A total of 110,000 ounces of gold was produced by the mines in McMurray Township between 1929 and 1968 (Ferguson et al., 1971).

Table 1. Gold Production from the Mines in the Study Area

Mine Name	Year(s)	Production (oz)	Grade (oz/ton)
Cooper	1938	1,625	0.333
Minto (JSZ)	1930-1934	21,266	0.366
Jubilee (JSZ)	1929-1939	14,915	0.125
Surluga (JSZ)	1968-1991	8,629	0.091
Parkhill	1929-1938	54,306	0.432
Grace-Darwin	1902-1937	17,634	0.387
Mariposa	1904	19	2.129

Source: Citadel Gold Mines Inc., 1991; Ferguson et al. (1971). JSZ = Jubilee Shear Zone.

Gold mineralization is widespread throughout the Michipicoten greenstone belt, and commonly occurs in quartz veins and vein systems hosted by regional-scale shear/ deformation zones. There are three main areas of current exploration and development

activity: Goudreou-Lochalsh, Renabie-Missinabe (marginal to the belt) and Michipicoten forming part of the so called "Wawa gold camp" (Tortosa et al., 1988). Of them, the Renabie-Missinabe area has seen significant gold production; over one million ounces has been obtained from the Renabie mine, about 70 km northeast of Wawa (Heather, 1989).

1.1. Problem and Objectives

Several aspects of the auriferous vein systems around Wawa are poorly understood at the present time. Some important questions regarding the mineralization are as follows:

1) *Are the minor structures in the hanging wall of the Jubilee shear related to the development of the Jubilee shear itself?* As smaller structures in many Archean gold deposits, such as branch faults, host the bulk of the gold (Gunning and Ambrose, 1937; Thomson, 1941; Kerrich, 1983, 1989; Colvine et al., 1988; Hodgson and Troop, 1988), it is important to understand the relationship between the major and minor structures in a given area. This problem can be approached in several ways:

(a) through a detailed structural analysis of the shear zones and enclosed vein systems and a comparison of their deformational histories, or

(b) through a comparative study of the hydrothermal fluid history of these zones on the basic premise that if these spatially distinct vein systems and shear zones are temporally related, they will have been infiltrated by similar fluids. This can be checked by studying the character of hydrothermal alteration assemblages and fluid inclusions in the shear zones and vein systems.

From the two approaches above, the second approach has been taken in order to answer the question addressed above concerning the mineralization in Wawa.

2) *How do these vein systems compare to the generally well-mineralized Archean systems described from greenstone belts around the world?* A comparison of alteration and fluid inclusion characteristics of the auriferous vein systems around Wawa to well-known, Archean gold-mineralizing systems may help assess their potential for significant gold mineralization.

3) *What were the depositional mechanisms for gold in these vein systems?* As gold precipitation may be caused by a variety of processes that induce physical and chemical changes in the hydrothermal fluid, a clear understanding of which mechanism(s) brought upon gold deposition in the veins may help predict the favorable horizons or sites in the veins for the occurrence of gold.

1.2. Previous Work

The mineralized deformation zones at Wawa have been described in a few regional geology studies of the area (Rupert, 1975, 1979; Sage, 1979), however, they have not received much attention with respect to the genesis of the mineralization. Of these regional studies, Rupert (1975) briefly dealt with the Jubilee Shear zone and made the important observation that shearing post-dated the formation of the early, gold-bearing quartz veins.

The only relevant previous work is restricted to a fluid inclusion study carried out by Paré (1989). Paré studied the Minto A and B zones, the Parkhill zone and the Mariposa vein system by carrying out microthermometric and Raman spectroscopic analyses of the fluid inclusions in quartz veins, most of which were secondary in origin. He concluded that the veins in the Minto A and B, and Parkhill zones were precipitated from relatively high-salinity (18-36 equiv. wt. % NaCl) fluids. He also concluded that the cause of gold deposition was fluid immiscibility. Because of a poor geological control on the age relationships between quartz veins, it is difficult to interpret his results in terms of an overall fluid evolutionary model for the area, as most of the shear zones were infiltrated by several generations of fluids.

1.3. Regional Geology

The Michipicoten Greenstone Belt (MGB) is located within the Superior Province of the Canadian Shield, and extends approximately 140 km northeast from Michipicoten Harbour on the eastern shore of Lake Superior (Figure 1).

The belt comprises at least three, possibly four, volcanic cycles with associated volcaniclastic sedimentary rocks (Table 2) (Goodwin, 1962; Attoh, 1980; Sage, 1981, 1986; Sage, 1979). Various granitic plutons have intruded this volcano-sedimentary sequence and may occur either completely within (internal plutons), or outside the belt (external plutons).

Each volcanic cycle consists of subalkaline tholeiitic massive and pillowed basalts at the base, progressing up to calc-alkaline andesites and rhyodacites (Thurston, 1986). The latter comprise feldspar porphyry, spherulitic and more massive, aphanitic flows, along with abundant felsic pyroclastic rocks. The pyroclastic rocks include breccias, lapilli tuff, feldspar crystal tuff and tuff breccia (Table 2).

Metasedimentary rocks occur throughout the stratigraphy, but are more abundant in the upper parts of the sequences. They consist of siderite-, pyrite-, or chert-magnetite iron formations, and/or massive greywacke, lithic greywacke, argillite,

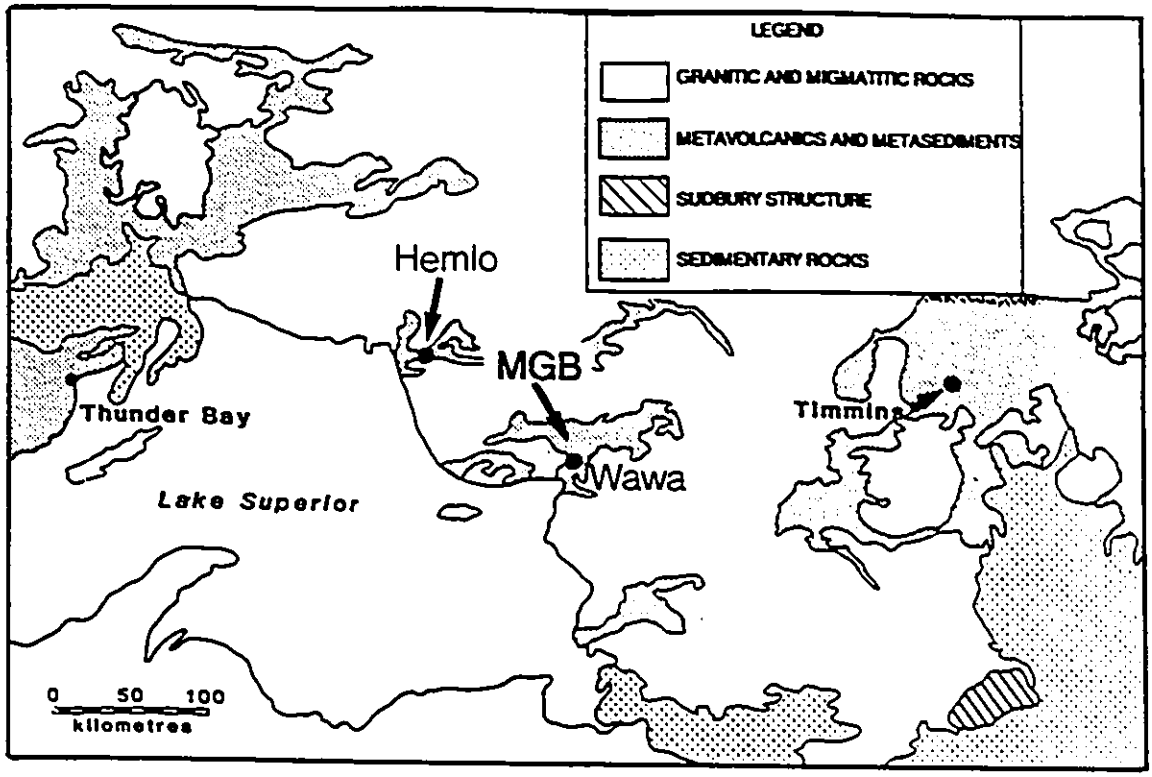

Figure 1. Regional Geology of the Michipicoten Greenstone Belt (MGB) (Modified after Sage, 1981). The solid circles represent some major gold camps and the approximate location of the study area in MGB.

siltstone, arkose and conglomerate (Sage et al., 1987). Sulphide- and oxide-facies iron formations typically cap each volcanic cycle (Table 2) (Sage et al., 1987).

The first two volcanic cycles have yielded maximum U-Pb ages of 2889 ± 9 Ma and 2749 ± 2 Ma, respectively, and the youngest cycle has been dated at 2694 ± 5 Ma (Turek et al., 1982, 1984 and 1988; Sullivan et al., 1985; Frarey and Krogh, 1986). From these ages, Turek et al.(1988) suggested that the greenstone belt evolved over a time span of at least 195 Ma.

The supracrustal rocks are intruded by synvolcanic sills and dikes of gabbroic to quartz-dioritic composition, and granodiorite or quartz-feldspar porphyry stocks and dike complexes (Table 2). Post-volcanic intrusions include various granitoid and syenitic plutons. The youngest date obtained from an internal granitoid is 2662 ± 5 Ma (Turek et al., 1984).

All supracrustal rocks have been regionally deformed and metamorphosed to greenschist grade (Arias and Helmsteadt, 1987, 1988). However, rocks at the margins

CENOZOIC	Quaternary	Pleistocene and Recent Unconformity	
PRECAMBRIAN	Proterozoic	Firesand River Carbonatite (1048) 1 Intrusive Contact Diabase dike Intrusive Contact	
	ARCHEAN	IV?	Diabase Intrusive contact Trondhjemite, granodiorite, quartz-monzonite Intrusive and fault contact High-Mg tholeiite and high-Fe tholeiite conformable contact
		III	Diorite, gabbro and quartz-diorite intrusives Intrusive contact Intermediate-felsic volcanics and assoc. sediments conformable contact Iron formation conformable contact high-Mg tholeiite and high-Fe tholeiite conformable and intrusive contact
		II	Gutcher Lake stock (272?± 1) 2 Intrusive contact Iron formation conformable and intrusive contact Jubilee Stock (2745± 3) 3 Jubilee porphyry (2742± 6) 3 Intrusive contact Diorite, gabbro, peridotite Intrusive contact Intermediate-felsic volcanics (Wawa tuffs)(2744± 10) 4 ? conformable contact ? Jubilee tuffs (2749± 2) 4, minor iron fm. ? conformable contact ? High-Mg tholeiite and high-Fe tholeiite Conformable contact
		I	Hawk Lake granite complex (2888± 2) 2 Intrusive contact Conformable and intrusive contact Diorite, gabbro, peridotite (?) Iron formation (Judith, 2889± 9) 5 Conformable contact Intermediate to felsic volcanics Conformable contact Peridotite and basaltic komatiites

Table 2. Supracrustal and intrusive rock units resulting from cyclic volcanism and intrusive activity (1 to 4? cycles) within the Michipicoten Greenstone Belt. (Modified after Sage and Heather, 1991). The numbers in brackets indicate geological ages: 1 = Gittens et al. (1967); 2 = Turek et al. (1984); 3 = Sullivan et al. (1985); 4 = Turek et al. (1982); 5 = Turek et al. (1988).

of the belt and in the vicinity of large external, granitoid bodies have undergone amphibolite-facies contact metamorphism (Ayres, 1978).

Late Archean and Proterozoic diabase, lamprophyre, and carbonatite dikes are also present in the area (Table 2) (Gledhill, 1927; Frohberg, 1932; Rupert, 1979; Sage, 1979, 1981). The Firesand River carbonatite complex is located 10 km east of Wawa and consists of an outer ring of sovite and mixed silicate-carbonate rocks and a core of ferruginous dolomitic and calcitic carbonatite. This complex has been dated at 1048 Ma (Gittens et al., 1967).

1.4. Geology of McMurray Township

The geology of McMurray Township has been studied in detail by Rupert (1975, 1979) and Sage (1979, 1981). Mafic and felsic metavolcanic rocks make up most of the rocks present in McMurray Township. These were interpreted by Sage (1979) to belong to the second cycle of volcanism (Table 2). This sequence has been intruded by an epizonal intrusion (the Jubilee Stock) of quartz-diorite to granodiorite composition (Figure 2). The Jubilee stock is interpreted as a subvolcanic intrusion emplaced within a caldera structure (Sage, 1979, 1981). The stock contains abundant xenoliths of volcanic rocks. The contact of the stock with the volcanic rocks is sharp and there is little evidence of assimilation or extensive contact metamorphism (Rupert, 1975, 1979; Sage, 1979).

To the east, south and southwest of the Jubilee stock, the country rocks comprise tuffs, feldspar-crystal tuffs, and lapilli tuffs of intermediate composition (andesite to dacite) and small amounts of felsic flows. Except in some highly localized deformation zones, these rocks were not extensively deformed, and thus lack a penetrative foliation (Rupert, 1979; Helmstaedt and Arias, 1988).

Northwest of the stock, and immediately south of Wawa, quartz-feldspar crystal tuffs are exposed, which in some cases contain lapilli and rare blocks (Rupert, 1975, 1979). Both the intermediate tuffs and the more felsic crystal tuffs northwest of the Jubilee stock have been interpreted to be effusive products of magmas associated with the emplacement of the Jubilee Stock (Sage, 1979). This interpretation is consistent with the U-Pb ages obtained from the Jubilee stock (2745 Ma, Sullivan et al., 1985) and from the crystal tuffs (2744 Ma, Turek et al., 1982). To the east and southeast of the stock and in isolated patches to the south of the stock, quartz-feldspar plugs are found and form a somewhat arcuate pattern around the stock (Sage, 1979). This crude

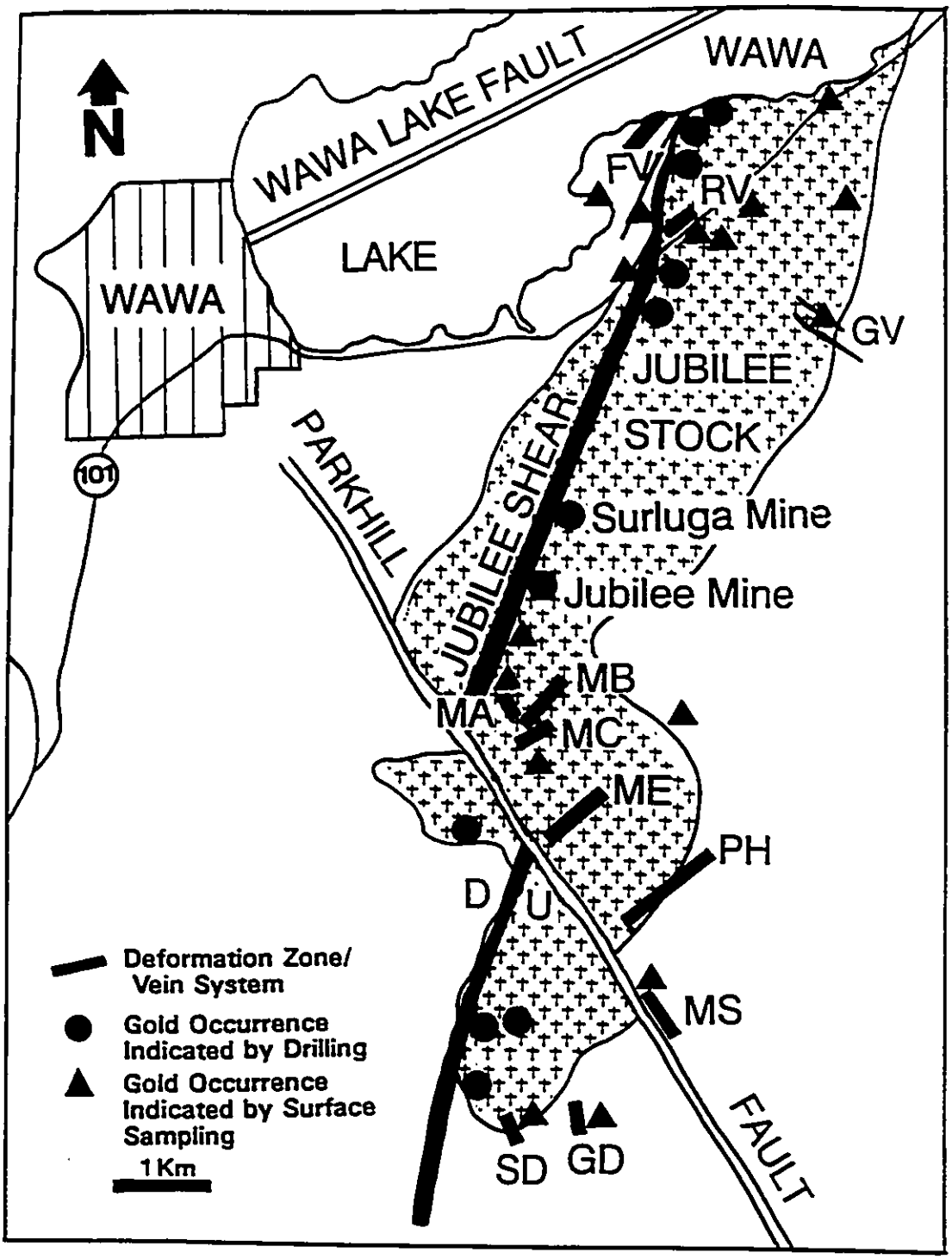

Figure 2. Simplified geology of part of McMurray Township showing the locations of the Jubilee Stock, deformation zones and gold mineralization (Adapted after Citadel Gold Mines Inc.). FV = Fat Vein zone; GD = Grace-Darwin zone; GV = Ganley Vein; MA = Minto A zone; MB = Minto B zone; MC = Minto C zone; ME = Minto E zone; MS = Mariposa Shaft; PH = Parkhill zone; RV = Root Vein zone; SD = Skunky Dog zone.

"ring-dike" pattern was suggested by Sage (1979) to represent a series of caldera-like fractures peripheral to the stock.

In the northeast corner of the township, steeply-dipping pillowed mafic to intermediate flows are present. These rocks belong to the first cycle of volcanism (Sage, 1979; 1981). The pillowed mafic to intermediate volcanics are separated from the tuffs marginal to the stock by a quartz-feldspar porphyry intrusion (Rupert, 1975, 1979; Sage, 1979, 1981).

The Helen Iron Range lies to the north of Highway 101, overlying the felsic tuffs and quartz porphyry flow units. The Iron Range is in turn overlain by massive mafic to intermediate metavolcanics that belong to the third cycle of volcanism (Sage, 1979). Disseminated sulphide mineralization (pyrite-pyrrhotite-arsenopyrite) and small pods of massive sulphide mineralization up to 1 metre thick are found on the south side of the iron formation above the felsic volcanics.

The metavolcanic sequence and the Jubilee stock are intruded by massive, fine- to medium-grained diabase dikes of post-Archean age, which generally trend east-west or northwest-southeast (Rupert, 1975, 1979).

Biotite- and olivine-rich lamprophyre dikes are very common in the area. They are generally less than 1 metre in width and have a northeast strike (Rupert, 1979; Sage, 1981, 1986 and 1987). Some of these dikes are probably associated with the intrusion of the Firesand River carbonatite complex. Radioactive carbonatite dikes occur in numerous road-cuts along Highway 101.

From a structural and economic geology point of view, the most important feature in the area is the Jubilee Shear, a brittle-ductile shear zone that extends south-southwest from the south shore of Wawa Lake for approximately 10 km to near the Mountain Lake (Figure 2). The shear zone dips 40 to 50° to the east and southeast (Rupert, 1975, 1979 and Sage, 1986). This zone is truncated by a northeast-trending fault (Wawa Lake fault) under Wawa Lake (Figure 2). In the south, the Jubilee shear is offset by the northwest-trending Parkhill fault (Figure 2) (Rupert, 1975; Sage et al., 1982). North of Highway 101, the Jubilee shear zone lies parallel to the margins of the Jubilee Stock, but further south, in the vicinity of the Surluga Mine, it is entirely within the stock (Figure 2). Near the Surluga Mine, the zone is approximately 30 to 50 m wide and dips 30-40° to the east (Helmstaedt, 1988). The Jubilee shear zone, which is exposed in the Fat Vein zone (FV in Figure 2), is characterized by an abrupt transition from relatively undeformed, non-foliated rocks to strongly-foliated buff schists which enclose numerous generations of quartz veins and breccias.

Smaller, northeast- and northwest-trending deformation zones and vein systems

occur in the hanging wall of the Jubilee shear (Figure 2) (Rupert, 1979; Sage, 1981). In addition to the Fat Vein zone and the Surluga Mine, both of which are located within the Jubilee shear zone, the Minto A, B, C and E deformation zones and vein systems (Figure 2) have been studied by the author.

1.5. Methodology

Representative samples of veins and rocks from within and outside the deformation zones were collected by the author and by Dr. I.M. Samson. Ninety five thin and polished-thin sections were prepared and examined by the author using transmitted and reflected light microscopy in order to establish the mineralogy and paragenesis of vein and alteration minerals. In addition, Raman spectroscopy has been used to distinguish between calcite and dolomite.

Thirty doubly-polished wafers were prepared by the author from representative vein samples for fluid inclusion analysis. These were examined in transmitted light in order to determine the fluid inclusion types present in each vein set. The compositions of the various fluid inclusion types were then determined using microthermometry and Raman spectroscopy. Raman spectroscopy was principally used to determine gas compositions and the identity of daughter minerals.

CHAPTER II
FIELD AND PETROGRAPHIC CHARACTERISTICS OF DEFORMATION ZONES AND VEIN SYSTEMS

2.1. Introduction

Characterization of the alteration and vein assemblages in the Jubilee shear zone and the other minor, mineralized deformation zones and vein systems involved a two-step approach. The first step was to establish the sequence of events for each individual zone. This involved extensive utilization of the detailed field observations of Samson and Holm (1991) on the stripped areas in those zones and of the information on the Surluga Mine provided by Citadel Gold Mines Inc.. The second step was to establish the petrographic characteristics of the rocks within the zones using transmitted and reflected light microscopy and Raman spectroscopy.

2.2. Jubilee Shear Zone

The Jubilee shear zone is a brittle-ductile shear zone hosted by the Jubilee Stock and associated felsic to intermediate crystal tuffs (not shown on the map) (Figure 2). The field relationships presented below are principally taken from Samson and Holm (1991).

2.2.1. Fat Vein Zone

The Fat Vein zone is a surface exposure of the Jubilee shear zone, north of Highway 101 (FV in Figure 2). Host rocks to the deformation zone comprise equigranular to porphyritic granodiorite and some felsic crystal tuffs. The shear zone comprises well-foliated, buff, muscovite schists and an enclosed pod of mafic schists. The zone also contains three generations of quartz veins and a mafic dike which cuts the deformation zone but is cut by the third vein set.

Veins

Vein Set 1 (V_1)

Vein set 1 comprises generally small, discontinuous grey-coloured, saccharoidal quartz veins which were isoclinally folded and boudinaged within the deformation zone. These veins typically occur as small boudins, a few mm up to 10 cm in width, within strongly foliated quartz-muscovite schists (Figure 3) in which the foliation is primarily defined by muscovite (Figure 3). These veins (V_1) consist of massive, fine-grained granoblastic quartz with subordinate amounts of dolomite, alkali feldspar, and

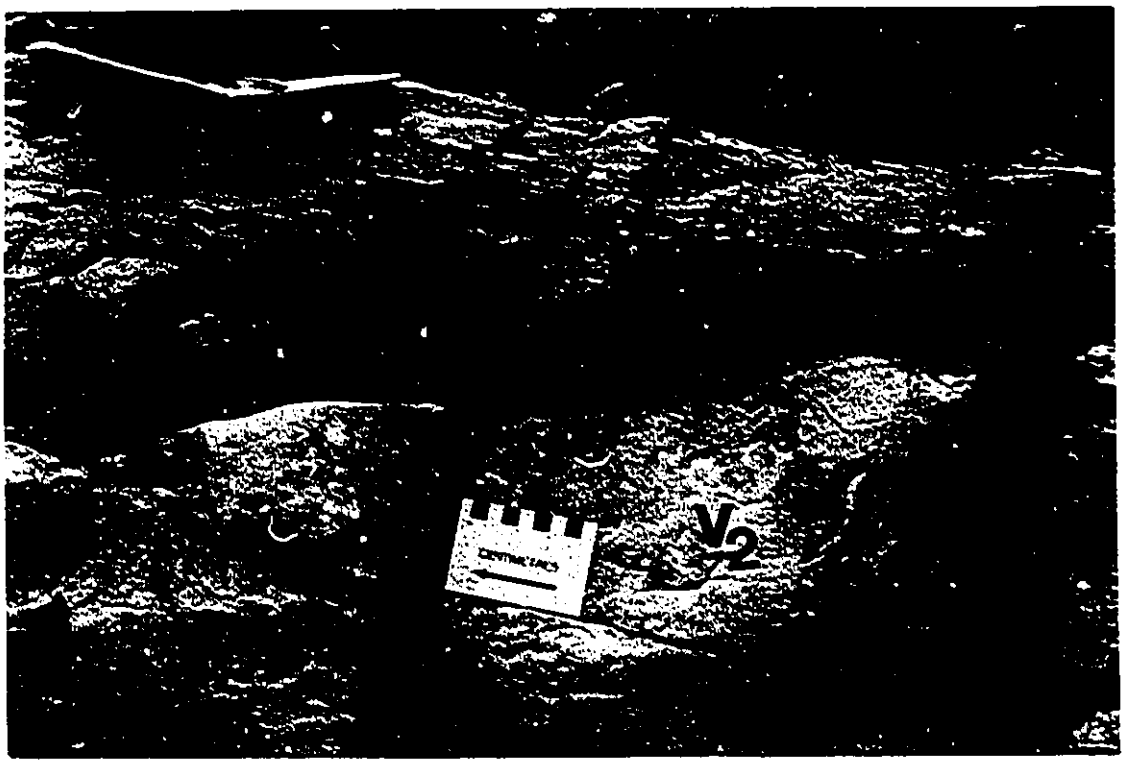

Figure 3. Vein set 1 (V_1) (boudinaged quartz veins) enclosed within buff, muscovite schists (MS) in the Fat Vein zone. Note also that vein set 2 (V_2) cross-cuts vein set 1 and the penetrative foliation (S_1).

and disseminated, coarse to fine-grained pyrite and chalcopyrite. These early veins are strongly deformed (boudinaged and folded) in the plane of the schistosity (S_1) (Figure 3). The axial planes of isoclinal folds and boudins are co-planar with the S_1 foliation. Deformation features in these veins include sutured grain boundaries and undulose extinction in quartz and feldspar grains.

Dolomite (identified using Raman spectroscopy) replaces quartz and alkali feldspar along fractures and grain boundaries. Inclusions of quartz and alkali feldspar occur within large ($\leq$ 5 mm) poikilitic dolomite grains. Dolomite also occurs as massive, coarse-grained aggregates. Dolomite grains are deformed as indicated by strong lamellar twinning, and undulose extinction. Hematite replaces dolomite along cleavage planes and fractures, which may suggest an Fe-rich composition for dolomite.

The sulphides in these veins commonly occur as coarse-grained, disseminated, euhedral to subhedral, brittlely-fractured grains up to 1 mm in size. They are paragenetically later than quartz and alkali feldspar, and are usually enclosed by

massive Fe-dolomite. Some fine-grained sulphides also occur interstitially to Fe-dolomite aggregates and recrystallized quartz.

Vein Set 2 (V_2)

Vein set 2 consists of massive, planar to lensoid quartz ± tourmaline veins (V_2) (Figure 3) that are podiform (boudinaged ?) within the deformation zone, but are relatively undeformed at the deformation zone margins (Samson and Holm, 1991). These veins cut the S_1 foliation and vein set 1 (Figure 3), but are offset by late, brittle faults within the shear zone. Tourmaline in this vein set was only observed in the veins at the shear zone margins, as disseminated fine-grained aggregates typically concentrated at the vein-wallrock contacts. These latter veins have a pinkish (feldspathic ?) alteration in wallrocks adjacent to these veins.

Vein Set 3 (V_3)

Vein set 3, which is known as "Jubilee Breccia", consists of undeformed quartz-ankerite veins (V_3) and breccias which display characteristic open-space filling textures such as crystal-lined vugs, cockade structures and single, large (up to 10-15 cm long), zoned quartz crystals with euhedral terminations (Samson and Holm, 1991). Ankerite in these veins is largely weathered to goethite. These veins cross-cut the foliation and vein sets 1 and 2.

Undeformed ankerite (?) veinlets, typically less than 0.5 mm in width, cross-cut the penetrative S_1 foliation in the schists, and form stockworks in places. There are also very thin ($\leq$ 0.5 mm in width), cross-foliation veinlets (V_3) of very small, fan-shaped, radiating crystal aggregates. In hand specimen, this mineral is white and soft, and in thin section, has very low birefrengence. These characteristics suggest that it may be kaolinite, or some other clay mineral. These thin veinlets are typically surrounded by hematitic alteration haloes. Minor chlorite and carbonate may occur at the margins of these veinlets. The relationship between these and the ankerite (?) veinlets is unclear, although both occur in late, separate fractures in a given sample.

Petrography of Host and Deformation-Zone Rocks

Host Rocks

The host rocks to the shear zone are non-foliated, medium- to coarse-grained granodiorites. They mainly consist of 30-35% plagioclase (andesine: An_{30-50}) (determined by the Michel-Levy method), 20-25% alkali feldspar, and 10-15% quartz.

Both plagioclase and alkali feldspar occur as large (1-5 mm), lath-shaped, euhedral to subhedral crystals with prominent zoning. Quartz occurs interstitially to these large feldspar crystals. Secondary minerals include sericite, biotite, chlorite, minor epidote and carbonate (altogether 5-10%). Sericite partially replaces feldspar and occurs as disseminated flakes or aggregates within and/or as narrow rims around feldspar. Biotite occurs as coarse-grained, euhedral to subhedral crystals up to 0.5 mm in size and also as polycrystalline aggregates. Biotite also occurs as large (0.5-2 mm), poikilitic crystals with quartz and feldspar inclusions.

Shear-Zone Rocks

The transition from undeformed to strongly foliated rocks occurs over less than a metre. The transitional rocks are weakly foliated chlorite-quartz-muscovite schists with minor carbonate (2%) and biotite (< 1%). A weak, anastomosing foliation (S_1) is usually defined by muscovite and chlorite. Coarse plagioclase grains are replaced and pseudomorphed by muscovite, and show minor recrystallization and fracturing. Quartz grains show undulatory extinction and are partially recrystallized around grain boundaries. Fine-grained aggregates of muscovite, carbonate and chlorite are commonly present in the pressure shadows of large, recrystallized quartz grains.

Rocks within the deformation zone contrast sharply, both mineralogically and texturally, with the rocks well outside the zone, and comprise buff-coloured, strongly foliated quartz-chlorite-Fe-dolomite-muscovite schists. They contain abundant (up to 50% of the rock) foliation-parallel quartz-Fe-dolomite augens (vein set 1) (Figure 3). The schistosity is defined by muscovite and chlorite which form ribbon-like, foliated masses wrapping around quartz and ferroan dolomite augens. Ferroan dolomite and quartz occur as polycrystalline aggregates both in the schist matrix and in the augens. Deformed plagioclase crystals display kink bands and partial recrystallization.

In addition to these muscovite-rich schists, there is a pod-shaped body of strongly foliated chlorite-Fe-dolomite schists which are conformably enclosed within the shear zone. The schistosity (S_1) in these rocks is defined by chlorite, which occurs as fibrous, foliated masses. The mafic schists have a well-developed crenulation cleavage (S_2), which is obvious in the field, but was not seen in thin section. This mafic schist unit also contains quartz-Fe-dolomite augens of vein set 1. Muscovite is absent in these rocks, which probably reflects a more mafic composition for the protolith of these schists, possibly a mafic dike or xenolith (Samson and Holm, 1991).

Late, fracture-related hematitic alteration is common throughout the Jubilee shear zone and is attributed to the emplacement of the Jubilee Breccias (Figure 4).

Figure 4. Photomicrograph of late hematitic (Hm) alteration in chlorite-muscovite schists. Hematite occurs as patchy masses in chlorite-rich areas. Field of view is 2.4 mm across (PPL). Sample #: IS89-50; Fat Vein zone.

A late biotitic alteration occurs as coarse-grained, randomly-oriented poikilitic biotite crystals which overgrow muscovite in the muscovite schists and thus, overprint the penetrative S_1 foliation. These large crystals contain abundant monazite (?) inclusions with pleochroic haloes. They are not affected by hematitic alteration, and may therefore be later than the hematitic alteration. However, the temporal relationship between the biotitic and hematitic alteration events remains speculative.

2.2.2. Surluga Mine

The Surluga mine is located within the Jubilee shear zone (Figure 2). The host rocks to the mineralized quartz veins mainly consist of strongly foliated quartz-Fe-dolomite-muscovite schists (S_1) which host three generations of veins (Helmstaedt, 1988 ; Samson and Holm, 1991). Some of the veins which belong to the second and third vein sets also occur in undeformed rocks.

Veins

Vein Set 1 (V_1)

The earliest set of veins in the mine comprise up to 0.5 m thick, discontinuous quartz veins and stringers that are strongly folded and boudinaged in the plane of the S_1 foliation. These veins (V_1) are principally composed of grey-coloured, fine-grained, saccharoidal quartz with lesser amounts of Fe-dolomite, alkali feldspar, tourmaline, chlorite, pyrite, pyrrhotite, arsenopyrite and gold. From an examination of some of the drill-core records from the Surluga Mine, it is evident that these veins, which have a high sulphide content (1-8%), always occur within strongly foliated muscovite schists. The schist intersections in the drill-cores vary in thickness from less than 1 metre up to 5 metres. High gold-assay values correspond to high sulphide contents in the veins, which suggests that most of gold is contained within, or associated with, the sulphides. In the Surluga mine the mineralized zones consist of these vein-schist "packages" which are arranged in an en-echelon fashion (R. Rupert, pers. comm., 1990).

The sulphide minerals usually occur as deformed, fine-grained, euhedral to subhedral crystals, or as polycrystalline aggregates, disseminated within quartz-Fe-dolomite boudins as well as in the schistose wallrocks. Pyrite and pyrrhotite are the most abundant sulphide minerals in the veins, with lesser amounts of chalcopyrite, arsenopyrite and fine-grained, ($\leq$ 50 μm) disseminated, native gold, all of which occur along fractures in quartz. Large rhomb-shaped arsenopyrite grains are enclosed by subhedral to anhedral pyrrhotite. Pyrite replaces pyrrhotite along fractures and grain-boundaries. All of the sulphides are commonly surrounded by thin ($\leq$ 1 mm wide) carbonate envelopes. Carbonate also occurs in late veinlets which are typically 0.5 to 1 mm in width. Within individual mineralized veins, a significant proportion of the sulphides occur near the vein-wallrock contacts. Large pyrite crystals display brittle deformation (fracturing) and replacement by late carbonate and/or chlorite along fractures and embayments. In some cases, the alteration envelopes (rims) around pyrite crystals are made up of fan-shaped, radiating crystals similar to the kaolinite (?) described from the Fat Vein zone.

Tourmaline occurs as disseminated, euhedral to subhedral crystals enclosed within the sulphides in the quartz veins. Some large ($>$ 1 mm) tourmaline crystals are colour zoned. Fe-dolomite replaces quartz in the veins along irregular fractures and grain-boundaries. This replacement is commonly accompanied by irregular patches of recrystallization in the quartz. Some large (~5 mm) ferroan dolomite grains display

lamellar twinning and fracturing and are replaced by chlorite along cleavage planes and irregular fractures.

Alkali feldspar occurs in subordinate amounts (up to 5%) within the quartz veins, as fractured grains interstitial to quartz, mostly at the vein margins.

Chlorite usually occurs as massive, lenticular masses in minor amounts (< 2%) at the vein margins, and is commonly accompanied by minor amounts of carbonate and tourmaline. When associated with tourmaline, chlorite completely encloses euhedral tourmaline crystals.

Vein Set 2 (V_2)

The second vein set, which is commonly termed the "Pinto Veins" in the Mine, comprises white, translucent, coarse-grained, equigranular quartz veins (V_2) which contain subordinate amounts of tourmaline, calcite (identified using Raman spectroscopy), and chlorite. Tourmaline typically occurs at the vein margins near the vein-wallrock contacts, where it forms laminae of fine-grained, euhedral to subhedral acicular grains.

Accessory calcite and chlorite occur interstitially to quartz. Chlorite also occurs as isolated patches and as fracture-fillings in quartz. These quartz veins are barren of gold (R. Rupert, pers. comm., 1990). These veins cross-cut the S_1 foliation (Figure 5) and vein set 1 but they are also deformed, as they are boudinaged and appear to have been rotated more or less parallel to the S_1 foliation (Helmstaedt, 1988a, 1988b).

Vein Set 3 (V_3)

The third vein set is the Jubilee Breccia, which consist of quartz-ankerite veins and breccias containing clasts of various intrusive and volcanic rocks, including an early set oflamprophyre dikes (R. Rupert, pers. comm., 1990). This breccia unit is commonly associated with a hematitic alteration and cross-cuts vein sets 1 and 2.
Late, thin (0.5-1 mm wide), cross-foliation kaolinite (?) veinlets with characteristic, fan-shaped, radiating crystals, similar to those described from the Fat Vein zone, also occur in the Surluga mine. These veinlets are commonly surrounded by hematitic alteration haloes.

Figure 5. A Pinto Vein (V_2) (vein set 2) in the Surluga Mine. Note that this vein cross-cuts the penetrative foliation (S_1).

Petrography of Deformation-Zone Rocks

The wallrocks to the veins described in the previous section are strongly foliated quartz-Fe-dolomite-muscovite schists in which the schistosity (S_1) is defined by muscovite. These schists have a well-developed crenulation cleavage (S_2) which is also defined by muscovite. Abundant, fine-grained, acicular rutile crystals also occur disseminated within the schist. Sulphide minerals (5-10% by volume), along with minor tourmaline and Fe-dolomite also occur disseminated throughout the schist. The tourmaline crystals lie parallel to the S_1 foliation. Basal sections of euhedral tourmaline crystals show prominent colour zoning.

Fe-dolomite occurs interstitially to quartz grains in the schist as disseminated, fine-grained, anhedral to subhedral grains and aggregates. In addition to the disseminated Fe-dolomite grains in the schist and in the veins, there are also fine-grained aggregates of carbonate along irregular fractures in, and as thin ($\leq$ 0.5 mm wide) envelopes around large pyrite grains in the schists.

Chlorite occurs in minor amounts in the schist; oriented parallel to S_1. In places, it is

pervasively hematized. Chlorite also occurs as a minor, late, alteration mineral after both Fe-sulphides and Fe-dolomite in which case it is massive.

Alkali feldspar occurs as large, poikiloblastic crystals with albite twinning, which overprint the penetrative S_1 fabric, as indicated by the enclosed quartz and tourmaline inclusions which have retained the orientation of the S_1 foliation.

Hematite replaces chlorite and Fe-sulphides and is restricted to areas where the late, fracture-related kaolinite (?) and carbonate veinlets occur in stockworks. A "salmon-red" coloured, fracture-related alteration commonly observed in the footwall rocks as well as in the mineralized zones in the Surluga Mine may be related to the emplacement of the Jubilee breccias (Figure 4) (Helmstaedt, 1988).

A late biotitic alteration is superimposed on muscovite in these schists, which overprints the S_1 foliation. Biotite occurs as large (up to 1.5 mm) euhedral to subhedral crystals. These crystals poikiloblastically enclose quartz and feldspar in the schists, and have not been subsequently altered or deformed.

2.2.3. Sequence of Events for the Jubilee Shear Zone

Figures 6 and 7 show a summary of the sequence of events within the Jubilee shear zone based on the field relationships and petrographic observations in the Fat Vein zone (Figure 6), and the Surluga Mine (Figure 7). The emplacement of the earliest vein set (V_1) appears to have been the first hydrothermal event in the Jubilee shear zone. This event is represented by the quartz-alkali feldspar-Fe-dolomite-sulphide veins in the Fat Vein zone (Figure 6) and by the auriferous quartz-alkali feldspar-Fe-dolomite-sulphide veins in the Surluga Mine (Figure 7). In these veins, Fe-dolomite and sulphide minerals are paragenetically later than the quartz-alkali feldspar assemblage (Figures 6 and 7). These veins were subsequently deformed during D_1 producing isoclinal folds and boudins (Figures 3, 6 and 7) (Samson and Holm, 1991). The deformed nature of these veins does not preclude the possibility that they were formed during the early stages of the D_1 deformation event (Figures 6 and 7). These veins are hosted by well-foliated quartz-muscovite-Fe-dolomite and chlorite-muscovite-Fe-dolomite schists in which the foliation (S_1) is primarily defined by muscovite and chlorite, and which is co-planar with the axial planes of the isoclinal folds and boudins. The development of the above mineral assemblages in the schists indicates that deformation (D_1) was predated or accompanied by a hydrothermal alteration event (A_1) (Figures 6 and 7). The quartz-muscovite-Fe-dolomite schists represent alteration of granodiorite and felsic tuffs whereas the chlorite-muscovite-Fe-dolomite schists represent alteration of an unidentified mafic protolith.

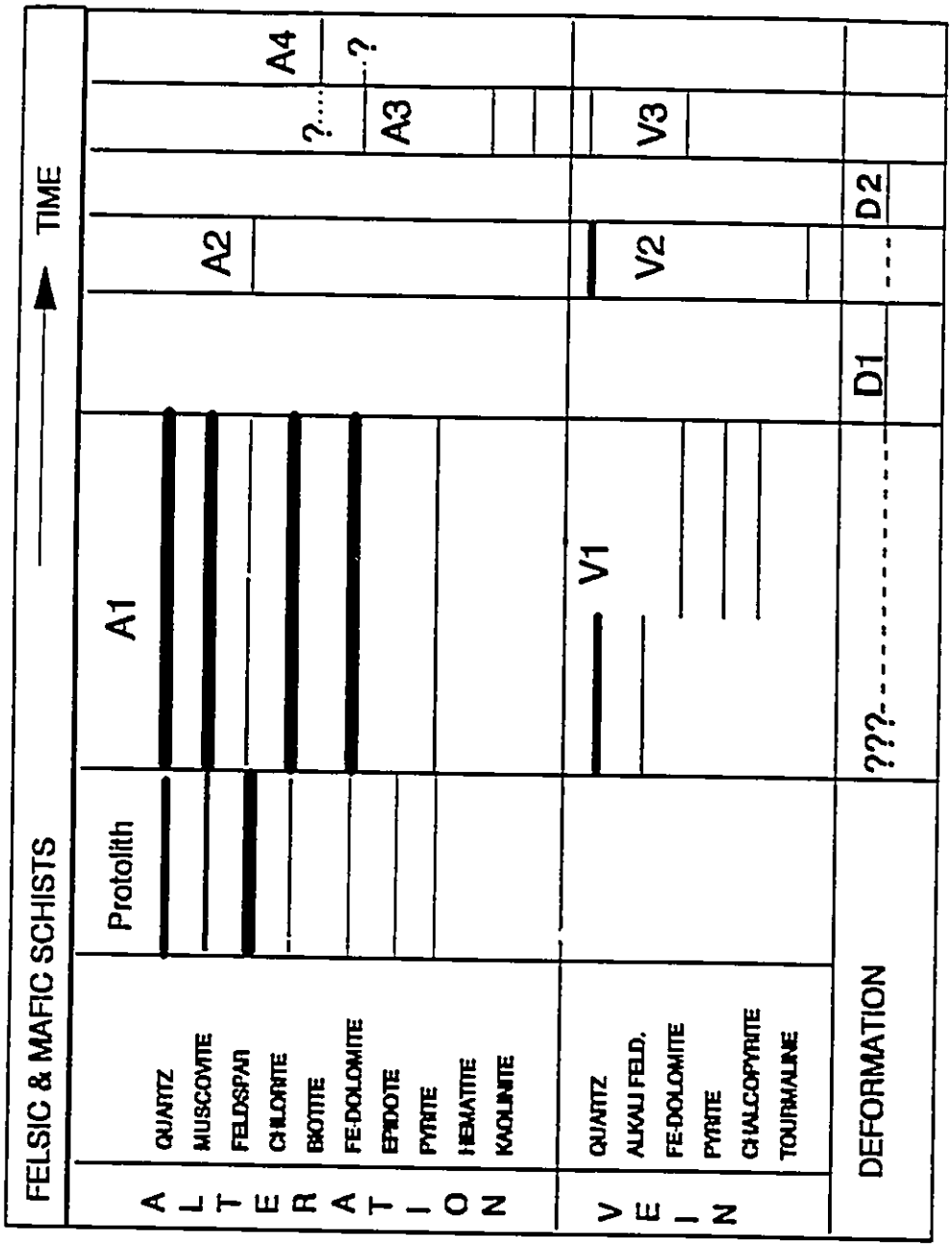

Figure 6. A summary of the paragenetic sequence of alteration and vein minerals in the Fat Vein zone. Variable thicknesses of lines indicate relative abundances of minerals. Broken lines indicate a possible temporal relationship between alteration and deformation events. V1,2,3 = vein sets 1, 2 and 3; A1,2,3,4 = alteration events 1, 2, 3 and 4; D1, 2 = deformation events 1 and 2, respectively.

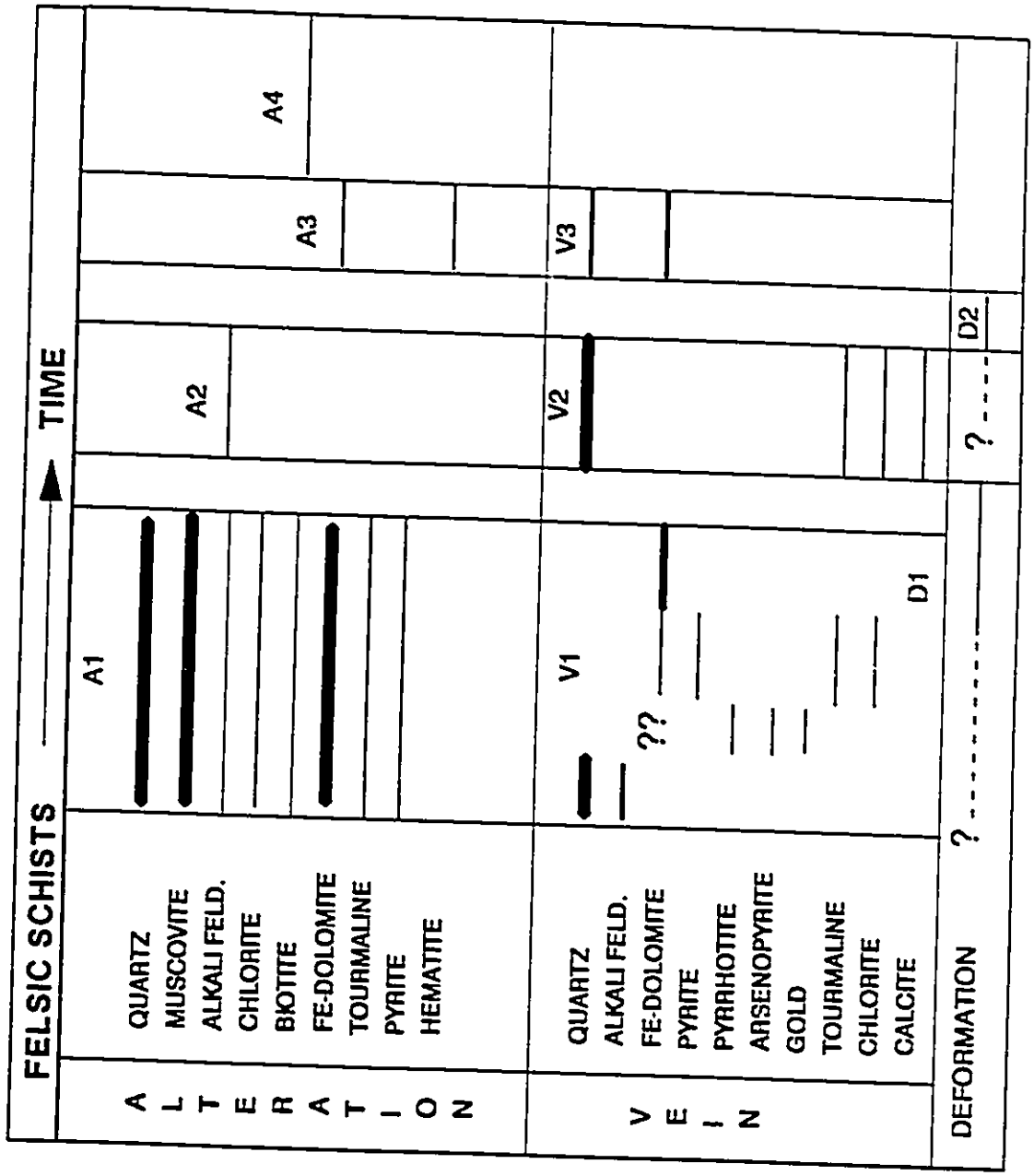

Figure 7. A summary of paragenetic sequence of alteration and vein minerals in the Suriuga Mine. Variable thicknesses of lines indicate relative abundances of minerals. V1,2,3 = vein sets 1, 2 and 3; A1,2,3,4 = alteration events 1, 2, 3 and 4; D1, 2 = deformation events 1 and 2, respectively.

The introduction of gold into the deformation zone must have taken place relatively early, as gold only occurs in the earliest vein set in the Surluga Mine (V_1) (Figure 7). But as discussed earlier, gold and sulphides are paragenetically later than the quartz in these veins. (Figures 6 and 7). This requires a brittle fracturing event following the precipitation of quartz in vein set 1 and possibly after its subsequent ductile deformation, as fractures hosting gold and sulphides cross-cut ductilely-deformed quartz grains. This brittle deformation event was probably penecontemporaneous with D_1, as the Pinto Veins (vein set 2) in both the Fat Vein zone and the Surluga Mine, all of which post-date D_1, are barren of gold (R. Rupert, pers. comm., 1990). The emplacement of the second vein set (V_2, Pinto veins) (quartz-calcite-chlorite-tourmaline) in the Surluga Mine (Figures 3 and 7) and by quartz $\pm$ tourmaline veins in the Fat Vein zone (Figures 3 and 6) took place after the D_1 deformation. A pinkish white (feldspathic ?) alteration (A_2) occurs in the wallrocks adjacent to these veins, which cross-cut the first vein set and the S_1 foliation and therefore post-date D_1 (Figures 3, 5 6 and 7). The deformed nature (boudinaging ?) of these veins, however, indicates a subsequent deformation event (D_2) following their emplacement (Figures 6 and 7). An alternative explanation for the generally lensoid shape of these veins may be that they are extensional veins that were emplaced during the development of brittle shear zones, as suggested by Samson and Holm (1991). This explanation is based on the observation of the similar quartz-tourmaline veins in the Root Vein zone, in the vicinity of the Fat Vein zone where they display an en-echelon arrangement which suggests that their lenticular form may be related to formation in a brittle shear zone rather than by boudinaging (Samson and Holm, 1991). The well-developed crenulation cleavage (S_2) in mafic schists (chlorite-Fe-dolomite) in the Fat Vein zone also requires a second deformation event (D_2) (Figure 6).

The Jubilee Breccia (V_3), which is represented by quartz-ankerite veins and breccias in the Fat Vein zone and in the Surluga Mine (Figures 6 and 7) was emplaced much later than the D_2 deformation in the Jubilee shear zone. These breccias were accompanied by hematization and fracture-related carbonate (ankerite ?) alteration (A_3) (Figures 4, 6 and 7). The kaolinite (?) veinlets are also possibly related to this late hematite and carbonate alteration, as these veinlets are usually surrounded by hematitic alteration haloes.

A late biotitic alteration (A_4) appears to post-date all the deformation and alteration events with the exception of hematitic alteration (Figures 6 and 7). The unaltered nature of biotite may suggest that this alteration post-dated the Jubilee breccia and the related

hematitic alteration. A possible genetic link between this biotitic alteration and the late, biotite-rich lamprophyre dikes may be considered as the latter are very abundant, especially in the Surluga Mine (Helmstaedt, 1988). This argument is supported by the fact that, biotization of wallrocks is very common in the Firesand River carbonatite (I. Samson, pers. comm., 1991).

2.3. Minto A Zone

This NNW-trending zone consists of at least four narrow (few centimetre to few metre wide) ductile deformation zones which are developed within a variety of lithologies (Samson and Holm, 1991). The general strike of the zone is 330° and the host rocks comprise a xenolith-rich granodiorite, felsic to intermediate crystal tuffs and some mafic pyroclastic units and dikes, which have been transformed into chlorite- and muscovite-rich schists within the deformation zones (Samson and Holm, 1991). The Minto A zone also hosts three sets of quartz veins, and thin carbonate and kaolinite (?) veinlets with hematitic haloes.

Lamprophyre dikes are present in the Minto A zone. These are 1 centimetre to 0.5 metres in width and intrude all deformation zones and vein set 2. Their relationship to vein set 3 is unclear. The lamprophyre dikes have bluish alteration haloes (fenitization), which usually extend for a few centimeters into the host rocks adjacent to them.

2.3.1. Veins

Vein Set 1 (V_1)

The first vein set consists of a planar quartz-alkali feldspar vein (V_1), which is located at the south end of the stripped area. A narrow, pinkish white, feldspathic (?) alteration halo exists around this vein. Chlorite is also present at the vein margins, and occurs as non-foliated, lath-shaped, fibrous crystals. This vein is cut by the second vein set.

Vein Set 2 (V_2)

The second vein set comprises abundant quartz $\pm$ Fe-dolomite $\pm$ chlorite veins which form a stockwork of planar veins outside the deformation zones (Samson and Holm, 1991). At the north end of the stripped area, flat-lying veins commonly contain Fe-dolomite at their margins, whereas steeply-dipping veins do not. Some veins belonging to the second vein set are deformed by the shear zones (Figure 8). In small

Figure 8. A field view of a planar quartz-Fe-dolomite vein (Fe-dolomite at the vein margins) (vein set 2) which was caught up in the deformation zone (DZ) and was boudinaged. Note also schistose (S_1) nature of the deformation zone in contrast with the undeformed, massive granodiorite host rock adjacent to it.

shear zones these veins can be traced into the zone (Figure 8); however, in larger zones, they simply terminate at the shear zone margin. Within the deformation zones the veins are folded and boudinaged (Figure 8, Samson and Holm, 1991). Axial planes of the folds are co-planar with the S_1 foliation.

Vein Set 3 (V_3)

The third vein set consists of a planar quartz-biotite vein in which the biotite occurs at the vein margin. This vein is undeformed and has a restricted exposure. Its relationship to the deformation zone and to the other vein sets is not known (Samson and Holm, 1991).

Vein Set 4 (V_4)

In addition to the quartz-rich veins described above, there are thin (0.1 to 1 mm thick) kaolinite (?) veinlets with associated hematitic alteration at the vein margins (c.f. the Fat Vein zone and the Surluga Mine). There are also stockworks of very thin (< 1 mm) carbonate veinlets. These veinlets cross-cut the planar quartz veins of vein set 1, boudins of vein set 2, and the S_1 foliation. But the relationship between carbonate stockworks and the kaolinite (?) veinlets is not known.

2.3.2. Petrography of Host and Deformation-Zone Rocks

Host Rocks

The host-rocks outside the deformation zones comprise non-foliated, relatively unaltered felsic crystal tuffs, mafic pyroclastic rocks and dikes, and medium- to coarse-grained granodiorite. The mineralogy of the granodiorite is similar to that described in the Jubilee shear. Secondary minerals both in the tuffs and granodiorite essentially consist of variable amounts of sericite and chlorite with minor amounts of epidote and carbonate. In mildly altered granodiorites, fracture-related sericitic alteration has affected plagioclase phenocrysts and the fine-grained groundmass. Chlorite also occurs in small amounts in association with the sericite. Minor amounts of carbonate occur as disseminated, fine-grained aggregates within these fractures.

In some cases, the granodiorites are pervasively altered to an assemblage containing up to 90% massive muscovite. Few relict plagioclase crystals can be recognized. This rock also contains abundant (around 5%), fine-grained, disseminated rod-shaped ilmenite crystals. A 1-2 cm wide massive, non-foliated chloritic alteration zone occurs within the pervasively sericitized rocks and contains inclusions of sericitized host rocks (Figure 9). The chlorite has a characteristic dark-green color and dark-brown birefrengence, suggesting that it is an Fe-Al-rich chlorite (Saggerson and Turner, 1982). This chloritic zone also contains accessory (< 1%) tourmaline which occurs as fine-grained aggregates and disseminated, euhedral crystals (Figure 9). Basal sections of some of the larger (0.5 mm) euhedral tourmaline crystals exhibit colour zoning. Trace amounts of Fe-dolomite are present in this chlorite-rich zone, as very small, rhomb-shaped crystals.

Relatively undeformed mafic fragmental rocks contain large plagioclase phenocrysts within a fine-grained groundmass of plagioclase and chlorite. Chlorite comprises up to 40% of the rock and occurs as felted, non-foliated masses which replace and

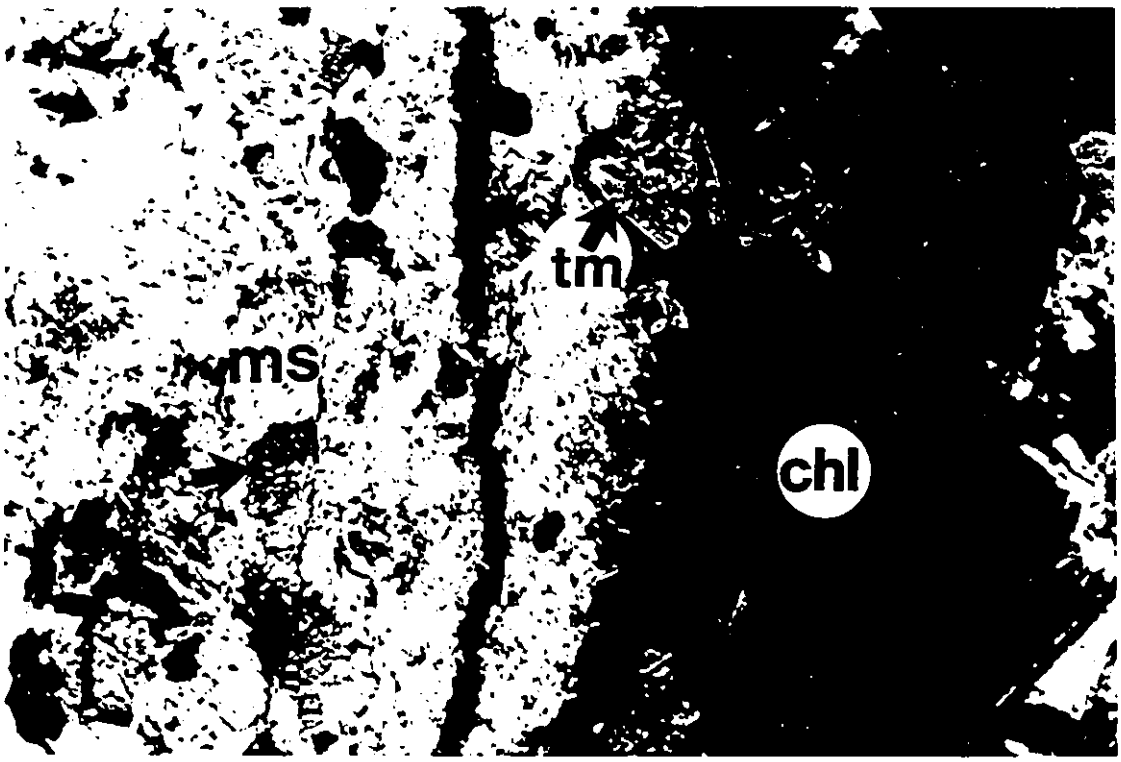

Figure 9. Photomicrograph of a 1 mm wide massive chloritic alteration zone (Chl, dark brown area) within the highly sericitized (Ms) rocks with relict feldspar grains (arrow). Note also the presence of minor tourmaline (Tm) in this alteration zone. Field of view is 2.4 mm across (XPL). Sample #: IS90-36; Minto A zone.

pseudomorph plagioclase phenocrysts. Riebeckite is present in these rocks, as fibrous, felted masses scattered throughout the rock.

Deformation-Zone Rocks

Deformation-zone rocks are distinguished from those outside the shear zone by their strongly foliated nature, and contrasting mineralogy. They have been divided, on the basis of their mineralogy, into mafic and felsic schists.

Mafic Schists

Rocks within a meter of the highly foliated rocks are weakly foliated chlorite-Fe-dolomite schists in which the anastomosing foliation is primarily defined by chlorite. Relict plagioclase grains display both brittle and ductile deformation features which

include irregular fractures, kink bands and recrystallization at grain boundaries. Chlorite and Fe-dolomite replace plagioclase along fractures. Chlorite also outlines the edges of plagioclase phenocrysts.

The well-foliated shear-zone rocks comprise chlorite-Fe-dolomite schists. They display a mylonitic texture, characterized by dynamically-recrystallized relict plagioclase porphyroclasts (~ 25%) and overall grain-size reduction of the matrix which is composed of plagioclase, chlorite and Fe-dolomite. The penetrative foliation (S_1) is defined by chlorite. Some rocks also display a weakly-developed crenulation cleavage (S_2) which is also defined by chlorite. Highly deformed (boudinaged and folded) quartz veins of vein set 2 occur in these schists. The foliation is generally parallel to the long axes of the quartz boudins (Figure 8).

Chlorite occurs as well-foliated fibrous masses (> 50% of the rock by volume) which contain abundant fine-grained, disseminated rutile crystals. Chlorite usually forms ribbon-like domains separated by Fe-dolomite-rich layers. Next in abundance to chlorite is Fe-dolomite (30-35%), which occurs interstitially to chlorite, as coarse to medium-grained disseminated elongate grains or aggregates (augens) parallel to the penetrative S_1 foliation. Minor riebeckite is present as fibrous, felted masses which replace Fe-dolomite along cleavage planes.

Felsic Schists

Felsic schists comprise quartz-Fe-dolomite-muscovite schists with mylonitic fabrics which contain large, polycrystalline quartz ± Fe-dolomite augens (vein set 2), up to 5 mm in diameter. Some of these augens are made up of a single, subhedral quartz crystal or polycrystalline quartz aggregate. Fe-dolomite occurs interstitially to quartz, as coarse-grained, subhedral to anhedral, grains. The Fe-dolomite has a brownish color and is commonly hematized along cleavage planes. Muscovite defines the S_1 foliation and occurs as ribbon-like masses wrapping around the polycrystalline quartz-Fe-dolomite augens (Figure 10).

There are minor (1%), disseminated, fine-grained, euhedral to subhedral pyrite grains and aggregates within the schist. These pyrite grains are brittlely deformed as indicated by irregular fractures in pyrite cubes which are filled with carbonate (vein set 4). Small (up to 0.5 mm), rounded patches of felted, blue, fibrous riebeckite-biotite aggregates are scattered throughout the schist. Riebeckite and biotite replace Fe-dolomite, as is indicated by riebekite and biotite overgrowing deformed Fe-dolomite grains.

Figure 10. Photomicrograph of quartz-muscovite schist enclosing deformed quartz veins (QV_1) (vein set 1). Note that the S_1 foliation is defined by muscovite (Ms). Field of view is 2.4 mm across (XPL). Sample #: MINA; Minto A zone.

2.3.3. Sequence of Events for the Minto A Zone

Figure 11 shows a summary of the major events in the Minto A zone. The first event in this zone was the emplacement of the quartz-feldspar-chlorite vein (V_1). Subsequently, quartz-Fe-dolomite veins (V_2) were emplaced, as they cross-cut vein set 1. A deformation event (D_1) must have taken place following the emplacement of the early vein sets (vein sets 1 and 2), as indicated by the deformed nature of the quartz-Fe-dolomite veins (vein set 2) (Figure 8). This deformation event was penecontemporaneous with, or pre-dated by, an alteration event (A_1) which produced the chlorite-Fe-dolomite assemblage in the mafic schists, and quartz-pyrite-Fe-dolomite-muscovite assemblage in the felsic schists (Figure 11). A second deformation event (D_2) is required to explain the crenulation cleavage in the mafic schists (Figure 11). The timing of the quartz-biotite vein (V_3) with respect to deformation and the emplacement of vein sets 1 and 2 is not known (Figure 11).

Late carbonate and kaolinite (?) veinlets (V_4) were emplaced at a later stage and

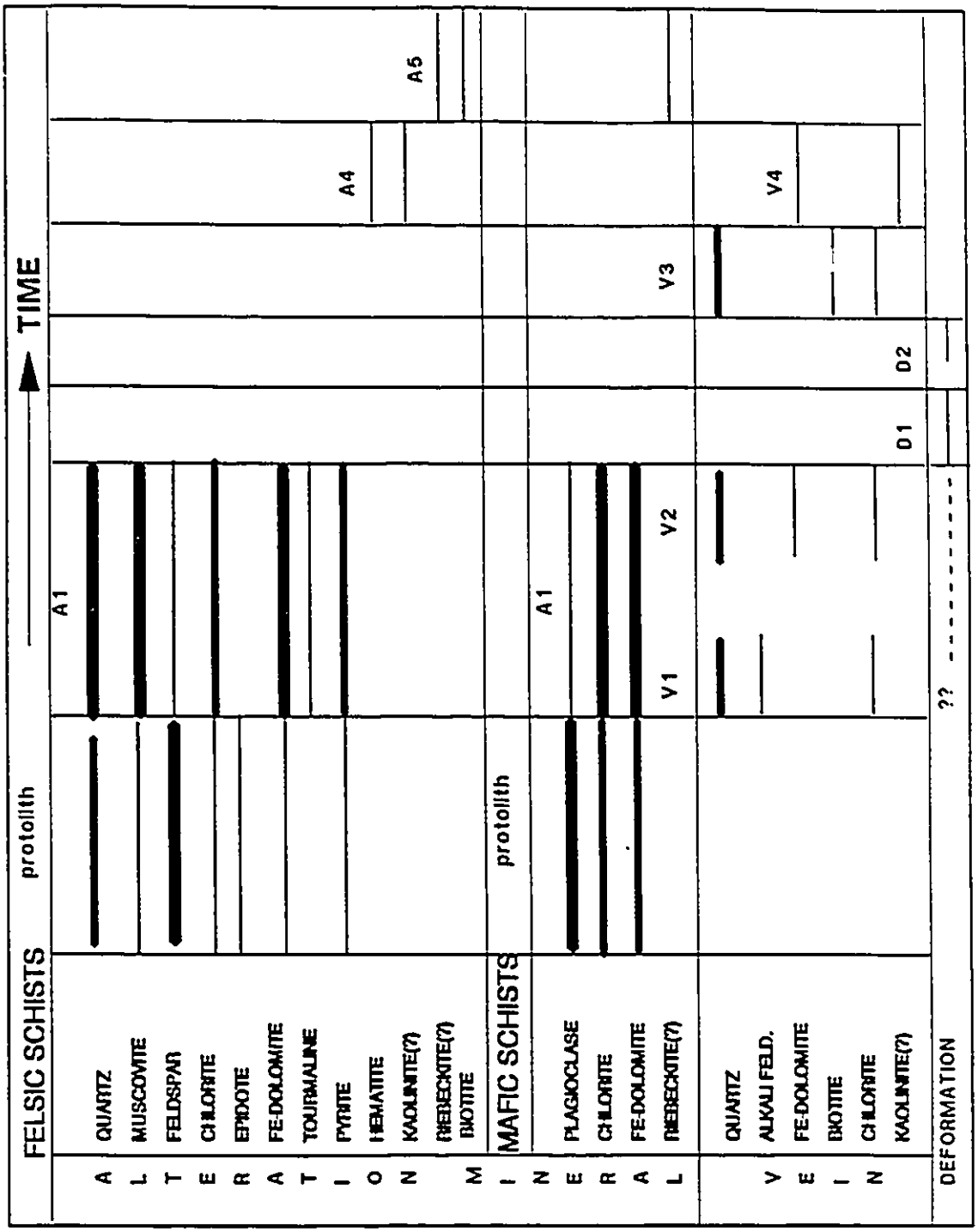

Figure 11. A summary of the paragenetic sequence of alteration and vein minerals in the Minto A zone. Variable thicknesses of lines indicate relative abundances of minerals. V1,2,3,4 = vein sets 1, 2, 3 and 4; A1,3,4,5 = alteration events 1, 3, 4 and 5; D1, 2 = deformation events 1 and 2, respectively.

were probably accompanied by hematization (A_4) (Figure 11). Finally, fenitization (A_5) took place during the emplacement of the lamprophyre dikes (Figure 11). The relationship of fenitization with respect to vein set 3 (quartz-biotite) is not known (Figure 11).

2.4. Minto B Zone

The Minto B zone is a ductile shear zone with a strike of approximately 45° and consists of intercalated felsic and mafic schists. The host rocks to the shear zone include quartzo-feldspathic tuffs, granodiorite, mafic fragmental rocks, and dikes. Mafic schists consist of chlorite-Fe-dolomite-biotite schists with a strong penetrative foliation (S_1) and, in places, a crenulation cleavage (S_2). The S_1 foliation is isoclinally folded in places along axial planes that lie approximately parallel to the S_1 foliation which may suggest that the original orientation of the S_1 foliation was at a steep angle to the deformation zone boundaries (Samson and Holm, 1991).

Felsic schists comprise quartz-chlorite-muscovite schists which contain a weak, disjunctive, anastomosing, spaced cleavage, mainly defined by muscovite and chlorite. These felsic schists contain disseminated sulphides, chiefly euhedral, coarse-grained pyrite. The contacts between the mafic and felsic units are sharp and lie parallel to the deformation zone margins. Some mafic units, however, pass along strike into the felsic units. In such cases, the mafic schist terminates as millimeter-thick whisps within the felsic units (Figure 12). These whispy zones contain relict quartz and feldspar phenocrysts (Samson and Holm, 1991).

The Minto B zone hosts numerous quartz veins (V_1, see below) which, within the mafic schists, generally lie parallel to the penetrative S_1 foliation where they are boudinaged and isoclinally folded. In the felsic units these veins are undeformed. Individual, undeformed quartz veins can be traced into deformed equivalents within the mafic schists (Samson and Holm, 1991).

Several diabase dikes and one lamprophyre dike cross-cut the deformation zone and the quartz veins. The lamprophyre dike is accompanied by fenitization which extends for a few tens of centimetres into the host rocks adjacent to it.

2.4.1. Veins

Vein Set 1 (V_1)

The first set of veins occurs in both mafic and felsic units and has a mineral assemblage of quartz-alkali feldspar ± tourmaline ± Fe-dolomite ± chlorite ± pyrite.

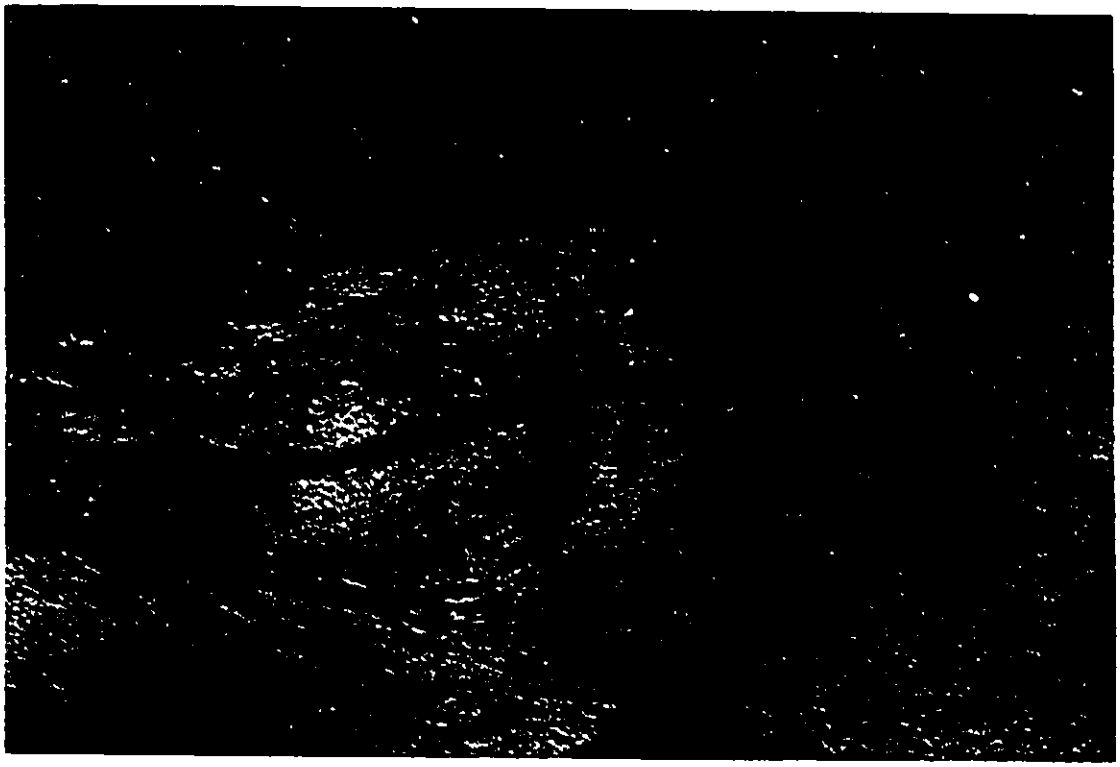

Figure 12. Whispy chloritic alteration zone in felsic schists, interfingering with weakly foliated felsic schists. Note the fine scale of interfingering. Pen as a scale.

The alkali feldspar occurs interstitially to quartz and is replaced by a chlorite-tourmaline-Fe-dolomite assemblage along fractures and grain boundaries. These veins are 1 to 50 cm wide and some of them are enveloped by non-foliated to weakly foliated massive chloritic haloes. Microscopic deformation features within the veins include sutured grain boundaries, recrystallization and undulose extinction in quartz and feldspar grains.

The sulphide minerals in these veins occur as disseminated, coarse-grained, anhedral to euhedral, brittlely-deformed crystals and polycrystalline aggregates up to 1 mm in size. They occur interstitially to Fe-dolomite and replace quartz and alkali feldspar along fractures, and hence are paragenetically later than them. Large, poikilitic Fe-dolomite grains enclose alkali feldspar and quartz inclusions. Fe-dolomite and pyrite are concentrated in areas where extensive recrystallization of quartz has occurred, as indicated by irregular zones of very fine-grained quartz within the coarse quartz crystals. Pyrite crystals are fractured and are replaced along these fractures, and along grain-boundaries by carbonate (c.f. the Fat Vein zone and the Surluga Mine).
Some small, planar, fibrous quartz $\pm$ chlorite veins occur in the felsic units. These

veins strike at a high angle to the trend of the shear zone and the S_1 foliation. The orientation of the fibers in these veins is approximately parallel to the general trend of the shear zone. This indicates that these are extension veins and are related to the development of the shear zone (Samson and Holm, 1991).

Vein Set 2 (V_2)

The second set of veins are thin (0.5 mm to 5 cm wide), planar, undeformed quartz-ankerite veins (V_2) with associated fracture-related ankeritic alteration (Samson and Holm, 1991). They cross-cut vein set 1 and the S_1 foliation (Figure 13). Some of these veins dominantly consist of ankerite and form stockworks which contain fragments of schist. There is also minor (1%) disseminated euhedral to subhedral pyrite grains which occur interstitially to both quartz and ankerite.

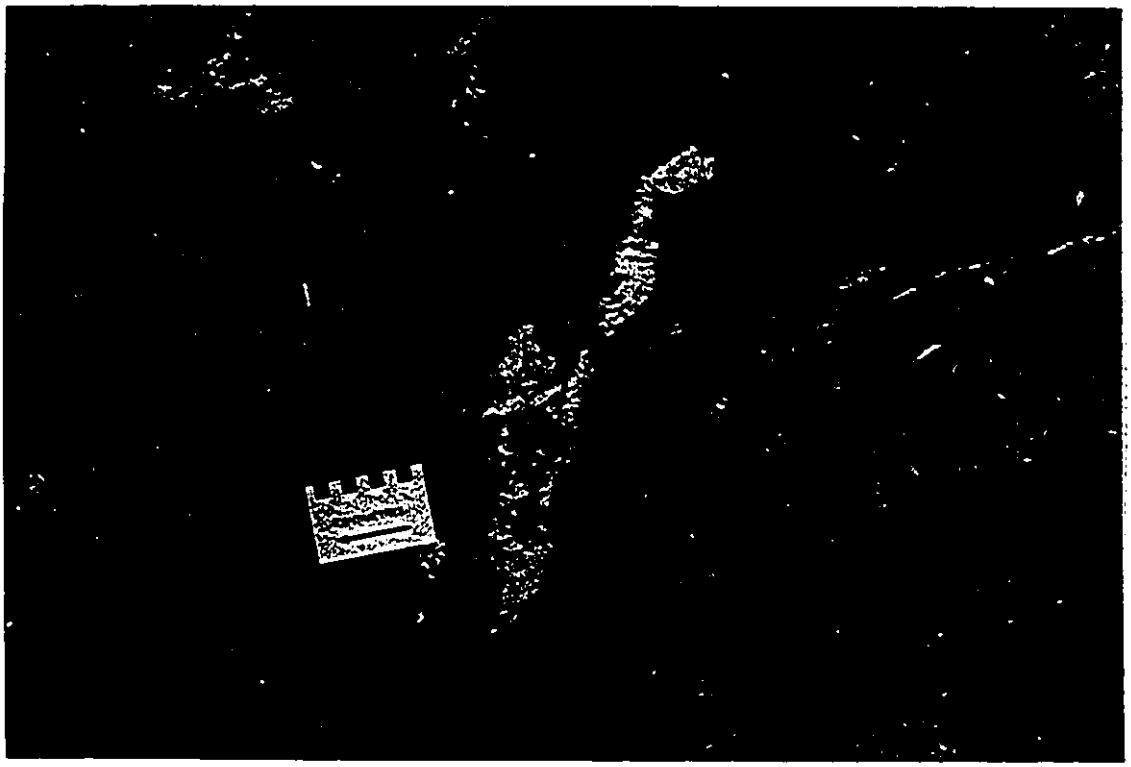

Figure 13. A field view of cross-cutting relationship between vein sets 1 and 2, the latter (V_2) cutting early, highly deformed veins (V_1) and the shear-zone foliation (S_1). Late planar veins are also accompanied by an ankeritic alteration.

2.4.2. Petrography of Host and Deformation-Zone Rocks

Host Rocks

Undeformed host rocks to the deformation zone consist of medium-grained granodiorite and quartzo-feldspathic crystal tuffs, and pervasively altered mafic fragmental rocks. The mineralogy of the granodiorite is similar to that described from other zones. The crystal tuffs contain large feldspar and quartz phenocrysts (1-5 mm) in a very fine-grained matrix of quartz and feldspar. Granodiorite and crystal tuffs contain very similar secondary mineral assemblages. Feldspar phenocrysts are mildly sericitized and chloritized along their edges and along fractures. Chlorite usually outlines the crystal margins whereas sericite occurs as fine-grained flakes dispersed throughout the crystal. Minor epidote occurs as fine, granular masses disseminated throughout feldspar crystals. Minor carbonate occurs interstitially to chlorite. Besides these minerals, there are small, disseminated, rounded patches of bluish-green, fibrous riebeckite. These patches are usually more common where biotite is abundant and they typically occur together with biotite. Biotite in these rocks occurs as poly-crystalline aggregates. Some carbonate is also present in these felted masses and in some cases these fibrous patches occur within carbonate grains.

In addition to these felsic rocks, there are some weakly-foliated mafic host rocks which are altered to a chlorite-epidote assemblage, with minor Fe-dolomite and ilmenite. Chlorite makes up 35-40% of the rock and occurs as weakly foliated masses enveloping relict plagioclase and biotite phenocrysts. Ferroan dolomite (5-10%) occurs as fine-grained aggregates, interstitially to chlorite. Some large ferroan dolomite crystals poikiloblastically enclose relict plagioclase phenocrysts. Epidote is abundant (15-25%) and occurs interstitially to chlorite, and as fine-grained, granular masses which pseudomorph plagioclase. Biotite occurs in subordinate amounts ($< 2\%$) and shows extensive replacement by chlorite. In addition, the mafic fragmental rocks contain minor amounts ($< 2\%$) of riebeckite, as scattered, fibrous, felted masses.

Deformation-Zone Rocks

Mafic Schists

The mafic schists consist of well-foliated, chlorite-Fe-dolomite-biotite schists with a well-developed penetrative foliation (S_1) (Figure 14). Some of these schists are mylonitic, as indicated by the presence of dynamically recrystallized plagioclase porphyroclasts. In some cases, these schists display a crenulation cleavage (S_2). The S_1 foliation is defined mainly by biotite and chlorite, which occur in

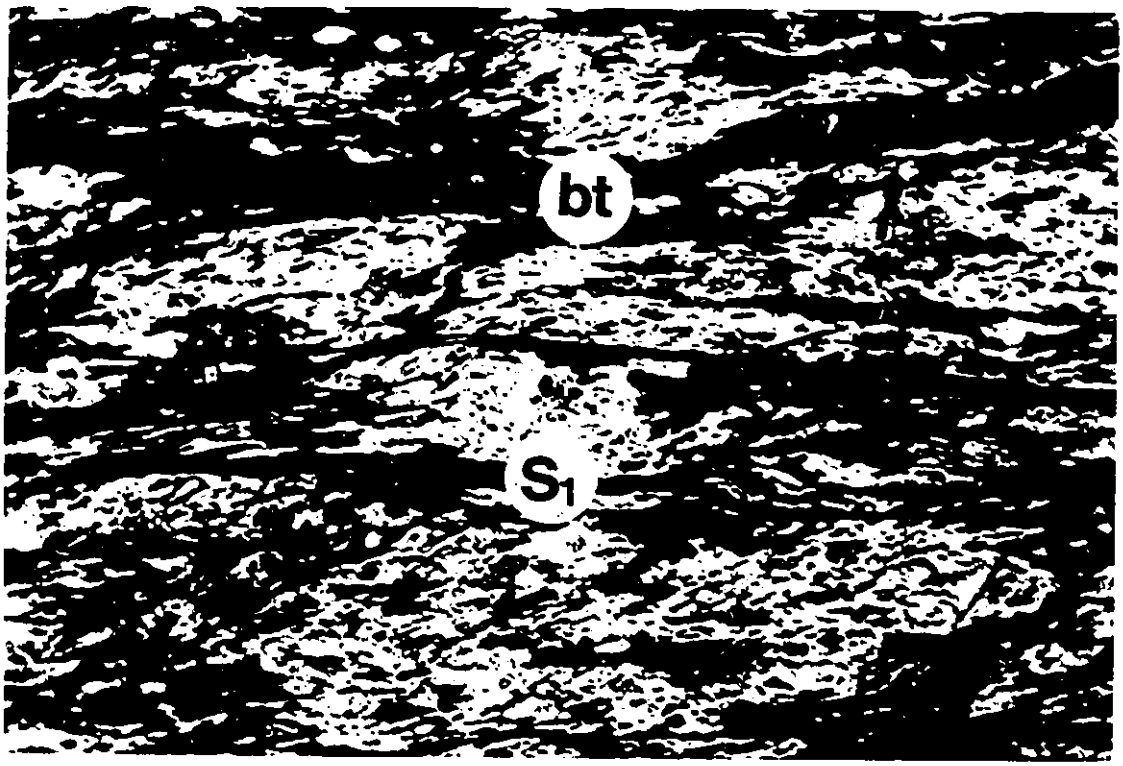

Figure 14. Photomicrograph of early biotitic alteration (biotite schist), biotite (Bt) defining continuous penetrative foliation (S_1). Note that biotite is concentrated in layers separated by chlorite-Fe-dolomite-rich domains. Field view is 2.4 mm across (PPL). Sample #: IS89-5; Minto B zone.

layers separated by quartzo-feldspathic layers (Figure 14). These biotite-rich schists contain abundant (15-25%), small, foliation-parallel, Fe-dolomite augens, typically less than 1 mm in diameter. These augens are composed of both single crystals and polycrystalline aggregates. The S_1 foliation defined by biotite is truncated by these augens. Biotite in these schists occurs in two ways: (1) as well-foliated masses (Figure 14); (2) as non-foliated, coarse-grained (up to 0.5 mm) poikilitic, euhedral to subhedral crystals and polycrystalline aggregates overgrowing chlorite and the S_1 foliation. Chlorite occurs as well-foliated felted masses and long, ribbon-like domains, which lie parallel to the S_1 foliation. It contains small amounts (2%) of fine-grained, disseminated euhedral to subhedral crystals of titanite. These crystals lie parallel to the S_1 foliation. The mafic schists also contain small amounts of disseminated and stringer pyrite and chalcopyrite.

Felsic Schists

Felsic schists in the Minto B zone are characterized by weakly foliated quartz-chlorite-epidote-muscovite schists, in which muscovite and chlorite define the S_1 foliation. In felsic schists, large, relict albite phenocrysts are altered to a muscovite-epidote-chlorite assemblage and occur in a fine-grained matrix of quartz, feldspar, sericite and chlorite. Minor carbonate occurs interstitially to chlorite in the matrix. In some samples, muscovite and epidote pseudomorph plagioclase phenocrysts. This alteration is accompanied by accessory (up to 2%) sulphides (pyrite and chalcopyrite) which occur as fine-grained, disseminated, euhedral to anhedral crystals and polycrystalline aggregates. Chlorite occurs along with muscovite and epidote, and forms well-foliated, irregular patches which enclose relict plagioclase grains and also fill the interstices between large plagioclase crystals. Chlorite is replaced by hematite in places.

Large (up to 2 mm), poikilitic biotite crystals overgrow muscovite in the schist matrix, and thus overprint the S_1 foliation (Figure 15). The poikilitic biotite crystals are restricted to the muscovite-rich domains in the schists, and contain abundant quartz and feldspar inclusions. Small amounts of riebeckite are also present in the felsic schists. Riebeckite replaces Fe-dolomite and occurs interstitially to biotite crystals, as fibrous, felted masses (Figure 16).

Vein-Related Alteration

The only alteration effects in the Minto B zone which can be directly related to vein emplacement are chloritic haloes which occur in the mafic schists around some of the quartz veins belonging to the first vein set (Samson and Holm, 1991). These "chloritic" haloes consist of biotite-chlorite schists. In the field, the haloes appear more massive than the enclosing schists and therefore appear to overprint the schists (Samson and Holm, 1991). However, in thin section they exhibit a well-developed S_1 foliation, and in some samples, a well-developed crenulation cleavage (S_2). Minor apatite and titanite occur within the chloritic haloes.

2.4.3. Sequence of Events for the Minto B Zone

Figure 17 shows a summary of the major events and a paragenetic sequence for the Minto B zone. The first event was the emplacement of the earliest vein set (V_1), which is represented by the quartz-Fe-dolomite-chlorite-tourmaline ($\pm$ pyrite, alkali feldspar)

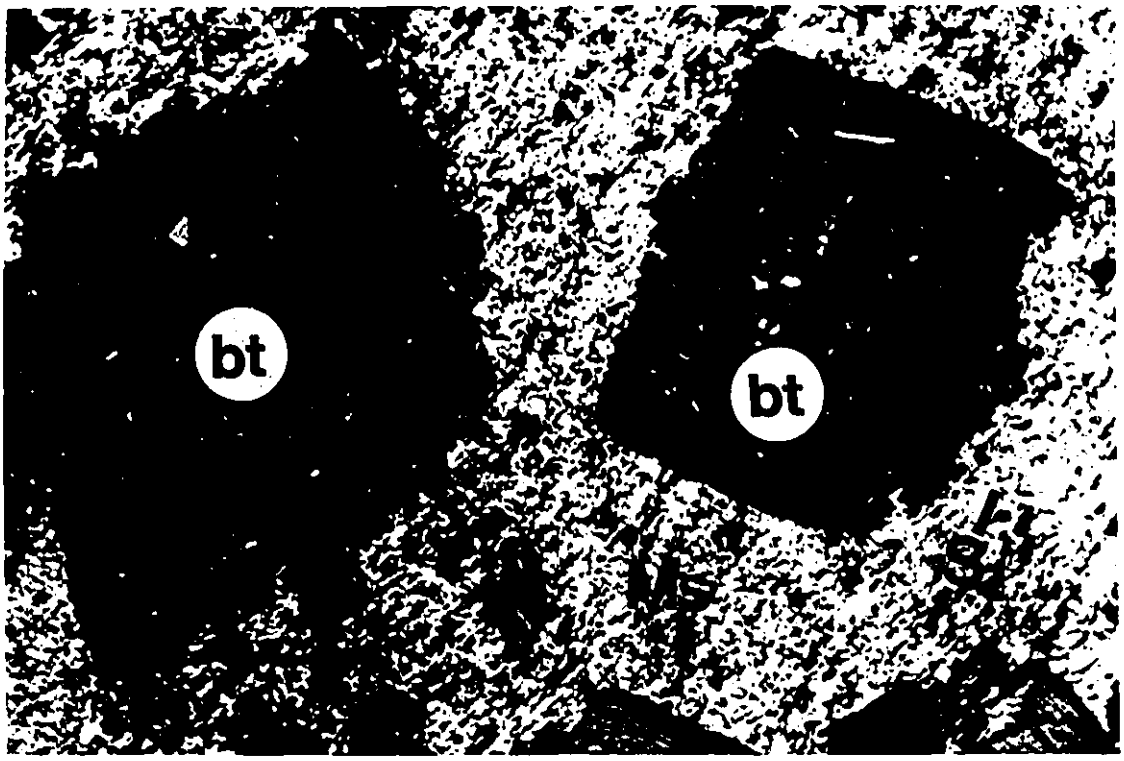

Figure 15. Photomicrograph of large poikilitic biotite crystals (Bt), overprinting the foliation (S_1) in muscovite schists (Ms). Note the presence of abundant quartz and feldspar inclusions (arrows) within large biotite crystals, also note their unaltered/undeformed nature. Field of view is 2.4 mm across (XPL). Sample #: IS90-43; Minto B zone.

veins (Figure 17). In these veins, Fe-dolomite, sulphides, chlorite and tourmaline are paragenetically later than quartz and alkali feldspar (Figure 17).

This early veining event (V_1) was accompanied by a vein-related alteration event (A_1) which produced the chloritic alteration haloes around some of the quartz veins in the mafic schists. The deformed nature of these alteration haloes suggest that this alteration and vein emplacement predated the deformation events which produced the S_1 and S_2 fabrics. However, as not all of the quartz veins have chloritic haloes, it is possible that there may have been two generations of quartz veining which predated the deformation event D_1 (Figure 17). A second deformation event (D_2) is indicated by the crenulation cleavage in the mafic schists and in the chloritic haloes (Figure 17). Planar, quartz-ferroan dolomite veins (V_2) were emplaced at a later stage (after D_2), and were accompanied by an ankeritic alteration event (A_2) (Figure 17). This alteration event may be related to the hematization in the felsic schists (Figure 17). A late, biotitic

Figure 16. Photomicrograph of fenitized host rock, with bluish-green, fibrous patches of riebeckite (Rb). Note that fibrous riebeckite replaces ferroan dolomite (Dol) and that the presence of biotite (Bt) in close association with riebeckite. Field of view is 2.4 mm across (PPL). Sample #: IS89-1; Minto B zone.

alteration (A_3) is present both in the mafic and felsic schists, and possibly represents fenitization, as riebeckite occurs interstitially to biotite (Figures 15 and 16).

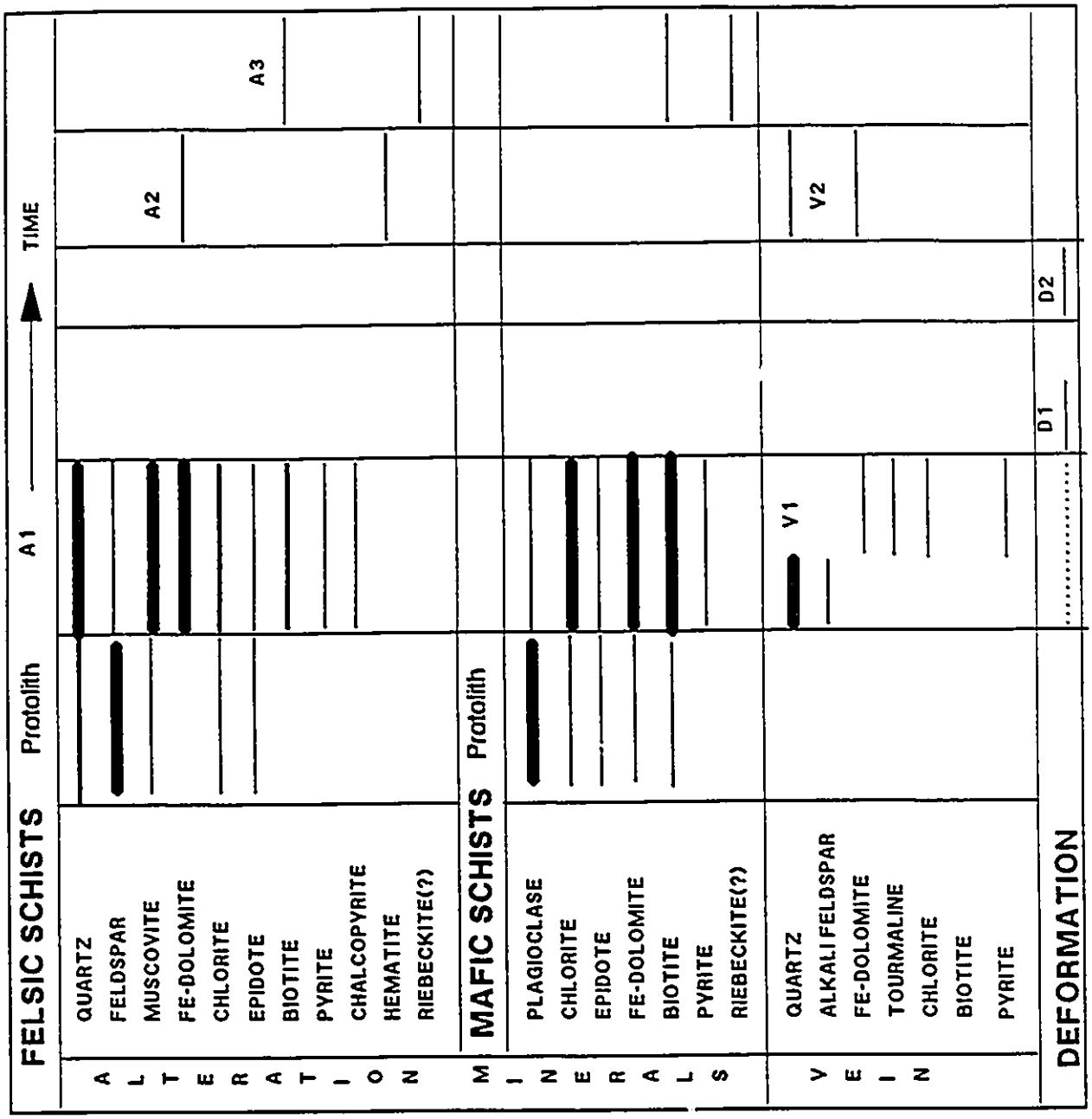

Figure 17. A summary of the paragenetic sequence of alteration and vein minerals in the Minto B zone. Variable thicknesses of lines indicate relative abundances of minerals. V1,2 = vein sets 1 and 2; A1,2,3 = alteration events 1, 2 and 3; D1,2 = deformation events 1 and 2.

2.5. Minto C Zone

The Minto C zone is a narrow (approx. 2 metre wide), ductile shear zone trending approximately 80/70°S which is in part localized at the contact of a biotite-rich granodiorite and mafic tuffs (Samson and Holm, 1991). The deformation zone consists of muscovite and biotite schists that are the altered and deformed equivalents of the granodiorite and the mafic unit, respectively. The zone contains a number of deformed quartz veins in the schists (vein set 1) and an undeformed quartz-tourmaline vein (vein set 2). A mafic dike cuts the zone and the first vein set and is affected by a hematitic alteration. A lamprophyre dike cuts everything in the zone and is accompanied by fenitization.

2.5.1. Veins

Vein set 1 occurs as deformed (boudinaged), recrystallized quartz veins in the schists. Vein set 2 occurs in the granodiorite, as a branching, undeformed quartz-chlorite-tourmaline-calcite vein. This vein has very similar mineralogical and textural characteristics, such as its coarse-grained, relatively undeformed nature, as the Pinto Veins in the Surluga Mine. Despite their deformed nature, the quartz veins belonging to vein set 1 could be temporally equivalent to vein set 2.

2.5.2. Petrography of Host and Deformation-Zone Rocks

Host Rocks

The host rocks to the shear zone comprise non-foliated, mafic crystal tuffs and a medium-grained granodiorite. The mafic crystal tuffs contain plagioclase and biotite phenocrysts in a fine-grained matrix of plagioclase, biotite, chlorite, sericite and epidote. These rocks have been altered to an assemblage of chlorite (~30%), muscovite (~10%), clinozoisite and zoisite (~10%), with minor carbonate. Plagioclase phenocrysts display variable amount of alteration, ranging from minor, disseminated muscovite flakes and granular epidote to complete replacement by a mixture of muscovite, chlorite and epidote. The latter assemblage commonly pseudomorphs these phenocrysts. Chlorite and minor carbonate partially replaces biotite.

The mineralogy of the granodiorite is similar to that described in the previous zones. The principal secondary minerals are muscovite (15-20%) and clinozoisite (5-10%), with minor chlorite and carbonate. In these rocks, muscovite and epidote typically pseudomorph plagioclase phenocrysts. Muscovite also occurs in alteration stockworks. Large (0.5 mm), euhedral to subhedral, poikilitic biotite crystals overgrow the

muscovite. These biotite crystals enclose small, anhedral granules of quartz and feldspar, resulting in a sieve-like texture (Figure 16). Minor fibrous riebeckite also occurs as small, rounded patches, some of which occur within large, poikilitic biotite crystals.

Deformation-Zone Rocks

Rocks within the deformation zone consist of strongly foliated quartz-muscovite schists and biotite-Fe-dolomite-chlorite schists. These schists contain quartz augens (few mm to few cm in width) which represent vein set 1.

The quartz-muscovite schists have a mylonitic fabric as they contain dynamically-recrystallized quartz and feldspar porphyroclasts in a fine-grained, homogeneous matrix of quartz, feldspar and muscovite. The S_1 foliation in these schists is defined by muscovite which occurs in long, foliated, ribbon-like masses separated by quartz-rich domains. The enclosed quartz augens (vein set 1) are both composed of single subhedral crystals (up to 5 mm) and polycrystalline aggregates. Large (up to 1 mm), subhedral to euhedral biotite crystals overprint muscovite and the S_1 foliation, and contain abundant monazite (?) crystals with pleochroic haloes.

In the biotite-Fe-dolomite-chlorite schists, the S_1 foliation is defined by biotite and chlorite which occur as foliated, fibrous masses. The rocks have a mylonitic texture. Large, poikilitic Fe-dolomite crystals contain inclusions of quartz and feldspar. Riebeckite is present in small amounts and occurs as small, felted masses scattered throughout the schist. In places, riebeckite occurs interstitially to poikilitic biotite crystals.

2.5.3. Sequence of Events for the Minto C Zone

Figure 18 shows a summary of major events and the paragenetic sequence of alteration and vein minerals for the Minto C zone. The first event was the emplacement of the first set of quartz veins (V_1) (Figure 18). The deformed nature of these veins requires a deformation event (D_1) following this veining event (Figure 18). This deformation was possibly penecontemporaneous with an alteration event (A_1) which produced the muscovite-rich and Fe-dolomite-chlorite-rich alteration assemblages in the granodiorite and mafic unit, respectively (Figure 18). The relationship of vein set 2 to the above alteration and veining events is not known (Figure 18). However, it may be possible that vein sets 1 and 2 are temporally related.

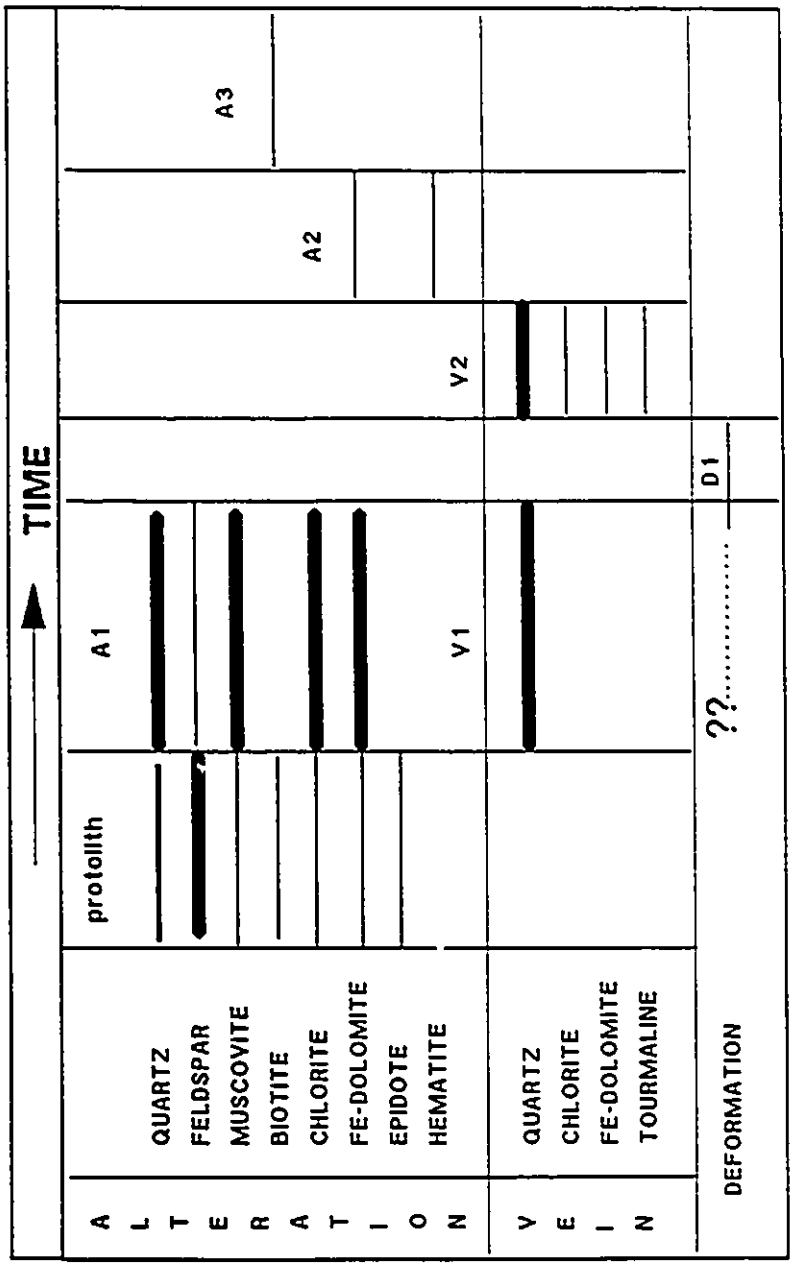

Figure 18. A summary of the paragenetic sequence of alteration and vein minerals in the Minto C zone. Variable thicknesses of lines indicate relative abundances of minerals. V1,2 = vein sets 1 and 2; A1,2,3 = Alteration events 1, 2 and 3; D1 = deformation event 1.

A mafic dike was emplaced after D_1. The hematized nature of this mafic dike requires a late hematitic alteration event (A_2) (Figure 18). A late biotitic alteration event (A_3) is manifested by the poikilitic biotite crystals which overprint the muscovite schists (Figure 18). Fenitization is possibly related to the late biotitic alteration as fibrous riebeckite crystals commonly occur interstitially to this biotite (Figure 18).

2.6. Minto E Zone

The Minto E zone comprises a narrow shear zone consisting of chlorite and muscovite schists which enclose abundant deformed and undeformed quartz veins (Samson and Holm, 1991). Two types of mafic dikes intrude the Minto E zone: one with no evidence of deformation and the other which is foliated and cut by the quartz veins. A few lamprophyre dikes are also present. These dikes cut the deformation zone and all of the quartz veins.

2.6.1. Veins

Planar, undeformed quartz veins occur in both mafic and felsic rocks outside the shear zone, some of which intersect and are deformed by the deformation zone. Some of the undeformed quartz veins contain massive chlorite and tourmaline. Within the mafic schists, there are abundant, deformed quartz-Fe-dolomite veins and veinlets.

2.6.2. Petrography of Host and Deformation-Zone Rocks

Host Rocks

Host rocks to the deformation zone comprise relatively undeformed medium-grained granodiorite, felsic and mafic crystal tuffs and mafic dikes. The granodiorite has very similar igneous and alteration mineral assemblages to those described from other deformation zones. Felsic crystal tuffs comprise albite and quartz phenocrysts in a fine-grained groundmass of quartz and feldspar. Felsic rocks do not show significant alteration except for minor amounts of chlorite, sericite and epidote which replace the feldspars. Mafic dikes are altered to a chlorite-epidote assemblage which partially pseudomorph plagioclase phenocrysts and replace feldspars in the groundmass. Epidote consists of both zoisite and clinozoisite, and occurs as disseminated granular masses. Chlorite occurs as massive, non-foliated masses which enclose relict plagioclase grains. Some relict hornblende (< 5%) also occurs as subhedral crystals replaced by chlorite.

Deformation-Zone Rocks

Rocks within the deformation zone consist of well-foliated felsic (quartz-chlorite-Fe-dolomite-muscovite) and mafic (epidote-Fe-dolomite-chlorite) schists.

Felsic Schists

Felsic schists consist of well-foliated quartz-chlorite-Fe-dolomite-muscovite schists which have a mylonitic texture. They contain abundant, disseminated, euhedral to subhedral pyrite crystals. Pressure shadows containing biotite occur around the pyrite. As in other zones, pyrite cubes are replaced by carbonate along fractures and grain margins.

Mafic Schists

Mafic crystal tuffs are pervasively altered to an epidote-Fe-dolomite-chlorite assemblage and are slightly deformed at the shear zone margins, as indicated by kinked, relict plagioclase and biotite phenocrysts. However, these rocks are transformed into strongly foliated epidote-Fe-dolomite-chlorite schists within the shear zone. The S_1 foliation is defined by chlorite, which occurs as well-foliated masses. These schists contain abundant, fine-grained, disseminated pyrite and enclose strongly deformed foliation-parallel quartz-Fe-dolomite veins. Minor amounts of riebeckite are present as fibrous, felted masses scattered throughout the schist.

2.6.3. Sequence of Events for the Minto E Zone

Figure 19 summarizes the major events and the paragenetic sequence for the Minto E zone. The earliest event appears to be the emplacement of quartz and quartz-chlorite-tourmaline-Fe-dolomite veins (V_1). This was followed by a deformation event (D_1) (Figure 19). The D_1 deformation was possibly accompanied by, or pre-dated by, an alteration event (A_1) which is represented by the chlorite-Fe-dolomite-muscovite assemblage in the granodiorite and felsic crystal tuffs, and by the epidote-Fe-dolomite-chlorite assemblage in the mafic crystal tuffs and mafic dikes (Figure 19). A late carbonate (ankerite ?) alteration (A_2) is indicated by fracture-related replacement veinlets within fractured pyrite crystals (Figure 19). Fenitization (A_3) took place at a later stage during the emplacement of the lamprophyre dikes into the zone (Figure 19).

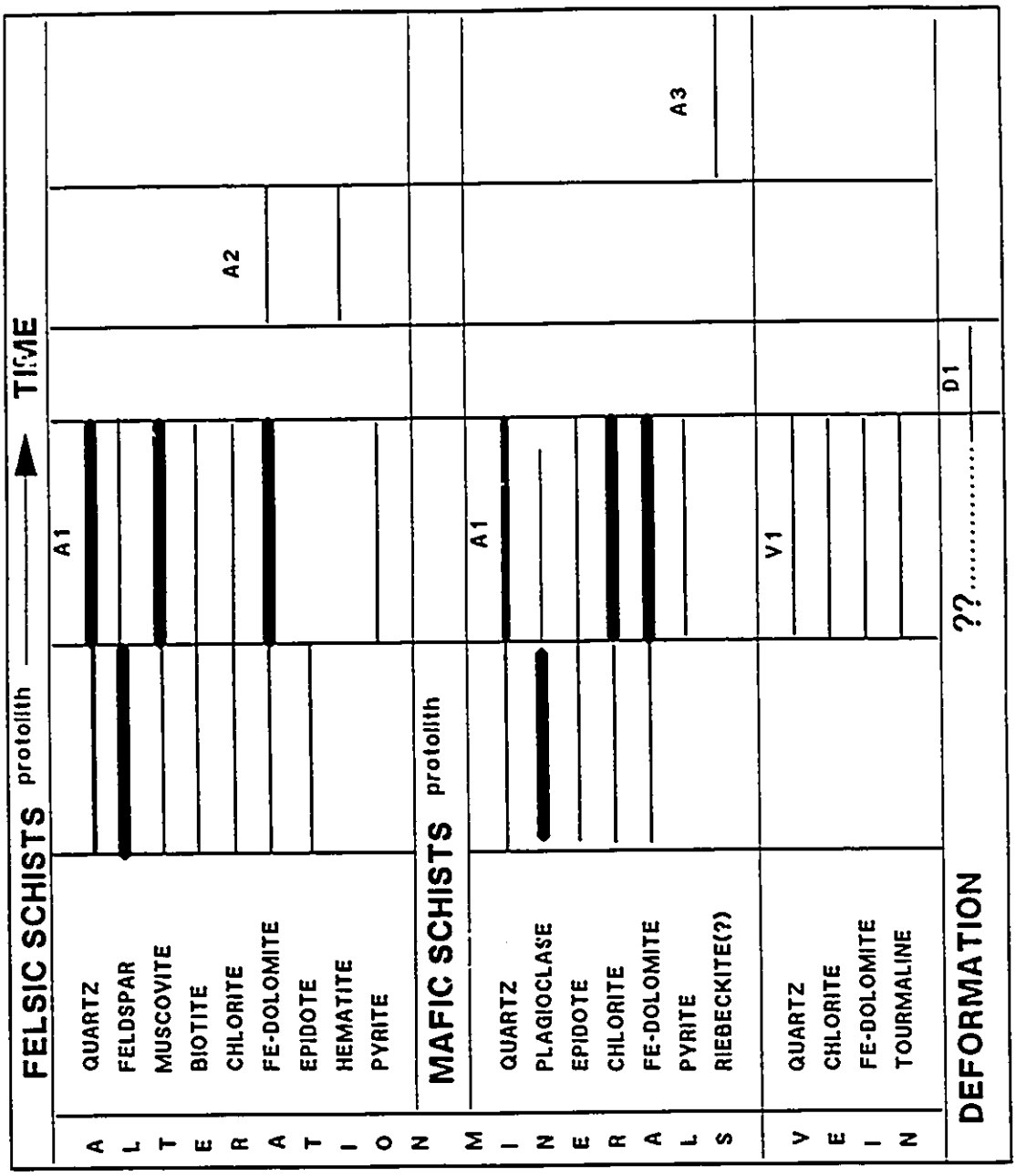

Figure 19. A summary of the paragenetic sequence of alteration and vein minerals in the Minto E zone. Variable thicknesses of lines indicate relative abundances of minerals. V1 = vein set 1; A1,2,3 = Alteration events 1 2 and 3; D1 = deformation event 1.

2.7. Discussion and Comparison of Hydrothermal Alteration

A comparative study of the hydrothermal fluid history of the deformation zones and the vein systems around Wawa has been partly accomplished through a detailed study of the petrographic characteristics of both host rocks and deformation-zone rocks, as described in the previous sections. The following is a summary of the field and petrographic observations.

2.7.1. Jubilee Shear Zone

A wide zone of well-foliated and altered, muscovite schists occurs in the Fat Vein zone. The host rocks include granodiorite and felsic crystal tuffs which are altered to a quartz-chlorite-Fe-dolomite-muscovite assemblage within the deformation zone. A restricted mafic schist unit comprises a chlorite-Fe-dolomite alteration assemblage. This early alteration event (A_1) in the Fat Vein zone involved the introduction of CO_2 and H_2O, as required by the carbonatization (Fe-dolomite) and hydration processes (chlorite and muscovite).

The early, vein-related hydrothermal alteration (A_1) in the Surluga Mine is represented by a quartz-Fe-dolomite-muscovite assemblage which contains abundant (up to 10 % by volume) sulphides and minor gold. There are also lesser amounts of tourmaline and chlorite. Sulphide mineralogy of the veins and the related hydrothermal alteration consists of pyrite, pyrrhotite and arsenopyrite. The alteration and vein assemblages in the Surluga Mine are similar to those in the Fat Vein zone. They differ in that they are richer in sulphides, and that they contain gold, arsenopyrite and tourmaline.

The emplacement of the second vein set (Pinto veins) was accompanied by a feldspathic (?) alteration (A_2) which is restricted to the immediate host rocks to these veins. This hydrothermal event most likely took place prior to, or during the second deformation event (D_2) as the veins cross-cut the early veins (vein set 1) and the S_1 foliation.

Two, temporally distinct, post-deformational alteration events followed A_1 and A_2. These are hematization and fracture-related ankeritic alteration (A_3) which are related to the emplacement of the Jubilee Breccia (V_3), and biotization and fenitization (A_4) which are interpreted to be related to the emplacement of lamprophyre dikes. The temporal relationship between A_3 and A_4 is not known.

2.7.2. Minto Zones

The Minto zones comprise felsic and mafic schists which represent variably altered and deformed protoliths of felsic and mafic composition, rather than fluids of different composition. This is indicated by the following:

1) the mineral assemblages observed in the partly altered mafic and felsic units are the same as those found in the mafic and felsic schists,

2) contacts between the interlayered mafic and felsic schists are generally sharp, which suggests original lithological layering, and

3) there is no evidence of overprinting of mafic and felsic mineral assemblages.

Felsic Schists

The early alteration (A_1) in felsic protoliths resulted in the following hydrothermal alteration assemblages:

1) Quartz-muscovite-Fe-dolomite-sulphides (Minto A)

2) Quartz-muscovite-chlorite-sulphides (Minto B)

3) Quartz-epidote-muscovite (Minto C)

4) Quartz-muscovite-Fe-dolomite-chlorite-sulphides (Minto E).

There are also small amounts of tourmaline in all these assemblages. The dominant alteration minerals are muscovite and Fe-dolomite. Chlorite is present in subordinate amounts, and epidote is significant only in the Minto C zone. The presence of epidote probably reflects a more Ca-rich, Fe-poor protolith composition. Fe-dolomite and sulphides are absent in the Minto C zone. Sulphides are far more abundant in the Minto B zone than the other Minto zones.

Mafic Schists

The early, hydrothermal alteration (A_1) assemblages in mafic protoliths comprise:

1) Chlorite-Fe-dolomite (Minto A)

2) Biotite-Fe-dolomite-chlorite-sulfides (Minto B)

3) Chlorite-Fe-dolomite-biotite-pyrite (Minto C)

4) Epidote-chlorite-Fe-dolomite-pyrite (Minto E)

The alteration assemblages developed in mafic protoliths in the Minto zones are dominated by chlorite and Fe-dolomite with the exception of the Minto B zone where biotite is abundant, and the Minto E zone where epidote is abundant. In the Minto B zone, biotite comprises more than 40% of the rock whereas in other Minto zones it is a relatively minor component. The similarities in hydrothermal alteration assemblages in

the Minto zones suggest that these spatially distinct deformation zones were infiltrated by similar H_2O-CO_2 fluids.

Veins

Pinto-Type Veins

The most abundant veins in the Minto zones are quartz ± chlorite ± tourmaline ± carbonate veins (Pinto veins). These veins represent different vein generations in different zones and are usually deformed when hosted by mafic schists, but relatively undeformed in felsic units. In the Minto A zone, these veins are represented by vein set 2 which consists of quartz ± Fe-dolomite ± chlorite stockworks. In the Minto B zone, they are represented by vein set 1 which comprises strongly-deformed quartz-alkali feldspar ± tourmaline ± chlorite ± Fe-dolomite veins in mafic schists. In the Minto B zone, some of these early veins have massive, chloritic alteration haloes. In felsic units outside the shear zone, planar, undeformed fibrous quartz ± chlorite veins occur and are probably of the same age as the deformed Pinto veins described above. The fibrous nature of these veins indicate their extensional origin. In the Minto C zone, Pinto veins are mainly represented by vein set 2 which comprises undeformed, branching quartz-chlorite-tourmaline-carbonate vein hosted by granodiorite, and possibly by highly deformed quartz veins belonging to vein set 1. In the Minto E zone, these veins are represented by abundant quartz ± chlorite ± tourmaline veins which occur both in and outside the deformation zone.

Quartz-Ankerite Veins

These veins consist of post-deformational (undeformed) quartz-ankerite veins which are commonly accompanied by a fracture-related ankeritic alteration. Such veins are represented by vein set 4 in the Minto A zone; vein set 2 in the Minto B zone, and are apparently absent in the Minto C and E zones.

Other Veins

In addition to these two major types of veins above, there are rare, planar quartz-alkali feldspar-chlorite veins with feldspathic alteration (V_1), and quartz-biotite veins (V_3) in the Minto A zone. The relationship of the latter to the deformation zone and other veins is not known.

2.7.3. Comparison of Hydrothermal Alteration in the Jubilee Shear Zone and the Minto Zones

Felsic schists in the Jubilee shear zone, and in the Minto zones have very similar alteration assemblages (Figure 20). However, felsic alteration assemblages in the Minto zones contain more sulphides than those in the Fat Vein zone, but less than those in the Surluga Mine. In comparison with the felsic alteration assemblages in the Surluga Mine, sulphides in the felsic schists in the Minto zones consist mainly of pyrite and do not contain visible gold or arsenopyrite and pyrrhotite. In both the Jubilee shear zone and the Minto zones, felsic schists generally contain more sulphides than mafic schists. The lack of significant amounts of sulphides within the mafic schists is not consistent with the common suggestion (Colvine et al., 1988) that sulphidation of wallrock Fe occurs more readily in mafic protoliths than in felsic protoliths. Sulphide precipitation, therefore cannot be explained by a simple sulphidation process driven by protolith composition, as felsic rocks have a lower Fe content than the mafic rocks. Thus, some other mechanism for the precipitation of Fe-sulphides (pyrite and pyrrhotite) must be considered.

Mafic schists in the Fat vein zone, and in the Minto Zones have very similar alteration assemblages (Figure 21), with the exception of the presence of biotite and epidote in the Minto B and E zones, respectively. In addition, alteration assemblages in mafic rocks in the Minto zones have minor amounts of pyrite and chalcopyrite, whereas those in the Fat Vein zone do not. Deformed quartz veins in the mafic schists in the Minto B zone have chloritic ($\pm$ tourmaline) alteration haloes, whereas the quartz veins present in any other zones lack such alteration haloes.

The presence of chlorite-Fe-dolomite and muscovite-Fe-dolomite alteration assemblages in the mafic and felsic schists (Figures 20 and 21) requires that a H_2O-CO_2 fluid caused the alteration. This early alteration event involved the addition of CO_2, H_2O, S, B, Au and As to the deformation-zone rocks, as indicated by the formation of hydrous minerals (H_2O), carbonate (CO_2), sulphides (S, As) and tourmaline (B). The Jubilee shear zone and the Minto zones also display later alteration effects. These are hematization and fracture-related ankeritic alteration (A_3), and biotitic alteration accompanied by riebeckite (fenitization) (A_4) (Figures 20 and 21).

From the above comparison of the alteration assemblages in the Jubilee and the Minto zones, it is clear that an H_2O-CO_2 fluid caused the early alteration event (A_1) in these separate deformation zones and vein systems, prior to, or penecontemporaneously with, the D_1 deformation. The late ankeritic alteration (A_3) was

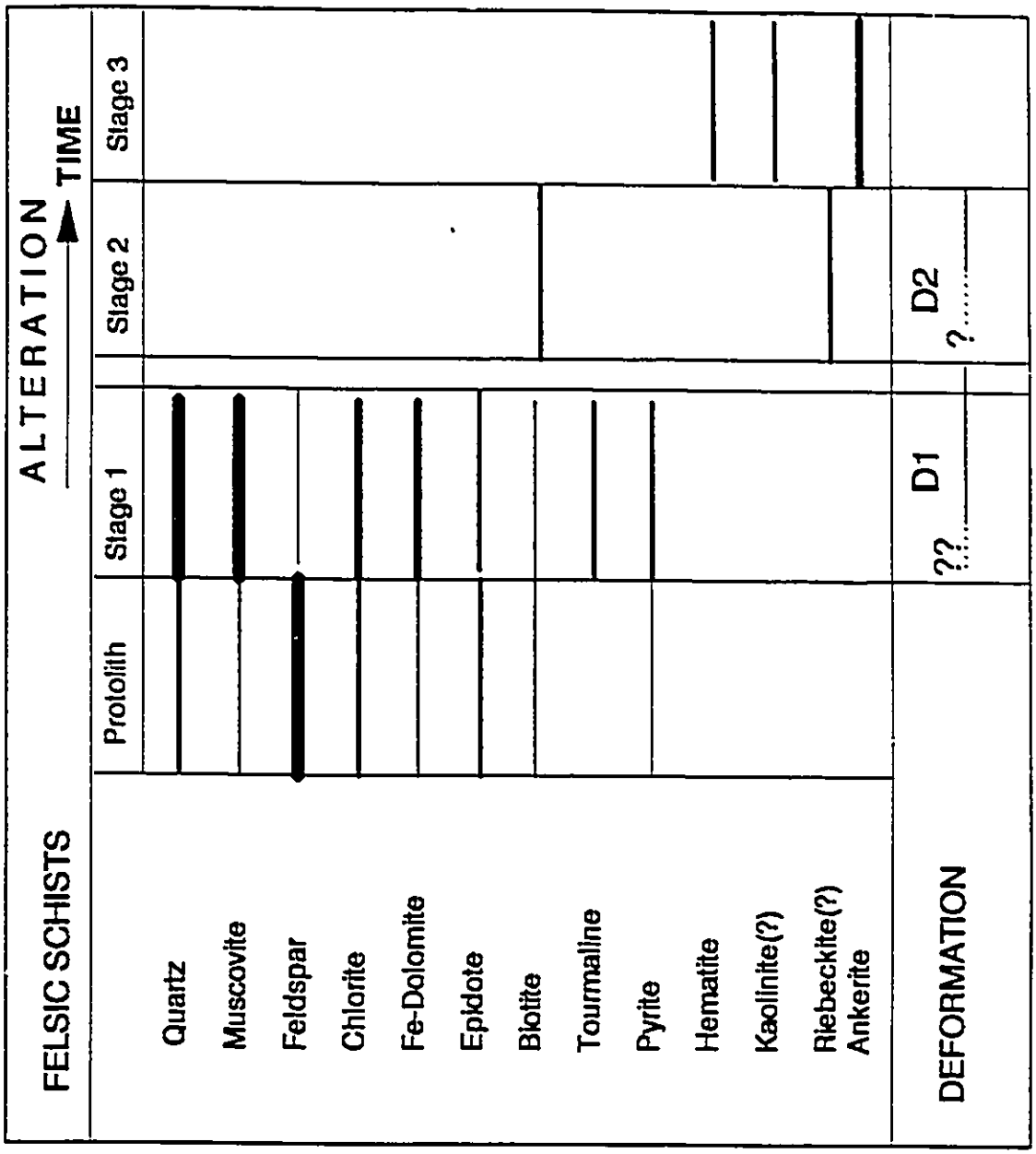

Figure 20. A summary of the paragenetic sequence of alteration mineral assemblages in felsic schists from the Jubilee and Minto deformation zones. Variable thicknesses of lines indicate relative abundances of minerals. D1, 2 = deformation events 1 and 2, respectively.

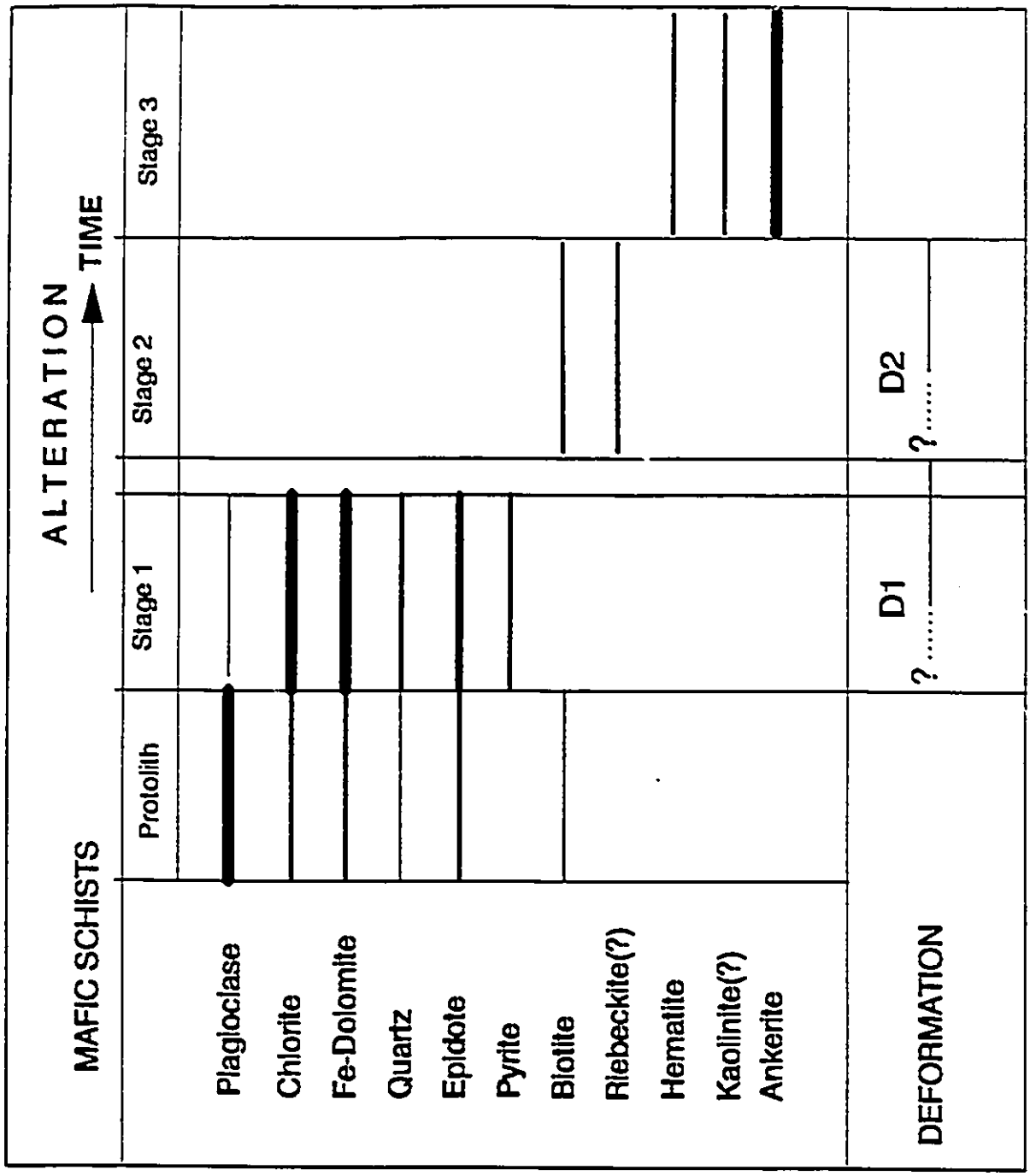

Figure 21. A summary of the paragenetic sequence of alteration mineral assemblages in mafic schists from the Jubilee and Minto deformation zones. Variable thicknesses of lines indicate relative abundances of minerals. D1, 2 = deformation events 1 and 2, respectively.

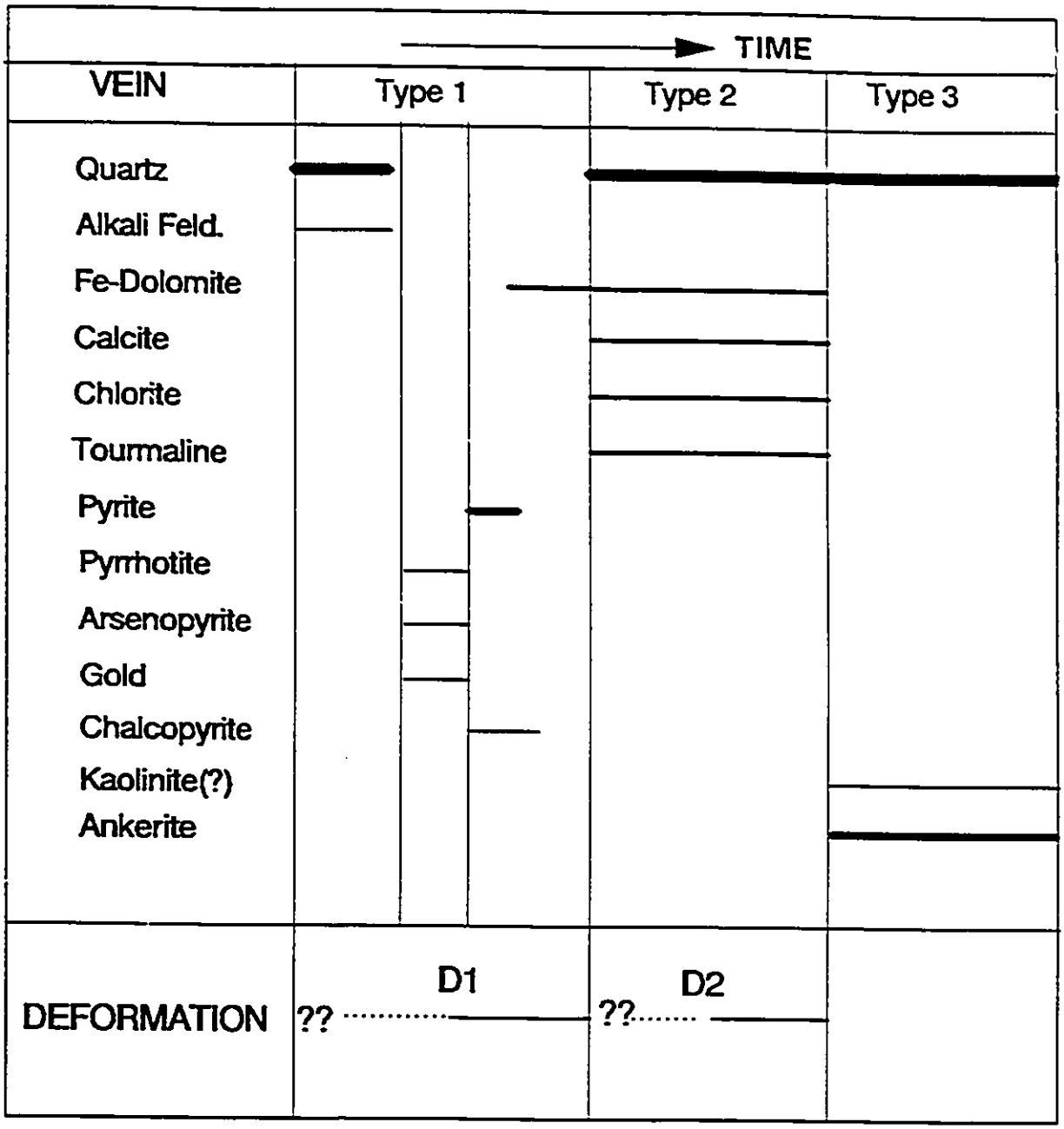

Figure 22. A summary of the paragenetic sequence of vein assemblages in the Jubilee and Minto deformation zones. Variable thicknesses of lines indicate relative abundances of minerals. D1, 2 = deformation events 1 and 2, respectively.

also caused by an aqueous-carbonic fluid which infiltrated the deformation zones after the D_1 and D_2 deformation events (Figures 20 and 21).

The presence of similar hydrothermal alteration assemblages in the studied deformation zones/vein systems strongly suggests that the smaller deformation zones in the hanging wall of the Jubilee Shear have recorded the effects of the same hydrothermal events which took place in the main shear zone. In this regard, these zones would be expected to have comparable fluid histories, a question which will be explored in Chapter 3 on fluid inclusions.

2.7.4. Comparison of Vein Types in the Jubilee Shear Zone and the Minto Zones

Three, distinct types of veins are recognized in the deformation zones at Wawa (Figure 22). The first type consists of the earliest set of veins which are represented by quartz-Fe-dolomite-alkali feldspar-sulphide veins in the Fat Vein zone, the auriferous quartz-Fe-dolomite-alkali feldspar-tourmaline-chlorite-sulphide veins in the Surluga Mine, and by quartz-alkali feldspar ± chlorite veins in the Minto A zone. The earliest veins in the Fat Vein zone and in the Surluga Mine display similar field relationships with respect to the Jubilee shear zone, but differ in that the latter veins contain tourmaline, chlorite, pyrrhotite, arsenopyrite and minor amounts of free gold. This type of mineralized veins is absent from the Minto zones.

The second vein type is the Pinto-type veins which occur in all deformation zones (Figure 22). These veins are represented by quartz ± chlorite ± tourmaline ± calcite veins in the Jubilee shear zone and by quartz-Fe-dolomite ± chlorite ± alkali feldspar ± tourmaline veins in the Minto zones. Some of the Minto zones (e.g., Minto C and E zones) consist exclusively of the Pinto-type veins. The Pinto Veins in all deformation zones are barren of sulphides and gold. These veins are relatively undeformed in the Jubilee shear zone, but are strongly deformed where hosted by mafic schists in the Minto zones. They are planar and undeformed in felsic units in the Minto zones.

The third vein type comprises undeformed, planar quartz-ankerite veins and breccia zones (Figure 22) in the Jubilee shear zone, and by quartz-ankerite veins in the Minto A and B zones. Quartz-ankerite veins are absent in the Minto C and E zones. Late, kaolinite (?) and ankerite (?) veinlets are also considered to be genetically related to these veins.

In addition to the three types of veins classified above, a single quartz-biotite vein (V_3) was observed in the Minto A zone (not shown in Figure 22). Its relationship to the other vein sets and to the deformation zones is not known.

CHAPTER III
FLUID INCLUSIONS

3.1. Introduction

All of the fluid inclusions described and measured are hosted by quartz. Six types of fluid inclusions are present in the quartz veins from Wawa. The types are distinguished on the basis of their phase ratios at room temperature, their cooling behavior down to about -25°C, and their behavior under slight heating (up to 31°C). Only inclusion sets with apparently consistent phase ratios at room temperature were selected for microthermometric and Raman spectroscopic analyses. The five dominant types are illustrated in Figure 23. The six inclusion types are:

1. Two-phase, liquid-vapour (LV) aqueous inclusions (Figure 23) that homogenize to the liquid phase. The vapour phase occupies 20-35% of the total inclusion volume.

2. Aqueous, liquid-vapor-solid inclusions (LVN). These inclusions contain a generally large (2-10 μm, 40% of inclusion volume) subhedral to euhedral, prismatic, highly birefrengent solid, identified as nahcolite (N) (see below) (Figure 23). These inclusions are sometimes associated with LV inclusions, in which case the latter probably represents part of a necked LVN inclusion.

3. One- or two-phase, liquid-rich inclusions (L $\pm$ N). These are commonly associated with LV inclusions and either represent the same fluid, but where a vapour bubble has failed to nucleate, or part of a necked inclusion. Where they are associated with LVN inclusions, they contain a solid similiar to that in LVN inclusions and thus, are clearly part of a necked inclusion.

4. Two- or three-phase, aqueous-carbonic inclusions (liquid-rich) (Figure 23). These inclusions usually occur in one of two ways:

a) as two-phase inclusions (LC) which resemble LV inclusions at room temperature. They are different from LV in that they nucleate a vapor phase inside the "vapor bubble" upon cooling down to -15°C (Figure 23);

b) as three-phase inclusions (LCV and LCVN) with a two-phase carbonic fluid at room temperature. In many cases, these inclusions contain a prismatic, birefrengent daughter mineral, identified as nahcolite, and are occasionally observed on the same planes together with LVN inclusions (Figure 23).

5. Two-phase, liquid-vapor (liquid-rich) carbonic inclusions (CV) (Figure 23) that homogenize to the liquid phase and commonly occur as negative crystals. They frequently occur in the same arrays together with with LVN and LCV(N) inclusions.

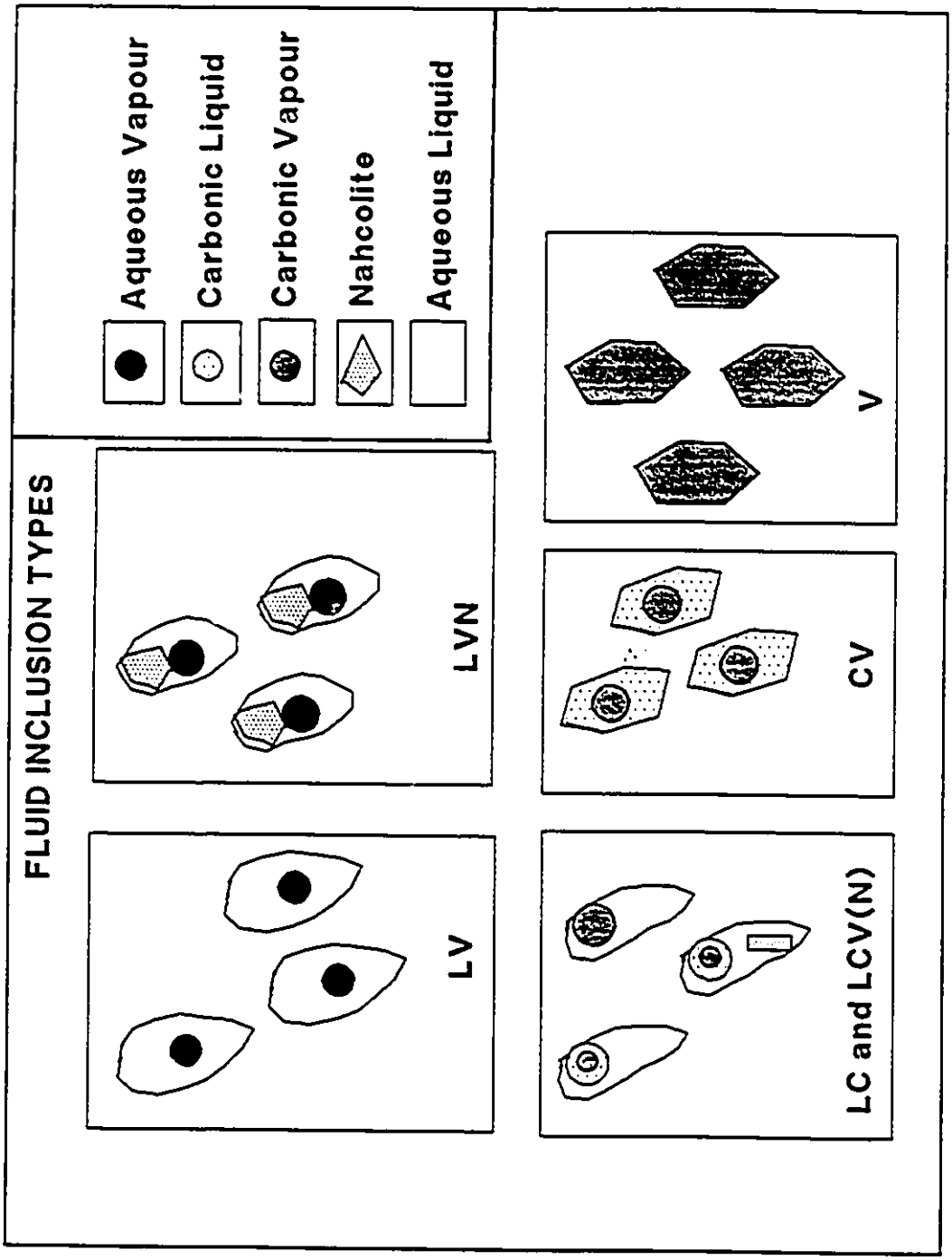

Figure 23. Major types of fluid inclusions present in quartz veins from Wawa.

In the latter case, they probably represent part of a necked inclusion.

6. One-phase vapor-rich inclusions with negative crystal shapes (V) (Figure 23). Rarely, these inclusions contain small birefrengent solids, identified as carbonate (see below) and may have tiny rims of aqueous liquid.

The fluid inclusion results will be presented and discussed in terms of the vein classification described at the end of Chapter 2:

Vein Set 1: Quartz-Fe-dolomite-alkali feldspar ± chlorite ± tourmaline ± sulphide ± gold veins,

Vein Set 2: Quartz ± chlorite ± tourmaline ± carbonate veins (Pinto Veins), and

Vein Set 3: Quartz-ankerite veins (Jubilee Breccia-type veins).

Results from fluid inclusions in the quartz-biotite vein from Minto A are plotted with vein set 3.

3.2. Nature of Fluid Inclusion Arrays

Tables 3, 4, 5 and 6 contain a summary of the characteristics of fluid inclusion arrays. Fluid inclusions occur in three different ways: 1) as transcrystalline planar arrays which cross-cut crystal boundaries, 2) as isolated, intracrystalline planar arrays within growth zones, and 3) as isolated inclusions or short intracrystalline planes.

3.2.1. Primary Inclusions

Only those inclusions that occur in growth zones in quartz from the Jubilee breccias in the Fat Vein zone are interpreted to be primary in origin (Roedder, 1984). They occur as short, isolated planar arrays. These growth zones consist exclusively of LC inclusions (Table 5).

3.2.2. Pseudosecondary Inclusions

Large (> 15 μm), LV inclusions in vein set 3 from both Fat Vein zone and the Surluga Mine, which occur on short, intracrystalline planes in a single crystal, and which are quite rare, are interpreted as pseudosecondary in origin (Table 3). In some samples, large, apparently isolated inclusions occur within a single crystal and may be primary or pseudosecondary in origin.

3.2.3. Secondary Inclusions

Most of the fluid inclusions observed in the quartz veins occur in planar arrays that

Table 3. Summary of characteristics of LV fluid inclusion arrays

DEFORMATION ZONE/VEINSET	CHARACTERISTICS OF LV FLUID INCLUSION ARRAYS
Fat Vein Zone - Vein set 1 quartz	secondary planes, associated with L ± N inclusions (necking), consistent liquid/vapour ratios
Fat Vein Zone - Vein set 3 growth-zoned quartz	large, isolated inclusions (rare) planes of same type of inclusions
Surluga Mine - Vein set 1 quartz	dense planar arrays, randomly-oriented, commonly occuring together with V inclusions
Surluga Mine - Vein set 2 quartz	long planes/trails cross-cutting grain boundaries consistent liquid/vapour ratios,
Surluga Mine - Vein set 3 quartz	large (~20 μm), isolated inclusions some contain trapped carbonate
Minto A Zone - Vein set 2 quartz	small inclusions in isolated planar arrays consistent liquid/vapour ratios,
Minto A Zone - Vein set 3 quartz	isolated short planes or 3-D arrays, some arrays contain small, birefrengent trapped (?) solids
Minto B Zone - Vein set 2 quartz	planar arrays of large (10-20 μm) inclusions consistent liquid/vapour ratios,
Minto E Zone quartz	randomly-oriented, dense planar arrays

Table 4. Summary of characteristics of LVN fluid inclusion arrays

DEFORMATION ZONE/VEINSET	CHARACTERISTICS OF LVN FLUID INCLUSION ARRAYS
Fat Vein Zone - Vein set 1 quartz	planar arrays of variable extent and density
Surluga Mine - Vein set 1 quartz	large (10-40 μm) inclusions on planes some are associated with LCV(N) inclusions
Surluga Mine - Vein set 2 quartz	large (10-50 μm) inclusions in dense planar arrays LCV(N) and CV inclusions usually dispersed among them
Minto A Zone - Vein set 2 quartz	long planar arrays cross-cutting grain boundaries
Minto A Zone - Vein set 3 quartz	planar arrays, associated with similiar planes containing small (1-5 μm) birefrengent solids
Minto B Zone - Vein set 2 quartz	planar arrays of large (10-25 μm) inclusions lots of necking, occasionally associated with trails of similiar solids in the host
Minto E Zone quartz	planar arrays with large (10-50 μm) inclusions usually associated with LCVN inclusions with similiar solids, abundant necking

Table 5. Summary of characteristics of LC and LCV(N) fluid inclusion arrays

DEFORMATION ZONE/VEINSET	LC AND LCV(N) FLUID INCLUSION ARRAYS
Fat Vein Zone - Vein set 1 quartz	large (~20 μm) isolated (?) inclusions and/or clusters
Fat Vein Zone- Vein set 3 growth-zoned quartz	isolated planar arrays containing usually small (2-15 μm) inclusions a large (~25 μm) inclusion is surrounded by an array of very small (2-5 μm) inclusions
Surluga Mine - Vein set 1 quartz	planar arrays cross-cutting grain-boundaries containing large (10-30 μm) inclusions with birefrengent solid
Surluga Mine - Vein set 2 quartz	generally small (5-10 μm) inclusions in dense planar arrays, abundant necking
Surluga Mine - Vein set 3 quartz	very small (1-5 μm) inclusions in isolated clusters, rarely contain a very small biref. solid
Minto A Zone- Vein set 2 quartz	planar arrays, contain a small rhombic to prismatic birefrengent solid, some on long, steep planes and prismatic in shape
Minto B Zone - Vein set 2 quartz fibrous vein with chlorite	planar arrays cross-cutting grain-boundaries, small (3-10 μm) inclusions
Minto B Zone - Vein set 2 quartz planar quartz-ankerite vein	long planar arrays of large (10-30 μm) inclusions with a birefrengent prismatic solid
Minto E Zone quartz	densely stacked planar arrays of large (10-40 μm) inclusions with variable liquid/vapour ratios commonly with prismatic, birefrengent solid

Table 6. Summary of characteristics of CV and V fluid inclusion arrays

DEFORMATION ZONE/VEINSET	CHARACTERISTICS OF CV FLUID INCLUSION ARRAYS
Surluga Mine - Vein set 2 Pinto quartz	generally small (1-10 μm) equant inclusions with negative crystal shapes in dense planar arrays
Surluga Mine - Vein set 3 quartz	very small (≤ 5 μm) isolated inclusions with negative crystal shapes;
Minto E Zone quartz	planar arrays of inclusions with negative crystal shapes
	CHARACTERISTICS OF V FLUID INCLUSION ARRAYS
Surluga Mine - Vein set 1 Au-bearing quartz	large (10-50 μm) inclusions in planar arrays restricted to a single crystal as well as long trails cross-cutting grain boundaries. There may have tiny rims of aqueous liquid, necked ?; usually negative crystals but also irregular
Minto B Zone - Vein set 2 quartz	small equant inclusions with negative crystal shapes
Minto E Zone quartz	dense planar arrays cross-cutting grain-boundaries large (10-30 μm) inclusions with negative crystal shapes, also contain tiny rims of aqueous liquid some inclusions in an array contain very small (≤ 2 μm) birefrengent solid

cross-cut grain-boundaries, and are therefore secondary in origin (Roedder, 1984). All types of fluid inclusions occur within such secondary planar arrays. But LVN, CV and V inclusions occur exclusively on such secondary planes (Tables 4 and 6).

Due to the high density of secondary planes in a given sample and a lack of any clear cross-cutting relationships between planes, it is impossible to establish any age relationships between those planes, and thus, to establish a fluid-inclusion chronology within a single sample.

3.3. Fluid Inclusion Compositions

3.3.1. Analytical Methods

Microthermometric measurements were carried out using a Linkam TH-600 heating-freezing stage calibrated with a variety of organic and inorganic calibration liquids and solids. The accuracy of measured temperatures range from $< \pm 0.3°$ below 0° to $\pm$ 4°C at 300°C. All microthermometric results are reported as the average value (ave) for a co-genetic group, along with the standard deviation (sd) for that group. Data points on diagrams also represent average values, and error bars represent the standard deviation for a group.

Raman spectroscopic data were collected at the University of Windsor on a Ramanor U-1000 spectrometer, fitted with a Spectra Physics Ar ion laser (514.5 nm green line) and a Nachet microscope (80X objective). Counting times were 1 second at spectral stepping intervals of 1 cm^{-1} over a spectral range of 0 to 1500 cm^{-1} for mineral analysis, and were 10 seconds at spectral stepping intervals of 0.5 cm^{-1} over the appropriate spectral range for each gas during volatile analysis. The details of Raman spectroscopic analysis are described in Wopenka and Pasteris (1987). Raman spectroscopy was principally utilized for further characterizing the composition of the non-aqueous portion of LC, LCV(N), CV and V inclusions. It was also used to identify solid phases in fluid inclusions and solid inclusions in quartz. Inclusions that were large enough ($\geq$ 10 μm in most cases) and which yielded $TmCO_2$ values significantly lower than -56°C were scanned for CO_2, CH_4 and N_2. In some cases H_2S was also analyzed for but was not detected. Inclusions containing a two-phase (liquid-vapour) carbonic fluid at room temperature were homogenized by heating the wafer chip to a temperature of 35°C on the fluid inclusion stage during the entire Raman analysis. This was done in order to obtain the bulk composition of the carbonic fluid as preferential partitioning of CH_4 and N_2 into the vapor phase would result in inaccurate peak intensities at room temperature, and hence in erroneous estimates of the molar proportions of the volatile species.

3.3.2. Calculation of Fluid Inclusion Compositions

All fluid inclusion types were initially analyzed using microthermometric methods in order to obtain semi-quantitative data on fluid composition (at low temperatures) and density (at high temperatures). The fluid inclusion types which contain a carbonic fluid phase (i.e., LC, LCV (N), CV and V) were also analyzed using Raman spectroscopy in order to determine quantitatively the composition of the carbonic fluid (see below). Composition (salinity) of the aqueous, LV and LVN inclusions was calculated using Potter et al.'s (1978) regression equation for salt solutions:

$$\text{Wt.\% NaCl} = 1.7698.D - 4.2384\times10^{-2}.D^2 + 5.2778\times10^{-4}.D^3 \quad (1)$$

where D is the final melting temperature of ice (TmICE). Salinity of the aqueous portion of the aqueous-carbonic fluid inclusions was calculated using Bozzo et al.'s (1973) salinity formula based on clathrate-melting temperature:

$$W_{NaCl} = 15.52022 - 1.02342.t - 0.05286.t^2 \quad (2)$$

where t = clathrate melting temperature in °C (TmCLATH, see Table 7 for definition of symbols), and W_{NaCl} = weight percent NaCl relative to H_2O.

The relative proportions of the volatile species in the carbonic fluid phase in CO_2-rich inclusions was derived from peak areas of these species. The peak areas were calculated from four co-added spectra, using standard numerical integration methods and are related to relative concentration through the following equation (Table 7):

$$C_a/C_b = (A_a/A_b) \cdot (F_a/F_b) \quad (3)$$

(Pasteris et al., 1988). The Raman quantification factors (F) represent a combination of the gas-specific scattering efficiencies and instrumental efficiency factors and, in addition, are dependent on the density (internal pressure) of the inclusion fluid (Pasteris et al., 1988; Wopenka and Pasteris, 1987). Low-density quantification factors were calculated by Wopenka and Pasteris (1987) for their Ramanor U-1000 instrument. These factors are 1.52 for CO_2 (1388 cm^{-1}) and 6.70 for CH_4 (2918 cm^{-1}), both values relative to N_2 (2329 cm^{-1}). Samson and Williams-Jones (1991) have checked the validity of these F-factors to calculate peak areas measured on the instrument at the University of Windsor by analyzing CO_2-N_2-O_2 gas standards. They concluded that calculated compositions are within 1 to 3% of the compositions calculated by Wopenka and Pasteris (1987) and thus using their factors is appropriate.

For CV and V inclusions, mole fractions of volatile species were calculated using Equation (3). For LC and LCV(N) inclusions the following equations were used:

$$nH_2O = (V_l.d_l)/(MW_l) \quad (4)$$

$$nCO_2 = [(V_v.ZCO_2)/\bar{V}_v] + [nH_2O.Z'CO_2] \cdot \quad (5)$$

Table 7. List of abbreviations used in the text

Microthermometry

Tf = Temperature of total freezing of inclusion contents

TfC = Temperature of freezing of non-aqueous portion of inclusion

TfH = Temperature of freezing of aqueous portion of inclusion

Te = Temperature of eutectic melting of ice and/or dry ice

TmICE = Temperature of ice melting

SAL = Salinity of aqueous liquid

TdV = Temperature of disappearance of vapour phase

TdDM = Temperature of dissolution of daughter mineral

$TmCO_2$ = Temperature of solid CO_2 (dry ice) melting

TmCLATH = Temperature of clathrate melting

ThC* = Temperature of homogenization of non-aqueous portion of LCV(N) inclusion in the presence of clathrate

ThC = Temperature of homogenization of CV and V inclusions, and of non-aqueous portion of LCV(N) inclusion in the absence of clathrate

ThTOT = Temperature of total homogenization of LC and LCV(N) inclusions

TD = Temperature of decrepitation of inclusion

Raman Spectroscopy

ni = Number of moles of species i in inclusion

Xi = Mole fraction of species i in inclusion

Zi = Mole fraction of species i in non-aqueous part of LC and LCV(N) inclusions

Z'i = Mole fraction of species i in aqueous part of LC and LCV(N) inclusions

Vl = Volume of aqueous part of LC and LCV(N) inclusions

Vv = Volume of non-aqueous part of LC and LCV(N) inclusions

dl = density of aqueous part of LC and LCV(N) inclusions

MWl = Molecular weight of aqueous part of inclusion

$\bar{V}v$ = Molar volume of non-aqueous part of LC and LCV(N) inclusions

C_a/C_b = molar ratio of species a and b

Ai = Raman peak area for species i

Fi = Raman quantification factor for species i

$$nCH_4 = (V_v.ZCH_4)/\bar{V}_v \quad (6)$$

$$nN_2 = (V_v.ZN_2)/\bar{V}_v \quad (7)$$

$$X_i = n_i/\Sigma n \quad (8)$$

(Samson and Williams-Jones, 1991).

A value of 0.025 was used for $Z'CO_2$ (Ellis and Golding, 1963). The density of the aqueous phase was calculated using a regression equation for the density of salt solutions (Potter and Brown, 1977):

$$dH_2O = (1{,}000.d_o + M_2.m.d_o)/(1{,}000 + A_o.m.d_o + B_o.m^{3/2}.d_o + C_o.m^2.d_o) \quad (9)$$

where d_o = density of water at 40°C in gcm^{-3} = 0.99164, M_2 = molecular weight of NaCl, m = molality of NaCl, A_o = 17.45, B_o = 1.71, and C_o = 0.040. The m value is calculated using Equation (2).

The volumes of the aqueous part of an inclusion (V_l) and of the non-aqueous part (V_v) were calculated from area ratios of liquid and vapor (measured with a planimeter from precise drawings made with a drawing tube). For flat inclusions, area ratios were assumed to be equal to volume ratios. For inclusions with a spherical or semi-spherical vapor phase, volumes were calculated taking the vapor-bubble diameter as the third dimension.

The XCH_4 and XN_2 values for H_2O-CO_2-CH_4-N_2 inclusions which did not show clathrate formation during microthermometry were calculated using the XCH_4-$\bar{V}$ projection of Heyen et al. (1982). In very few cases when calculating molar volumes and bulk compositions of the vapor phase in H_2O-CO_2-CH_4 inclusions which yielded clathrate melting data, a projection method developed by Seitz et al. (1987) was utililized. The details of the projection method are given in Seitz et al. (1987). However, this method has the limitation (Seitz et al., 1987) that the carbonic phases must homogenize to either liquid or vapor between the temperatures at which clathrate nucleates and melts. Therefore, the composition of LCV(N) inclusions with ThC values greater than TmCLATH values can not be interpreted using this method. Because most LCV(N) inclusions from Wawa have ThC values much greater than TmCLATH, molar volumes were calculated from ThC and Raman-derived ZCH_4 using the XCH_4-$\bar{V}$ projection of Heyen et al. (1982). Molar volumes of those inclusions which yielded a ZCO_2 value of 1 from Raman analyses were calculated using the program FLINCOR (Brown, 1989), and the equation of state of Bottinga and Richet (1981).

3.3.3. LV Inclusions

Petrographic characteristics of LV inclusion arrays are given in Table 3. The LV inclusions occur in three ways: 1) as dense, randomly-oriented, planar arrays that cross-cut grain-boundaries (Figure 24); 2) as large (> 10 μm), isolated inclusions; and 3) as short, planar arrays or 3-D clusters within a single crystal. Those inclusions which occur in the third mode are restricted to the third vein sets (Jubilee Breccia) from the Fat Vein zone and the Surluga mine (Table 3).

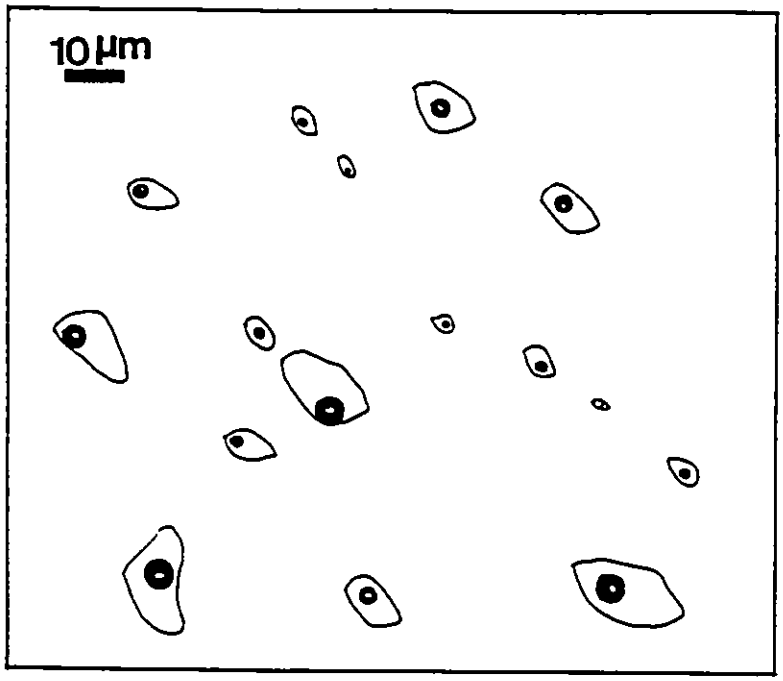

Figure 24. Precise drawing of LV inclusions on secondary planes in quartz in vein set 2 from the Surluga Mine.

Microthermometric Results

Table 8 contains a summary of all the microthermometric results obtained on LV inclusions.

Eutectic melting temperatures (Te) of LV inclusions ranged from -31 to -13°C (Table 8). Temperatures of the final melting of ice (TmICE) ranged from -21 to nearly 0°C (Figure 25 A, B and C).

LV inclusions homogenize to the liquid phase at temperatures of between 93 and

Table 8. Summary of Microthermometry Data for LV Fluid Inclusions

SAMPLE #	MIN	SET	TYPE	OR	#	Tf	Te		TmICE		SAL	TdV		TD	
							ave	sd	ave	sd		ave	sd	ave	sd
FAT VEIN - VEIN SET 1															
IS90-4	CQ	1	LV	S	4	-37	-	-	-0.1	0.0	0	281	11	-	-
IS90-4	CQ	2	LV	S	2	-37	-	-	-1.3	0.1	2	273	1	-	-
IS90-4	CQ	3	LV	S	3	-35	-	-	-0.8	0.0	2	256	0	-	-
IS90-4	CQ	4	LV	S	2	-32	-	-	-0.3	0.0	1	245	7	-	-
MINTO B - VEIN SET 2															
IS90-43	FQ	1	LV	S	3	-54	-21.0	0.0	-7.6	0.1	11	147	8	-	-
IS90-43	FQ	2	LV	S	2	-52	-20.0	0.0	-7.9	0.1	12	157	2	-	-
IS90-43	FQ	3	LV	S	5	-61	-24.0	0.3	-13.5	0.3	17	163	3	-	-
MINTO E															
IS90-53b	CQ	1	LV	S	4	-40	-	-	-6.8	1.3	10	153	19	-	-
IS90-53a	CQ	2	LV	S	6	-36	-21.0	1.1	-6.5	1.0	10	158	40	-	-
SURLUGA MINE - VEIN SET 1															
IS89-65	CQ	1	LV	S	4	-48	-31.0	0.0	-21.0	0.1	23	192	9	-	-
IS89-65	CQ	2	LV	S	3	-46	-27.0	0.2	-18.0	0.0	21	196	10	-	-
IS89-70B	CQ	3	LV	S	5	-45	-22.0	0.0	-14.0	0.0	18	191	3	-	-
IS89-70A	CQ	4	LV	S	3	-48	-31.0	0.2	-18.4	1.2	22	180	8	296	64
IS89-70A	CQ	5	LV	S	4	-46	-29.0	0.8	-18.6	0.8	22	169	2	291	18
IS89-70A	CQ	6	LV	S	11	-	-30.0	0.0	-17.0	0.1	21	277	5	316	65
IS89-70A	CQ	7	LV	S	13	-49	-30.0	0.0	-16.5	0.0	20	236	12	282	29
IS89-70A	CQ	8	LV	S	6	-54	-28.0	0.4	-16.7	0.5	20	242	40	210	27
IS89-70A	CQ	9	LV	S	4	-48	-28.0	0.2	-15.2	0.8	19	207	4	-	-
IS89-70A	CQ	10	LV	S	6	-45	-24.0	0.0	-13.5	0.1	18	199	4	-	-
S280-613	CQ	11	LV	S	4	-52	-31.0	0.0	-16.0	0.0	20	203	3	-	-
S280-613	CQ	12	LV	S	4	-51	-23.0	0.0	-17.5	0.0	21	186	3	-	-
MINTO A - VEIN SET 2															
IS89-54	FQ	1	LV	S	6	-56	-22.0	0.0	-13.0	0.4	17	197	16	-	-
IS89-54	FQ	2	LV	S	6	-49	-23.0	0.0	-13.0	0.4	17	190	8	-	-
IS89-54	FQ	3	LV	S	4	-46	-21.0	0.1	-14.0	0.5	18	186	11	-	-
IS89-54	FQ	4	LV	S	6	-45	-23.0	0.2	-12.8	0.6	16	198	10	-	-
IS89-54	FQ	5	LV	S	3	-43	-20.0	0.2	-13.2	0.3	17	213	13	-	-
IS89-54	FQ	6	LV	S	8	-45	-22.0	0.5	-13.4	0.6	17	197	8	-	-

Table 8 (Continued)

SAMPLE #	MIN	SET	TYPE	ORI	#	Tf	Te ave	Te sd	TmICE ave	TmICE sd	SAL	TdV ave	TdV sd	TD ave	TD sd
SURLUGA MINE - VEIN SET 2															
IS89-63	CQ	1	LV	S	6	-46	-22.0	1.2	-10.8	1.9	15	142	15	-	-
IS89-63	CQ	2	LV	S	12	-45	-19.0	0.0	-11.5	0.0	16	93	6	-	-
IS89-63	CQ	3	LV	S	5	-43	-20.0	0.0	-11.6	0.0	16	128	0	-	-
IS89-64	CQ	4	LV	S	5	-42	-	-	-7.5	0.4	11	118	5	-	-
IS89-64	CQ	5	LV	S	8	-41	-21.0	0.2	-11.9	0.6	16	188	19	-	-
IS89-64	CQ	6	LV	S	8	-48	-22.0	0.8	-8.5	0.9	12	140	4	-	-
IS89-64	CQ	7	LV	S	4	-37	-22.0	0.0	-6.1	0.3	10	109	6	-	-
IS89-64	CQ	12	LV	S	5	-55	-25.0	1.1	-12.7	1.2	17	209	16	-	-
IS89-64	CQ	13	LV	S	2	-42	-21.0	0.0	-8.2	0.1	12	175	4	-	-
FAT VEIN - VEIN SET 3															
IS90-100	CQ	1	LV	PS	2	-39	-13.0	0.0	-5.6	0.0	9	161	6	-	-
IS90-100	CQ	2	LV	PS	3	-41	-15.0	0.0	-5.7	0.1	9	225	0	-	-
IS90-100	CQ	3	LV	PS	3	-36	-	-	-2.8	0.1	5	293	23	-	-
IS90-100	CQ	4	LV	PS	1	-37	-	-	-0.3	-	1	208	-	-	-
MINTO A ZONE - VEIN SET 3															
IS90-10	CQ	1	LV	PS	2	-63	-	-	-18.0	0.0	21	188	4	-	-
IS90-10	CQ	2	LV	PS	4	-61	-23.0	0.0	-16.0	0.9	19	189	4	-	-
IS90-10	CQ	3	LV	PS	2	-56	-	-	-17.0	0.7	20	196	5	-	-
IS90-10	CQ	4	LV	PS	2	-57	-	-	-16.0	0.8	19	189	9	-	-
IS90-10	CQ	5	LV	PS	3	-61	-27.0	0.4	-19.0	0.8	22	200	5	-	-
SURLUGA MINE - VEIN SET 3															
IS89-69	CQ	1	LV	P?	3	-35	-14.0	0	-4.3	0.1	7	235	4	-	-
IS89-69	CQ	2	LV	P?	1	-41	-	-	-0.5	-	1	267	-	-	-
IS89-69	CQ	3	LV	P	1	-39	-	-	-0.8	-	2	262	-	-	-
IS89-69	CQ	5	LV	P	2	-39	-	-	-0.4	0.1	1	265	3	-	-
IS89-69	CQ	6	LV	P	1	-41	-	-	0.0	-	0	222	-	-	-
IS89-69	CQ	7	LV	PS	1	-40	-	-	-6.8	-	10	172	-	193	-
IS89-69	CQ	8	LV	PS	1	-39	-18.0	-	-7.2	-	11	187	-	-	-

ORI=origin of inclusion; MIN=host mineral; SET=co-genetic group of inclusions;
CQ=coarse quartz; FQ=fine quartz; #=number of inclusions in a co-genetic group

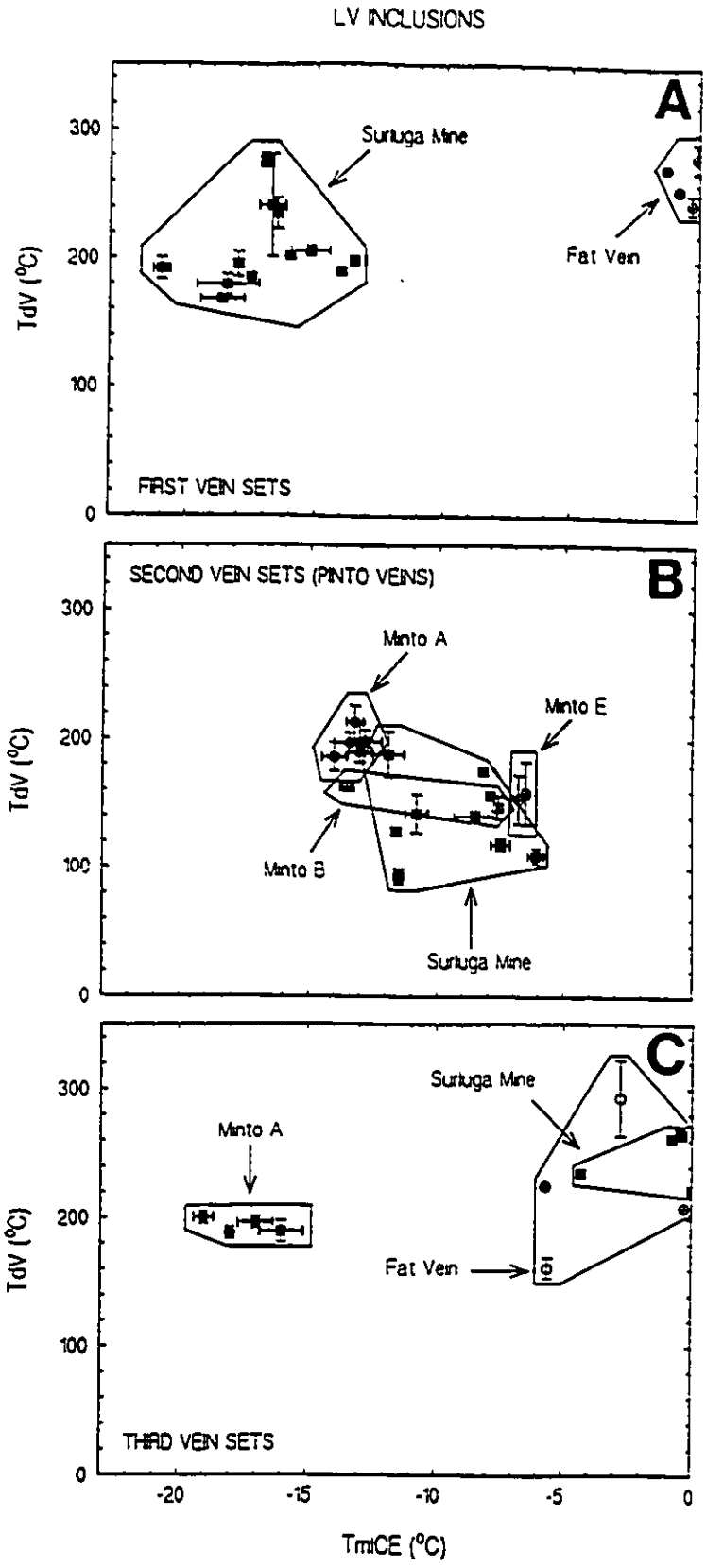

Figure 25. TdV-TmICE plots of LV inclusions in (A) first vein sets; (B) second vein sets (Pinto veins); and (C) third vein sets.

277°C (Figure 25). A significant number of LV inclusions in the first vein set from the Surluga Mine decrepitated between 210 and 316°C, before final homogenization. This probably indicates the presence of minor amounts of CO_2 and/or $CH_4 \pm N_2$ in the inclusion. Few LV inclusions were analyzed using Raman spectroscopy. When analyzed, no gases were detected, possibly due to the dislocation of the vapor bubble as a result of heating from the laser beam during the analysis.

The highest TmICE values were obtained from the inclusions in vein set 3 from both the Surluga Mine and the Fat Vein zone and from inclusions in vein set 1 from the Fat Vein zone (Figure 25 A and C). TmICE values below -15°C are restricted to the first vein set from Surluga Mine, and to vein set 3 (quartz-biotite vein) from the Minto A zone (Figure 25 A and C). LV inclusions in vein set 2 from the Minto A zone and the Surluga Mine, and similar veins from the the Minto B (vein set 2) and E zones (namely, Pinto veins) have higher and similar TmICE values that range from -13.4 to -6.1°C (Figure 25B).

TdV values for all vein sets are similar (147 to 293°C) with the highest values restricted to vein set 3 in the Surluga Mine and Fat Vein zone, and to vein set 1 in the Fat Vein zone (Figure 25). Most TdV values from the first and second vein sets are lower than 200°C. The lowest values of TdV (147-163°C) occurred in vein set 2 from the Minto B and E zones.

Fluid Compositions

Salinities of LV inclusions were calculated in terms of the H_2O-NaCl system due to generally high ($\geq$ -30°C) eutectic melting temperatures (Table 8). Calculated salinities range from 0.4 to 23 equiv. wt. % NaCl. The salinities of the high-TmICE inclusions which occur in vein set 3 from the Surluga Mine and in vein sets 1 and 3 from the Fat Vein zone range from nearly 0 to 11 wt.% NaCl (Table 8). Salinities of the low-TmICE inclusions ($<$ -15°C) which are are restricted to the first vein set from the Surluga Mine, and to vein set 3 from the Minto A zone (Figure 25 A and C) range from 18 to 22 wt.% NaCl (Table 8).

3.3.4. LVN Inclusions

Table 4 summarizes the petrography of LVN inclusion arrays. All LVN inclusions occur in planar arrays of variable extent and density, which cross-cut crystal grain-boundaries. These inclusions are generally large, ranging in size from 10 to 80 μm (Figure 26).

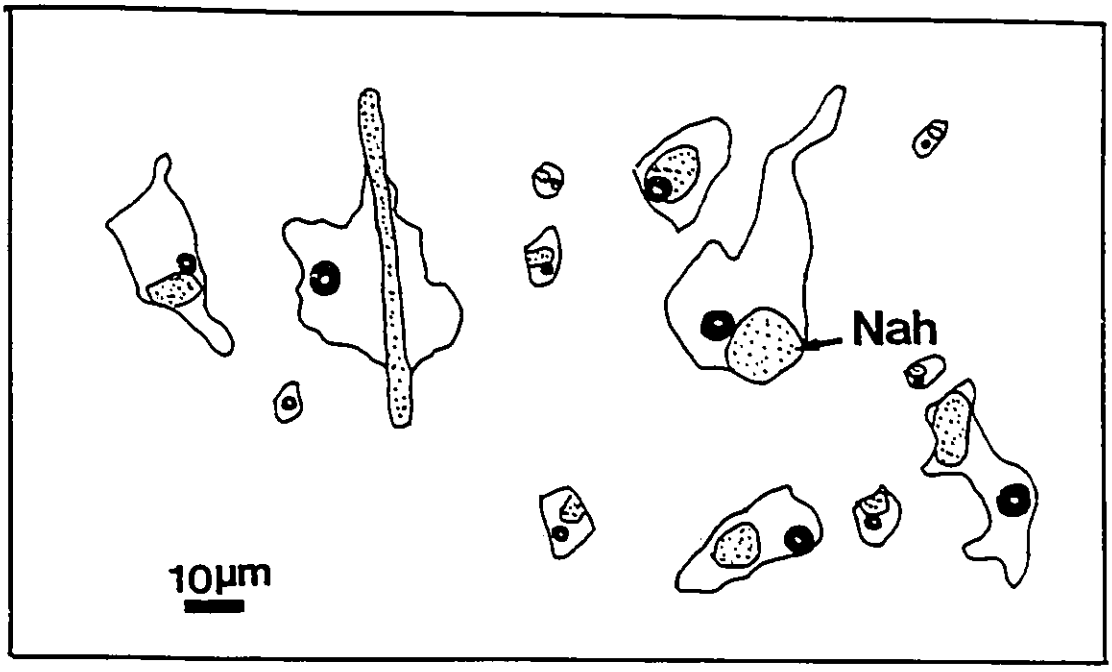

Figure 26. Precise drawing of LVN inclusions in quartz in vein set 2 from the Surluga Mine. Nah = Nahcolite.

Raman Spectroscopy

LVN inclusions contain a colourless, highly birefrengent, prismatic to acicular, euhedral to subhedral solid. A Raman spectrum of this solid is shown in Figure 27. The bands at 686, 1046, 1269 and 1435 cm^{-1} correspond to those of nahcolite ($NaHCO_3$) (Dhamelincourt et al., 1979). Of these bands, the one at 1046 cm^{-1} was always present in numerous spectra collected from LVN inclusions from different vein sets and zones. Nahcolite was also observed as planar arrays of solid inclusions in Pinto quartz veins from the Surluga Mine. The Raman spectrum obtained from these solid inclusions is identical to that shown in Figure 27. In some rare cases, these planar arrays of nahcolite were observed to merge with dense secondary planes of LVN inlusions. In such cases, LVN inclusions are clearly related to those planar arrays of solid inclusions. Solid inclusions of calcite was also identified in quartz and the corresponding Raman spectrum is given in Figure 28. The bands at 283, 715 and 1085 cm^{-1} correspond to calcite (Griffith, 1975).

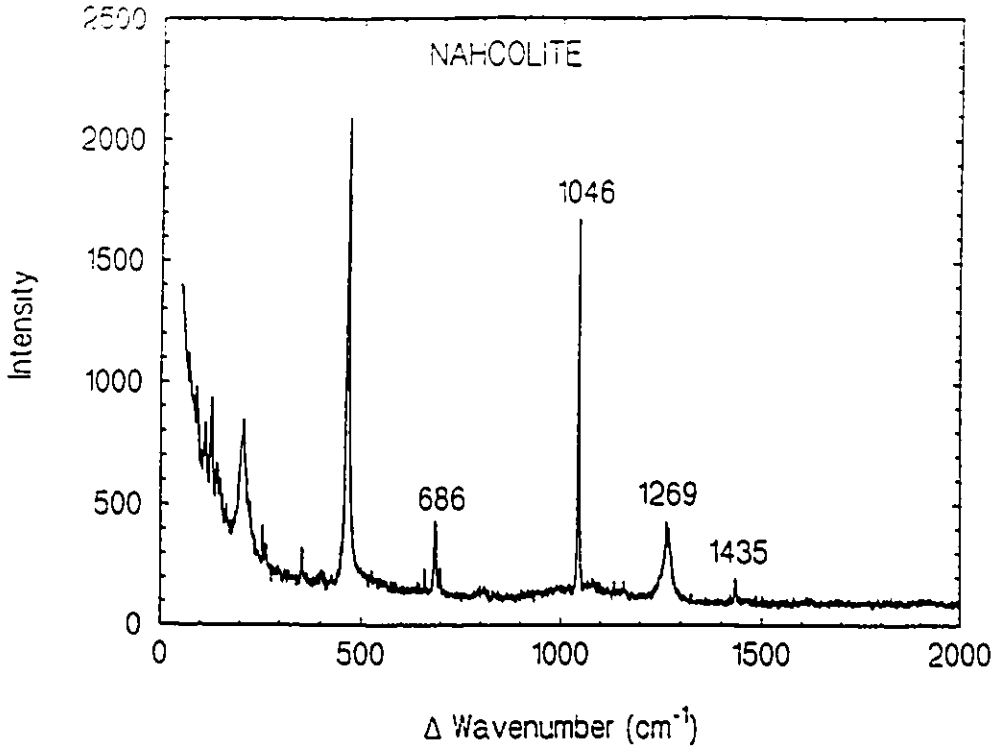

Figure 27. Raman Spectrum of nahcolite daughter mineral in LVN inclusions. Unlabeled peaks belong to the host quartz.

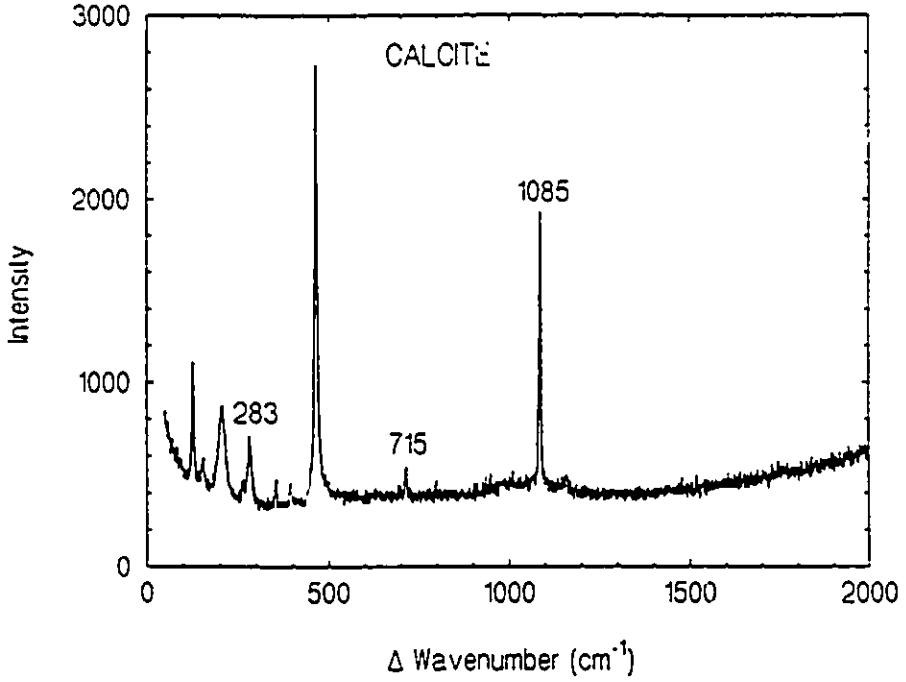

Figure 28. Raman spectrum of calcite solid inclusion in quartz in vein set 2 from the Surluga Mine. Unlabeled peaks belong to host quartz.

Table 9. Summary of Microthermometry Data for LVN Fluid Inclusions

SAMPLE #	MIN	SET	TYPE	OR	#	Tf	Te ave	Te sd	TmICE ave	TmICE sd	SAL	TdV ave	TdV sd	TdDM ave	TdDM sd	TD av	TD sd
FAT VEIN - VEIN SET 1																	
IS90-4	CQ	1	LVN	S	5	-38	-14	-	-3.6	0.1	6	166	4	214	13	-	-
IS90-4	CQ	2	LVN	S	5	-36	-18	0.1	-4.1	0.1	7	173	9	198	7	-	-
IS90-4	CQ	3	LVN	S	6	-39	-	-	-5.4	0.1	9	181	18	225	22	-	-
IS90-4	CQ	4	LVN	S	3	-35	-20	0.3	-3.2	0	[illegible]	175	4	187	14	-	-
IS90-4	CQ	5	LVN	S	4	-38	-	-	-4.5	0.1	[illegible]	156	5	175	4	-	-
MINTO A - VEIN SET 2																	
IS89-24	CQ	1	LVN	S	2	-42	-16	0.1	-6.5	0.1	10	151	3	189	4	205	5
IS89-24	CQ	2	LVN	S	4	-44	-15	0	-7.1	0.2	11	164	15	194	5	215	10
IS89-24	CQ	3	LVN	S	4	-43	-19	0	-6.8	0.2	10	166	7	196	2	-	-
IS89-24	CQ	4	LVN	S	7	-47	-18	0	-7.2	0.1	11	145	3	205	9	213	12
IS89-24	CQ	5	LVN	S	8	-39	-20	0	-7.2	0.1	11	163	5	187	6	196	18
IS89-24	CQ	6	LVN	S	7	-45	-22	0.2	-7.2	0.1	11	194	18	180	9	-	-
IS89-24	CQ	7	LVN	S	8	-44	-21	0.1	-7.2	0.1	11	139	8	204	6	-	-
IS89-24	CQ	8	LVN	S	10	-50	-20	0.3	-7.8	0.3	12	140	9	213	11	-	-
IS89-24	CQ	9	LVN	S	4	-47	-22	0.2	-6.7	0.2	10	158	16	214	14	-	-
IS89-24	CQ	10	LVN	S	9	-44	-18	0.4	-7.2	0.2	11	169	9	199	4	-	-
IS89-54	FQ	1	LVN	S	5	-57	-25	0.2	-15	0.7	19	144	4	194	9	-	-
IS89-54	FQ	2	LVN	S	2	-48	-23	0.1	-15.3	0.8	19	148	4	189	8	-	-
IS89-54	FQ	3	LVN	S	3	-48	-	-	-13	0.2	17	162	7	201	11	-	-
IS89-54	FQ	4	LVN	S	3	-46	-22	0.3	-15	0.4	19	154	4	193	14	-	-
IS89-54	FQ	5	LVN	S	4	-48	-	-	-13	0.2	17	148	7	189	9	-	-
IS89-54	FQ	6	LVN	S	4	-52	-24	0.2	-17	0.3	20	164	10	196	11	-	-
MINTO B - VEIN SET 2																	
IS90-34	CQ	1	LVN	S	4	-55	-24	0.3	-9.4	0.7	13	152	4	173	5	-	-
IS90-34	CQ	2	LVN	S	6	-60	-20	0.4	-12	0.9	16	130	5	153	7	-	-
MINTO E																	
IS90-53A	FQ	1	LVN	S	6	-48	-26	2.6	-6	1	9	146	31	184	12	-	-
IS90-53C	CQ	2	LVN	S	5	-46	-26	2.2	-6.1	1.1	10	139	30	181	12	-	-
IS90-53B	CQ	3	LVN	S	11	-48	-20	2.5	-7.6	1.6	11	143	26	186	21	-	-
IS90-53B	CQ	4	LVN	S	10	-45	-	-	-7.6	1.6	11	148	22	189	20	-	-
IS90-53A	CQ	5	LVN	S	5	-43	-	-	-6.1	1.1	9	179	61	207	16	-	-
IS90-53B	CQ	6	LVN	S	4	-43	-	-	-8.2	1.1	12	147	21	19[illegible]	15	-	-
IS90-53B	CQ	7	LVN	S	5	-42	-	-	-8.7	0.8	13	151	21	191	24	-	-
IS90-53B	CQ	8	LVN	S	13	-43	-18	0.6	-9.1	0.5	13	155	21	192	26	-	-
IS90-53B	CQ	9	LVN	S	4	-45	-	-	-9.8	0	14	176	0	222	0	-	-
IS90-53B	FQ	10	LVN	S	8	-45	-	-	-9	0.4	13	139	18	170	19	-	-
IS90-50C	CQ	11	LVN	S	4	-42	-27	2	-9.4	0	14	156	0	151	0	-	-

Table 9 (Continued)

SAMPLE #	MIN	SET	TYPE	ORI	#	Tf	Te ave	Te sd	TmICE ave	TmICE sd	SAL	TdV ave	TdV sd	TdDM ave	TdDM sd	TD av	TD sd
SURLUGA MINE - VEIN SET 1																	
IS89-65	CQ	1	LVN	S	2	-48	-21	0.3	-8.6	0.2	13	173	17	151	25	-	-
IS89-65	CQ	2	LVN	S	2	-35	-14	0.1	-8.6	0.1	13	173	3	136	10	-	-
IS89-70A	CQ	3	LVN	S	1	-43	-21	-	-11.0	0.3	15	140	7	193	21	285	-
IS89-70A	CQ	4	LVN	S	6	-48	-20	0.5	-12.3	0.2	16	140	10	200	12	290	15
IS89-70A	CQ	5	LVN	S	4	-45	-23	0	-10.8	0	15	202	5	167	5	268	8
SURLUGA MINE - VEIN SET 2																	
IS89-63	CQ	1	LVN	S	5	-46	-22	0.8	-8.6	0.9	13	116	9	174	1	-	-
IS89-63	CQ	2	LVN	S	5	-43	-20	3.7	-8.0	0.2	12	127	10	175	18	-	-
IS89-63	CQ	3	LVN	S	10	-46	-20	0	-8.1	0.1	12	129	10	166	8	-	-
IS89-63	CQ	4	LVN	S	15	-45	-20	0	-7.0	0.1	11	144	8	183	13	-	-
IS89-63	CQ	5	LVN	S	6	-43	-21	0.2	-7.1	0	11	136	8.2	181	12	-	
IS89-63	CQ	6	LVN	S	4	-42	-24	0	-8.0	0.6	12	135	6	181	2	-	-
IS89-63	CQ	7	LVN	S	10	-48	-20	0	-6.3	0	10	156	8	178	17	-	-
IS89-63	CQ	8	LVN	S	4	-46	-	-	-5.8	0	9	139	8	184	11	-	-
IS89-63	CQ	9	LVN	S	5	-48	-21	0.7	-7.2	0.2	11	169	12	199	10	-	-

ORI=origin of inclusion; MIN=host mineral; SET=co-genetic group of inclusions; CQ=coarse quartz; FQ=fine quartz; #=number of inclusions in a co-genetic group

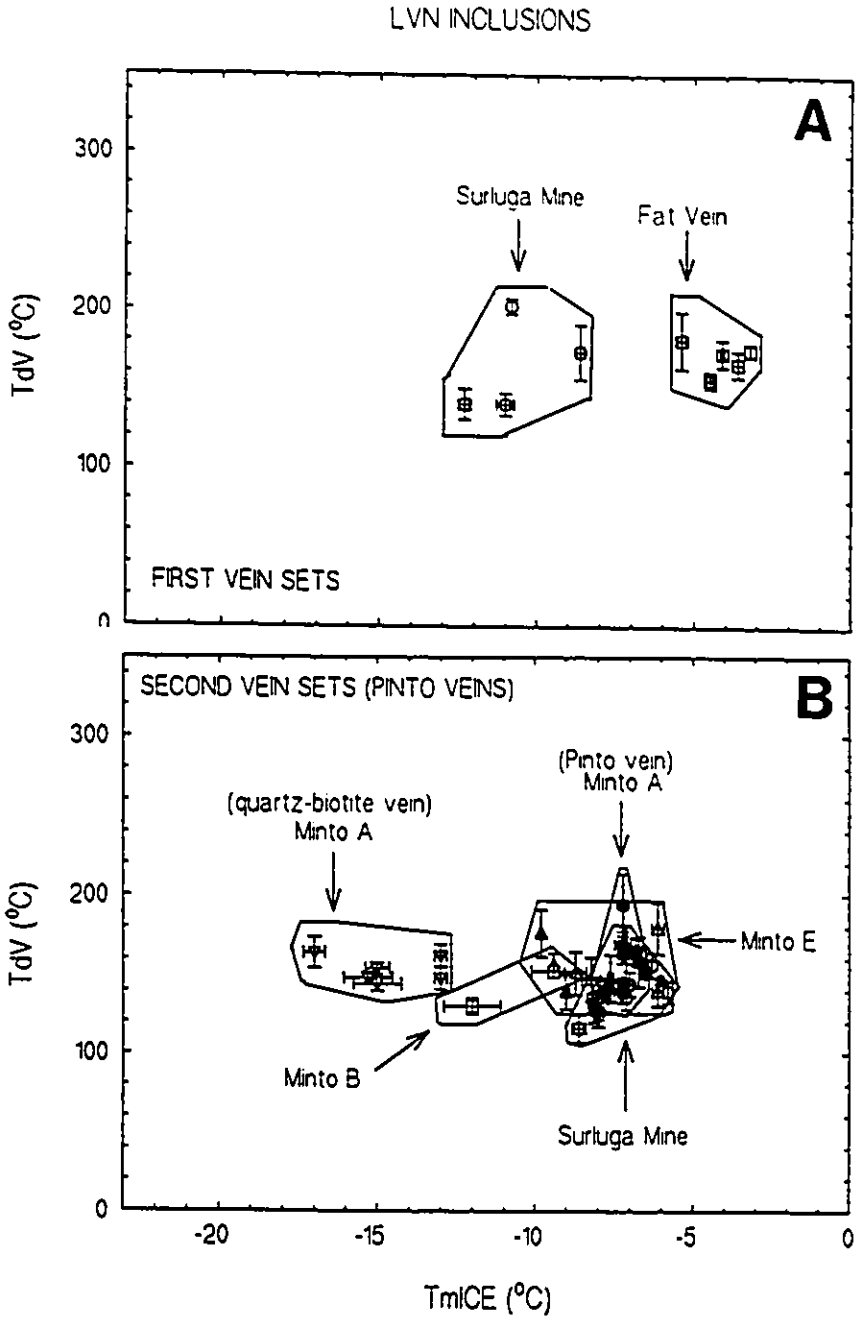

Figure 29. TdV-TmICE plots of LVN inclusions in (A) vein set 1, and (B) vein set 2.

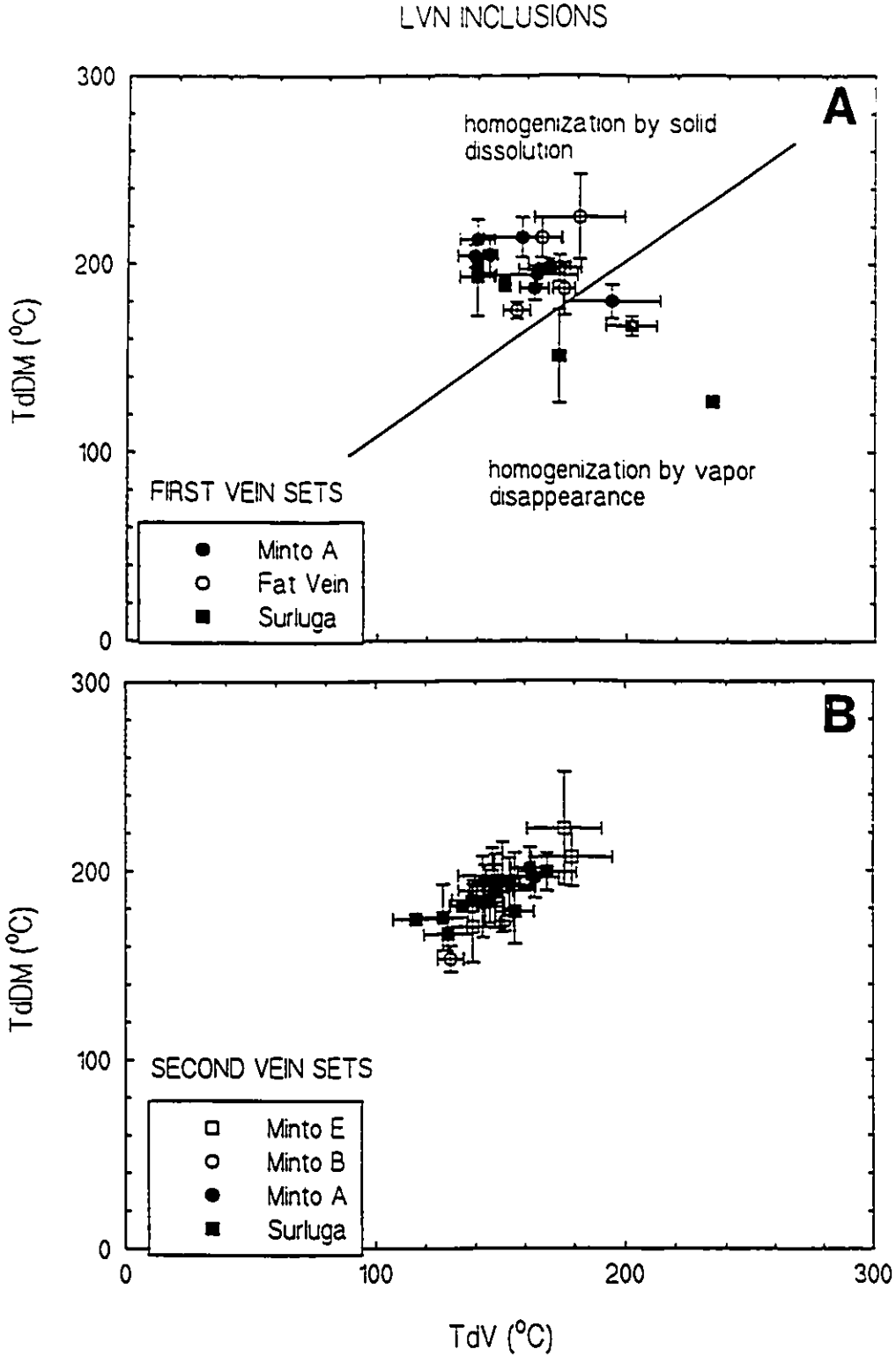

Figure 30. TdV-TdDM plots of LVN inclusions in (A) vein set 1, and (B) vein set 2.

Microthermometric Results

Table 9 contains a summary of the microthermometric results obtained on LVN inclusions.

Eutectic melting temperatures of LVN inclusions ranged from -27 to -14°C (Table 9). Final ice-melting occurred at temperatures of between -17 and -3.6°C (Figure 29 A and B). Most TmICE values obtained on LVN inclusions fall within a relatively narrow range between -9 and -3.6°C (Figure 29). The lowest TmICE values are from LVN inclusions in vein set 2 from the Minto A zone, which range from -17 to -13°C (Figure 29B). These TmICE values are similiar to those obtained on LV inclusions in vein set 2 from the same zone (compare Figures 25B and 29B).

LVN inclusions usually homogenize to the liquid phase by the dissolution of nahcolite at temperatures (TdDM) ranging from 136 to 225°C. Most TdDM values lie between 165 and 185°C (Figure 30 A and B). LVN inclusions with consistent solid size in a group yielded TdDM within a 10 to 20°C range, as indicated by the small standard deviations of the TdDM values, indicating that in these cases, the nahcolite is a daughter mineral (Figure 30). Some LVN inclusions were observed to homogenize by vapor disappearance following dissolution of nahcolite (for example, 50% of LVN inclusions in veinset 1 from the Surluga mine, Table 9, Figure 30A).

Average temperatures of disappearance of vapour ranged from 116 to 202°C, with most values between 116 and 165°C (Figure 30). In comparison to LV inclusions, LVN inclusions yielded relatively consistent microthermometric results, regardless of the vein sets and deformation zones in which they occur (compare Figures 25, 29 and 30).

Fluid Compositions

The salinity of LVN inclusions ranges from 5 to 20 equiv. wt.% NaCl (Table 9). The salinity of the LVN inclusions in vein set 2 from the Surluga Mine (16-19 wt.% NaCl) and in vein set 2 from the Minto B zone (13-16 wt. % NaCl), and in vein set 2 from the Minto A zone (17-20 wt. % NaCl) are slightly higher than the LVN inclusions in other vein sets (Table 9).

3.3.5. LC and LCV(N) Inclusions

Most LCV(N) inclusions occur in planes of variable extent and orientation which cut grain-boundaries, and are therefore secondary in origin (Table 5; Figure 31A). However, LC inclusions in vein set 3, from the Fat Vein zone, occur on short isolated

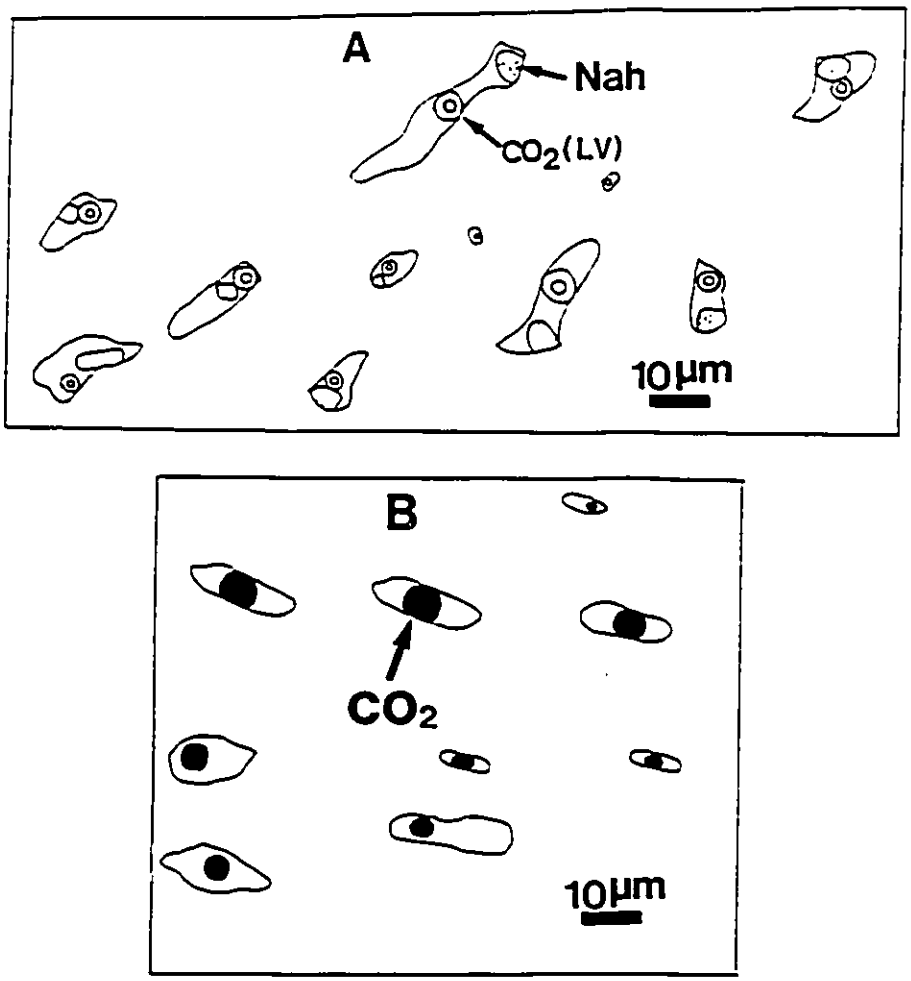

Figure 31. Precise drawings of LCVN and LC inclusions (A) secondary inclusions in planar arrays in vein set 2 from the Surluga Mine, and (B) primary inclusions in short planar arrays in growth-zoned quartz (vein set 3) from the Fat Vein zone. Nah = Nahcolite; L and V = liquid and vapor, respectively.

planes in growth zones, and thus are primary in origin (Figure 31B) (Roedder, 1984). Most LCV inclusions contain nahcolite (Figure 31A) and sometimes occur together with LVN inclusions in the same planar arrays.

Raman Spectroscopy

Results of Raman analyses of the non-aqueous portions of the LC and LCV(N) inclusions are shown in Table 10, and Figure 32. The related microthermometric and aqueous liquid volume (V_l) data on those inclusions are also given in Table 10. The mole fraction of CO_2 in the carbonic portion (ZCO_2) of a significant proportion ($\approx$ 50%) of these inclusions has a value of 1, even although they have final CO_2

Table 10. Microthermometry and Raman Data for LC and LCV(N) Fluid Inclusions

Incl.	Sample	Type	Vl	TmCO2	TmICE	TmCLATH	ThC	ZCO2*	ZCH4*	ZN2*	Vv
FAT VEIN - VEINSET 1											
A1	IS90-4	LC	0.94	-58.3	-3	n.v.	-7.2(l)	1.00	0.00	0.00	45
A2	IS90-4	LC	0.8	-58.4	n.v.	n.v.	-7.5(l)	1.00	0.00	0.00	45
SURLUGA MINE - VEINSET 1											
A1	IS89-70A	LCV	0.56	-59.6	-14.4	6.8	26.5(l)	0.95	0.05	0.00	70
B1	IS89-70A	LCV	0.90	-59.6	n.v.	6.8	27.0(l)	0.97	0.03	0.00	70
C1	IS89-70A	LC	0.53	-63.9	n.v.	7.3	-16.5(l)	0.71	0.26	0.02	45
C2	IS89-70A	LC	0.62	-65.4	n.v.	8.3	-20.5(l)	0.72	0.25	0.03	40
C4	IS89-70A	LC	0.55	-65.4	n.v.	8.3	-20.5(l)	0.75	0.17	0.08	40
C5	IS89-70A	LC	0.56	-66.0	n.v.	8.1	-20.5(l)	0.65	0.30	0.05	40
C6	IS89-70A	LC	0.51	-66.0	n.v.	8.1	-20.5(l)	0.71	0.24	0.06	40
MINTO B - VEINSET 2											
A1	IS90-43	LCV	0.82	-59.3	n.v.	1.4	30.8(v)	0.92	0.05	0.03	90
A2	IS90-43	LCV	0.86	-59.3	n.v.	1.4	30.8(v)	0.95	0.05	0.00	90
A4	IS90-43	LCV	0.87	-59.4	n.v.	2.0	28.9(l)	0.88	0.08	0.04	70
A6	IS90-43	LCV	0.86	-59.1	n.v.	2.1	28.8(l)	1.00	0.00	0.00	70
A7	IS90-43	LCV	0.80	-59.1	n.v.	2.1	30.0(l)	1.00	0.00	0.00	70
MINTO E											
K1	IS90-53B	LCVN	0.52	-59.1	-12.4	7.2	22.7(l)	0.94	0.02	0.04	60
K2	IS90-53B	LCVN	0.18	-59.1	-12.4	7.2	22.4(l)	0.99	0.01	0.00	60
K3	IS90-53B	LCVN	0.85	-58.9	-12.4	8.3	20.9(l)	1.00	0.00	0.00	60
K4	IS90-53B	LCVN	0.83	-58.8	n.v.	5.2	21.3(l)	1.00	0.00	0.00	60
L3	IS90-53B	LC	0.81	-59.3	n.v.	7.0	15.2(l)	0.95	0.00	0.05	60
L4	IS90-53B	LCVN	0.80	-59.0	n.v.	7.1	22.4(l)	0.98	0.02	0.00	60
S1	IS90-53C	LCVN	0.75	-58.9	n.v.	6.2	26.7(l)	1.00	0.00	0.00	70
MINTO A ZONE - VEINSET 2											
A1	IS89-19	LCV	0.91	-59.7	-13.0	3.5	30.0(l)	0.95	0.05	0.00	75
A3	IS89-19	LCV	0.88	-59.7	n.v.	3.7	28.0(l)	0.85	0.12	0.03	70
A5	IS89-19	LCV	0.89	-59.7	-13.0	3.7	29.2(l)	1.00	0.00	0.00	70
B2	IS89-19	LCV	0.75	-59.4	n.v.	3.4	29.8(l)	0.92	0.08	0.00	75
B3	IS89-19	LCV	0.86	-59.4	n.v.	3.7	30.0(l)	1.00	0.00	0.00	75

Table 10 (continued)

Incl.	Sample	Type	Vl	TmC	TmICE	TmCLATH	ThC	ZCO2*	ZCH4*	ZN2*	Vv
MINTO A ZONE - VEINSET 2											
C1	IS89-21	LCV	0.82	-58.0	n.v.	5.3	29.6(l)	0.96	0.04	0.00	75
C4	IS89-21	LCV	0.88	-58.0	n.v.	4.6	29.2(l)	0.95	0.03	0.02	70
D3	IS89-21	LCV	0.81	-57.9	n.v.	n.v.	30.5(l)	1.00	0.00	0.00	75
D4	IS89-21	LCV	0.85	-58.0	n.v.	5.3	30.1(l)	0.98	0.02	0.00	75
E2	IS89-21	LCV	0.83	-57.9	-13.4	n.v.	29.4(l)	1.00	0.00	0.00	70
SURLUGA MINE - VEINSET 2											
Q3	IS89-64	LCVN	0.79	-58.7	n.v.	n.v.	26.0(l)	1.00	0.00	0.00	70
Q5	IS89-64	LCVN	0.75	-59.0	n.v.	2.7	25.4(l)	1.00	0.00	0.00	70
Q7	IS89-64	LCVN	0.62	-59.0	n.v.	n.v.	25.3(l)	1.00	0.00	0.00	70
S4	IS89-63	LCVN	0.64	-59.5	-12.4	6.3	23.3(l)	0.93	0.07	0.00	65
S5	IS89-63	LCVN	0.87	-59.4	-12.4	n.v.	20.7(l)	0.98	0.02	0.00	55
MINTO B - VEINSET 2											
B1	IS89-6	LCV	0.83	-58.1	n.v.	4.2	30.0(l)	1.00	0.00	0.00	70
B2	IS89-6	LCV	0.79	-58.1	n.v.	n.v.	29.4(l)	0.98	0.02	0.00	70
B4	IS89-6	LCV	0.90	-58.1	n.v.	n.v.	22.2(l)	0.96	0.04	0.00	60
B5	IS89-6	LCV	0.95	-58.1	n.v.	3.9	29.6(l)	1.00	0.00	0.00	70
B7	IS89-6	LCV	0.93	-58.1	n.v.	n.v.	22.2(l)	0.95	0.05	0.00	60
B8	IS89-6	LCV	0.87	-58.1	n.v.	4.1	22.2(l)	1.00	0.00	0.00	60
FAT VEIN - VEINSET 3											
B1	IS90-100	LC	0.88	-58.1	n.v.	8.5	-8.4(l)	0.98	0.02	0.00	45
B2	IS90-100	LC	0.85	-57.9	n.v.	n.v.	-8.1(l)	1.00	0.00	0.00	45
B5	IS90-100	LC	0.92	-58.7	n.v.	n.v.	-6.7(l)	0.95	0.05	0.00	45
B6	IS90-100	LC	0.87	-59.1	n.v.	-	-	0.90	0.07	0.03	cc
B7	IS90-100	LC	0.83	-58.2	n.v.	-	-	1.00	0.00	0.00	cc
B9	IS90-100	LC	0.76	-58.3	n.v.	-	-	1.00	0.00	0.00	cc

* calculated from Raman analyses
l and v = homogenization into the liquid and vapor phases
n.v. not visible

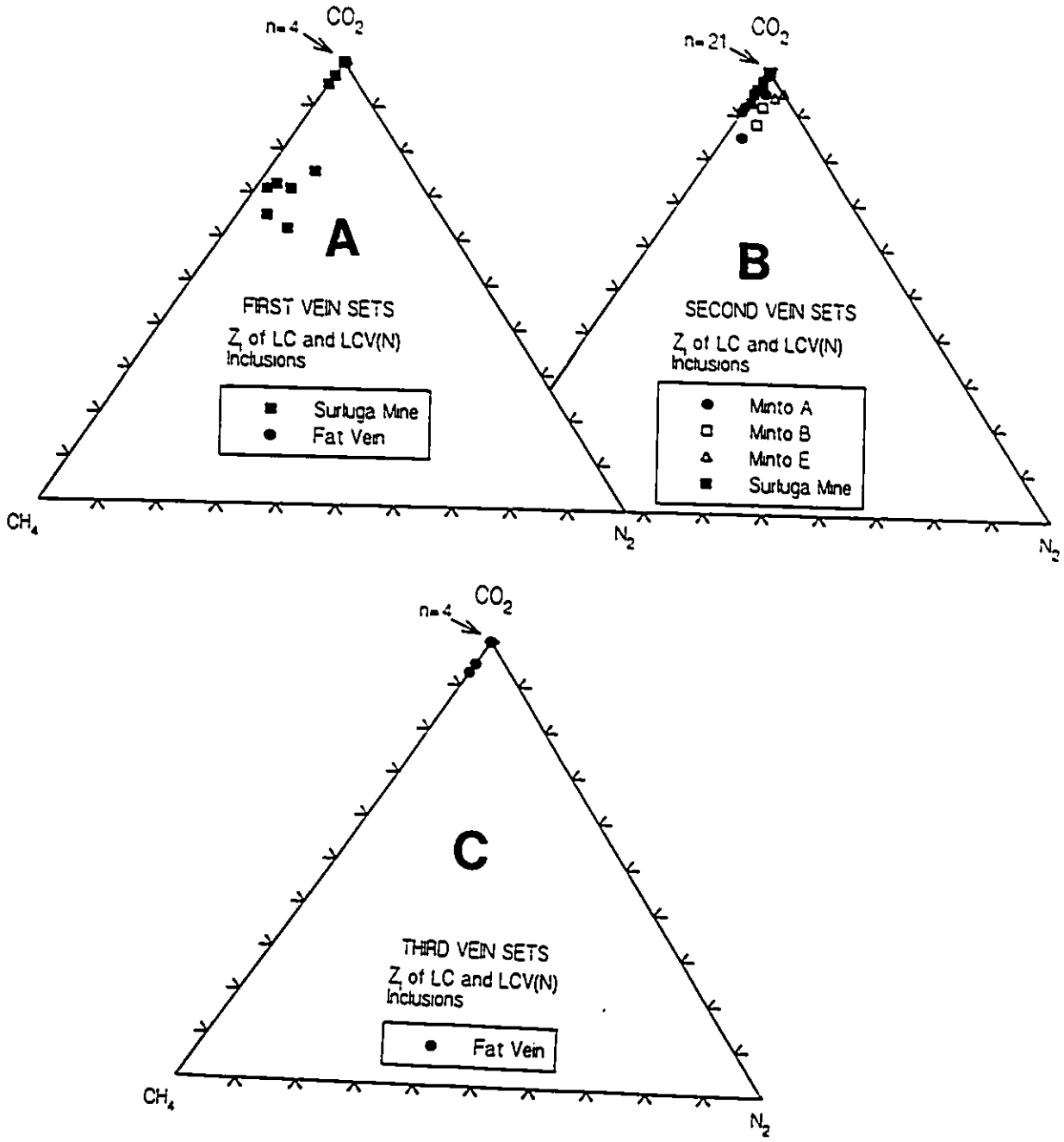

Figure 32. Molecular proportions (Z_i) of CO_2, CH_4 and N_2 in the non-aqueous part of LC and LCV(N) inclusions in (A) vein set 1, (B) vein set 2, and (C) vein set 3, as determined by Raman analyses.

melting temperatures ($TmCO_2$) of less than -56.6°C. The latter data indicate that low concentrations of other gases are present, below the detection limits of the Raman spectrometer (Figure 32). Inclusions in vein set 2 have ZCO_2 values that range from 0.65 to 1, with the highest values restricted to the inclusions from the Minto E and the Fat Vein zones (Figure 32A).

ZCH_4 ranges from 0 to 0.30, with the highest values (0.17-0.30) occurring in the inclusions in vein set 1 from the Surluga Mine (Figure 32A). ZCH_4 for the inclusions from vein set 2 range from 0 to 0.12 (Figure 32B).

ZN_2 ranges from 0 to 0.06, with the highest values restricted to inclusions from vein set 1 in the Surluga Mine. (Figure 32A). Very few Raman analyses yielded distinct N_2 peaks. Inclusions which yielded distinct N_2 peaks at room temperature yielded poorly-defined peaks at 35°C. This is due to preferential partitioning of N_2 into the vapour phase at room temperature. An example of a multi-region Raman spectrum collected from such inclusions is shown in Figure 33.

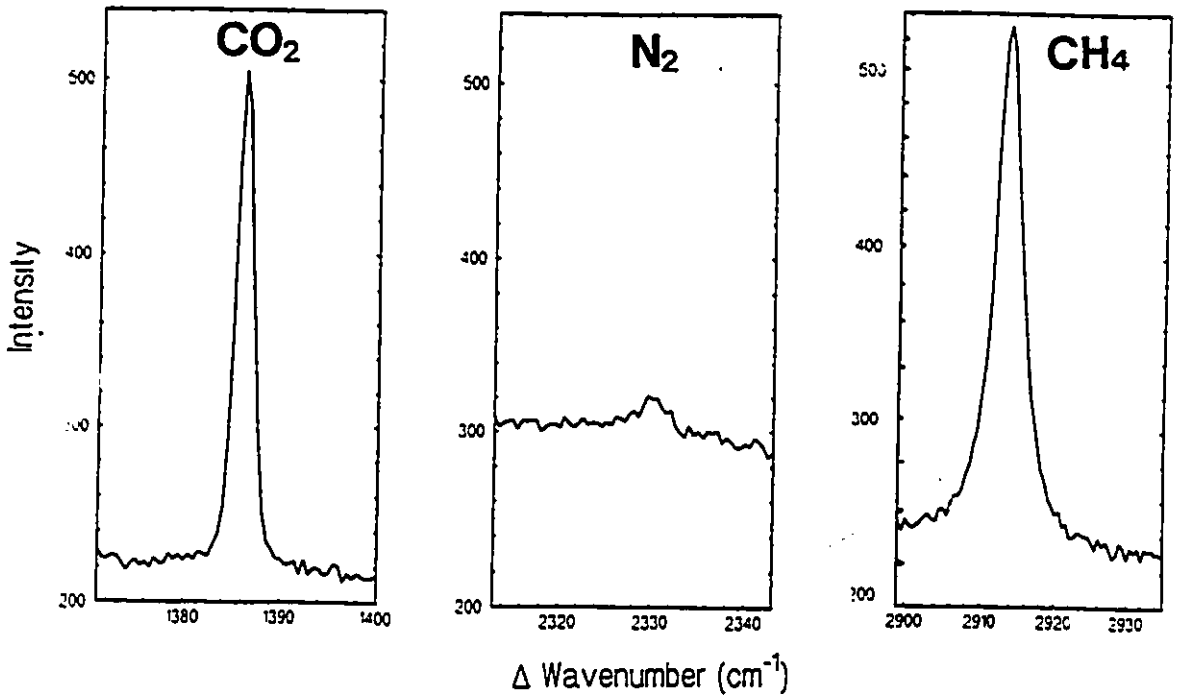

Figure 33. Multi-region/multi-scan Raman spectra collected from non-aqueous part of an LC inclusion with very low $TmCO_2$.

LCV(N) inclusions in vein set 2 from the Minto A, B and E zones, and from the Surluga Mine have similar ZCO_2, ZCH_4 and ZN_2 values to inclusions with low ZCH_4 in vein set 1 (Figure 32B). The high-ZCH_4 inclusions from the Surluga Mine are not present in vein set 2. The similarity in composition between some of these inclusions may indicate that inclusions with low CH_4 content in vein set 1 represent an overprint from fluids related to vein set 2.

The primary LC inclusions in vein set 3 from the Fat Vein zone have ZCO_2, ZCH_4 and ZN_2 values of between 0.90 and 1; 0 and 0.07, and 0 and 0.03, respectively (Figure 32C). These values are very similiar to those for other vein sets with the exception of vein set 1 from the Surluga Mine (Figure 32).

Microthermometric Results

Table 11 and Figure 34 summarize the microthermometric results obtained on LC and LCV(N) inclusions.

$TmCO_2$ values for LC and LCV(N) inclusions range from -66 to -57.8°C (Figure 34). These inclusions can be classified into two groups on the basis of their $TmCO_2$ values: 1) inclusions with low $TmCO_2$ values ranging from -66 to -63.9°C; and 2) inclusions with high $TmCO_2$ values, falling between -59.8 and -57.8°C (Figure 34 A, B and C). Of these, low-$TmCO_2$ inclusions are exclusively found in vein set 1 from the Surluga Mine (Figure 34A). Most of the high-$TmCO_2$ inclusions contain a two-phase carbonic fluid at room temperature, and in some cases, contain nahcolite.

Final melting of clathrate (TmCLATH) was usually difficult to observe owing to the small size of most inclusions, but where observed, ranged from 2.8 to 9.1°C (Table 11). In many cases, the final clathrate-melting temperature was taken as when a jagged meniscus between the aqueous and non-aqueous portions became smooth and rounded. These values of TmCLATH indicate minimum salinities of between 1 and 14 equiv. wt. % NaCl (Bozzo et al., 1973) (Table 11). The salinity of the inclusions in the high-$TmCO_2$ group will be slightly underestimated (2-4 wt. % NaCl). This is due to the small amount (< 1-5 mole %) of CH_4 and/or N_2 present in the inclusions, as indicated by the depressed $TmCO_2$ values, which will have raised the TmCLATH value (Hollister and Burruss, 1976). However, the error in calculated salinities based on clathrate-melting temperatures in the case of the low-$TmCO_2$ inclusions will be significantly higher due to the greater (10-35 mole%) amounts of dissolved gases within the carbonic part of these inclusions, as indicated by lower $TmCO_2$ values (-66 to -63.9°C) (Figure 34A).

Table 11. Summary of Microthermometry Data for LC and LCV(N) Fluid Inclusions

SAMPLE #	MIN	SET	TYPE	ORIG	#	TfC	Te	TmCO2 ave	TmCO2 sd	TmCLATH ave	TmCLATH sd	ThC* ave	ThC* sd	ThC ave	ThC sd	TfH	TmICE	SAL	TdDH ave	TdDH sd	ThTOT ave	ThTOT sd	TD a	TD sd
FAT VEIN - VEINSET 1																								
IS90-4	CQ	1	LC	PS?	3	-97	-	-58.3	0.05	8.1	0.1	7.5	0.0	-7	0.2	-42	-4.2	4	-	-	260	8	-	-
IS90-4	CQ	2	LC	PS?	6	-98	-	-58.2	0.1	8.6	0.1	7.9	0.2	-6.9	0.1	-45	-6	3	-	-	193	11	-	-
IS90-4	CQ	3	LC	?	1	-81	-	-58.3	-	9.1	-	8.1	-	-7.2	-	-36	-2.7	2	-	-	-	-	157	-
IS90-4	CQ	4	LC	?	1	-97	-68?	-58.4	-	9.3	-	7.8	-	-7.5	-	-41	n.v	1	-	-	-	-	230	-
MINTO B - VEINSET 2 (PINTO VEIN)																								
IS90-43	FQ	1	LCV	S	5	-101	-	-59.3	0	1.7	0	-	-	30.8	0	-55.9	n.v	14	-	-	-	-	183	8
IS90-43	FQ	2	LCV	S	3	-101	-	-59.1	0	2.4	0	-	-	30	0	-53.8	n.v	13	-	-	-	-	195	14
IS90-43	FQ	3	LCV	S	2	-101	-	-59.1	0	2.4	0	-	-	27.7	1.2	-54	n.v	13	-	-	-	-	186	17
IS89-6	CQ	1	LCV	S	6	-93	-	-58.1	0.1	4.2	0.2	-	-	29.6	0.2	-40	n.v	10	-	-	-	-	166	14
IS89-6	CQ	1	LCV	S	3	-93	-	-58.2	0.1	4.1	0.1	-	-	22.2	0	-38	n.v	10	-	-	-	-	175	9
MINTO E (PINTO VEIN)																								
IS90-53B	CQ	1	LCVN	S	4	-95	-	-59.1	0.1	6.8	1	-	-	22.7	0.1	-40	-7.2	6	-	-	-	-	165	6
IS90-53B	CQ	2	LCVN	S	2	-99	-	-58.8	0	5.2	0.05	-	-	21.3	0.1	-45	n.v	9	-	-	-	-	171	21
IS90-53B	CQ	3	LCVN	S	4	-96	-	-58.9	0.3	6.2	1	-	-	26.7	0.2	-37	-6.5	7	-	-	-	-	175	14
IS90-53B	CQ	4	LCVN	S	3	-95	-	-59.1	0.1	7.2	0.05	-	-	28.5	0.3	-43	-8.2	5	-	-	-	-	181	12
IS90-53C	CQ	5	LCVN	S	3	-92	-	-59	0.1	7.1	0.1	-	-	22.4	1.3	-42	-11	6	-	-	-	-	160	11
IS90-53C	CQ	6	LC	S	5	-96	-	-59.3	0.1	7	0.1	-	-	15.2	0.4	-46	-8.3	6	-	-	-	-	175	9
SURLUGA MINE - VEINSET 1																								
IS89-70A	CQ	1	LCVN	S	4	-92	-	-58.4	0.1	5.6	0.1	-	-	28.1	0.2	-48	n.v.	8	156	15	195	18	-	-
IS89-70A	CQ	2	LCVN	S	5	-94	-	-58.8	0.05	5.1	0.1	-	-	26.3	0.2	-41	-15	9	135	12	-	-	235	23
IS89-70A	CQ	3	LCVN	S	1	-106	-	-63.9	-	7.3	-	-17	-	-	-	-61	n.v.	5	-	-	365	14	-	-
IS89-70A	CQ	4	LCVN	S	7	-106	-	-65.5	0.5	8	0.3	-20	0.9	-	-	-63	n.v.	4	-	-	-	-	265	18
IS89-70A	CQ	5	LCVN	S	4	-108	-	-66	0.6	6.2	0.1	-26.5	0.1	-	-	-	n.v.	7	-	-	267	15	-	-
IS89-70A	CQ	6	LCVN	S	2	-107	-	-65.3	0	7.5	0.1	-25	0	-	-	-54	n.v.	5	-	-	-	-	257	21
IS89-70A	CQ	7	LCVN	S	3	-106	-	-65.5	0.5	7.8	0.3	-22.8	0.2	-	-	-	n.v.	4	-	-	279	31	-	-

Table 11 (continued)

SAMPLE	#	HIN	SET	TYPE	ORIG	#	TfC	Te	TmCO2 ave	TmCO2 sd	TmCLATH ave	TmCLATH sd	ThC* ave	ThC* sd	ThC ave	ThC sd	TfH	TmICE	SAL	TdDH ave	TdDH sd	ThTOT ave	ThTOT sd	TD a	TD sd
HINTO A - VEINSET 2 (PINTO VEIN)																									
IS89-19	CQ	1	LCV	S		2	-97	-	-59.7	0	3.8	0	-	-	30.2	0.2	-44	-13	11	-	-	30	0	-	-
IS89-19	CQ	2	LCV	S		3	-96	-	-59.8	0.1	4	0.1	-	-	26.7	0.9	-49	-13	11	-	-	-	-	229	17
IS89-19	CQ	3	LCV	S		4	-100	-	-59.4	0	4	0	-	-	30.5	0.4	-37	-10	11	-	-	296	8	-	-
IS89-19	CQ	4	LCV	S		4	-100	-	-59.4	0	4	0	-	-	27.3	0.7	-37	-10	11	-	-	289	7	-	-
IS89-21	CQ	1	LCV	S		8	-96	-	-58	0.1	4.7	0.2	-	-	29.4	0.1	-46	-12	10	-	-	-	-	-	-
IS89-21	CQ	2	LCV	S		4	-95	-	-57.9	0.1	5.1	0.2	-	-	30.4	0.3	-45	n.v	9	-	-	-	-	-	-
IS89-21	CQ	3	LCV	S		5	-96	-	-58	0.1	5.1	0.1	-	-	29.7	0.2	-48	n.v	9	-	-	-	-	-	-
IS89-21	CQ	4	LCV	S		6	-98	-	-58.2	0.1	3.7	0.2	-	-	20.2	0.1	-48	-13	11	-	-	-	-	266	8
IS89-21	CQ	5	LCV	S		2	-97	-	-57.9	0.1	5.7	0.1	-	-	29.1	0.3	-65	-12	8	-	-	-	-	233	10
IS89-21	CQ	6	LCV	S		2	-96	-	-57.8	0	5.1	0.1	-	-	30.4	0.1	-60	-13	9	-	-	-	-	224	0
SURLUGA MINE - VEINSET 2 (PINTO VEIN)																									
IS89-63	CQ	1	LCV	S		2	-98	-	-59.6	0.3	4.2	0	-	-	23.4	2.5	-45.8	-12	11	-	-	-	-	202	13
IS89-63	CQ	2	LCVN	S		3	-100	-	-59.7	0	6.5	0.1	-	-	31	0	-50	-12	7	156	23	215	25	-	-
IS89-63	CQ	3	LCVN	S		4	-98	-	-58.5	0.4	5.7	0.5	-	-	26.3	2.1	-	-9.7	10	145	0	190	24	-	-
IS89-63	CQ	4	LCVN	S		4	-95	-70	-59.1	0	4.1	0.2	-	-	22.8	2.8	-45	-13	10	138	15	227	36	-	-
IS89-64	CQ	5	LCV	S		8	-96	-	-58.7	0.2	2.8	0.2	-	-	25.1	0.4	-	n.v	12	-		202	7	-	-
FAT VEIN - VEINSET 3																									
IS90-100	CQ	1	LC	P		5	-97	-	-57.8	0.1	8.8	0.2	7.8	0.8	15.7	0.2	-42	n.v	2	-		-	-	227	37
IS90-100	CQ	2	LC	P		1	-103	-	-59.1	-	4.2	-	3.6	-	-8.9	-	-43	n.v	10	-		187	-	-	-
IS90-100	CQ	3	LC	P		5	-96	-	-57.8	0	7.4	0	4.3	0	13	0.1	-45	-7	5	-		-	-	215	21
IS90-100	CQ	4	LC	P		5	-97	-	-58	0	8.8	0	4.8	0	-8.6	0	-45	n.v	2	-		-	-	180	16
IS90-100	CQ	5	LC	P		4	-93	-	-58.2	0	7.8	0	2.1	0.3	-6.1	0.2	-45	-10	4	-		185	2	-	-
IS90-100	CQ	6	LC	P		1	-98	-	-58.3	-	5.8	-	3.8	-	-4.3	-	-43	n.v	8	-		-	-	136	-

ORIG=origin of inclusion; HIN=host mineral; SET=co-genetic group of inclusions; CQ=coarse quartz; FQ=fine quartz;
#=number of inclusions in co-genetic group; n.v. not visible

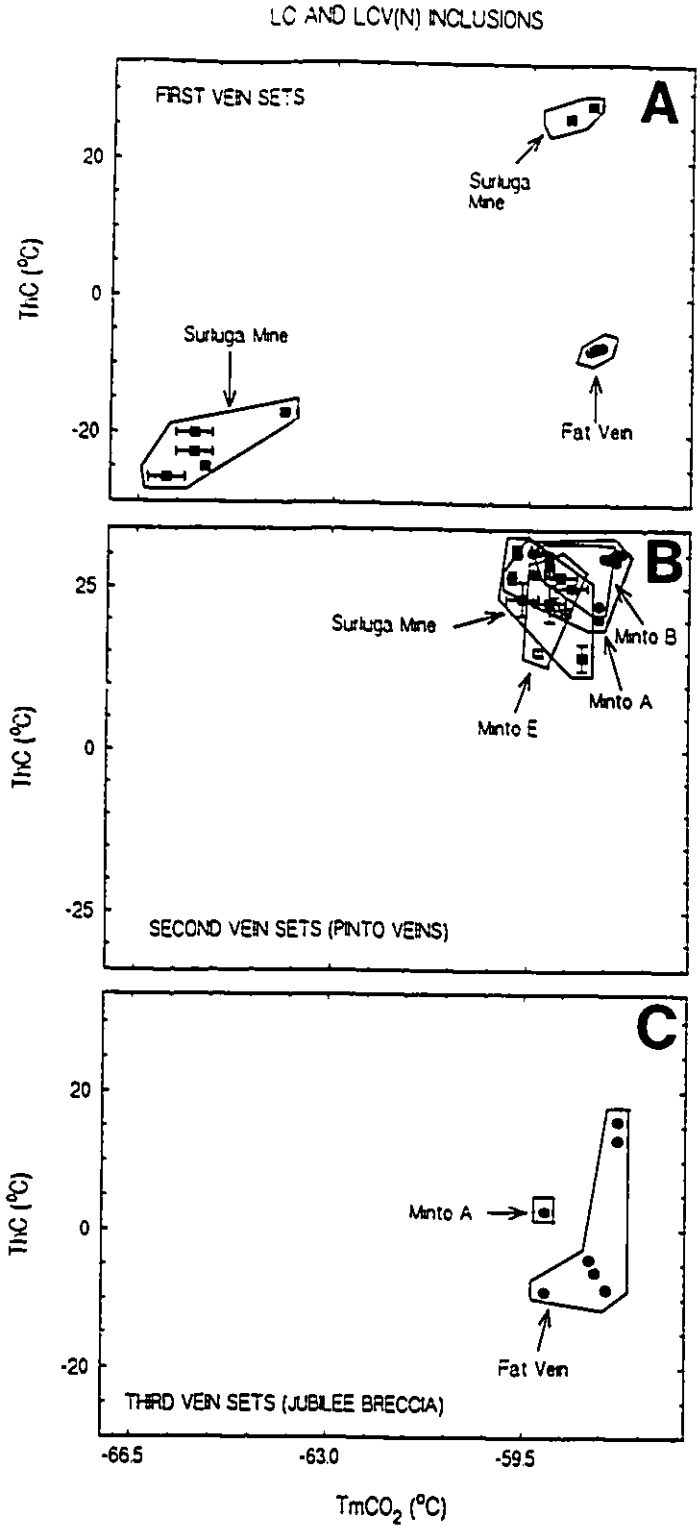

Figure 34. ThC-$TmCO_2$ plots of LC and LCV(N) inclusions in (A) vein set 1, (B) vein set 2, and (C) vein set 3.

Where possible, homogenization of the non-aqueous portion of an inclusion (ThC) was observed both in the presence (ThC^*) and absence (ThC) of clathrate by using the temperature-cycling technique described by Seitz et al. (1987). The non-aqueous portion of many LCV(N) inclusions homogenized above the clathrate melting temperature so that ThC^* could not be measured. ThC and ThC^* were occasionally measured in the same inclusion. Homogenization in the presence of clathrate (ThC^*) was only clearly observed in LC inclusions from vein sets 1 and 3 in the Fat Vein zone. ThC^* values for these inclusions ranged from 7.5 to 8.1°C in vein set 1 and from 2.1 to 7.8°C in vein set 3 (Table 11). ThC values for the same inclusions ranged from -7.5 to -6.9°C and from -8.7 to 15.7°C, respectively (Figure 34 A and C).

For most of the inclusions with a two-phase (liquid and vapor) carbonic fluid at room temperature, only ThC values were obtained, which ranged from 22.2 to 31°C (Figure 34). Except in cases where ThC was greater than or equal to 30.5°C, the non-aqueous portion of most LCV(N) inclusions homogenized to the liquid phase (Table 11).

ThC values are generally high (13 to 31°C) for inclusions in all of the vein sets, with the exception of those in vein set 1 from the Surluga Mine (-27 to -17°C); and those in vein sets 1 and 3 in the Fat Vein Zone (-8.9 to -4.2°C) (Figure 34).

Temperatures of total homogenization (ThTOT) were obtained from only a few inclusions as most inclusions decrepitated at temperatures of between 136 and 266°C, before final homogenization. Values of ThTOT ranged from 185 to 365°C (Figure 35). Only two ThTOT values were obtained from the primary LC inclusions in growth-zoned quartz (vein set 3) in the Fat Vein zone. These values are 185 and 187°C (Figure 35). A few total homogenization temperatures were obtained on the low-$TmCO_2$ inclusions and range from 269 to 365°C (Figure 35). All of the LC and LCV(N) inclusions from the Minto B and E zones decrepitated at temperatures of between 160 and 195°C (Table 11). For LCVN inclusions with nahcolite, values of TdDM ranged from 138 to 156°C (Table 11).

Inclusions with low $TmCO_2$ (-66 to -63.9°C) and low ThC (-26.2 to -17°C) occur exclusively in vein set 1 from the Surluga Mine. In some cases, these inclusions occur in the same plane as CV inclusions with low $TmCO_2$ and ThC, indicating that the two types are related through necking. In contrast, inclusions with high $TmCO_2$ (-59.8 to -57.8°C) and high ThC (-8.6 to 30.7°C) occur in all vein sets. Where this latter type occur together with LVN inclusions, they may contain nahcolite, indicating that these two inclusion types are closely related. Moderately low ThC values (-7.8 to -6.8°C) in

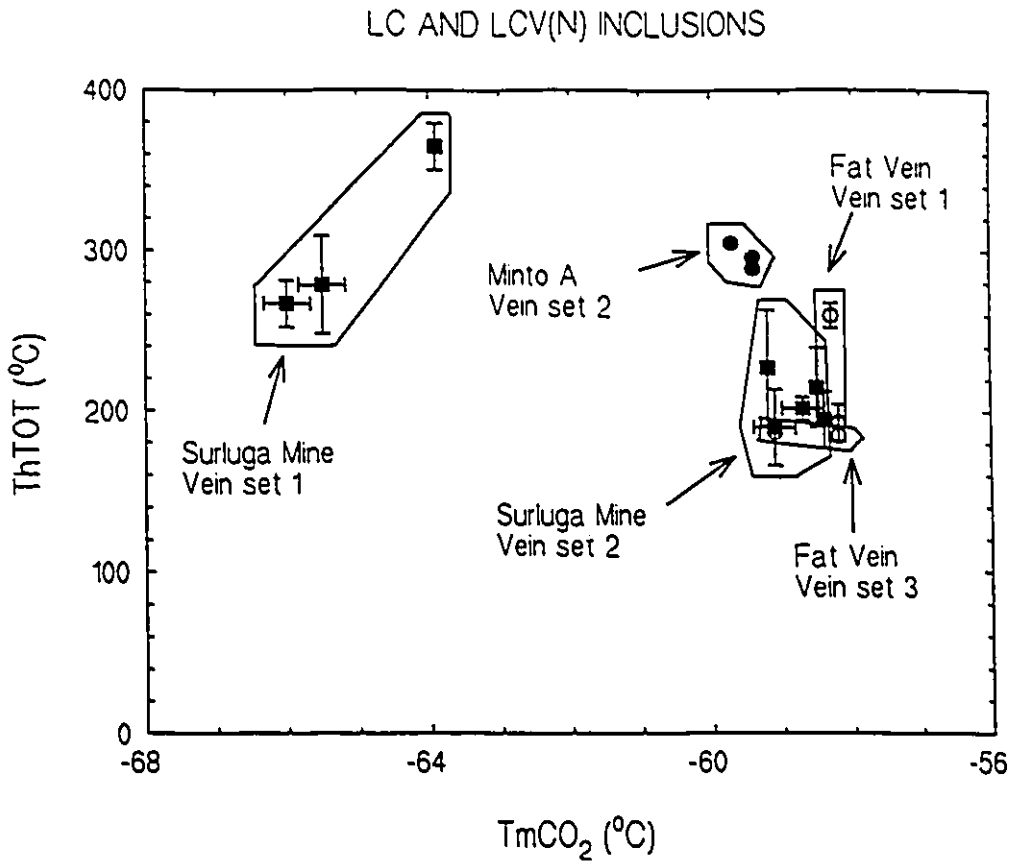

Figure 35. ThTOT-$TmCO_2$ plot of LC and LCV(N) inclusions from all vein sets.

the high-$TmCO_2$ inclusions were only observed in the primary inclusions from vein set 3 in the Fat Vein zone (Figure 34C).

Most of the LCV(N) inclusions in vein sets 1 and 2 in the Surluga Mine, and in vein set 2 from the Minto A, B and E zones have very similiar $TmCO_2$ and ThC values of between -59.3 and -58.4°C, and between 26.3 and 30.8°C, respectively (Figure 34 A and B). The primary LC inclusions in vein set 3 from the Fat vein zone have similiar $TmCO_2$ values as those in other vein sets, ranging from -59.1 to -57.8°C (Figure 34C).

Fluid Compositions

The bulk fluid compositions of LC and LCV(N) inclusions are given in Table 12 and in Figure 36.

Values of XH_2O range from 0.47 to 0.96, with most values between 0.74 and 0.96 (Table 12, Figure 36). Values of XH_2O for inclusions in vein set 2 from the Surluga Mine and Minto A, B and E zones are very similar, and range from 0.91 to 0.96 (Figure 36B).

Table 12. Bulk Compositions of LC and LCV(N) Fluid Inclusions

Incl	nH2O	nCO2	nCH4	nN2	XH2O	XCO2	XCH4	XN2
MINTO A ZONE - VEINSET 2								
A1	0.05	0.00	0.00	0.00	0.95	0.05	0.00	0.00
A3	0.05	0.00	0.00	0.00	0.94	0.05	0.00	0.00
A5	0.05	0.00	0.00	0.00	0.94	0.06	0.00	0.00
B2	0.04	0.00	0.00	0.00	0.89	0.10	0.01	0.00
B3	0.04	0.00	0.00	0.00	0.94	0.06	0.00	0.00
C1	0.05	0.00	0.00	0.00	0.93	0.07	0.00	0.00
C4	0.05	0.00	0.00	0.00	0.94	0.06	0.00	0.00
D3	0.05	0.00	0.00	0.00	0.92	0.08	0.00	0.00
D4	0.05	0.00	0.00	0.00	0.94	0.06	0.00	0.00
E2	0.05	0.00	0.00	0.00	0.93	0.07	0.00	0.00
FAT VEIN - VEINSET 1								
A1	0.09	0.00	0.00	0.00	0.96	0.04	0.00	0.00
A2	0.08	0.02	0.00	0.00	0.76	0.24	0.00	0.00
FAT VEIN - VEINSET 3								
B1	0.07	0.02	0.00	0.00	0.75	0.25	0.00	0.00
B2	0.07	0.02	0.00	0.00	0.75	0.25	0.00	0.00
B5	0.08	0.02	0.00	0.00	0.77	0.23	0.00	0.00
B6	0.05	0.02	0.00	0.00	0.66	0.34	0.00	0.00
B7	0.06	0.02	0.00	0.00	0.71	0.29	0.00	0.00
B9	0.05	0.02	0.00	0.00	0.65	0.35	0.00	0.00
SURLUGA MINE - VEINSET 1								
A1	0.04	0.01	0.00	0.00	0.83	0.16	0.01	0.00
B1	0.06	0.00	0.00	0.00	0.95	0.05	0.00	0.00
C1	0.04	0.01	0.00	0.00	0.78	0.16	0.05	0.00
C2	0.05	0.01	0.00	0.00	0.82	0.14	0.04	0.00
C4	0.04	0.01	0.00	0.00	0.78	0.17	0.03	0.02
C5	0.04	0.01	0.00	0.00	0.78	0.15	0.06	0.01
C6	0.04	0.01	0.00	0.00	0.74	0.19	0.06	0.01
SURLUGA MINE - VEINSET 2								
Q3	0.04	0.00	0.00	0.00	0.91	0.09	0.00	0.00
Q5	0.04	0.00	0.00	0.00	0.89	0.11	0.00	0.00
Q7	0.03	0.01	0.00	0.00	0.83	0.17	0.00	0.00
S4	0.04	0.01	0.00	0.00	0.86	0.13	0.01	0.00
S5	0.05	0.00	0.00	0.00	0.93	0.06	0.00	0.00
MINTO B - VEINSET 2								
A1	0.04	0.00	0.00	0.00	0.93	0.07	0.00	0.00
A2	0.04	0.00	0.00	0.00	0.94	0.06	0.00	0.00
A4	0.04	0.00	0.00	0.00	0.94	0.06	0.00	0.00
A6	0.04	0.00	0.00	0.00	0.93	0.07	0.00	0.00
A7	0.04	0.00	0.00	0.00	0.91	0.09	0.00	0.00

Table 12 (continued)

Incl	nH2O	nCO2	nCH4	nN2	XH2O	XCO2	XCH4	XN2
MINTO B - VEINSET 2								
B1	0.04	0.00	0.00	0.00	0.93	0.07	0.00	0.00
B2	0.04	0.00	0.00	0.00	0.91	0.09	0.00	0.00
B4	0.05	0.00	0.00	0.00	0.94	0.06	0.00	0.00
B5	0.05	0.00	0.00	0.00	0.96	0.04	0.00	0.00
B7	0.05	0.00	0.00	0.00	0.95	0.05	0.00	0.00
B8	0.05	0.00	0.00	0.00	0.93	0.07	0.00	0.00
MINTO E								
K1	0.04	0.01	0.00	0.00	0.80	0.19	0.00	0.01
K2	0.01	0.01	0.00	0.00	0.47	0.53	0.00	0.00
K3	0.07	0.00	0.00	0.00	0.94	0.06	0.00	0.00
K4	0.06	0.00	0.00	0.00	0.93	0.07	0.00	0.00
L3	0.06	0.00	0.00	0.00	0.92	0.08	0.00	0.00
L4	0.06	0.00	0.00	0.00	0.92	0.08	0.00	0.00
S1	0.06	0.01	0.00	0.00	0.92	0.08	0.00	0.00

LC inclusions in vein set 3 from the Fat Vein zone have overall lower XH_2O values than those above, that range from 0.65 to 0.82, with most values between 0.65 and 0.77 (Figure 36C). Inclusions in vein set 2 from the Surluga Mine have higher XH_2O (0.83-0.93) than those in vein set 1 (0.74-0.83) (Figure 36 A and B).

XCO_2 variations of LC and LCV(N) inclusions from different vein sets and zones essentially mimic the patterns shown by XH_2O, as for most inclusions the relationship $XCO_2 = 1 - XH_2O$ is valid (Figure 36). XCH_4 values range from 0 to 0.06, with the highest values restricted to the inclusions in vein set 1 from the Surluga Mine (0-0.06) (Table 12, Figure 37A). N_2 was only detected in a few samples, most of which came from vein set 1 in the Surluga Mine. XN_2 values range from 0 to 0.01 (Table 12, Figure 37B).

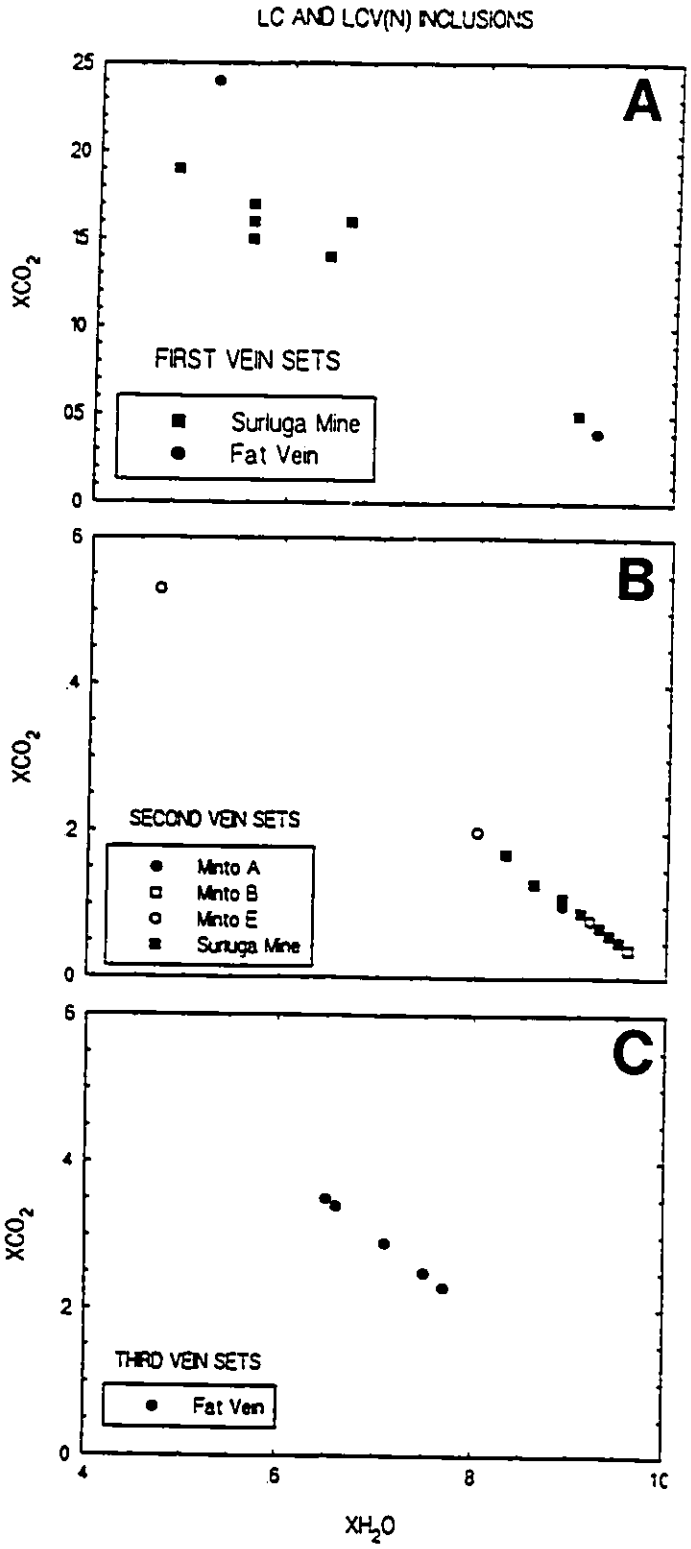

Figure 36. XCO_2-XH_2O plots of LC and LCV(N) inclusions in (A) vein set 1, (B) vein set 2, and (C) vein set 3.

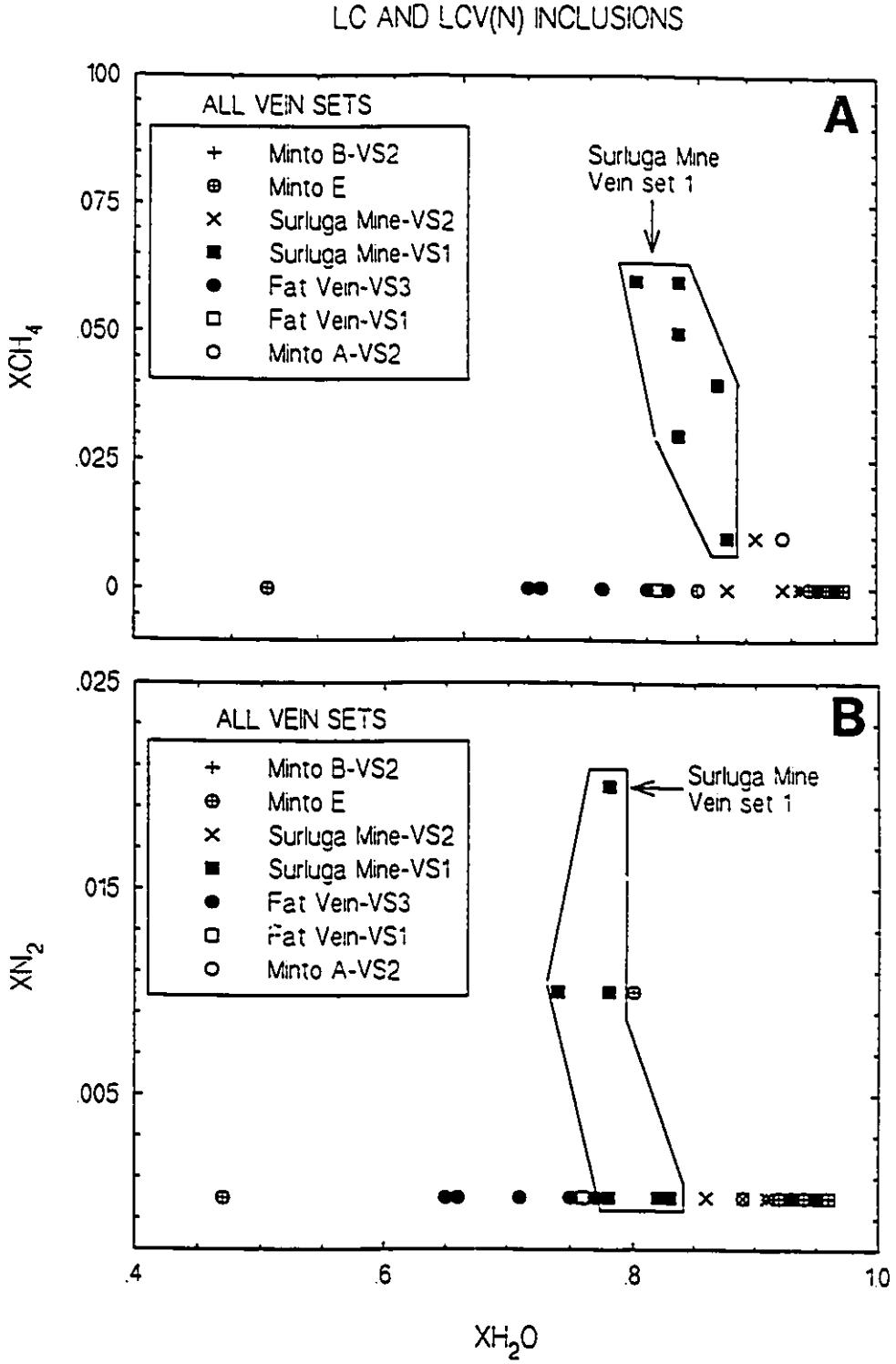

Figure 37. (A) XCH_4-XH_2O and (B) XN_2-XH_2O plots of LC and LCV(N) inclusions in all vein sets.

3.3.6. CV Inclusions

Table 6 contains a summary of the petrographic characteristics of CV inclusion arrays. CV inclusions occur in dense, extensive planar arrays, as negative crystal-shaped inclusions (Figure 38). These inclusions are generally small, usually ranging in size from 1 to 10 μm. The planes which contain CV inclusions are usually dispersed among the planar arrays containing LVN and LCVN inclusions. Where CV and LCVN inclusions occur in the same planar arrays, CV inclusions probably resulted from necking of LCVN inclusions. These inclusions were only observed in vein set 2 from the Surluga Mine (Table 6).

Raman Spectroscopy and Fluid Compositions

Table 13 shows Raman spectroscopy results on CV inclusions, along with selected microthermometry data. XCO_2 values for CV inclusions fall within a narrow range from 0.93 to 1.00. XCH_4 values range from 0 to 0.07 (Table 13, Figure 39). No N_2 was detected in these inclusions.

Microthermometric Results

Table 14 summarizes the microthermometric results obtained on CV inclusions. Values of $TmCO_2$ fall within a narrow range from -59 to -57.4°C (Table 14, Figure 40). These inclusions homogenize to the liquid phase at temperatures of between 11.4 and 28.7°C, with most values between 25.4 and 28.7°C (Figure 40).

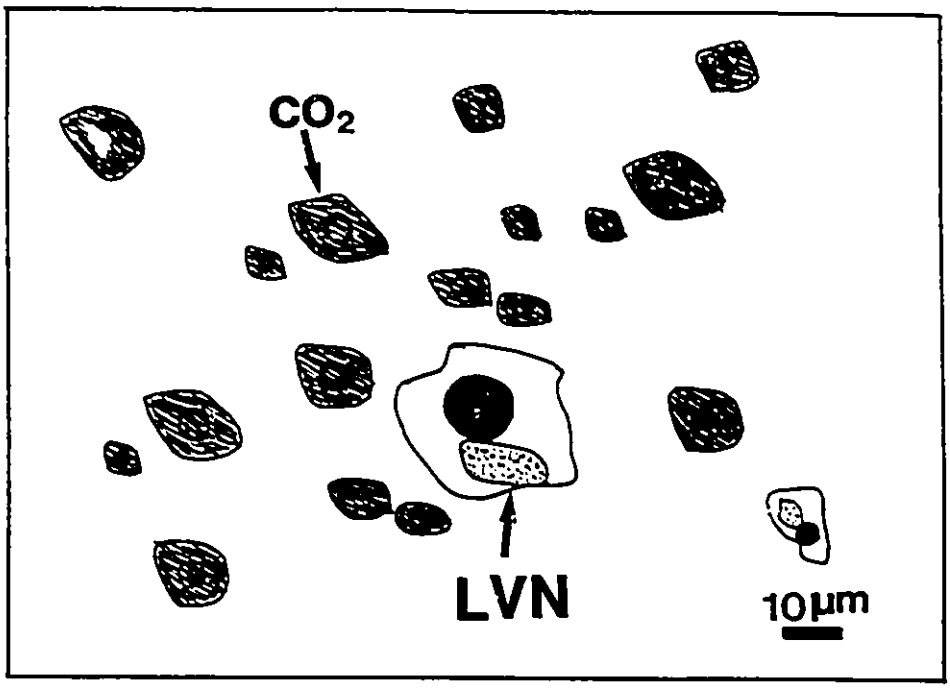

Figure 38. Precise drawing of CV inclusions in quartz in vein set 2 from the Surluga Mine.

Table 13. Microthermometry and Raman Data for CV inclusions

Incl.	Sample #	Type	TmCO2	ThC	XCO2*	XCH4*	XN2*
SURLUGA MINE - VEINSET 2							
T1	IS89-64	5	-58.6	23.7(l)	0.93	0.07	0.00
T2	IS89-64	5	-58.5	24.2(l)	0.97	0.03	0.00
T3	IS89-64	5	-57.8	27.6(l)	1.00	0.00	0.00
U1	IS89-63	5	-58.0	23.4(l)	1.00	0.00	0.00
U2	IS89-63	5	-58.3	26.5(l)	1.00	0.00	0.00
U3	IS89-63	5	-58.7	24.8(l)	0.97	0.03	0.00
V1	IS89-63	5	-58.6	25.5(l)	0.95	0.05	0.00
V2	IS89-63	5	-57.9	27.5(l)	0.98	0.02	0.00

* calculated from Raman analyses
l = homogenization into the liquid phase

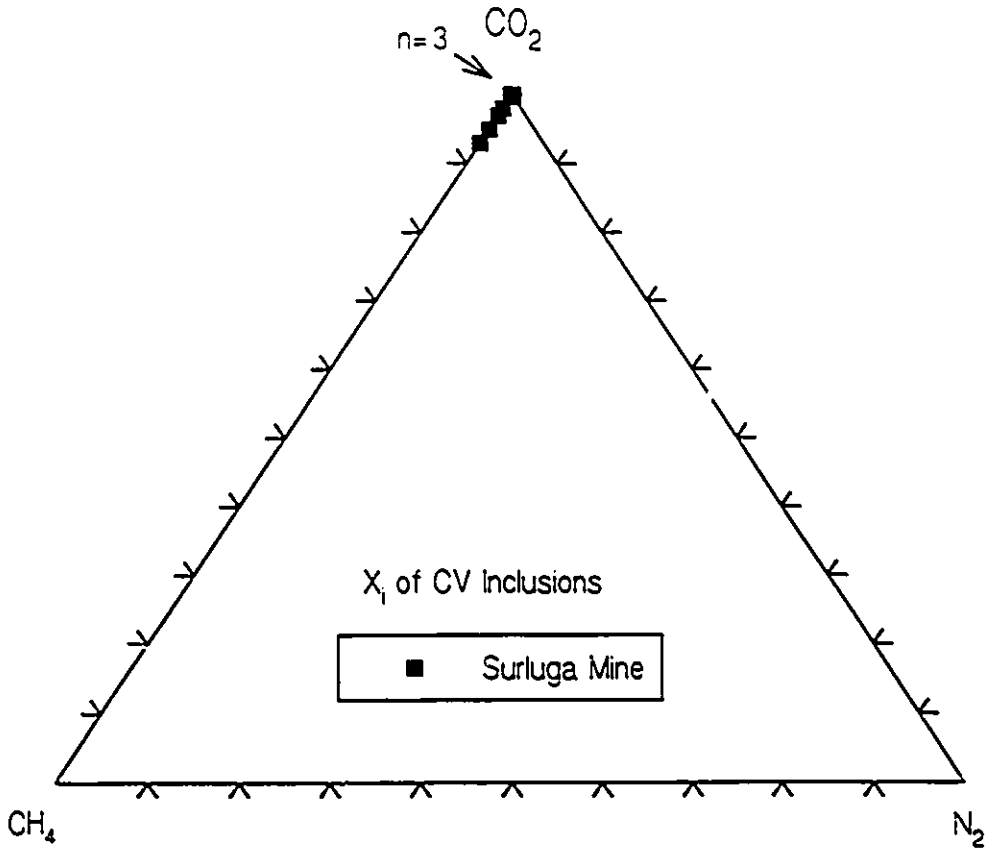

Figure 39. Molecular proportions (X_i) of CO_2, CH_4, and N_2 in CV inclusions as determined by Raman analyses.

Table 14. Summary of Microthermometry Data for CV Fluid Inclusions

SAMPLE	MIN	SET	TYPE	ORIG	#	TfC	Te ave	Te sd	TmCO2 ave	TmCO2 sd	ThC ave	ThC sd
SURLUGA MINE - VEINSET 2												
IS89-63	CQ	1	CV	S	5	-90	-	-	-57.4	0	11.4	1
IS89-63	CQ	2	CV	S	3	-93	-	-	-58.6	0	27	0
IS89-64	CQ	1	CV	S	5	-93	-	-	-58.4	0	28.7	0.4
IS89-64	CQ	2	CV	S	2	-98	-	-	-58.0	0	25.8	0
IS89-64	CQ	3	CV	S	4	-100	-	-	-57.7	0	25.4	1.9
IS89-64	CQ	4	CV	S	3	-98	-	-	-57.9	0	27	0

ORIG=origin of inclusion; MIN=host mineral; SET=co-genetic group of inclusions
CQ=coarse quartz; #=number of inclusions in co-genetic group

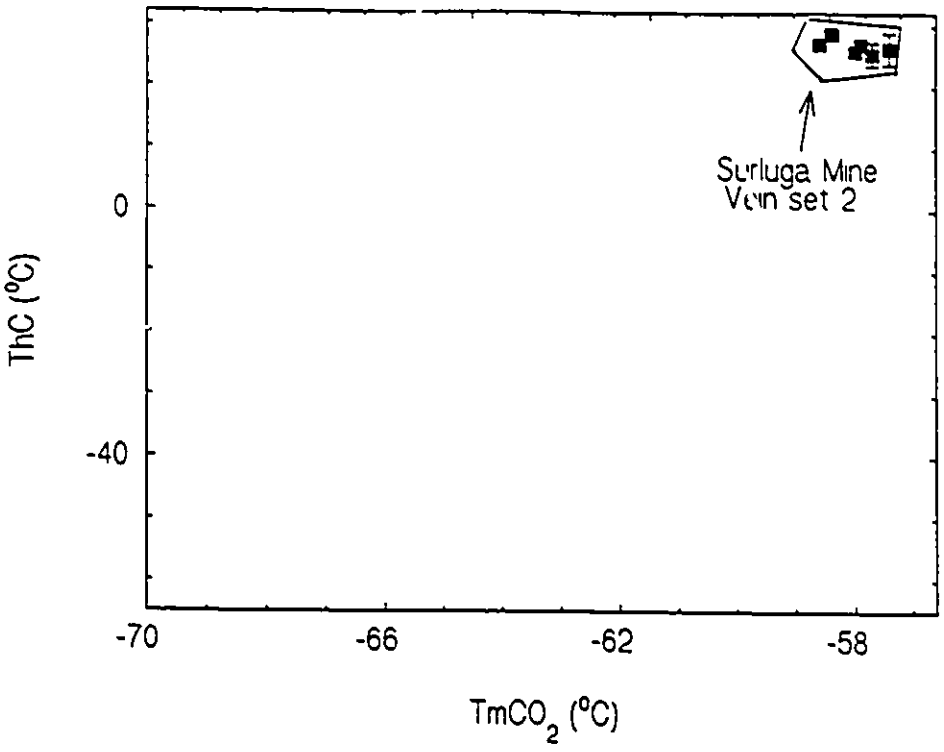

Figure 40. ThC-$TmCO_2$ plot of CV inclusions.

3.3.7. V Inclusions

V inclusions are very abundant (approx. 80% of total inclusion population) in samples IS89-70A, IS89-70B and S280-613, all from vein set 1 in the Surluga Mine (Table 6). In a visible gold-bearing sample (IS89-70A), V inclusions occur on intracrystalline planes, along with a large subhedral gold grain (Figure 41).
V inclusions are also present in the second vein sets from the Minto B and E zones. These inclusions occur on planes in all orientations and sizes, and usually have negative crystal or globular shapes. Because of their large size (usually > 15μm), they were fully characterized using both microthermometry and Raman spectroscopy.

Raman Spectroscopy and Fluid Compositions

Table 15 contains the Raman spectroscopic results for V inclusions, along with the microthermometric data on inclusions on which Raman data were obtained.

In vein set 1 from the Surluga Mine, three different compositional groups can be identified on the basis of XCO_2, XCH_4 and XN_2:

1) a CO_2-rich group with minor CH_4 and no N_2,

Table 15. Microthermometry and Raman Data for V Inclusions

Incl.	Sample #	Type	TmCO2	ThC	XCO2*	XCH4*	XN2*
SURLUGA MINE - VEINSET 1							
L1	IS89-70B	6	-58.7	5.8(l)	0.98	0.02	0.00
L2	IS89-70B	6	-59.3	3.5(l)	0.95	0.05	0.00
M1	IS89-70A	6	-65.3	-21.0(l)	0.73	0.20	0.07
M2	IS89-70A	6	-64.9	-20.5(l)	0.65	0.28	0.07
M3	IS89-70A	6	-66.0	-25.1(l)	0.60	0.32	0.08
M4	IS89-70A	6	-65.2	-20.6(l)	0.60	0.35	0.05
M5	IS89-70A	6	-64.9	-23.8(l)	0.71	0.25	0.04
N1	S280-613	6	-	-	0.00	1.00	0.00
N2	S280-613	6	-	-89.0(v)	0.07	0.76	0.17
N3	S280-613	6	-	-83.5(v)	0.04	0.86	0.10
N4	S280-613	6	-	-	0.00	1.00	0.00
N5	S280-613	6	-	-	0.00	1.00	0.00
MINTO B - VEINSET 2							
Q1	IS90-43	6	-59.3	13.2(l)	0.95	0.05	0.00
Q2	IS90-43	6	-59.0	3.6(l)	0.98	0.02	0.00
Q3	IS90-43	6	-59.1	11.5(l)	1.00	0.00	0.00
MINTO E							
G3	IS90-53B	6	-58.4	13.4(l)	1.00	0.00	0.00
G4	IS90-53B	6	-59.2	18.3(l)	0.98	0.02	0.00
G5	IS90-53B	6	-59.4	15.6(l)	0.95	0.05	0.00
G6	IS90-53B	6	-58.4	19.9(l)	1.00	0.00	0.00
I5	IS90-53C	6	-58.3	8.9(l)	0.99	0.01	0.00
I6	IS90-53C	6	-58.2	9.4(l)	1.00	0.00	0.00
J1	IS90-53B	6	-58.4	17.3(l)	0.96	0.04	0.00
J2	IS90-53B	6	-58.3	18.6(l)	1.00	0.00	0.00

* calculated from Raman analyses
l and v = homogenization into the liquid and vapor phases
n.v. not visible

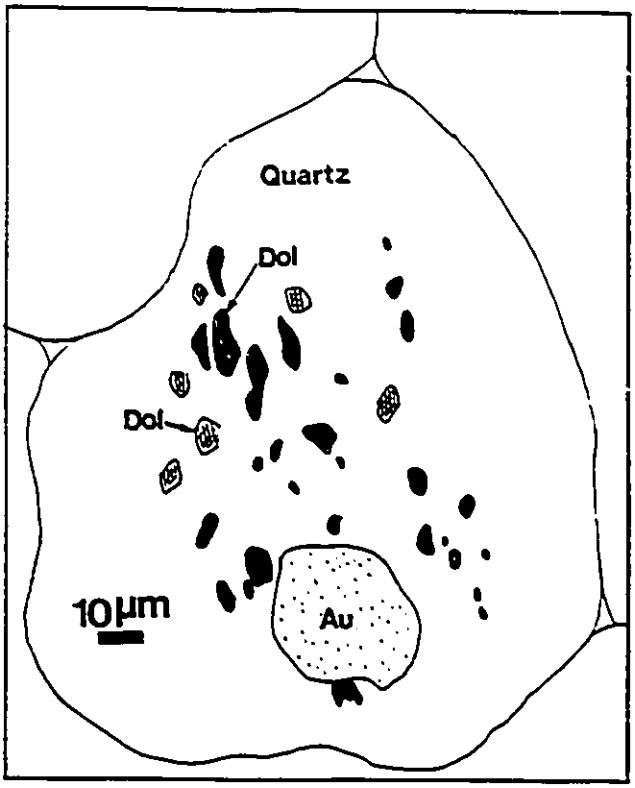

Figure 41. Precise drawing of V inclusions in gold-bearing quartz vein (vein set 1) from the Surluga Mine. Au = gold, Dol = Fe-dolomite.

XCO_2 in this group ranges from 0.95 to 0.98, and CH_4 from 0.02 to 0.05 (Table 15, Figure 42).

2) a CO_2-rich group with significant CH_4 and minor N_2, XCO_2 of this group ranges from 0.60 to 0.73, XCH_4 from 0.20 to 0.35 and XN_2 from 0.04 to 0.08 (Table 15, Figure 42). This group corresponds to the low-TmCO_2/low-ThC V inclusions (see below).

3) a CH_4-rich group with significant N_2 and minor CO_2, XCO_2 of this group falls within a narrow range between 0 and 0.07; XCH_4 from 0.76 to 1, and XN_2 from 0 to 0.17 (Table 15, Figure 42).

V inclusions which occur in vein set 2 (Pinto veins) from the Minto B and E zones have XCO_2 values of between 0.95 and 1, and XCH_4 values of between 0 and 0.05 (Table 15, Figure 42). No N_2 was detected in these inclusions. These inclusions have similiar compositions to the first group of inclusions described above from the Surluga Mine.

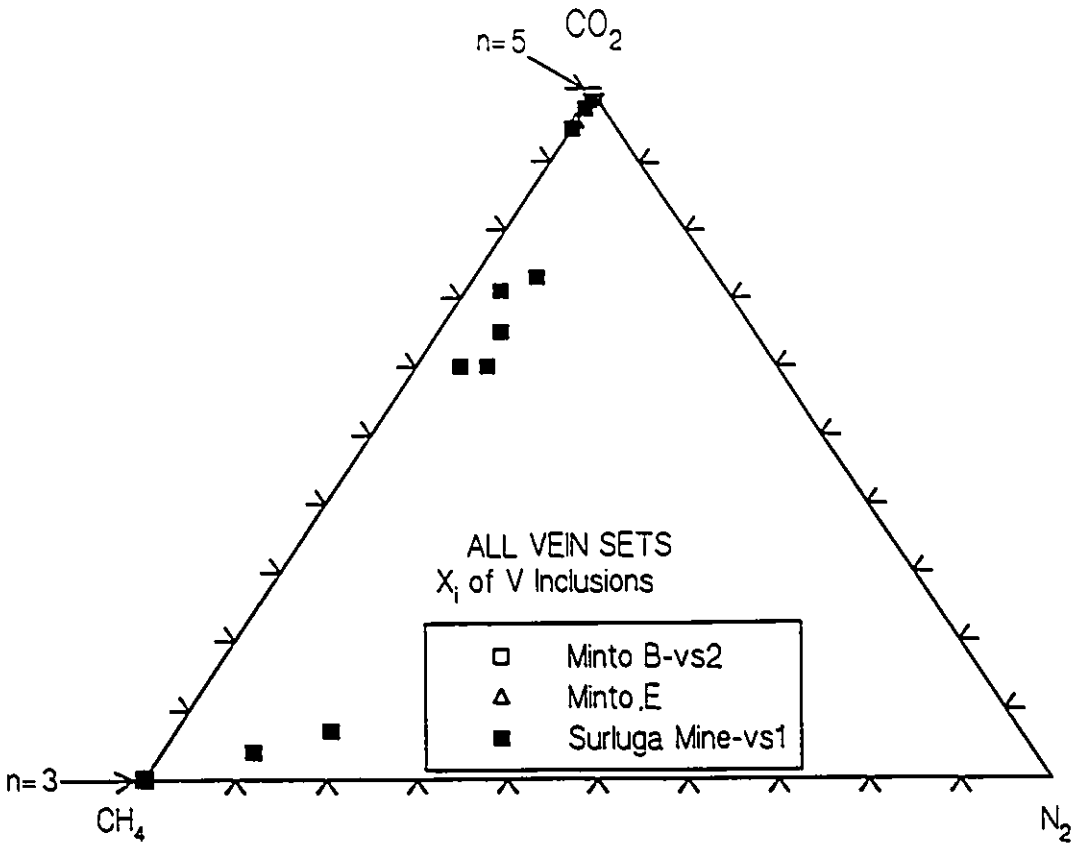

Figure 42. Molecular proportions (X_i) of CO_2, CH_4 and N_2 in V inclusions, as determined by Raman analyses. Note that all Minto inclusions fall on the CO_2 apex.

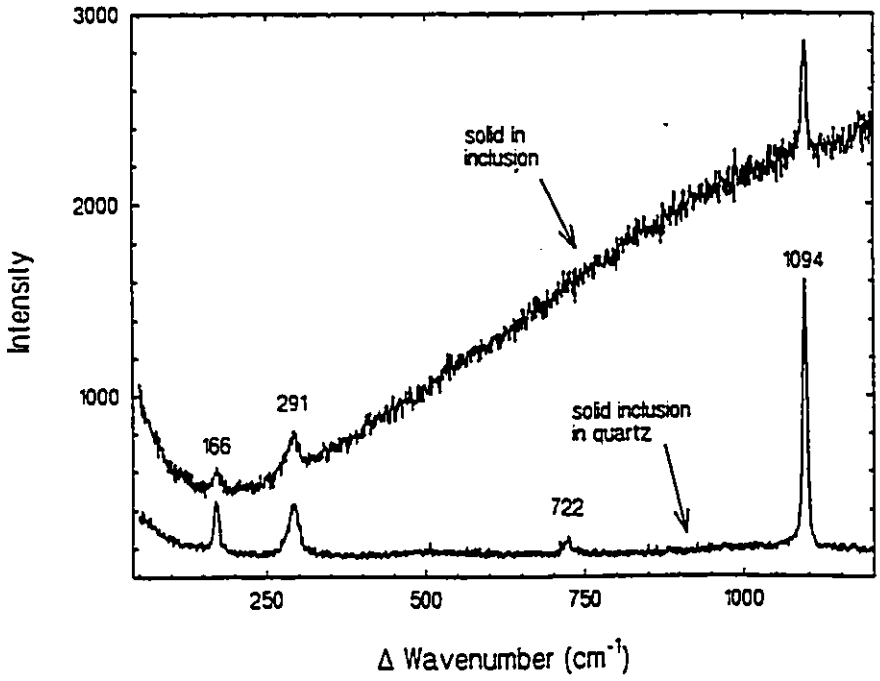

Figure 43. Raman spectra of Fe-dolomite both as a solid inclusion in quartz and as a solid (trapped phase ?) within V inclusion in quartz vein with visible gold (vein set 1) from the Surluga Mine.

In some V inclusions (less than 5% of a given group), volumetrically small amounts (less than 1% of the total inclusion volume) of an aqueous liquid occur as thin rims around the carbonic phase. This aqueous liquid was not considered in calculating bulk fluid-composition, and the resultant errors are negligible.

A few V inclusions in sample IS89-70A from vein set 1 in the Surluga Mine contain Fe-dolomite. Fe-dolomite also replaces quartz in the sample, along grain-boundaries and microfractures. The Raman spectra of Fe-dolomite in the fluid inclusion and in the quartz host are shown in Figure 43. The bands at 171, 292, 722 and 1095 cm^{-1} correspond to those of dolomite (Griffith, 1975), however an Fe component is inferred on the basis of hematized nature and brownish colour of dolomite. Some V inclusions from the Minto E zone contain a very small (much less than 5 μm), highly birefrengent solid. Raman analysis of this solid was unsuccessful.

Microthermometric Results

Table 16 and Figure 44 summarize the microthermometric results obtained on V inclusions.

V inclusions are identified by their characteristic phase behavior upon cooling down to -25°C, which involves the nucleation of a vapour phase within an originally homogeneous, one-phase "vapour-rich" inclusion. Eutectic temperatures were obtained in a few cases, and ranged from -101 to -65°C (Table 16). Values of $TmCO_2$ ranged from -67 to -57.6°C (Figure 44). These inclusions are divided into two groups on the basis of their $TmCO_2$ values: 1) inclusions with low $TmCO_2$ values (-67 to -64.9°C (Table 16, Figure 44), and 2) inclusions with high $TmCO_2$ values (-59.3 to -57.6°C) (Table 16, Figure 44).

V inclusions homogenize to the liquid phase between -55 and 7.5°C. Homogenization of low-$TmCO_2$ inclusions occurred between -55 and -11°C to the liquid phase (Figure 44), indicating high fluid densities and/or high concentrations of CH_4 and/or N_2. Homogenization of high-$TmCO_2$ inclusions occurred to the liquid phase between 1.3 and 7.5°C (Figure 44). Low ThC values were only observed in the inclusions with very low $TmCO_2$ values (-67 to -65°C) (Figure 44).

The phase behavior of the V inclusions observed in sample S280-613 is very different from those described above. Most of the inclusions in this sample do not show any phase change upon cooling down to about -150°C (practical limit of the stage). Where observed, the only phase change in these inclusions during cooling was the condensation of minor amounts of liquid at temperatures near -135°C, but freezing of

Table 16. Summary of Microthermometry Data for V Fluid Inclusions

SAMPLE	MIN	SET	TYPE	ORIG	#	TfC	Te		TmCO2		ThC	
							ave	sd	ave	sd	ave	sd
MINTO B - VEINSET 2												
IS90-43	FQ	1	V	S	4	-76	-	-	-59.3	0	12.9	1.9
IS90-43	FQ	2	V	S	8	-98	-	-	-59.4	0	7.3	4.7
IS90-43	FQ	3	V	S	8	-100	-	-	-59.2	0	11.0	5.5
MINTO E												
IS90-53	CQ	1	V	S	3	-94	-	-	-58.3	0	16.7	0.5
IS90-53	CQ	2	V	S	3	-99	-	-	-58.9	0.2	14.5	0.3
IS90-53	CQ	3	V	S	5	-98	-	-	-58.5	0	14.3	0.1
IS90-53	CQ	4	V	S	4	-98	-	-	-58.5	0	15.2	0
IS90-53	CQ	5	V	S	11	-99	-	-	-58.6	0.1	17.9	0.03
IS90-53	CQ	6	V	S	3	-98	-	-	-58.4	0	19.9	0
IS90-53	CQ	7	V	S	2	-96	-	-	-58.4	0	7.6	0.05
IS90-53	CQ	8	V	S	9	-100	-	-	-60.2	0	4.2	0.1
SURLUGA MINE - VEINSET 1												
S280-61	CQ	1	V	S	15	-	-	-	-	-	-89	0.5
IS89-70	CQ	1	V	S	4	-96	-	-	-59.3	0.1	2.2	0.55
IS89-70	CQ	2	V	S	4	-96	-	-	-58.9	0	4.7	0.5
IS89-70	CQ	3	V	S	4	-96	-65	0	-59.3	0	1.3	0.3
IS89-70	CQ	4	V	S	16	-99	-	-	-57.8	0	7.5	0.7
IS89-70	CQ	5	V	S	8	-	-	-	-57.8	0	5.4	1.1
IS89-70	CQ	1	V	S	13	-98	-	-	-59.1	0	3.9	0.6
IS89-70	CQ	2	V	S	4	-98	-	-	-58.3	0	2.7	0
IS89-70	CQ	3	V	S	6	-100	-	-	-57.6	0	3.1	0
IS89-70	CQ	4	V	S	7	-110	-101	2	-65.0	0	-21	0.1
IS89-70	CQ	5	V	S	10	-110	-96	0	-66.0	0.2	-26	0
IS89-70	CQ	6	V	S	21	-	-101	0.6	-66.0	0.2	-19	3.7
IS89-70	CQ	7	V	S	13	-115	-	-	-65.1	0	-20	1
IS89-70	CQ	8	V	S	4	-115	-	-	-66.0	0	-55	0
IS89-70	CQ	9	V	S	5	-110	-	-	-64.9	0.3	-21	2.5
IS89-70	CQ	10	V	S	10	-110	-	-	-65.2	0	-11	0.1
IS89-70	CQ	11	V	S	8	-111	-	-	-67.0	0	-54	1.1
IS89-70	CQ	12	V	S	5	-110	-	-	-66.0	0	-55	0
IS89-70	CQ	13	V	S	3	-117	-	-	-67.0	0	-54	1.1

ORIG=origin of inclusion; MIN=host mineral; SET=co-genetic group of inclusions
CQ=coarse quartz; #=number of inclusions in co-genetic group

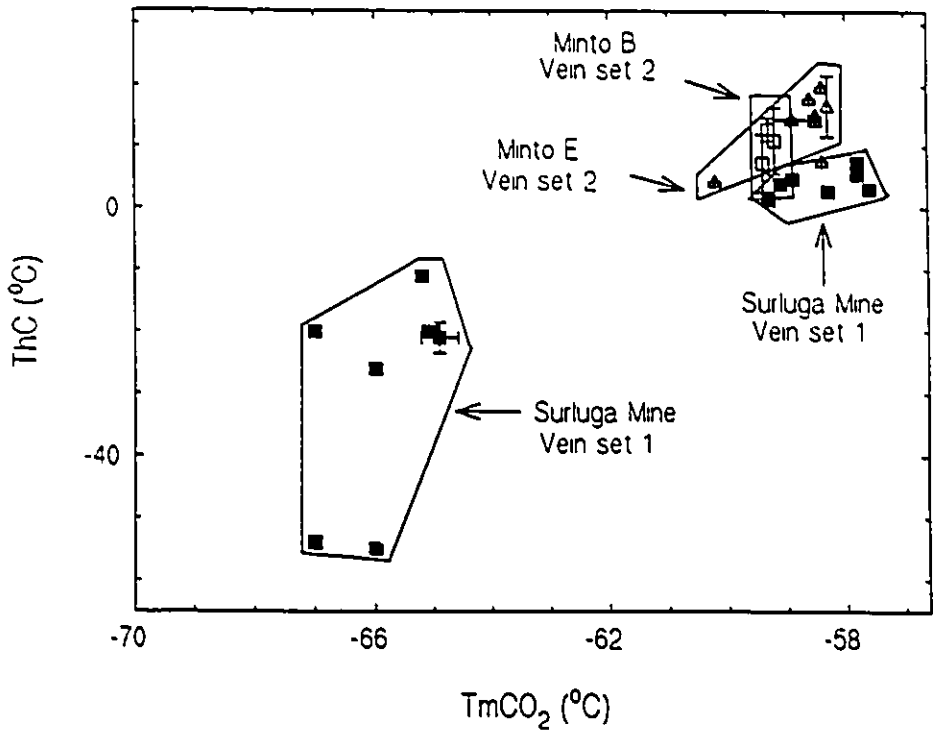

Figure 44. ThC-$TmCO_2$ plot of V inclusions.

the inclusion was not achieved even at very low temperatures. A few inclusions displayed homogenization to the vapor phase at temperatures ranging from -89 to -83°C (Table 16). These inclusions correspond to the third compositional group with high XCH_4 above (Figure 42).

3.4. Discussion of Fluid-Inclusion Results

3.4.1. Introduction

As pointed out earlier, most of the fluid inclusions observed in the quartz veins at Wawa are secondary in origin. However, the restriction of certain fluid inclusion types with particular vein sets suggests that these inclusions trapped fluids which were emplaced during a brittle deformation event (fracturing of quartz) in the quartz veins. Therefore, those secondary fluid-inclusion arrays occuring in a certain vein set may be spatially and temporally related to the fluids which were responsible for the fracture-healing in quartz.

3.4.2. LV Inclusions

LV inclusions can be divided into three groups on the basis of their salinity:

1) Relatively high salinity (18-23 equiv. wt.% NaCl) (low TmICE) inclusions which are only found in vein set 1 from the Surluga Mine and in vein set 3 from the Minto A zone (Figure 25 A and C). The restricted occurrence of these inclusions in these two vein sets suggests a genetic link between the inclusions and vein formation, and also between the vein sets.

2) Intermediate salinity inclusions (10-18 equiv. wt. % NaCl) which occur only in vein set 2 from the Surluga Mine and Minto zones (Figure 25B). The absence of these inclusions from the third vein sets indicates that they predate this vein set. Their restricted occurrence in the Pinto veins suggests a genetic link between this group to those veins, although their absence from vein set 1 in both the Fat Vein zone and the Surluga Mine may be an artifact of insufficient sampling of these veins.

3) Low salinity (~0-10 wt. % NaCl) (high TmICE) inclusions which occur in vein set 3 from the Surluga Mine and the Fat Vein zone and also in vein set 1 from the Fat Vein zone (Figure 25 A and C). The occurrence of secondary, low-salinity LV inclusions, and of primary H_2O-CO_2 inclusions in vein set 3 indicates that the low-salinity, aqueous fluid post-dates the formation of vein set 3. Low salinity LV inclusions in vein set 1 from the Fat Vein zone probably represent a late overprint.

3.4.3. LVN Inclusions

The range in salinity of the LVN inclusions is less than that of the LV inclusions, but some differences between vein sets and deformation zones still exist. LVN inclusions in vein set 1 from the Surluga Mine have relatively low TmICE values (high salinity), inclusions in vein set 2 from the Minto zones have intermediate TmICE values, and inclusions in vein set 1 from the Fat Vein zone have high TmICE values (low salinity) (Figure 29 A and B). These relative groupings are similiar to those described for the LV inclusions. An analogous pattern of TmICE distribution for LV and LVN inclusions is observed in the second vein sets from both the Surluga Mine and the Minto zones (compare Figures 25B and 29B). Despite the variations in TmICE, the occurrence of these nahcolite-bearing LVN inclusions in all of the deformation zones indicates that a similar fluid existed in all the zones. The absence of LVN inclusions from vein set 3 (Jubilee Breccia) in all the deformation zones indicates that the fluid that these inclusions trapped was introduced into the deformation zones prior to the emplacement of the third vein sets.

3.4.4. LC and LCV(N) Inclusions

The most significant aspect of LC and LCV(N) inclusions is that inclusions with relatively high XCH_4 (0.03-0.06) only occur in vein set 1 from the Surluga Mine (Figure 36A). In addition, these inclusions do not contain nahcolite. Similar inclusions in other vein sets have low XCH_4 values (0-0.01) (Figure 36).

Primary LC inclusions in vein set 3 (Jubilee Breccia) from the Fat Vein zone are notable in that they have high XCO_2 and low XCH_4 values (Figure 36). Similiar inclusions in vein set 1 from the Fat vein zone are probably an overprint from vein set 3 as they have the same $TmCO_2$ and ThC values (Figure 34 A and C).

LCV inclusions which occur in vein set 2 from the Surluga Mine, and the Minto zones mostly contain nahcolite as a daughter mineral, and therefore are probably related to the LVN inclusions. Such a relationship is obvious in some cases where LVN and LCVN inclusions occur in the same planar arrays, where they are probably related through necking.

LCVN inclusions in vein set 1 from the Surluga Mine are probably the result of overprinting from the fluid found in vein set 2 (Pinto veins). The absence of nahcolite from the primary LC inclusions in vein set 3 in the Fat Vein zone, along with their high XCO_2 values, suggests that these inclusions trapped a later, unrelated fluid.

3.4.5. CV Inclusions

CV inclusions are restricted to vein set 2 in the Surluga Mine, and are thus probably temporally related to this vein set. The microthermometric and Raman results obtained on these inclusions are very similar to those obtained on LCV(N) inclusions in vein set 2 (Figures 34, 36, 39 and 40). The absence of these inclusions in the early veins (vein set 1) may be explained if these inclusions originated through necking as they have fluid compositions identical to LCV(N) inclusions. The variable XCO_2 values (0.06-0.17) for LCVN inclusions in vein set 2 from the Surluga Mine (Figure 36B) may also be attributable to necking.

3.4.6. V Inclusions

Low-$TmCO_2$/high-XCH_4 V inclusions only occur in vein set 1 from the Surluga Mine (Figures 42 and 44). The absence of such inclusions in other vein sets and deformation zones may suggest that these inclusions are temporally related to this vein set. Field relationships suggest that vein set 1 in the Fat Vein zone is equivalent to the

auriferous, vein set 1 in the Surluga Mine (Samson and Holm, 1991). However, the fluid inclusion data does not support this contention, as vein set 1 in the Fat Vein zone lacks LC and V inclusions with high CH_4 content, and relatively high-salinity, aqueous, LV inclusions (Figures 25 and 42).

V inclusions with high XCH_4 values in the Surluga Mine may be related to the LC inclusions in the same vein set with comparable XCH_4 values, as is suggested by their similar microthermometric and Raman data (Figures 34A, 36A, 42 and 44).

CHAPTER IV
DISCUSSION OF HYDROTHERMAL FLUID CHARACTERISTICS OF AURIFEROUS SHEAR ZONES AT WAWA

4.1. Introduction

From an analysis of the petrographic data on alteration assemblages in the deformation zones, and of the fluid inclusion data from the quartz veins, it is clear that at least three temporally distinct fluids were introduced into the deformation zones in McMurray Township. Alteration effects which were accompanied by the introduction of these fluids can only be inferred for the first and last fluid infiltration events.

4.1.1. First Fluid-Infiltration Event

The earliest fluid was an aqueous-carbonic fluid of low salinity (4 to 7 wt.% NaCl, see below), containing up to 20 mole% CO_2 and $\leq$ 10 mole% CH_4+N_2. This early fluid is only observed in vein set 1 from the Surluga Mine. Three types of fluid inclusions appear to be restricted to vein set 1 in the Surluga Mine: 1) LC inclusions with high CH_4 content, 2) relatively high-salinity (18-23 equiv. wt.% NaCl), aqueous LV inclusions, and 3) high-XCH_4+N_2, V inclusions. The restricted occurrence of these fluid inclusion types in vein set 1 from the Surluga Mine may represent:

1) fluids derived from a low-salinity H_2O-CO_2-CH_4-N_2-salt fluid through fluid immiscibility, or
2) temporally different fluids associated with the episodic brittle fracturing of the early, quartz veins at the Surluga Mine.

The available fluid inclusion data fits the first model above best based on the following evidence: a) the "high" CH_4 content of the LC inclusions in vein set 1 from the Surluga Mine supports a link between these inclusions and the high-XCH_4 V inclusions in the same vein set, and b) the presence of the relatively high-salinity, aqueous LV inclusions in this vein set can be explained by fluid immiscibility, as during such fluid immiscibility, salt will be partitioned into the H_2O-rich phase; whereas CH_4, N_2 and, to a lesser extent, CO_2 will be partitioned into the vapour phase (Bowers and Helgeson, 1983; Holloway, 1984). In this fluid-immiscibility model, it is postulated that this parent fluid is represented by the high-XCH_4 LC inclusions, the salinity of which ranges from 4 to 7 wt. % NaCl. Whereas, the relatively high-salinity, aqueous LV inclusions and the high-XCH_4 V inclusions are interpreted to have been derived from the above parent fluid through fluid immiscibility.

In the second model (temporally distinct fluids), the interpreted parent fluid of the

first model above (i.e., low-salinity, high-XCH_4, LC inclusions), and the high-salinity, aqueous LV inclusions may represent a continuum in fluid composition. However, much higher salinity of the latter contradicts this model.

In Sample IS89-70A with visible gold, randomly-oriented trails of V inclusions yielded quite different homogenization temperatures, which can not be accounted for by necking, but can be explained if individual trails represented temporally different (episodic) brittle fracturing and fluid-infiltration events (Robert and Kelly, 1987). Robert and Kelly (1987) attributed such trails of variable fluid densities to fluctuations of fluid pressure in the hydrothermal reservoir in a dynamic tectonic environment.

It is also important to note that LC and V inclusions with high XCH_4 values occur exclusively in the gold-bearing sample from vein set 1 in the Surluga Mine are associated with a significant amount of late Fe-dolomite alteration (replacement) of quartz in these veins. The Fe-dolomite occurs along fractures which also host the above inclusions. In contrast, similar inclusions with high XCO_2 but low XCH_4 values (0.95-0.98) were observed in sample IS89-70B, from the same vein set above, which shows no evidence of mineralization and late Fe-dolomite alteration. These observations suggest that gold mineralization is genetically (temporally) related to high-XCH_4 LC and V inclusions, and the late, Fe-dolomite alteration in the auriferous quartz veins.

Field relationships of the earliest veins (vein set 1) in the Fat Vein zone and Surluga Mine suggest that these veins are temporally related (Samson and Holm, 1991). On this presumtion it would be expected that these veins would have been infiltrated by the same early, gold-bearing fluids. However, the fluid inclusion data on vein set 1 from the Fat Vein zone shows that these early fluids did not record this early fluid infiltration event. The different fluid histories of the early veins in the Jubilee Shear zone may suggest that these veins were formed at different times, and hence are not temporally equivalent. This also suggests that vein set 1 from the Surluga Mine were emplaced earlier than vein set 1 in the Fat Vein zone. This means that vein set 1 in the Fat Vein zone was emplaced after the earliest, auriferous fluid passed through the Jubilee Shear zone and deposited gold and sulphides in microfractures in the early quartz veins in the Surluga Mine. Alternatively, focussing of the early, auriferous fluids along the most permeable (most dilatant ?) segments of the Jubilee Shear zone might have happened. This may also suggest that the Fat Vein zone was not sufficiently permeable for fluid flow or that this zone was outside the focal point of the auriferous fluid discharge in the Jubilee Shear zone. This alternative model would also explain the lack of visible gold and sulphides in the early quartz veins in the Fat Vein zone. However, further fluid-

inclusion study of this vein set is required in order to test this model.

The absence of the early, auriferous fluids from the Pinto Veins (vein set 2) in the Jubilee and Minto deformation zones suggests that these early fluids were introduced into the Jubilee Shear zone before the emplacement of these veins. On the other hand, the absence of these fluids in the Minto zones suggests the early, auriferous fluids infiltrated only the Jubilee Shear zone and not the Minto deformation zones. This was probably due to higher permeability in the Jubilee shear zone compared to the Minto zones. For this question to be fully resolved, timing relationships between the main deformation zone and the other minor zones would have to be determined.

In the Surluga Mine, auriferous veins (V_1) are surrounded by hydrothermally-altered rocks which consist of muscovite-Fe-dolomite schists (A_1). These veins and the schists occur as vein-schist "packages" in the Mine (R. Rupert, pers. comm., 1990). Thus, the early, hydrothermal alteration is clearly vein-related. On the other hand, the restricted occurrence of high-XCH_4 LC and V, and relatively high-salinity, aqueous LV inclusions in the early, auriferous veins (V_1) suggests a genetic link between the early hydrothermal fluid and these veins. Therefore, it may be concluded from the above evidence that the early, auriferous fluids caused the A_1 alteration in the Jubilee Shear zone. However, the absence of these fluids in the Minto zones rules out any genetic link between the early, auriferous fluids and the early alteration (A_1) in those zones although the mineral assemblages in the Minto zones are very comparable to those in the Jubilee Shear zone. In general, the commonly observed alteration assemblages in the felsic schists (muscovite-Fe-dolomite-chlorite) and those in the mafic schists (chlorite-Fe-dolomite) are compatible with the infiltration of the deformation zones by a CO_2-H_2O fluid. On the other hand, the development of the similar alteration assemblages in different deformation zone suggests that these zones were formed penecontemporaneously and prior to the infiltration by an early, CO_2-H_2O fluid which caused the A_1 alteration in these discreet zones. However, the early, gold-depositing fluid appears to pre-date this fluid.

4.1.2. The Second Fluid-Infiltration Event

The second fluid is an aqueous fluid of low to moderate salinity (5 to 16 wt.% NaCl) with up to 10 mole % CO_2 and minor CH_4. These fluids also contained dissolved Na and HCO_3^{2-}, as is indicated by the presence of nahcolite as a daughter mineral. Moderate-salinity, aqueous LV and LVN inclusions, and low-XCH_4 LCV (no nahcolite) and LCVN inclusions represent this fluid. The absence of nahcolite-bearing

LVN and LCVN inclusions in vein set 3 in all deformation zones indicates that the fluid which was trapped in these inclusions was introduced before the emplacement of vein set 3 (Jubilee Breccia). This relationship is clear in the Fat Vein zone and the Surluga Mine, where vein sets 1 and 2 contain nahcolite-bearing LVN and LCVN inclusions, but vein set 3 (Jubilee Breccia) does not.

Most of the fluid inclusions which represent this second fluid were observed in the Pinto veins (vein set 2) in the Surluga Mine and Minto zones. They are particularly abundant (approx. 90% of total inclusions) in samples from the Minto E zone and Surluga Mine. As nahcolite is a common daughter mineral in fluid inclusions in carbonatites, it is likely that this second fluid is related to the emplacement of the lamprophyre-carbonatite dike suite associated with the nearby Firesand River carbonatite complex. Lamprophyre dikes are abundant in both the Minto E zone and the Surluga Mine, as revealed by field observations at the Minto E zone, and by drill-core records from the Surluga Mine. LVN and LCV(N) inclusions always occur in secondary planes in quartz, therefore a genetic link between the second fluid and lamprophyre dikes is possible. The lamprophyre dikes are commonly accompanied by fenitization (including late biotitic alteration) of the host rocks, suggesting a possible link between this alteration event and the second fluid.

From the above discussion it follows that the fluids which are related to LVN and LCVN inclusions were not responsible for the precipitation of the Pinto Veins (vein set 2) in the Jubilee and Minto deformation zones. Thus, it would appear that such fluids were not present in these veins. However, moderate-salinity, aqueous LV inclusions or low-XCH_4, LCV inclusions (without nahcolite) in vein set 2 could represent the fluids which precipitated these veins, although it appears that the LV inclusions are probably related to LVN inclusions because of their comparable salinity. Thus, the nature of the fluids responsible for the Pinto Veins is not known.

The Pinto veins do not display any visible alteration effects with the exception of pinkish (feldspathic ?) haloes at the vein-wallrock contacts. The nature of this alteration and the composition of the responsible fluids are not known.

4.1.3. The Third Fluid-Infiltration Event

The third fluid type is represented by a low-salinity (2-10 wt.% NaCl), aqueous fluid with significant amounts of CO_2 (XCO_2 = 0.23-0.35). This fluid is represented by primary, high-XCO_2/low-XCH_4, LC and LCV inclusions (without nahcolite) which occur exclusively in late, planar, undeformed quartz-ankerite veins (vein set 3) in the

Jubilee and Minto deformation zones (A and B).

The primary nature of LC inclusions in growth-zoned quartz from the Jubilee Breccia shows that these, late quartz-ankerite veins were precipitated from this third fluid. Late ankeritic and hematitic alteration associated with the Jubilee Breccias may also be attributed to this fluid.

In addition to the three fluid infiltration events above, there is also a very late fluid infiltration event (fourth ?) which post-dates the emplacement of the Jubilee Breccias. This fluid is represented by low-salinity (~0-11 equiv. wt. % NaCl), aqueous LV inclusions in vein sets 1 and 3 from the Fat Vein zone and in vein set 3 from the Surluga Mine (Figure 25 A and C).

In conclusion, the Jubilee Shear zone and the Minto deformation zones were infiltrated by similar fluids with the exception of the early, auriferous fluids which are absent in the Minto zones. The second fluid was pervasive as is indicated by its common occurrence in all deformation zones with the exception of the Minto E zone. This late fluid was associated with the emplacement of the Jubilee Breccias. Figure 45 summarizes a correlation of veins, fluid inclusion types and hydrothermal alteration effects observed in the Jubilee and Minto deformation zones.

4.2. Comparison of Hydrothermal Alteration and Fluid Inclusion Characteristics at Wawa to Other Archean Gold Deposits

As stated in Chapter 1, a comparison of hydrothermal alteration and fluid inclusion characteristics at Wawa to those of well-studied Archean gold-mineralizing systems may prove useful in appraising the gold potential of the Wawa systems.

4.2.1. Hydrothermal Alteration Associated with Archean Gold Deposits

Most Archean gold deposits are accompanied by extensive wallrock alteration. The nature of hydrothermal alteration associated with Archean lode gold deposits varies with the nature of the host rocks. Alteration is normally best developed in mafic and ultramafic rocks, and is most cryptic in metasediments (Groves et al., 1987, 1988). The most common types of alteration are extensive carbonatization and chloritic alteration. Other types of alteration include albitization, potassic alteration, sulphidation and silicification, the first two types being commonly associated with mineralization in felsic igneous or clastic sedimentary rocks (Nesbitt and Muehlenbachs, 1988, 1989).

Alteration of mafic lithologies is more extensive than the mineralization itself, and may involve complete replacement of the host rock (Colvine et al., 1984, 1988; Boyle,

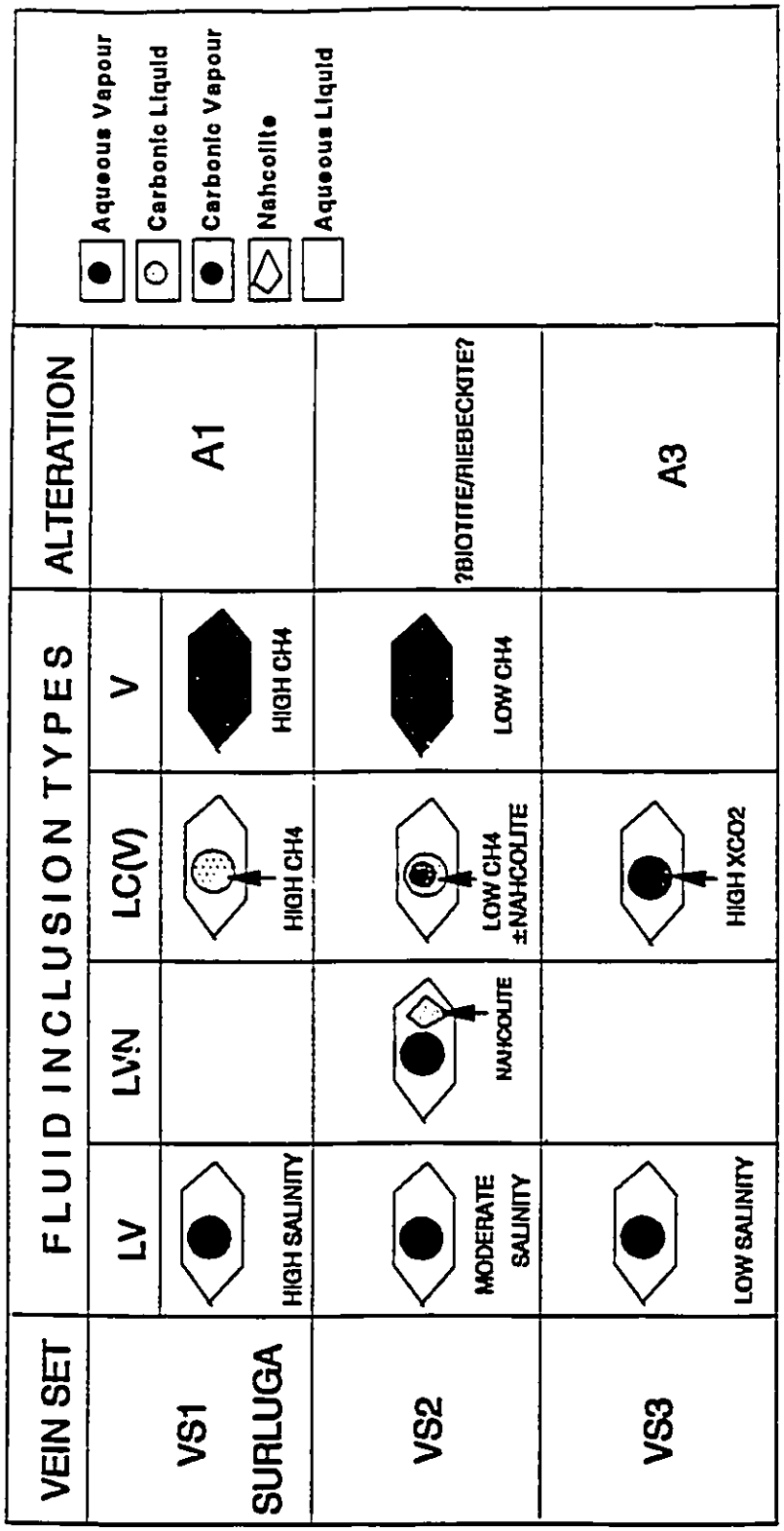

Figure 45. A summary of the correlation of veins, fluid inclusion types and hydrothermal alteration effects in the Jubilee and Minto deformation zones. VS1, VS2 and VS3 = vein sets 1, 2 and 3; A1, A2 = alteration events 1 and 3, respectively.

1979). Mafic rocks commonly display an alteration assemblage consisting of chlorite, carbonate (calcite, dolomite-ankerite), sericite, quartz and sulphides. In general, mafic rocks display a dramatic enrichment in CO_2, K_2O, and S and depletion in Na_2O and SiO_2 within the alteration zone (Boyle, 1979).

Intermediate and felsic rocks are less susceptible to hydrothermal alteration, mainly due to the higher amounts of quartz in these rocks. The most common alteration minerals are muscovite/sericite, calcite, quartz, albite and chlorite. Alteration in felsic rocks is generally fracture-related and limited to the zones immediately adjacent to the veins. Associated geochemical changes include increases in CO_2, H_2O, S and K_2O and decreases in Na_2O and SiO_2 (Boyle, 1979; Colvine et al., 1988).

In general, the geochemical changes associated with Archean lode gold deposits involve significant enrichment in Au, CO_2, H_2O, K_2O and S with lesser increases in As, Sb, Mo, B, Ag, Li, Ba, Se, Te, F, Cl, Bi, Rb, Cr and sporadic increases in Cu, Zn, Pb, Fe (Colvine et al., 1988; Boyle, 1979; Roberts, 1987). Thus, it may be assumed that the auriferous hydrothermal fluids must have been enriched in CO_2, H_2O, K_2O, S, and a wide array of trace elements. The most common alteration minerals in Archean lode gold deposits are carbonate (calcite, dolomite-ankerite), K-rich phyllosilicates (muscovite/sericite and biotite), Cr-bearing phyllosilicates (fuchsite), chlorite, quartz and Fe-sulphides. A variety of other minerals may be locally important, including scheelite, tourmaline, fluorite, hematite, chloritoid, staurolite, cordierite and anthophyllite. Of these, last four minerals exclusively occur in gold deposits hosted by the rocks of higher metamorphic grade (Mathieson and Hodgson, 1984; Pattison et al., 1986; Smith, 1986).

The occurrence of alteration minerals (paragenetically related to gold) both in the mineralized veins and in the surrounding wallrocks suggests a close temporal relationship between the alteration process and gold deposition (Colvine et al., 1988).

The relative timing of hydrothermal alteration and shear-zone deformation is not usually emphasized in many studies of hydrothermal alteration associated with Archean gold deposits (Phillips, 1990). However, the studies on many Archean gold deposits in the Superior Province of the Canadian Shield suggests a close temporal relationship between deformation, alteration and gold mineralization (Colvine et al., 1988 and references therein). Both hydrothermal alteration and gold mineralization are generally considered to be syn- to late kinematic (Robert and Brown, 1986; Kerrich, 1989; Colvine, 1989; Colvine et al., 1988). It is also generally accepted that the first-order control on the distribution of Archean gold deposits and associated hydrothermal

alteration is structural, specifically shear zones (Gunning and Ambrose, 1937; Kerrich, 1989; Hodgson, 1989; Sibson, 1990). It is also accepted that gold-hosting structures were sufficiently permeable to maintain the focussed fluid flow only when they were actively undergoing deformation at the time of gold deposition and hydrothermal alteration (Robert et al., 1990).

Hodgson (1989) has studied the patterns of gold mineralization in a large number of Archean gold deposits and has concluded that in most deposits the main stage of shear-related vein formation and associated hydrothermal alteration occurred after the host shear zone was established as a zone of high strain. This is based on the orientations and deformed nature of the veins (folding and boudinaging) and genetically-related alteration mineral assemblages (for example, Sigma Mine, Val d'Or, Quebec: Robert and Brown, 1986).

Poulsen and Robert (1989) have studied the deformational and mineralogical characteristics of the auriferous shear zones in the southern Canadian Shield and have concluded that hydrotharmal alteration accompanied deformation based on the restriction of hydrothermally-altered rocks to the deformation zones.

4.2.2. Comparison of Hydrothermal Alteration at Wawa to Archean Gold Deposits

The aurifereous shear/deformation zones at Wawa are hosted by a compositionally diverse group of felsic, intermediate and mafic protoliths. In the Jubilee shear zone, host rocks comprise granodiorite, felsic crystal tuffs and an unidentified mafic protolith (dike or xenolith ?). The felsic rocks are altered to a quartz-chlorite-Fe-dolomite-muscovite assemblage whereas the mafic protolith was altered to a chlorite-Fe-dolomite assemblage. This early alteration event (A_1) resulted in the introduction into the shear zone of CO_2 and H_2O, as indicated by the carbonatized and hydrated nature of the shear-zone rocks. In the Surluga Mine the early, gold-related alteration (A_1) is clearly vein-related and is represented by a quartz-Fe-dolomite-muscovite assemblage with sulphides (chiefly pyrite, pyrrhotite and arsenopyrite) and minor gold. There are also subordinate amounts of tourmaline and chlorite. These mineralogical changes require the addition of CO_2, H_2O, S, As, B and Au by the hydrothermal fluid.

In the Minto zones, protolith composition is highly variable. Felsic protoliths commonly display an alteration assemblage consisting of quartz, Fe-dolomite, muscovite, epidote and subordinate amounts of chlorite, tourmaline and sulphides (pyrite and chalcopyrite). Mafic protoliths, on the other hand, are pervasively altered to an assemblage of chlorite-biotite-Fe-dolomite with lesser amounts of sulphides. Felsic protoliths contain more sulphides than mafic protoliths. Biotite is an important

alteration mineral only in the Minto B zone. The mineralogical changes to the host rocks in the Minto zones require the introduction into the deformation zones of CO_2, H_2O, S and B.

In general, the mineralogical and chemical changes in deformation zones at Wawa are similar to those associated with many, well-studied Archean gold deposits. However, the lack of a detailed geochemical data on altered and unaltered host rocks at Wawa limits the extent of any comparison between these zones and Archean gold deposits in terms of gains and losses of chemical components through fluid-rock interaction. Nevertheless, it may be safe to assume that the auriferous hydrothermal fluids which caused the observed alteration effects at Wawa are compatible with those involved in the formation of other Archean gold deposits.

Some differences in the hydrothermal alteration characteristics between Wawa and other Archean systems also exist:

1) Unlike most Archean systems in which the hydrothermal alteration associated with the gold mineralization hosted by felsic protoliths is generally fracture-related and is restricted to the zones immediately adjacent to the mineralized veins (Colvine et al., 1988), the early, gold-related hydrothermal alteration at Wawa has usually no clear-cut spatial relationship to the veins. This is best exemplified by the Fat Vein zone where a 20-30 m wide zone of hydrothermal alteration (muscovite-carbonate schists) with three generations of veins occur without any clear relationship to the early, strongly-deformed veins (augens). However, the exception to the above is in the Surluga Mine where the early auriferous veins are always surrounded by zones of intense alteration of limited thickness (1-5 m in drill-core intersections) forming "vein-schist packages".

2) As stated earlier, the hydrothermal alteration associated with Archean gold-mineralizing systems is commonly interpreted to have occurred more or less synchronously with gold deposition as gold is paragenetically related to the alteration minerals in the wallrock. The timing of gold emplacement and the related hydrothermal alteration in Archean systems is usually interpreted to be synchronous with, or to post-date, the major episode of shearing (Kerrich, 1989; Colvine, 1989; Colvine et al., 1988). Although the temporal relationship between gold deposition and hydrothermal alteration at Wawa is not unambiguously established at the present level of investigation, the strongly deformed character of the alteration mineral assemblages indicates a pre- or syn-shear (D_1 deformation) origin of the early hydrothermal alteration. However, the restriction of hydrothermal alteration to the deformation zones suggests a possible genetic, if not temporal, relationship between the D_1 deformation

and the hydrothermal alteration. Such a restricted occurrence of the alteration implies a structural control on the focussed fluid flow which caused the hydrothermal alteration. The resultant strain incompatibilities of unaltered and altered rocks probably promoted further localization of deformation (e.g., the Jubilee shear in Jubilee Stock) (Cobbold and Gapais, 1987; Poirier, 1980).

3 Gold mineralization hosted by mafic protoliths in Archean gold deposits is commonly associated with significant sulphidation (dominantly pyrite) of these protoliths in comparison with the felsic protoliths (Colvine et al., 1988 and references therein). However, at Wawa most of the pyritic alteration occurs in the Fe-poor felsic protoliths. This difference suggests that the precipitation of pyrite at Wawa can not be accounted for simply through the sulphidation of wallrock Fe.

4) Late, hydrothermal alteration events which clearly post-date the deformation, early hydrothermal alteration and gold mineralization are present at Wawa. They are fracture-related ankeritic alteration and hematization which is attributed to the emplacement of the Jubilee Breccia in the Jubilee shear zone, and fenitization (including late biotitic alteration) which is probably related to fluids associated with the emplacement of lamprophyre dikes. These late alteration events are not documented from other Archean systems, and are unrelated to gold mineralization at Wawa.

4.2.3. Fluid Inclusion Characteristics of Archean Gold Deposits

Table 17 briefly summarizes some recent fluid inclusion studies on Archean gold deposits. The fluid interpreted to have been trapped during the precipitation of gold in Archean gold deposits was of low salinity (< 6 wt. % NaCl equiv.), H_2O-rich with variable amounts of CO_2 (up to 20 mole %) (Table 17).

The available fluid inclusion data on Archean gold deposits (Table 17) indicate that the most common fluid inclusion types are (Kesler, 1990):

1) H_2O-CO_2 inclusions which consist of a low-salinity (< 6 wt. % NaCl) aqueous fluid with variable CO_2 content ($\pm$ CH_4 and N_2),
2) CO_2 inclusions which mainly consist of CO_2, with small amounts of H_2O and variable amounts of CH_4 and N_2, and
3) H_2O inclusions with salinity $\geq$ 10 wt. % NaCl ($\pm$ $CaCl_2$, KCl etc.) and with relatively low gas contents.

Most of the described fluid inclusions from Archean gold deposits are pseudosecondary and secondary in origin (Table 17, Kesler, 1990). However, the pseudosecondary and secondary nature of the fluid inclusions is in line with the

Table 17. Fluid Inclusion Data From Recent Studies of Archean Gold Deposits (Modified After Robert and Kelly, 1987; Colvine et al., 1988)

DEPOSIT/AREA/REFERENCE	SUMMARY OF FLUID INCLUSION DATA	INTERPRETATION
Auriferous veins, Yellowknife area, N.W.T English (1981)	Primary H2O-rich (10-30 vol% CO2; 5 wt % NaCl; Th = 200-330°C) and CO2-rich inclusions (95 vol% CO2, Th = 280-322°C); secondary H2O inclusions (11 wt % NaCl, Th = 120-150°C)	Early auriferous fluid: heterogeneous entrapment; late fluid in fractures: late fluid in fractures: low-salinity aqueous
McIntyre-Hollinger mine, Timmins, Ontario Smith et al. (1984)	Pseudosecondary and/or primary H2O-CO2 inclusions in quartz (3-24 mole % CO2 and minor CH4; <2 wt % NaCl; Th=220°-350°C); and secondary CO2-bearing aqueous inclusions (0-20 wt % NaCl; Th=160°-385°C) all inclusions "GOLD-RELATED"; in a graphite-bearing quartz vein, pseudosecondary to primary CO2-CH4 rich inclusions (> 26 mole % CH4), and secondary one-phase CH4-rich inclusions	Early auriferous fluid: homogeneous entrapment with possible fluid unmixing; fluids buffered by QFM
Hollinger mine, Timmins, Ontario Wood et al. (1986)	Primary H2O-CO2 inclusions in scheelite, quartz and carbonate with both constant and variable phase ratios (4 wt % NaCl; 6 mole % CO2; Th=225°-355°C)	Early auriferous fluid: homogeneous entrapment; accompanied by intermittent fluid unmixing
Pamour mine, Porcupine, Ontario Walsh et al. (1984)	Coexisting secondary H2O-rich (5-10 wt % NaCl) and CO2-rich (± CH4) inclusions in healed fractures in vein quartz	Heterogeneous fluid in the late fractures,
O'Brien mine, Cadillac, Quebec Krupka et al. (1977)	Primary H2O-CO2 inclusions in quartz with constant phase ratios; coexisting secondary vapor-rich (± CO2 ?) and liquid-rich (H2O-rich ?) inclusions in healed fractures contemporaneous with gold veinlets in quartz (Th of both types of inclusions = 210°-380°C)	Early auriferous fluid: homogeneous entrapment; late fluid in fractures: late fluid in fractures: heterogeneous fluid entrapment

Table 17 (continued)

DEPOSIT/AREA/REFERENCE	SUMMARY OF FLUID INCLUSION DATA	INTERPRETATION
Nine deposits from Yilgarn block, Western Australia Ho et al. (1985)	Primary H_2O-CO_2 inclusions in quartz with both constant and variable phase ratios (20-30 mole % CO_2; <2 wt % NaCl; Th=200°-390°C) "GOLD-RELATED"; coexisting primary H_2O-rich and CO_2-rich inclusions in late fractures in quartz	Early auriferous fluid: homogeneous entrapment with intermittent unmixing; Late fluid in fractures: heterogeneous entrapment
Sigma mine, Val d'Or, Quebec Robert and Kelly (1987)	Secondary H_2O-CO_2 inclusions in late fractures in quartz (<10 wt % NaCl; 15-30 mole % CO_2; Th=285°-395°C) coexisting secondary, high salinity (25-34 wt % salt) H_2O Th=60°-295°C) and CO_2-rich inclusions in healed fractures contemporaneous with gold-bearing fractures, all inclusions are "GOLD-RELATED"	Late auriferous fluid in fractures: mainly heterogeneous entrapment, with intermittent entrapment of homogeneous fluid
Red Lake, Ontario Brown and LaKind (1986)	Primary low-salinity H_2O-CO_2 inclusions with variable phase ratios and higher CO_2 density (Th=110°-360°C) "GOLD-RELATED"; secondary low-salinity H_2O-rich inclusions (Th= > 350°C); secondary low-salinity (<10 equiv. wt % NaCl) mixed H_2O-CO_2 inclusions with low CO_2 density	Early auriferous fluid: heterogeneous entrapment with possible fluid unmixing; Late fluid: homogeneous entrapment

common assumption that in most Archean gold deposits crack-seal processes play significant role in the development of auriferous veins (Robert and Brown, 1986; Durney and Ramsay, 1973; Ramsay and Huber, 1987).

Homogenization temperatures for the H_2O-CO_2 fluid inclusions range from 250° to 350°C (Table 17), whereas most H_2O inclusions, and particularly high-salinity ones, homogenize at temperatures of between 150° and 250°C (Table 17, Kesler, 1990). Fewer homogenization temperatures are available for the CO_2-rich inclusions and they are usually similar to those obtained on H_2O-CO_2 inclusions.

Among numerous detailed studies of the fluid inclusion characteristics of Archean gold deposits, very few have demonstrated or implied a direct genetic link between the observed fluid inclusions and gold itself (Table 17). Of these studies, Robert and Kelly (1987) have described fluid inclusions which contained gold in them and also gold inclusions in the same planar arrays of fluid inclusions in quartz.

4.2.4. Comparison of Fluid Inclusion Characteristics at Wawa to Archean Gold Deposits

Most of the fluid inclusion studies on other Archean gold deposits (Table 17) tend to concentrate on the fluid inclusion populations which are more or less paragenetically related to gold mineralization. The results of these studies are generally consistent in terms of fluid types and compositions but vary considerably in the interpretation of the data from a genetic point of view. The fluid inclusion data on Archean gold deposits have been interpreted either to suggest unmixing of a homogeneous fluid or to argue heterogeneous entrapment of several types of fluid. Although these results are generally comparable to those obtained on fluid inclusions at Wawa, in that the fluids associated with the gold mineralization are of a CO_2-rich, low-salinity, aqueous type. Among numerous studies summarized in Table 17, the most comparable data to those obtained on fluid inclusions in the auriferous quartz veins at Wawa are given by Smith et al. (1984) on the Hollinger-McIntyre Mine in Timmins, Ontario, and by Robert and Kelly (1987) on the Sigma Mine in Val d'Or, Quebec.

The gold-related fluid inclusions in the Hollinger-McIntyre Mine consist of pseudosecondary and/or primary H_2O-CO_2 inclusions in quartz (Table 17) which contain 3-24 mole % CO_2 and are of low salinity (< 2 wt. % NaCl) (Smith et al., 1984). The homogenization temperatures for these inclusions range from 220° to 350°C. Smith et al. (1984) interpreted that these fluid inclusions trapped a homogeneous, auriferous fluid (Table 17). In addition, Smith et al. (1984) have

reported pseudosecondary and secondary CO_2-bearing aqueous fluid inclusions (Table 17). The salinity of these fluid inclusions ranges from 0 to 20 wt. % NaCl and their homogenization temperatures range from 160° to 385°C (Table 17). Apart from these inclusions in quartz, pseudosecondary CO_2-CH_4 (> 24 mole % CH_4) and secondary CH_4-rich inclusions were observed in a graphite-bearing quartz vein (Smith et al., 1984).

The H_2O-CO_2 fluid inclusions at the Hollinger-McIntyre Mine are compositionally comparable to those described from the auriferous quartz veins (vein set 1) in the Surluga Mine. However, the H_2O-CO_2 inclusions in the Surluga Mine have a narrower range of CO_2 contents (XCO_2 = 17-26 mole %) and significant amounts of CH_4 (up to 6 mole %) and minor (≤ 1 mole %) N_2. The homogenization temperatures for H_2O-CO_2 inclusions in the Surluga Mine (265-365°C) are comparable and slightly higher than those at the Hollinger-McIntyre Mine (220-350°C). The salinity of these inclusions at both mines is low and comparable (< 2 wt. % NaCl for Hollinger-McIntyre; 4-7 wt. % NaCl for the Surluga Mine).

The CO_2-bearing aqueous inclusions at the Hollinger-McIntyre Mine have salinities (0-20 wt. % NaCl) that are comparable with those of the relatively high-salinity (18-23 wt. % NaCl), aqueous LV inclusions in the auriferous vein at the Surluga Mine. Decrepitation of the LV inclusions at temperatures as high as 320°C indicate the presence of gases, possibly CO_2.

In the Hollinger-McIntyre Mine, the early gold-related fluid was interpreted by Smith et al. (1984) to have been homogeneously entrapped and have undergone possible unmixing (Table 17). This fluid is represented by the low-salinity H_2O-CO_2 inclusions. The relatively saline (up to 20 wt. % NaCl), CO_2-bearing aqueous fluid inclusions have been interpreted to have been produced by such an unmixing. Similarly, the equivalent fluid at Wawa has also been interpreted to have undergone significant unmixing and have possibly acted as a trigger for gold deposition (see later). However, the only real difference between the mineralizing fluids at the Hollinger-McIntyre Mine and the Surluga Mine is that the latter fluids in the latter are significantly richer in CH_4.

Pseudosecondary and primary, CH_4-rich and CO_2-CH_4 fluid inclusions (> 26 mole % CH_4) were described from a graphite-bearing quartz vein at the Hollinger-McIntyre Mine (Smith et al., 1984; Table 17). These inclusions are compositionally very comparable with the high-XCH_4 V inclusions which occur only in vein set 1 from the Surluga Mine. Some of them (e.g. those in sample S280-613 from the mine) occur as almost pure CH_4 inclusions. However, the quartz vein in which these inclusions are observed does not contain graphite, and, most importantly, these inclusions are

paragenetically related to the auriferous fluid described above. Similar inclusions from the Hollinger-McIntyre Mine are not related to the mineralizing fluids, as indicated by the virtual absence of CH_4 in the ore fluid (Smith et al., 1984; Table 17).

Robert and Kelly (1987) have described aqueous inclusions with possible nahcolite, that may be analogous to the the nahcolite-bearing, aqueous LVN inclusions at Wawa. However, there is great uncertainity about whether the identified solid is actually nahcolite, although its highly birefrengent and water-soluble character (Robert and Kelly, 1987) resembles nahcolite in the LVN inclusions at Wawa. At the Sigma Mine, the aqueous, nahcolite (?)-bearing inclusions are more saline (25-34 wt. % salt) than the LVN inclusions (5-20 wt. % NaCl) at Wawa. However, the mineralogy of the quartz veins from which these inclusions were described is analogous to the Pinto Veins in that they contain tourmaline, calcite and chlorite (Robert and Kelly, 1987). The main difference between these aqueous inclusions at the Sigma and Surluga Mines is that the inclusions described by Robert and Kelly (1987) are related to gold mineralization, whereas at Wawa they are not (see below).

The secondary, aqueous-carbonic inclusions (15-30 mole % CO_2) described by Robert and Kelly (1987) from the Sigma Mine commonly occur in late, healed microfractures in quartz (Table 17). These inclusions are of low salinity (< 10 wt. % NaCl) and coexist with the high salinity, nahcolite(?)-bearing, aqueous inclusions described above. Both inclusion types occur along the the same fracture planes, which also contain visible gold, and are hence paragenetically related to gold. Robert and Kelly (1987) have interpreted that the fluid inclusions observed at the Sigma Mine were generated through unmixing of an originally homogeneous, low-salinity, H_2O-CO_2 fluid in response to dynamic fluid-pressure fluctuations in an active deformation zone. They also attempted to describe the generation of the high-salinity (25-34 wt. % salt) aqueous fluid by preferential partitioning of salt into the aqueous fluid phase. Robert and Kelly (1987) have also concluded that the "onset of gold deposition at the Sigma Mine coincided with the onset of fluid unmixing".

With the exception of the possible presence of nahcolite (?) and the virtual absence of CH_4, these inclusions are reminescent of the inclusions associated with the auriferous veins (vein set 1) from the Surluga Mine. A similar fluid unmixing process is also proposed by the author to explain the co-existence of high-salinity, aqueous (minor CO_2 ?) and low-salinity/high-CH_4 H_2O-CO_2 and CO_2-CH_4 inclusions ($\pm$ H_2O) in vein set 1 from the Surluga Mine. The secondary origin of these inclusions at Wawa is probably due to their emplacement during a late, brittle deformation (fracturing) of the early,

ductilely-deformed quartz veins, which may also be attributed to fluid-pressure fluctuations in the shear zone, as suggested by Robert and Kelly (1987) for the Sigma Mine. Furthermore, the common occurrence of visible gold and sulphides in microfractures in quartz at the Surluga Mine may imply a possible genetic relationship between gold deposition and unmixing of the CH_4-rich, aqueous-carbonic fluid (see later) as was concluded for the Sigma Mine (Robert and Kelly, 1987; Table 17).

As can be seen from the above discussion, the fluid inclusion characteristics of the auriferous quartz veins at the Surluga Mine are comparable to those described from some typical Archean gold deposits, one being the Hollinger-McIntyre lode gold-system, one of the largest, and most productive deposits in the world. The salinity and CO_2 content of the fluid that is paragenetically related to gold at Wawa are also comparable with the ranges described from other Archean gold deposits (i.e., $<$ 10 wt. % NaCl; up to 30 mole % CO_2) (Roedder, 1984; Table 17). Similarly, the few total homogenization temperatures obtained from the H_2O-CO_2 inclusions which occur in the mineralized veins in the Surluga Mine (250-350°C) are consistent with the temperatures from other Archean gold deposits (Robert and Kelly, 1987; Colvine et al., 1988; Kesler, 1990; Table 17).

4.2.5. Possible mechanism(s) of gold precipitation at Wawa

Bisulphide complexing of gold (e.g., $Au(HS)_2^-$) is generally accepted as the main transport mechanism for gold in the hydrothermal fluids that form Archean gold deposits (Colvine et al., 1988; Seward, 1984). Precipitation of gold from such fluids may occur mainly as a result of:

1) Sulphidation of host rock iron;
2) Increase in oxygen fugacity and pH as a result of CO_2-CH_4 immiscibility;
3) Fluid-rock interaction (hydrothermal alteration).

1) ***Sulphidation of host rock iron***: Destabilization of gold transported as a bisulphide complex may be brought about through the sulphidation of host rocks, in which Fe-bearing oxide and silicate minerals are replaced by Fe-sulphides, commonly pyrite, pyrrhotite and arsenopyrite (MacDonald 1984; Phillips and Groves, 1984; Roberts, 1987). In this process, gold precipitation occurs due to decreasing ligand activity (H_2S and HS^-) and the resultant oversaturation of gold in the hydrothermal fluid and concomittant gold precipitation (Seward, 1973, 1984; Romberger, 1986). This mechanism is most relevant to gold deposits associated with banded iron formations and Fe-rich igneous host rocks (Groves et al., 1987; Neall and Phillips, 1987). An abundance of pyrite, pyrrhotite and arsenopyrite paragenetically related to gold in a

deposit hosted by Fe-rich rocks is strong evidence for this process (Colvine et al., 1988).

Host rocks to the deformation zones in McMurray Township are granodioritic in composition, and thus are low in Fe. Although there are mafic schists in the deformation zones at Wawa, they do not contain as much sulphides as the felsic schists. There is also no significant sulphidation in the granodioritic rocks, especially in the Surluga Mine. Therefore, this mechanism can not be considered important for gold deposition in the study area.

2)*Increase in oxygen fugacity and pH as a result of CO_2-CH_4 immiscibility*:

It has been shown for many Archean gold deposits in low- to medium-grade metamorphic terrains that gold was deposited from low-salinity hydrothermal fluids rich in CO_2 and/or CH_4 (Boyle, 1979; Smith et al., 1984; Walsh et al., 1988; Robert and Kelly, 1987; Colvine et al., 1988; Naden and Shepherd, 1989; Table 17). Fluid immiscibility has been proposed as a mechanism for bringing about gold precipitation in these deposits (Robert and Kelly, 1987; Walsh et al., 1988; Colvine et al., 1988). In a recent study, Naden and Shepherd (1989) have demonstrated that the addition of even small amounts ($\leq$ 5 mole %) of CH_4 to the hydrothermal fluid dramatically enlarges the pressure-temperature field of fluid immiscibility and will trigger gold deposition. This is due to the low solubility of this gas within aqueous brines over a wide range of P-T conditions (up to 3 kbars and 400°C). This also implies that, if the CH_4 is added at the site of gold deposition, the degree of fluid-rock interaction necessary to initiate fluid immiscibility in the hydrothermal fluid will be minimal (Naden and Shepherd, 1989).

However, due to the greater solubility of CO_2 (up to 15 mole %) in aqueous brines under similiar P-T conditions, the extent of such fluid-rock interaction required for bringing about fluid immiscibility and hence, gold precipitation, will be much greater (Naden and Shepherd, 1989).

Fluid immiscibility may also take place as a result of a decrease in temperature and/or pressure. The partitioning into a non-aqueous vapor phase, of acid species such as CO_2 and reduced species such as H_2S and CH_4 results in an increase in pH (due to the loss of CO_2) and oxygen fugacity (due to the loss of both H_2S and CH_4) which will destabilize gold-bisulphide complexes and will bring about gold precipitation (Romberger, 1986; Shenberger and Barnes, 1989; Seward, 1973, 1984). This precipitation mechanism has been proposed to account for the presence of Archean gold deposits in Fe-poor granitoids or felsic volcanics, in which sulphidation of wallrock Fe cannot account for gold precipitation (Colvine et al., 1988; Spooner et al., 1987). The

presence of co-existing CO_2-CH_4-rich and H_2O-rich fluid inclusions in gold-bearing veins may provide evidence for fluid immiscibility.

The restricted occurrence of one-phase CH_4-CO_2-N_2 and CO_2-rich inclusions with high CH_4 contents (up to 35 mole %) in vein set 1 in the Surluga Mine and their association with relatively high-salinity, aqueous inclusions strongly suggests that fluid immiscibility may have caused gold deposition in the Jubilee shear zone. The absence of these fluid inclusion types in the Minto zones may be explained by that these zones were probably formed at a later stage than the infiltration of an early, auriferous fluid. Alternatively, greater permeability along the Jubilee shear zone might have caused focussing of this fluid into the main shear zone, thus depriving Minto zones of the auriferous fluid.

3) ***Fluid-rock interaction***: Apart from fluid immiscibility, increases in oxygen fugacity and pH of the gold-mineralizing fluids can also be caused by fluid-rock interaction, and resultant hydrothermal alteration of the country rocks. As pointed out earlier, hydrothermal alteration in the Jubilee Shear zone has developed at a relatively early stage with respect to mineralization as gold commonly occurs in late fractures in ductilely deformed, early quartz veins which are enveloped by intensely altered and deformed host rocks in the Surluga Mine. Thus, wallrock alteration is an unlikely control mechanism for the late gold deposition in the veins, as also pointed out earlier by Robert and Kelly (1987) for the Sigma Mine where the timing relationship between gold deposition and wallrock alteration is similar to that at Wawa.

CHAPTER V
CONCLUSIONS

The hydrothermal alteration and fluid inclusion characteristics of the auriferous deformation zones and vein systems at Wawa lead to the following conclusions:

1. The Jubilee Shear zone and the Minto zones have been affected by a similar, early hydrothermal alteration event (A_1) which resulted in the development of a quartz-chlorite-Fe-dolomite-muscovite assemblage in felsic to intermediate protoliths, and a chlorite-Fe-dolomite assemblage in mafic protoliths. Hydrothermal alteration was more intense in mafic protoliths than in felsic protoliths. The mineralogical changes seen in the deformation zones require the introduction of mainly CO_2 and H_2O, and subordinate amounts of S, Au, As and B.

2. Textures exhibited by alteration minerals such as muscovite, chlorite and Fe-dolomite suggest a pre- or syn-shear origin for the early, hydrothermal alteration. However, the restricted occurrence of hydrothermally altered rocks to the deformation zones suggests a genetic relationship between hydrothermal alteration and the deformation processes.

3. The presence of the same, deformed, hydrothermal alteration assemblages in both the Minto zones and in the Jubilee shear zone suggests that these deformation zones were formed penecontemporaneously.

4. Gold deposition was most likely caused by fluid unmixing, as indicated by the inferred co-existence in the auriferous quartz veins (vein set 1) in the Surluga Mine of: a) high-XCH_4, CO_2-H_2O inclusions, b) CO_2-CH_4 ($\pm$ N_2) inclusions, and c) moderately saline, CO_2-bearing, aqueous fluid inclusions. Gold, along with sulphides, was deposited in fractures in quartz during an episode of late, brittle deformation within the Jubilee Shear zone, which post-dated ductile deformation of this early vein set. The high-XCH_4+N_2, H_2O-CO_2 and, CO_2 fluid inclusions which occur in the auriferous veins in the Surluga Mine are absent in the early veins from both the Fat Vein zone and the Minto zones. The

different fluid histories of these deformation zones could be best explained if the early, auriferous fluids (CH_4-rich) were highly-focussed, and thus infiltrated only parts (most dilatant ?) of the Jubilee shear zone.

In addition to their occurence in the early veins, gold and sulphides also occur in hydrothermally altered wallrock to the veins in the Surluga Mine, and are paragenetically related to the hydrothermal alteration minerals, which may suggest a contemporaneity between gold deposition and hydrothermal alteration. However, wallrock alteration probably played a less significant role, if any, in gold deposition.

5) The conclusions above imply that fluid inclusion composition can aid in the location of potential zones of high-grade gold mineralization in the deformation zones at Wawa and other areas. In comparison hydrothermal alteration may only serve as a broad guide for target-area selection in the Michipicoten greenstone belt.

6. On the basis of fluid inclusion and mineralogic characteristics, it may be .pm5 concluded that most of the veins in the Minto zones, if not all, are temporally equivalent to the Pinto veins (vein set 2) in the Surluga Mine.

7. Fluid inclusion compositions and hydrothermal alteration assemblages at Wawa are comparable to those described from other Archean gold-mineralizing systems. However, the fluids associated with gold mineralization at Wawa contain more CH_4 than those involved in the formation of most Archean gold deposits.

8. Late fenitization, including biotitic alteration, is most likely related to the emplacement of carbonatite-lamprophyre intrusive complex in the area. Nahcolite-bearing fluid inclusions possibly represent the fluids associated with the intrusion of carbonatite-lamprophyre dikes. The absence of such inclusions in the Jubilee Breccias from the Fat Vein zone strongly suggests a pre-Jubilee Breccia origin for these fluids.

9. Late hematization and fracture-related ankeritic alteration, which are commonplace in almost all deformation zones, are probably related to the emplacement of the Jubilee Breccias into the Jubilee shear zone. These breccias were associated with a low-salinity/high-XCO_2 H_2O-CO_2 fluid.

REFERENCES

Arias, Z.G. and Helmstaedt, H. (1988): Regional structural geology related to gold mineralization in the Goudreau-Lochalsh Area, District of Algoma. **In** Summary of Field Work and Other Activities, 1987, Ontario Geol. Survey, Misc. Paper **137**, 146-154.

Arias, Z.G. and Helmstaedt, H. (1989): Structural evolution of central and east-central Michipicoten (Wawa) greenstone belt, Superior Province. **In** Summary of Research 1988-1989, Ontario Geol. Survey, Misc. Paper 143, pp. 210-226.

Attoh, K. (1980): Stratigraphic relations of the volcanic-sedimentary successions in the Wawa greenstone belt, Ontario. **In** Current Research, pt. A, Geol. Survey Canada, Paper 80-1A, 101-106.

Ayres, L.D. (1978): Metamorphism in the Superior Province of Northwestern Ontario and its relationship to crustal development. **In** Metamorphism in the Canadian Shield, Geol. Survey Canada Paper 78-10, pp. 25-36.

Bottinga, Y. and Richet, P. (1981): High pressure and temperature equation of state and calculation of the thermodynamic properties of gaseous carbon dioxide. **Am. J. Sci. 281, 615-660.**

Brown, P.E. and LaKind, J.S. (1986): Fluid inclusion study of selected quartz veins, Red Lake gold camp, northwestern Ontario, Canada. Unpubl. manuscript, 44p.

Bowers, T.S. and Helgeson, H.C. (1983): Calculation of the thermodynamic and geochemical consequences of non-ideal mixing in the system H_2O-CO_2-NaCl on phase relation in geologic systems: Equation of state for H_2O-CO_2-NaCl fluids at high pressures and temperatures. **Geochim. Cosmochim. Acta. 47, 1247-1275.**

Boyle, R.W. (1979): The geochemistry of gold and its deposits, **Geol. Survey Canada Bull. 280, 584p.**

Bozzo, A.T., Chen, J.R., and Barduhn, A.J. (1973): The properties of the hydrates of chlorine and carbon dioxide. **In** 4th Intl. Conf. Fresh Water from the Sea, A. Delyannis and E. Delyannis (eds.), vol. 3, 437-451.

Cobbold, P.R. and Gapais, D. (1987): Shear criteria in rocks: An introductory review. **J. Structr. Geol. 9, 521-523.**

Colvine, A.C. (1989): An empirical model for the formation of Archean gold deposits: Products of final cratonization of the Superior Province, Canada, pp. 37-53. **In** The Geology of Gold Deposits: The Perspective in 1988, R.R. Keays, W.R.H. Ramsay and D.I. Groves (eds.), **Econ. Geol. Monograph 6**, 1989, 667p.

Colvine, A.C., Andrews, A.J., Cherry, M.E., Durocher, M.E., Fyon, A.J., Lavigne, M.J., MacDonald, A.J., Marmont, S., Poulsen, K.H., Springer, J.S., and Troop, D.J. (1984): An integrated model for the origin of Archean lode gold deposits. Ontario Geol. Survey, Open File Rep. **5524**, 98p.

Colvine, A.C., Fyon, J.A., Heather, K.B., Marmont, S., Smith, P.M., and Troop, D.G. (1988): Archean lode gold deposits in Ontario. Ontario Geol. Survey Misc. Paper **139**, 210p.

Dhamelincourt, P., Beny, J-M, Dubessy, J. and Poty, B. (1979): Analyse d'inclusions fluides à la microsonde MOLE à effet Raman. **Bull. Minéral. 102, 600-610.**

Ellis, A.J. and Golding, R.M. (1963): The solubility of carbon dioxide above 100°C in water and in sodium chloride solutions. **Am. J. Sci. 261, 47-60.**

English, P.J. (1981): Gold-quartz veins in metasediments of the Yellowknife Supergroup, Northwest Territories: A fluid inclusion study. Unpubl. M.Sc. Thesis, University of Alberta, Edmonton, 108p.

Ferguson, S.A., Groen, H.A. and Haynes, R. (1971): Gold deposits of Ontario, Part 1, Districts of Algoma, Cochrane, Kenora, Rainy River and Thunder Bay. Ontario Dept. Mines, Min. Res. Circ. No. **13**, 315p.

Frarey, M.J. and Krogh, T.E. (1986): U-Pb zircon ages of late internal plutons of the Abitibi and eastern Wawa Subprovinces, Ontario and Quebec, pp. 43-48. **In** Current Research, pt. A, Geol. Survey Canada, Paper **86-1A**, 826p.

Frohberg, M.H. (1935): The gold deposits of the Michipicoten area, Ontario Dept. Mines, Annual Rep. vol. **36**, pt. 8, pp.39-83.

Gledhill, T.L. (1927): Michipicoten gold area, District of Algoma, Ontario Dept. Mines, Annual Rep. vol. **36**, pt.2, pp.1-49.

Goodwin, A.M. (1962): Structure, stratigraphy and origin of iron formations in the Michipicoten area, Algoma District, Ontario, Canada. **Geol. Assoc. America Bull., 73, pp.561-586.**

Griffith, W.P. (1975): Raman spectroscopy of terrestrial minerals. **In** Infrared and Raman Spectroscopy of Lunar and Terrestrial Minerals, Karr, C. (ed.), pp.299-323.

Groves, D.I., Phillips, G.N., Falconer, L.J., Houstoun, S.M., Ho, S.E., Browning, P., Dahl, N. and McNaughton, N.J. (1987): Evidence for an epigenetic origin for BIF-hosted gold deposits in greenstone belts of the Yilgarn Block, Western Australia, pp. 167-179. **In** Recent Advances in Understanding Precambrian Gold Deposits, S.E. Ho and D.I. Groves (eds.), joint issue by the Geology Department and University Extension, University of Western Australia, Publ. no. 11, 368p.

Gittens, J., MacIntyre, R.M. and York, D. (1967): The ages of carbonatite complexes in eastern Canada. **Can. J. Earth Sci. 4, 651-655.**

Gunning, H.C. and Ambrose, J.W. (1937): Cadillac-Malartic area, Quebec. **Can. Inst. Min. Metall. Transc. vol. 40, 341-362.**

Heather, K.B. (1989): The geological and structural setting of gold mineralization in the Renabie portion of the Missanabi-Renabie gold district, Wawa gold camp. **In** Summary of Field Work and Other Activities 1989, Ontario Geol. Survey Misc. Paper **146**, pp. 99-107.

Heyen, G., Ramboz, C., and Dubessy, J. (1982): Simulation des équilibres de phases dans le systéme CO_2-CH_4 en dessous de 50°C et de 500 bar. Application aux inclusions fluides. **C.R. Acad. Sci. Paris, Ser. II 294, 203-206.**

Ho, S.E., Groves, D.I. and Phillips, D.N. (1985): Fluid inclusions as indicators of the nature and source of ore fluids and ore depositional conditions for Archean gold deposits of the Yilgarn block, Western Australia. **Geol. Soc. South Africa Trans. v.88, pt.1, pp.149-158.**

Hodgson, C.J. and Troop, D.J. (1988): A new computer-aided methodology for area selection in gold exploration: A case study from the Abitibi greenstone belt. **Econ. Geol. 83, 952-977.**

Hollister, L.S. and Burruss, R.C. (1976): Phase equilibria in fluid inclusions from the Khtada Lake metamorphic complex. **Geochim. Cosmochim. Acta. 40, 163-175.**

Holloway, J.R. (1984): Graphite-CH_4-H_2O-CO_2 equilibria at low-grade metamorphic conditions. **Geology 12, 455-458.**

Kerrich, R. (1983): Geochemistry of gold deposits in the Abitibi greenstone belt. **Can. Inst. Min. Metall. Spec. Vol. 27, 75p.**

Kesler, S.E. (1990): Nature and composition of mineralizing solutions, pp. 86-90. **In** Greenstone Gold and Crustal Evolution, **NUNA Conference (1990, Val d'Dor, Quebec) Volume**, F. Robert, P.A. Sheahan and S.B. Green (eds.), Geol. Assoc. Canada, Mineral Deposits Division, 252p.

Krupka, K.M., Ohmoto, H. and Wickman, F.E. (1977): A new technique in neutron activation analysis of Na/K ratios of fluid inclusions and its application to the gold-quartz veins at the O'Brien Mine, Quebec. **Canada, Can. J. Earth Sci. 14, 2760-2770.**

MacDonald, A.J. (1984): Gold mineralization in Ontario, I: the role of banded iron formation, p.412-430. **In** Chibougamau-Stratigraphy and Mineralization, J. Guha and E.H. Chown (eds.), **Can. Inst. Min. Metall. Spec. Vol. 34, 534p.**

Naden, J. and Shepherd, T.J. (1989): Role of methane and carbon dioxide in gold deposition. **Letters to Nature 342, 793-795.**

Neall, F.B. and Phillips, G.N. (1987): Fluid-wallrock interaction in Archean hydrothermal gold deposit: A thermodynamic model for the Hunt Mine, Kambalda. **Econ. Geol. 82, 1679-1694.**

Paré, C. (1989): A fluid inclusion study of the gold-bearing quartz veins in McMurray Township, Unpubl. B.Sc Thesis, University of Windsor, 123p.

Pasteris, J.D., Wopenka, B. and Seitz, J.C. (1988): Practical aspects of quantitative laser Raman microprobe spectroscopy for the study of fluid inclusions. **Geochim. Cosmochim. Acta 52, 979-988.**

Pattison, E.F., Sauerbrei, J.A., Hannila, J.J. and Church, J.F. (1986): Gold mineralization in the Casa Berardi area, Quebec, Canada. **In** MacDonald, A.J. (ed.), Proceedings of Gold'86, Konsult International, Toronto, pp. 170-183.

Phillips, G.N. (1990): Wallrock alteration and P-T environments of gold deposition, pp. 98-99. **In** Greenstone Gold and Crustal Evolution, **NUNA Conference (1990, Val d'Dor, Quebec) Volume**; F. Robert, P.A. Sheahan and S.B. Green (eds.), Geol. Assoc. Canada, Mineral Deposits Division, 252p.

Phillips, G.N. and Groves, D.I. (1984): Fluid access and fluid-wallrock interaction in the genesis of the Archean gold-quartz vein deposit at Hunt Mine, Kambalda, Western Australia, pp. 389-416. **In** Proceedings of Gold'82: The Geology, Geochemistry, and Genesis of Gold Deposits, R.P. Foster (ed.), **Geol. Soc. Zimbabwe, Spec. Publ. 1, 753p.**

Poirier, J.P. (1980): Shear localization and shear instability in materials in the ductile field. **J. Structr. Geol. 2, 135-142.**

Potter, R.W.,II, and Brown, D.L. (1977): The volumetric properties of aqueous sodium chloride solutions from 0° to 500°C, and pressures up to 2000 bars based on a regression of available data in the literature. **U.S. Geol. Survey Bull. 1421-C, 36p.**

Potter, R.W., II, Clynne, M.A. and Brown, D.L. (1978): Freezing point depression of aqueous sodium chloride solutions. **Econ. Geol. 73, 284-285.**

Poulsen, K.H. and Robert, F. (1989): Shear zones and gold: Practical examples from the southern Canadian Shield, pp. 239-299. **In** Mineralization and Shear Zones, J.T. Bursnall (ed.), Geol. Assoc. Canada Short Course Notes vol. 6, 300p.

Robert, F. and Brown, A.C. (1986): Archean gold-bearing quartz veins at the Sigma Mine, Abitibi greenstone belt, Quebec: Part II. Vein paragenesis and hydrothermal alteration. **Econ. Geol. 81, 593-616.**

Robert, F. and Kelly, W. (1987): Ore-forming fluids in Archean gold-bearing quartz veins at the Sigma Mine, Abitibi Greenstone belt, Quebec, Canada. **Econ. Geol. 82, 1464-1482.**

Robert, F., Phillips, G.N. and Kesler, S.E. (1990): Greenstone gold and crustal evolution: Scope and results of the conference, pp. 2-7. **In** Greenstone Gold and Crustal Evolution, **NUNA Conference (1990, Val d'Dor, Quebec) Volume**; F. Robert, P.A. Sheahan and S.B. Green (eds.), Geol. Assoc. Canada, Mineral Deposits Division, 252p.

Roberts, R.G. (1987): Ore deposit models, no.11: Archean lode gold deposits. **Geoscience Canada, vol. 14, p.37-52.**

Roedder, E. (1984): Fluid inclusions. **Rev. in Mineralogy**, P.H. Ribbe (ed.), vol. **12**, Min. Soc. America, 644p.

Romberger, S.B. (1986): Ore deposit models, no. 9: Disseminated gold deposits. **Geoscience Canada 13, 23-31.**

Rupert, R.J. (1975): McMurray Township and parts of surrounding townships, District of Algoma, Ontario Divison of Mines, Preliminary Map p. 828, Geological Series Scale 1 inch to 1/4 mile. Compilation 1970 thru 1972.

Rupert, R.J. (1979): Geology of McMurray Township and surrounding townships, District of Algoma. Ontario Geol. Survey Open File Rep. **5283**, 170p.

Sage, R.P. (1979): Wawa area, District of Algoma; p.48-53. **In** Summary of Field Work, 1979, V.G. Milne, O.L. White, R.B. Barlow, and C.R. Kustra (eds.), Ontario Geol. Survey Misc. Paper **90**, 245p.

Sage, R.P. (1981): Preliminary interpretation of the relationship between economic mineralization and volcanic stratigraphy in the Wawa area. **In** Summary of Field Work 1981, Ontario Geol. Survey Misc. Paper **100**, pp. 41-44.

Sage, R.P. (1986): Stratigraphic correlation in the Wawa area. **In** Volcanology and Mineral Deposits, J. Wood and H. Wallace (eds.), Ontario Geol. Survey, Misc. Paper **129**, pp.62-68.

Sage, R.P. (1987): Geology of the Goudreau-Lochalsh and Kabenung Lake areas. **In** Summary of Field Work and Other Activities, 1987, Ontario Geol. Survey, Misc. Paper **137**, pp. 134-137

Sage, R.P. and Heather, K.B. (1991): The structure, stratigraphy and mineral deposits of the Wawa area. GAC-MAC, SEG, Joint Ann. Mtg., Toronto'91, Field Trip A6 Guidebook, 118p.

Sage, R.P., Thorpe, R. and Berdusco, E. (1987): Geology of the Michipicoten Iron Formation. Institute on Lake Superior Geology 33rd Annual Mtg., Wawa, Ontario, Field Trip Guidebook.

Saggerson, E.P. and Turner, L.M. (1982): General comments on the identification of chlorites in thin sections. **Mineral. Mag. 46, 469-473.**

Samson, I.M. and Holm, P.E. (1991): Geological relationships in mineralized deformation zones in McMurray Township, Wawa, Ontario, Unpubl. report.

Samson, I.M. and Williams-Jones, A.E. (1991): C-O-H-N-salt fluids associated with contact metamorphism, McGerrigle Mountains, Quebec: A Raman spectroscopic study. **Geochim. Cosmochim. Acta. 55, 169-177.**

Seitz, J.C., Pasteris, J.D. and Wopenka, B. (1987): Characterization of CO_2-CH_4-H_2O fluid inclusions by microthermometry and laser Raman microprobe spectroscopy: Inferences for clathrate and fluid equilibria. **Geochim. Cosmochim. Acta. 51, 1651-1664.**

Seward, T.M. (1973): Thio complexes of gold and the transport of gold in hydrothermal ore solutions. **Geochim. Cosmochim. Acta. 37, 370-399.**

Seward, T.M. (1984): The transport and deposition of gold in hydrothermal systems. **In** Foster, R.P. (ed.), Gold'82: The Geology, Geochemistry and Genesis of Gold Deposits, A.A. Balkema, pp. 165-181.

Shenberger, D.M. and Barnes, H.L. (1989): Solubility of gold in aqueous sulfide solutions from 150° to 350°C. **Geochim. Cosmochim. Acta. 53, 269-278.**

Smith, T.J., Cloke, P.L., and Kesler, S.E. (1984): Geochemistry of fluid inclusions from the McIntyre-Hollinger gold deposit, Timmins, Ontario, Canada. **Econ. Geol. 79, 1265-1285.**

Spooner, E.T.C., Burrows, D.R., Callan, N.J., De Ronde, C.E.J., and Wood, P.C. (1987): High hydrothermal fluid pressures, hydraulic fracturing and fluid pressure dilation of shear zones in Archean Au-quartz vein systems (Abstr.). In Geol. Assoc. Canada Progr. Abstr., Summer Field Mtg., Yellowknife.

Sullivan, R.W., Sage, R.P., and Card, K.D. (1985): U-Pb zircon age of the Jubilee Stock in the Michipicoten greenstone belt near Wawa, Ontario; In Current Research, pt.B, Geol. Survey Canada, Paper 85-1B, p.361-365.

Thurston, P.C. (1986): Volcanic cyclicity in mineral exploration: The caldera cycle and zoned magma chambers. In Volcanology and Mineral Deposits, Ontario Geol. Survey Misc. Paper 129, pp. 104-123.

Turek, A., Van Schmus, W.R., and Sage, R.P. (1988): Extended volcanism in the Michipicoten Greenstone Belt, Wawa, Ontario. GAC-MAC Progr. Abstr. 13, p. A127.

Turek, A., Smith, P.E. and Van Schmus, W.R. (1984): U-Pb zircon ages and the evolution of the Michipicoten plutonic-volcanic terrane of the Superior Province, Ontario. **Can. J. Earth Sci. 21, 457-464.**

Turek, A., Smith, P.E. and Van Schmus, W.R. (1982): Rb-Sr and U-Pb ages of volcanism and granite emplacement in the Michipicoten greenstone belt, Wawa, Ontario. **Can. J. Earth Sci. 19, 1608-1626.**

Walsh, J.F., Cloke, P.L. and Kesler, S.E. (1984): Fluid (H_2-CO_2) immiscibility and fO_2 as factors in gold deposition: Pamour No. 1 Mine, Timmins, Ontario. (abs.): Geol. Soc. America Abstr. with Programs, v. 16, p. 686.

Wood, P.C., Burrows, D.R., Thomas, A.V. and Spooner, E.T.C. (1986): The Hollinger-McIntyre Au-quartz vein system, Timmins, Ontario, Canada: Geologic characteristics, fluid properties, and light stable isotope geochemistry; pp. 56-80. In Proceedings of Gold'86, an International Symposium on the Geology of Gold, A.J. Macdonald (ed.), Konsult International Inc., Toronto, 517p.

Wopenka, B. and Pasteris, J.D. (1987): Raman intensities and detection limits of geochemically relevant gas mixtures for a laser Raman microprobe. **Anal. Chem. 59, 2165-2170.**

APPENDIX A

DETAILED PETROGRAPHY OF HOST AND DEFORMATION ZONE ROCKS

FAT VEIN ZONE

Host Rocks: Felsic granodiorite, and quartz-feldspar crystal tuffs

Sample #: IS90-6: undeformed dioritic host rock to the deformation zone; **Location**: Fat Vein zone, outside the shear zone; **Hand specimen Description**: undeformed medium grained quartz-diorite with slight chloritic alteration; **Field Interpretation**: undeformed dioritic host rock to the shear zone; **Thin section Description**: coarse-grained, phaneritic granodiorite with an original igneous mineralogy of plagioclase (> 50% of total feld.), alkali feldspar and quartz interstitial to feldspar laths; fine-grained, non-foliated biotite replacing alkali feldspars, some monazite (?) within biotite, as inclusions with pleochroic haloes; apatite and disseminated opaques (pyrite ?); other secondary minerals: chlorite (with anomalous, berlin-blue biref.), muscovite (sericite) and epidote disseminated throughout plagioclase and alkali feldspar phenocrysts.

***

Deformation Zone Rocks: Buff, muscovite-rich schists and a pod-shaped body of mafic schists

Sample #: IS89-50; **Location**: within the Jubilee shear zone; **Hand specimen Description**: well-foliated, muscovite-carbonate-chlorite schist with pervasive pink hematitic (?) alteration, some minor folding (?); **Field Interpretation**: foliated host rock with late, pink, fracture-related alteration (hematite ?); **Thin section Description**: quartz-chlorite-dolomite/ankaerite-muscovite schist with abundant carbonate, relict plagioclase and alkali feldspar grains; secondary minerals: muscovite, dolomite-ankerite, chlorite and late, fracture-related kaolinite (?) veinlets with hematitic alteration haloes, cross-cutting the main foliation (S_1); deformational features: good foliation defined primarily by muscovite, enclosing deformed quartz-carbonate veins/veinlets containing the inclusions of foliation.

***

Sample #:WJN-5; **Location**: within the Jubilee shear zone; **Hand specimen Description**: weakly foliated chlorite-biotite-carbonate schist with prominent pinkish alteration (hematization); **Field Interpretation**: Mafic sill within the shear zone or a xenolith within the Jubilee Stock (granodiorite); well-foliated chlorite-carbonate schist, marginally hematized; display good crenulation cleavage (S_2); **Thin Section Description**: well-foliated chlorite-

dolomite/ankerite schist with some relict feldspar phenocrysts (plagioclase), contains minor sphene; pervasive carbonatization and chloritization; deformational features: good S_1 foliation defined primarily by chlorite wrapping around quartz-carbonate augens.

***

Sample #: WJN-6; Location: right at the shear zone boundary; Hand specimen Description: altered host rock, slightly schistose with some pinkish alteration (carbonate-hematite); Field Interpretation: Altered host rock right at the deformation zone boundary, slightly schistose and containing some pinkish (K-feldspar ?) veins/veinlets, hematized; Thin Section Description: quartz-chlorite-carbonate (dolomite/ankerite)-muscovite schist with relict plagioclase and alkali feldspar grains, minor rutile and opaques (pyrite ?); large poikiloblastic biotite (biotitic alteration) overprinting muscovite and the main foliation; chlorite, carbonates and vein quartz paragenetically related; deformational features: a weak foliation defined by muscovite, quartz-carbonate veinlets with chlorite slightly deformed (ductilely).

***

Sample #: WJN-7; Location: 3 meters into the shear zone from the shear-zone boundary; Hand specimen Description: well-foliated chlorite-biotite-carbonate-muscovite schist with pinkish alteration (carbonate+hematite); Field Interpretation: Chlorite schist, 3 meters away from the Jubilee shear-zone boundary (inwards); contain chlorite-biotite porphyroblasts; pinkish alteration veins cross-cutting the schistosity; Thin Section Description: well-foliated, quartz-chlorite-biotite-carbonate (dolomite/ankerite)-muscovite schist enclosing quartz-carbonate augens; minor rutile; large, poikilitic biotite (late alteration) and hematitic alteration; also stockwork of late quartz-carbonate veins cross-cutting S_1 foliation; carbonate grains in stockworks are hematized.

***

Sample #:WJN-8; Location: 6 meters into the Jubilee shear zone from the shear-zone boundary, Hand specimen Description: well foliated chlorite-biotite-carbonate-muscovite schist with prominent pinkish alteration (carbonate+hematite); Field Interpretation: chloritic schist, 6 meters away from the deformation-zone boundary (inwards), highly schistose chlorite-biotite schist with abundant cross-foliation and foliation-parallel quartz-feldspar veins/veinlets, pinkish in color due to abundant potassic alteration (?); Thin Section Description: well-foliated quartz-chlorite-dolomite/ankerite-muscovite schist, minor apatite, and disseminated rutile and pyrite; deformational features: a well-developed S_1 foliation defined by muscovite and chlorite, along which quartz and carbonate augens (early quartz-carbonate veins/veinlets) are deformed; large biotite grains (phenocrysts ?) highly deformed and altered to chlorite.

***

Sample #: WJN-9; Location: 9 meters into the Jubilee S.Z. from the boundary; Hand specimen Description: massive, pinkish alteration rock; Field Interpretation: buff alteration rock (muscovite-rich) within the shear zone, slightly schistose, pinkish alteration (potassic ?) pervasive; Thin Section Description: a porphyritic, felsic to intermediate igneous rock with an original mineralogy of quartz (10-15%), alkali feldspar(20-25%), plagioclase (albite, An_{30}), undeformed & relatively unaltered lithon within the shear zone; fracture-related muscovite-carbonate (dolomite/ankerite) alteration stockworks; late hematitic alteration along cleavages and margins of the carbonate grains.

***

Sample #: IS90-5; Location: within the Jubilee shear zone; Hand specimen Description: well-foliated muscovite-biotite-chlorite schist with some carbonate; Field Interpretation: oriented sample of mafic schist with a lineation 175 at 30° and foliation 60/75S; Thin section Description: well-foliated chlorite-muscovite-dolomite/ankerite-biotite schist with enclosed quartz-carbonate augens (early quartz-dolomite/ankerite-sulphide veins/veinlets); alteration: pervasive carbonate, muscovite and, chloritic alteration of ferromagnesian minerals and plagioclase); sulphide and carbonates occurring interstitially and later than quartz in veins, as fracture fillings and replacement zones in recrystallized coarse quartz.

***

SURLUGA MINE

Host Rocks: same host rocks as in the Fat Vein zone.

Deformation Zone Rocks: strongly foliated quartz-muscovite-carbonate schists.

Sample #: IS89-66; Location: the Surluga Mine within the Jubilee shear zone; Hand specimen Description: well-foliated buff-coloured, quartz-carbonate-muscovite schist with disseminated sulphides; Field Interpretation: strongly-foliated wallrock to early, auriferous vein set (vein set 1); Thin Section Description: well-foliated quartz-chlorite-dolomite/ankerite-muscovite schist with weakly-developed crenulation cleavage (S_2); contains highly deformed (brittle-ductile) sulphide (pyrite, chalcopyrite) lenses within and at the margins of quartz-carbonate veins/veinlets; tourmaline disseminated within schist matrix, closely associated with sulphides; late chlorite-carbonate replacing pyrite cubes as thin rims around them, and also along fractures within pyrite euhedra; late fracture-related kaolinite (?) (fan-shaped, radiating, low-birefrengence) crystals stringer veins with hematitic alteration haloes, cross-cutting S_1 foliation.

***

Sample #: IS89-71; Location: the Surluga Mine within the Jubilee shear zone; Hand specimen Description: well-foliated quartz-muscovite-carbonate schist with quartz-carbonate augens; Field Interpretation: strongly-foliated wallrock to auriferous, early quartz vein (vein set 1) with buff alteration associated; Thin Section Description: well-foliated quartz-muscovite-

dolomite/ankerite schist with enclosed augens (up to 0.5 cm in diameter) of early quartz-dolomite/ankerite-pyrite-arsenopyrite ± pyrrhotite ± chalcopyrite ± gold veins; sulphides are deformed brittlely in a ductile matrix and are elongate in shape, are commonly associated with clusters of euhedral tourmaline disseminated within the schist matrix; sulphide lenses (augens) are surrounded by thin rims of late carbonate alteration; carbonates and quartz in augens are granoblastic in texture and deformed indicated by sutured grain boundaries, undulatory extinction in quartz; and lamellar twinning in carbonates; a late feldspathic alteration (lath-shaped alkali feldspar ?) overprinting the S_1 fabric indicated by the inclusions of quartz and tourmaline with the preserved (inherited) S_1 foliation; schist displays a weakly-developed crenulation cleavage (S_2) defined by muscovite which also defines the S_1 foliation.

***

MINTO A ZONE

Host Rocks: xenolith-rich granodiorite and felsic fragmental rocks

Sample #: IS89-17; Location: outside the Minto A deformation zone; Hand specimen Description: non-foliated felsic crystal tuff with chloritic alteration; Field Interpretation: undeformed felsic fragmental host rock; Thin Section Description: non-foliated chloritized crystal tuff with a mineralogy of quartz, alkali feldspar (k-feldspar/albite), plagioclase phenocrysts set in fine-grained matrix of the above minerals and sericite, biotite, chlorite, epidote (clinozoisite/zoisite) and opaques; undeformed, planar quartz-alkali feldspar veins in non-foliated chloritized tuffs; chlorite has a fibrous texture;

***

Sample #: IS89-21; Location: host rock outside the deformation zone; Hand specimen Description: non-foliated, medium- to coarse-grained granodiorite; Field Interpretation: wallrock to quartz vein (vein set 2); Thin Section Description: slightly altered and deformed quartz-diorite or granodiorite with an original mineralogy of plagioclase (andesine, An_{30}) (35-40%), alkali feldspar (25-30%), quartz (15-20%), quartz being interstitial to large lath-shaped feldspar crystals; secondary minerals: muscovite-sericite, chlorite, carbonate and disseminated opaques within chlorite hematized in places, muscovite and chlorite outlining feldspar crystals.

***

Sample #: IS89-18A; Location: outside the Minto A deformation zone; Hand specimen Description: non-foliated felsic crystal tuff with sericitic, ankeritic and chloritic alteration, pinkish color due to hematitic alteration; Field Interpretation: wallrock in a zone of mafic schist and quartz vein with disseminated ankeritic alteration; Thin Section Description: minerals present: quartz, k-feldspar, plagioclase, sericite, carbonate (dolomite/ankerite, < 5% in abundance), chlorite, hematite and minor rutile; phenocrysts of k-feld and plag suggesting a

porphyritic nature of the rock; alteration observed: sericitic, ankeritic, chloritic and hematitic; chloritic alteration is fracture related and overprinting the sericitic alteration.

Sample #: IS89-19; Location: outside the deformation zone; Hand specimen Description: non-foliated, felsic crystal tuff with planar quartz vein and incipient alteration, and late hematitic alteration; Field Interpretation: felsic fragmental host rock containing small, planar, undeformed quartz veins; Thin Section Description: non-foliated felsic to intermediate crystal tuff with a mineralogy of quartz, k-feldspar and, plagioclase; secondary minerals: sericite, hematite; fracture-related stockworks of sericitic alteration; planar quartz veins are undeformed and are surrounded by sericite-rich alteration haloes.
Sample #: IS89-20; Location: outside the deformation zone; Hand specimen Description: pervasive muscovite alteration rock , felsic tuff?, with massive chloritic alteration zone; Field Interpretation: massive chlorite alteration zone within felsic fragmental host rock; Thin Section Description: highly altered granodiorite, pervasively altered to an assemblage of muscovite, tourmaline and minor carbonate and rutile; hematized in places; relict feldspar grains can be recognized.

***

Sample #:IS90-65; Location: outside the deformation zone, 150 meters W of the Minto A zone; Hand specimen Description: undeformed felsic quartz-feldspar crystal tuff; Field Interpretation: non-foliated felsic crystal tuff; Thin Section Description: undeformed and unaltered felsic crystal tuff with large unstrained quartz and K-feldspar phenocrysts in a fine-grained matrix of quartz and feldspar.

***

Sample #: IS89-20A; Location: outside (?) the deformation zone; Hand specimen Description: highly altered (buff alteration) felsic rock with massive chloritic alteration zone; Field Interpretation: massive chloritic alteration zone within felsic fragmental host rock; Thin Section Description: pervasively altered (to muscovite) granodiorite, relict feldspar crystals can be identified; massive chloritic alteration zone, chlorite Fe-rich variety as it is green pleochroic with dark brown birefrengence; disseminated to massive tourmaline replaced by chlorite, tourmaline concentrated at the chloritic zone and wallrock (massive muscovite-rich rock) contact; minor, disseminated hematized dolomite/ankerite crystals within chlorite; minor opaques (ilmenite ?) disseminated throughout muscovite alteration rock.

***

Sample #: IS90-10; Location: outside the deformation zone; Hand specimen Description: undeformed felsic fragmental rock containing a planar quartz vein with chloritic or biotitic alteration halo; Field Interpretation: planar quartz vein with biotite selvages and bleached alteration halo; Thin section Description: non-foliated, probably mafic fragmental host rock

with planar, relatively strain-free quartz vein; alteration: chlorite replacing deformed (kinked) muscovite fragments, two types of chlorite observed: 1) green pleochroic with anomalous berlin-blue birefrengence, associated with and replacing muscovite, 2) colorless to yellowish pleochroic with dark brown birefrengence, replacing muscovite along fractures; chlorite possibly earlier than planar quartz vein since the chlorite inclusions are enclosed within the vein; late, fracture-related kaolinite (?) veinlets with hematitic alteration haloes (c.f. the Fat Vein zone), cross-cut the planar quartz vein.

***

Deformation Zone Rocks: felsic and mafic schists with enclosed quartz veins
Sample #: IS89-18B; Location: within the Minto A deformation zone
Hand specimen Description: weakly foliated mafic rock with quartz vein and disseminated carbonate alteration (dolomite/ankerite); Field Interpretation: alteration rock in a zone of mafic schist and quartz vein with disseminated ankeritic alter.; Thin Section Description: weakly foliated quartz-muscovite-carbonate-chlorite schist, foliation defined by chlorite and muscovite; carbonate is dolomite/ankerite identified by Raman spectroscopy, and is greater than 10% in abundance; highly-deformed (brittlely) plagioclase and alkali feldspar phenocrysts are altered to an assemblage of muscovite-carbonate-chlorite along fractures within the feldspar phenocrysts; carbonate grains are henmatized along edges and cleavage planes.

***

Sample #: IS89-18C; Location: within the deformation zone; Hand specimen Description: highly altered and well-foliated, mafic, chlorite-dolomite/ankerite schist with a mylonitic (?) texture and foliation-parallel quartz-dolomite/ankerite augens (ealy veins);
Field Interpretation: mafic schist and qtz veins in the deformation zone;
Thin Section Description: quartz-muscovite-dolomite/ankerite-chlorite schist with disseminated minor rutile; dolomite/ankerite alteration (35-40% in abundance) overprinting S_1 foliation defined by chlorite and muscovite-rich zones; chlorite probably replacing ankerite; strongly developed mylonitic fabric grain-size reduction and dynamic rextallization (deformation-induced), also slight crenulation cleavage development in the schists and probly some C-S fabrics.

***

Sample #: IS89-53; Location: within the deformation zone; Hand specimen Description: well-foliated quartz-muscovite schist with disseminated pyrite, buff alteration;
Field Interpretation: mylonite with pervasive silicification and ankeritic alteration and fine-grained, disseminated pyrite; Thin Section Description: strongly foliated quartz-muscovite schist with mylonitic texture; large (1-5 mm) single and polycrystalline quartz augens enclosed within the schist matrix; relict plagioclase crystals dynamically recrystallized; late carbonate

(dolomite/ankerite) in fractures cross-cutting the quartz augens and the S_1 foliation, as well as cross-foliation stringer veins/veinlets of kaolinite (?) with fan-shaped, radiating low-birefrengence crystals associated with hematitic alteration haloes.

***

Sample #: IS90-63; Location: within the deformation zone; Hand specimen Description: crenulated chlorite-biotite-carbonate schist; Field Interpretation: oriented sample of foliation in small inclusions of chlorite schist truncated by quartz veins; Thin Section Description: strongly foliated muscovite-carbonate (dolomite/ankerite)-chlorite schist with mylonitic fabric as indicated by dynamically recrystallized plagioclase crystals.

***

Sample #: IS90-64; Location: within the deformation zone; Hand specimen Description: well-foliated chlorite schist containing foliation-parallel quartz stringers; massive quartz vein enclosing mafic schist inclusions; Field Interpretation: mafic schist within quartz vein; Thin Section Description: well-foliated chlorite-carbonate (dolomite/ankerite) schist with protomylonitic (?) fabric; coarse-grained carbonate grains highly deformed (ductilely) and disseminated and concentrated between chlorite-rich layers; dynamically recrystallized plagioclase relicts enclosed within schist matrix.

***

MINTO B ZONE

Host Rocks: medium to coarse-grained granodiorite, felsic to intermediate fragmental rocks, and mafic sills (?)

Sample #: IS90-29; Location: outside the shear zone; Hand specimen Description: relatively undef. slightly carbonatized and chloritized coarse-grained quartz-diorite; Field Interpretation: undeformed (?) diorite; Thin Section Description: undeformed, coarse-grained granodiorite with an igneous mineralogy of plagioclase (35-45%), alkali feldspar (25-30%) and quartz (10-20%) interstitial to feldspar laths; alteration: selective sericitic and chloritic alteration of feldspars; fenitization indicated by riebeckite(?) occurring as fibrous, felted masses and small patches scattered all over the rock; minor carbonate (calcite ?) disseminated within chlorite.

***

Sample #: IS90-33; Location: outside the shear zone; Hand specimen Description: fine-grained undeformed (?) quartz-diorite; highly chloritized (?) with late, pink-coloured hematite+carbonate alteration stockworks; Field Interpretation: deformed (?) and altered diorite; Thin Section Description: non-foliated, medium-grained, altered granodiorite with a similar original mineralogy as IS90-29; secondary minerals: sericite and chlorite altering

feldspar phenocrysts; late, subhedral biotite crystals overgrowing sericite, poikilitic in texture,

with quartz and feldspar inclusions.

***

Sample #:IS89-1; Location: outside the shear zone; Hand specimen Description: undeformed felsic crystal tuff with bluish alteration (fenitization); Field Interpretation: fenitized host rock; Thin Section Description: fenitized felsic fragmental rock with an igneous mineralogy of quartz, alkali feldspar, plagioclase phenocrysts within a fine-grained matrix of quartz, feldspar, carbonate, sericite and chlorite and biotite; bluish green, fibrous, small patches of riebeckite (?) (fenitization) commonly occur interstitially with subhedral biotite crystals, but replacing carbonates (dolomite/ankerite) along cleavage planes and grain margins.

***

Sample #: IS89-8; Location: outside the shear zone; Hand specimen Description: non-foliated medium-grained, chloritized felsic fragmental rock; Field Interpretation: patchy chloritic alteration with ankerite and disseminated pyrite; Thin Section Description: non-foliated felsic fragmental rock with quartz and alkali feldspar/plagioclase phenocrysts within a very fine-grained matrix of quartz, feldspar, chlorite, sericite and epidote; alteration: selective pervasive muscovite, chlorite and minor epidote (clinozoisite and zoisite) alteration of feldspar phenocrysts, occasionally well-developed ghost textures due to complete replacement of feldspars; minor hematite after chlorite.

***

Sample #: IS89-16; Location: Minto B zone; Hand specimen Description: altered mafic dike, massive and very fine grained and veined; Field Interpretation: alteration within mafic dike; Thin Section Description: mafic rock with an original mineralogy of hornblende and plagioclase; fibrous vein filled with a low-birefrengence mineral (kaolinite) containing the inclusions of mafic dike.

***

Sample #:IS89-10; Location: outside the shear zone; Hand specimen Description: non-foliated felsic fragmental rock; Field Interpretation: chlorite schist outside the shear zone; Thin Section Description: chlorite-epidote-biotite schist, weakly foliated quartz-feldspar crystal tuff with an original mineralogy of plagioclase, alkali feldspar, quartz and biotite; chl-quartz-carbonate veins cross-cutting weak S_1 foliation defined by chlorite; pervasive chlorite and epidote alteration pseudomorphing plagioclase and alkali feldspar phenocrysts.

***

Deformation Zone Rocks: intercalated mafic/felsic schists and felsic pyroclastics

Sample #: IS89-4; Location: within the shear zone; Hand specimen Description: chloritized felsic fragmental rock (tuff ?) with quartz veins; Field Interpretation: quartz vein with pervasive chloritization (chloritic halo around vein set 1); Thin Section Description: well-

foliated, chlorite-biotite schist with fairly well-developed crenulation cleavage (S_2); minor rutile and apatite disseminated within the schist; S_1 and S_2 defined by chlorite and biotite.

***

Sample #: IS89-5; Location: within the shear zone; Hand specimen Description: mafic schists with deformed quartz veins/veinlets and disseminated pyrite; Field Interpretation: biotite schist with discontinuous stringers of quartz and ankerite, and abundant, disseminated, coarse-grained, euhedral pyrite; Thin Section Description: strongly foliated quartz-carbonate (dolomite/ankerite)-biotite schist with foliation-parallel, deformed quartz-carbonate-alkali feldspar veins (augens) with disseminated pyrite; carbonate grains are highly deformed in the foliation planes; S_1 foliation is defined by biotite, and is truncated by carbonate augens, slight fenitization indicated by bluish green fibrous, felted riebeckite crystals replacing carbonate grains.

***

Sample #: IS89-9; Location: from the center of the shear zone; Hand specimen Description: carbonate-biotite schist with quartz-carbonate veins; Field Interpretation: quartz-carbonate-rich biotite schist at the center of the deformation zone; Thin Section Description: quartz-chlorite-dolomite/ankerite-biotite schist with undeformed quartz-carbonate (dolomite/ankerite) veins/veinlets containing the inclusions of foliation, thus quartz-carbonate veining post-dates chloritic and biotitic alteration, and deformation (foliation).

***

Sample #: IS90-31; Location: within the shear zone; Hand specimen Description: well-foliated chlorite-biotite schist with abundant carbonate veins (stockwork ?);
Field Interpretation: mafic schist in shear zone; Thin Section Description: well-foliated biotite-chlorite-carbonate schist; biotite replaced by chlorite-carbonate (dolomite/ankerite) assemblage; incipient fenitization (fibrous, felted masses of riebeckite); late, unaltered biotite with poikilitic texture indicated by abundant inclusions of quartz an feldspar, and also abundant zircon (?) inclusions with pleochroic haloes; carbonate grains are deformed in the plane of foliation, forming augens.

***

Sample #: IS90-32; Location: within the shear zone; Hand specimen Description: well-foliated biotite-chlorite-muscovite schist with abundant sulphides, and foliation-parallel quartz (±ankerite) veins ((folded and boudinaged), late hematitic alteration; Field Interpretation: felsic schist with sulphides; Thin Section Description: well-foliated quartz-chlorite-carbonate-muscovite schist with minor tourmaline, pyrite, alkali feldspar; pyrite occurring interstitially to tourmaline; ankerite (?) replacing quartz; euhedral pyrite crystals are brittlely deformed and are replaced by carbonate along fractures and crystal edges (carbonate rims), vein quartz highly

fractured; pyrite-chlorite-tourmaline-carbonate assemblage overprinting the S_1 fabric defined by muscovite; chlorite is massive, non-foliated.

***

Sample #: IS90-35; Location: within the shear zone; Hand specimen Description: slightly deformed mafic dike probably diabase; Field Interpretation: boudinaged mafic dike Thin Section Description: weakly foliated mafic schist with a granoblastic texture; relict hornblende surrounded by biotite-chlorite-carbonate alteration assemblage, chlorite-carbonate replacing biotite.

***

Sample #: IS90-36; Location: within the shear zone; Hand specimen Description: chlorite-biotite schist with crenulation cleavage and contain boudinaged quartz (± dolomite/ankerite) veins; late hematitic alteration; Field Interpretation: crenulated chlorite schist truncated by biotite schist (dike ?) foliation; tourmaline at the margins of quartz boudins which are surrounded by chloritic alteration haloes (schistose); Thin Section Description: refolded chlorite-biotite schist enclosing a relatively undeformed altered diorite with relict plagioclase phenocrysts altered to an assemblage of chlorite, quartz and carbonate (ankerite ?); chlorite also occurs in the foliated schist; carbonate is replaced by chlorite and some quartz veinlets have carbonate rims.

***

Sample #: IS90-37; Location: within the shear zone; Hand specimen Description: chlorite schist with boudinaged (?) quartz-ankerite veins; late hematitic alteration; Field Interpretation: massive chloritic alteration halo around quartz boudin within biotite schist; Thin Section Description: pervasive chloritic alteration of early carbonate-quartz vein, carbonate is dolomite-ankerite as determined by Raman spectroscopy.

***

Sample #: IS90-38; Location: right at the shear zone contact; Hand specimen Description: weakly foliated biotite-chlorite schist (probably deformed diorite or mafic dike ??); Field Interpretation: contact between biotite schist and massive chloritic alteration halo around the early quartz veins; Thin Section Description: well-foliated chlorite-carbonate-biotite schist (weak crenulation cleavage ?); alteration effects: biotite replaced by chlorite and carbonate (dolomite/ankerite); anastomosing foliation well-developed in chlorite-biotite-rich domains.

***

Sample #: IS90-40; Location: within the shear zone; Hand specimen Description: weakly foliated biotite-rich mafic dike with abundant pyrite but no quartz veins; Field Interpretation: poorly foliated mafic dike with no quartz veins (late ?); Thin Section Description: weakly to non-foliated quartz-carbonate-biotite schist; large carbonate (ankerite ?) grains have inclusions

of feldspar and quartz (sieve textures); quartz-carbonate vein probably deformed ?; minor apatite; it appears that carbonate & biotite alteration overprint the early deformational fabric (weak S_1 foliation).

***

Sample #: IS90-41; Location: within the shear zone; Hand specimen Description: crenulated (?) well-foliated biotite schist with quartz-carbonate augens, minor disseminated pyrite; Field Interpretation: biotite schist with quartz augens; Thin Section Description: well-foliated biotite-carbonate schist with abundant carbonate (dolomite/ankerite?) veins/veinlets deformed in the plane of foliation (boudins/augens) as well as cross-cutting the foliation ?; it appears that carbonate veins/veinlets predate the deformation causing the crenulation cleavage; boudinaged carbonate veins have abundant disseminated pyrite grains with carbonate rims and also cut by late carbonate veinlets; incipient fenitization with blue fibrous, felted masses of riebeckite (?) overgrowing carbonates and paragenetically related to late, poikilitic biotite overprinting the S_1 and S_2 fabrics.

***

Sample #: IS90-42; Location: within the shear zone; Hand specimen Description: well-foliated and chlorite-carbonate-rich mafic schist with thin (~1cm across) light green coloured, well foliated zone with whispy ends, containing feldspar and quartz relicts; Field Interpretation: sliver of mafic schist with whispy ends; Thin Section Description: weakly-foliated, altered mafic fragmental rock with plagioclase phenocrysts (brittlely deformed =fractures); selective to pervasive chlorite-carbonate-biotite alteration both in hostrock and also in the veins; chlorite-biotite intergrowths show decussate fabrics suggesting an equlibrium relationship between these minerals; carbonate veinlets replacing plagioclase along fracture planes; massive carbonate (dolomite/ankerite) vein with chlorite at the vein margins (alteration ?), carbonate grains are hematized in the vein; late, undeformed, planar quartz-carbonate vein with strain-free quartz grains.

***

Sample #: IS90-44; Location: within the shear zone; Hand specimen Description: well-foliated chlorite schist with deformed (boudinaged) quartz-carbonate veins and minor pyrite, late hematitic alteration; Field Interpretation: chlorite schist adjacent to quartz boudins, replacement of biotite by chlorite ?; Thin Section Description: well-foliated chlorite schist with crenulation cleavage (?), also containing deformed quartz-alkali feldspar-carbonate vein, vein margins are recrystallized and show serrated grain-boundary development; carbonate replacing quartz in the vein and there are large, disseminated pyrite grains with carbonate alteration rims (replacement) and late hematitic alteration along the fractures within carbonate grains; chlorite schist has disseminated sphene grains and this schist unit could be an early

hydrothermal alteration of a mafic dike ?

MINTO C ROCKS

Host Rocks: granodiorite and mafic volcanic (fragmental) rock units

Sample #: IS90-26A; **Location**: outside the deformation zone; **Hand specimen Description**: medium-grained fresh quartz-diorite with some fracture related carbonate alteration (stockwork ?); **Field Interpretation**: biotite-rich diorite; **Thin Section Description**: non-foliated granodiorite with incipient alteration of feldspars to sericite, chlorite and carbonate mixture, and a late biotitic alteration.

***

Sample #: IS90-27A; **Location**: outside the deformation zone; **Hand specimen Description**: undeformed biotite-rich mafic tuff; **Field Interpretation**: chlorite schist; **Thin section Description**: undeformed mafic volcanic breccia with an alteration assemblage of quartz-chlorite-epidote (clinozoisite and zoisite); epidote pseudomorphing plagioclase phenocrysts; this rock may be described as chlorite-epidote hornfels due to a lack of deformational features.

***

Sample #: IS90-27B; **Location**: outside the deformation zone; **Hand specimen Description**: fine-grained diorite with patchy carbonate alteration; **Field Interpretation**: biotite-chlorite schist; **Thin Section Description**: non-foliated, highly altered felsic crystal tuff ?; alteration: early pervasive sericitization and epidote psedomorhing feldspars; carbonatization: ankerite? replacing biotite crystals; also late fracture-related, chl veinlets replacing biotite crystals along fractures, biotite has abundant zircon ? inclusions and also undergone britle-ductile deformation indicated by kinking and brittle fracturing of biotite.

***

Deformation Zone Rocks: muscovite- and biotite-rich schists

Sample #: IS89-12; **Location**: within the deformation zone; **Hand specimen Description**: weakly foliated chlorite schist; **Field Interpretation**: mafic fragmental host rock; **Thin Section Description**: highly sericitized and chloritized mafic tuff with a mineralogy of plagioclase, quartz and biotite; an alteration assemblage of chlorite, sericite, epidote (clinozoisite and zoisite) and some carbonate, and a vein assemblage of quartz, chlorite, carbonate and disseminated pyrite.

***

MINTO E ZONE

Host Rocks: mafic and felsic fragmental rock units and diabase dikes

Sample #: IS90-52; **Location**: outside the deformation zone; **Hand specimen Description**: massive vein quartz with chloritic alteration haloes within felsic tuff; **Field Interpretation**:

quartz vein with chloritic selvages; Thin Section Description: undeformed and unaltered felsic crystal tuff containing a planar quartz vein with disseminated epidote and carbonate (probably replaced by quartz); the vein material is highly fractured and quartz being replaced by sericite along fractures within the vein; small quartz stringers are cut and displaced by fractures containing sericitic alteration suggesting that sericitic alteration later than quartz veining event.

***

Sample #: IS90-54A; Location: outside the deformation zone; Hand specimen Description: undeformed diabase; Field Interpretation: undeformed mafic dike; Thin Section Description: undeformed mafic dike rock: a nonfoliated, highly chloritized and carbonatized porphyritic mafic dike rock; chlorite-carbonate-white mica alteration assemblage after the breakdown of plagioclase and biotite crystals; chlorite typically occurs at the margins of carbonate veinlets; a late hematitic alteration along the fractures within carbonate grains.

***

Deformation Zone Rocks: chlorite and muscovite (sericite) schists

Sample #: IS90-50A and B; Location: within the deformation zone; Hand specimen Description: (A) biotite schist with thin (<0.5 mm), deformed quartz-carbonate veinlets (host rock: probably mafic tuff); (B): quartz-sericite-biotite schist with foliation-parallel disseminated pyrite (host rock: probably felsic xtall tuff); Field Interpretation: shear zone in mafic (A) and felsic rocks (B); Thin Section Description: (A) shear zone in mafic rock: weakly foliated, highly chloritized and carbonatized mafic volcanic tuff with planar undeformed quartz-carbonate-chlorite veins/veinlets, quartz-carbonate stringers; biotite in host rock is replaced by an alteration assemblage consisting of chlorite, epidote (clinozoisite and zoisite) and carbonate. (B) shear zone in felsic rock (crystal tuff ?): well-foliated, sericite schist; pervasive sericitic alteration with disseminated, large, euhedral pyrite with biotite crystals growing in their pressure shadows; pyrite cubes have typical carbonate replacement rims (c.f. Fat Vein zone, Surluga Mine).

***

Sample #: IS90-54A; Location: within the deformation zone; Hand specimen Description: deformed mafic dike (?); Field Interpretation: deformed mafic dike; Thin Section Description: well-foliated chlorite schist; pervasive chloritization and carbonatization with disseminated pyrite, and also deformed coarse-grained quartz-carbonate-chlorite veins; carbonate grains in these veins show strong preferred orientation and display lamellar twinning due to deformation.

APPENDIX B

ALL MICROTHERMOMETRY DATA

PART I: MICROTHERMOMETRY DATA FOR AQUEOUS FLUID INCLUSIONS

FAT VEIN ZONE

TABLE 1. WAWA MICROTHERMOMETRY DATA FOR AQUEOUS INCLUSIONS
FAT VEIN ZONE

SAMPLE	MI	SET	TYPE	ORI	Tf	Te	TmICE	SAL	TdV	TD	COMMENTS
VEIN SET 1											
IS90-4(A1)	CO	1	LV	S	-37	-	-0.1	0.44	300	-	aqueous inclusions with constant L/V ratios
IS90-4(A1)	CO	1	LV	S	-36	-	-0.1	0.44	275	-	same as above
IS90-4(A1)	CO	1	LV	S	-37	-	-0.1	0.44	270	-	same as above
IS90-4(A1)	CO	1	LV	S	-37	-	-0.1	0.44	280	-	same as above
IS90-4(A2)	CO	2	LV	S	-37	-	-1.3	2.48	272	-	aqueous inclusions with constant L/V ratios
IS90-4(A2)	CO	2	LV	S	-36	-	-1.2	2.31	274	-	aqueous inclusions with constant L/V ratios
IS90-4(A6)	CO	3	LV	S	-36	-	-0.8	1.64	256	-	aqueous inclusions with constant L/V ratios
IS90-4(A6)	CO	3	LV	S	-35	-	-0.75	1.56	256	-	same as above
IS90-4(A6)	CO	3	LV	S	-35	-	-0.8	1.64	256	-	same as above
IS90-4(A8)	CO	4	LV	S	-33	-	-0.3	0.79	252	-	aqueous inclusions with constant L/V ratios
IS90-4(A8)	CO	4	LV	S	-32	-	-0.32	0.82	238	-	aqueous inclusions with constant L/V ratios
VEIN SET 3 "JUBILEE BX"											
IS90-100(A1)	CO	1	LV	PS?	-39	-13	-5.6	8.87	155	-	aqueous inclusions with constant L/V ratios
IS90-100(A1)	CO	1	LV	PS?	-39	-13	-5.6	8.87	167	-	same as above
IS90-100(A1)	CO	2	LV	PS?	-41	-15	-5.7	9.01	225	-	same as above
IS90-100(A1)	CO	2	LV	PS?	-40	-15	-5.7	9.01	225	-	same as above
IS90-100(A1)	CO	2	LV	PS?	-41	-15	-5.6	8.87	225	-	same as above
IS90-100(A1)	CO	3	LV	PS?	-36	-	-2.8	-	262	-	same as above
IS90-100(A1)	CO	3	LV	PS?	-35	-	-2.9	-	300	-	same as above
IS90-100(A1)	CO	3	LV	PS?	-37	-	-2.8	-	316	-	same as above
IS90-100(A1)	CO	4	LV	PS?	-37	-	-0.3		208		

TABLE 2. WAWA MICROTHERMOMETRY DATA FOR AQUEOUS INCLUSIONS
SURLUGA MINE

SAMPLE	MIN	SET	TYPE	ORI	Tf	Te	TmICE	SAL	TdV	Tddm	Th	TD	COMMENTS
VEIN SET 1													
IS89-65(A1)	CQ	1	LVS	S		-22	-9.2	13.3	28	169	280		decrepitated before final homo.
IS89-65(A1)	CQ	1	LVS	S		-21	-8.1	12	260	n.	260		solid not dissolved
IS89-65(A1)	CQ	2	LV	S?			-8	11.9	123		123		no decrepitation at 350oC
IS89-65(A1)	CQ	2	LV	S?			-7	10.7	113		113		no decrepitation at 350oC
IS89-65(A5)	CQ	1	LVS	S		-13	-8.8	12.8	175	175	175		final hom. by dissol.and disapp. of vapor
IS89-65(A5)	CQ	1	LVS	S		-14	-8.5	12.5	170	126	170		
IS89-65(A5)	CQ	2	LV	S		-23	-12.1	16.3	180		180	195	decrepitated, TD=195oC
IS89-65(A5)	CQ	2	LV	S		-23	-13.2	17.3	263		263		
IS89-65(A5)	CQ	2	LV	S		-20	-12.8	17	110		110		probably necked ??
IS89-70b(A1)	CQ	1	LV	S		-22	-10.7	14.9	170		170		Surluga mine vs1 qtz vein with no v.g.;
IS89-70b(A1)	CQ	1	LV	S		-22	-12.3	16.5	210		210		aqueous LV and LVS-type inclusions
IS89-70b(A1)	CQ	1	LV	S		-22	-11.7	15.9	170		170		closely associated with CO2-rich inclusions
IS89-70b(A1)	CQ	1	LV	S		-22	-12.5	16.7	180		180		consistent phase ratios
IS89-70b(A1)	CQ	1	LV	S		-22	-12.1	16.3	210		210		
VEIN SET 1 "AU-QTZ"													
IS89-70a(A2)	CQ	1	LVS	S	-43	-21	-11.3	15.5	267	126	267	285	large inclusion with prismatic biref. solid
IS89-70a(A2)	CQ	1	LV	S	-45	-21	-11.2	15.4	323	-	323	337	vb didnot completely disappear upon freezing
IS89-70a(A2)	CQ	1	LV	S	-42	-21	-11.3	15.5	-	-		205	small inclusion (5µ)
IS89-70a(A2)	CQ	1	LV	S	-45	-21	-11.2	15.4	292	-	292	345	large incl. (10µ)
IS89-70a(A3)	CQ	1	LV	S		-23	-10	14.1	140		140		Surluga mine vs1 Au-qtz;
IS89-70a(A3)	CQ	1	LV	S		-24	-7.8	11.7	135		135		large aqueous LV inclusions
IS89-70a(A3)	CQ	1	LV	S		-25	-8	11.9	145		145		
IS89-70a(A3)	CQ	1	LV	S		-25	-8.3	12.2	138		138		
IS89-70a(A3)	CQ	2	LV	S			-17.1	20.6	275		275	278	aqueous LV-type inclusion associated with
IS89-70a(A3)	CQ	2	LV	S			-17	20.5	275		275	278	CO2-rich inclusions on secondary trail(s)
IS89-70a(A3)	CQ	2	LV	S		-22	-16.8	20.4	272		272	278	same as above
IS89-70a(A3)	CQ	2	LV	S			-16.9	20.5	285		285	428	same as above
IS89-70a(A3)	CQ	3	LVS	S			-17.2	20.7	143	165	165		biref. solid trapped phase ?
IS89-70a(A3)	CQ	3	LVS	S		-21	-17	20.5	143	215	215		prismatic biref. solid trapped phase ?
IS89-70a(A3)	CQ	3	LVS	S		-20	-15	18.9	124			286	decrepitated at 286°C
IS89-70a(A4)	CQ	3	LVS	S		-20	-15	18.9	145			295	decrepitated at 295°C
IS89-70a(A4)	CQ	3	LVS	S		-20	-15	18.9	143			290	
IS89-70a(A4)	CQ	3	LVS	S		-20	-15	18.9	140	200	200		

TABLE 2 (CONT'D)- SURLUGA MINE

SAMPLE	MIN	SET	TYPE	ORI	Tf	Te	TmICE	SAL	TdV	Tdda	Th	TD	COMMENTS
VEIN SET 1 "AU-QTZ"													
IS89-70a(A3)	CQ	3	LV	S		-23	-18	21.3	208		208		aqueous LV inclusions (a group of 10 incl.'s)
IS89-70a(A3)	CQ	3	LV	S		-23	-18	21.3	204		204		on a long secondary trail; large inclusions
IS89-70a(A3)	CQ	3	LV	S		-23	-18	21.3	208		208		consistent l/v ratios, ave. size ~ 10 microns
IS89-70a(A3)	CQ	3	LV	S		-23	-18	21.3	183		183		same as above
IS89-70a(A3)	CQ	3	LV	S		-23	-18	21.3	183		183		same as above
IS89-70a(A3)	CQ	3	LV	S		-23	-18	21.3	176		176		same as above
IS89-70a(A3)	CQ	3	LV	S		-23	-18	21.3	187		187		same as above
IS89-70a(A3)	CQ	3	LV	S		-23	-18	21.3	197		197		same as above
IS89-70a(A3)	CQ	3	LV	S		-23	-18	21.3	212		212		same as above
IS89-70a(A3)	CQ	3	LV	S		-23	-18	21.3	197		197		same as above
IS89-70a(A3)	CQ	3	LV	S		-23	-18	21.3	202		202		same as above
IS89-70a(A4)	CQ	1	LVS	S	-45	-23	-10.2	14.4	-	149		294	aqueous incl. with biref. prism. solid
IS89-70a(A4)	CQ	1	LVS	S	-45	-23	-10.2	14.4	-	149		242	solid highly soluble
IS89-70a(A4)	CQ	1	LV	S	-45	-23	-10.2	14.4	-	-		294	decrepiated
IS89-70a(A4)	CQ	1	LV	S	-45	-23	-10.2	14.4	-	-		230	decrepiated
IS89-70a(A4)	CQ	1	LV	S	-45	-23	-10.2	14.4	254	-	254	300	homogen. into L
IS89-70a(A4)	CQ	1	LV	S	-45	-23	-10.2	14.4	-	-	-	294	decrepiated
IS89-70a(A4)	CQ	2	LVS	S	-46	-24	-10.9	15.1	?	?			very large (25 mic.) aqueous incl. with biref. solid
IS89-70a(A4)	CQ	2	LVS	S	-45	-24	-10.4	14.6	?	?			small (~10 mic.) incl. with solid
IS89-70a(A4)	CQ	2	LVS	S	-46	-23	-10.6	14.8	?	?			small (~10 mic.) incl. with solid
IS89-70a(A4)	CQ	2	LVS	S	-49	-25	-12.4	16.6	?	?			very large (> 20 mic.) incl. with biref. prismatic solid
IS89-70a(A4)	CQ	3	LV	S	-47	-23	-13.4	17.5	?				medium- to large size inclusions
IS89-70a(A4)	CQ	3	LV	S	-47	-23	-11.1	15.3	?				associated with mixed-type ones; may contain some
IS89-70a(A4)	CQ	3	LV	S	-47	-23	-11.1	15.3	?				carbonic vapor phase within vapor bubble
IS89-70a(A4)	CQ	3	LV	S	-47	-23	-11.1	15.3	?				same as above
IS89-70a(A4)	CQ	3	LV	S	-47	-23	-11.1	15.3	?				same as above
IS89-70a(A4)	CQ	3	LV	S	-47	-23	-11.1	15.3	?				same as above
IS89-70a(A4)	CQ	3	LV	S	-47	-23	-11.1	15.3	?				same as above
IS89-70a(A4)	CQ	3	LV	S	-47	-23	-11.1	15.3	?				same as above
IS89-70a(A4)	CQ	3	LV	S	-47	-23	-11.1	15.3	?				same as above
IS89-70a(A4)	CQ	3	LV	S	-47	-23	-11.1	15.3	?				same as above
IS89-70a(A5)	CQ	1	LV	S	-49	-22	-16.5	20.1	232		- 232		secondary inclusion on short plane, ave. size 10 microns
IS89-70a(A5)	CQ	1	LV	S	-49	-22	-16.5	20.1	230		- 230		relatively consistent l/v ratios; assoc. with lvs-type incl.'s
IS89-70a(A5)	CQ	1	LV	S	-49	-22	-16.5	20.1	232		- 232		with bluish-biref. solid (incl. set # 2)
IS89-70a(A5)	CQ	1	LV	S	-49	-22	-16.5	20.1	227		- 227		same ns above

TABLE 2 (CONT'D)- SURLUGA MINE

SAMPLE	MIN	SET	TYPE	ORT	Tf	Te	TmICE	SAL	TdV	Tddm	Th	TD	COMMENTS
VEIN SET 1 "AU-QTZ"													
IS89-70a(A5)	CQ	1	LV	S	-49	-22	-16.5	20.1	227	-	227		same as above
IS89-70a(A5)	CQ	1	LV	S	-49	-22	-16.5	20.1	227	-	227		same as above
IS89-70a(A5)	CQ	1	LV	S	-49	-22	-16.5	20.1	224	-	224		same as above
IS89-70a(A5)	CQ	1	LV	S	-49	-22	-16.5	20.1	220	-	220		same as above
IS89-70a(A5)	CQ	1	LV	S	-49	-22	-16.5	20.1	245	-	245		same as above
IS89-70a(A5)	CQ	1	LV	S	-49	-22	-16.5	20.1	247	-	247		same as above
IS89-70a(A5)	CQ	1	LV	S	-49	-22	-16.5	20.1	252	-	252		same as above
IS89-70a(A5)	CQ	1	LV	S	-49	-22	-16.5	20.1	262	-	262		same as above
IS89-70a(A5)	CQ	1	LV	S	-49	-22	-16.5	20.1	247	-	247		same as above
IS89-70a(A5)	CQ	2	LVS	S	-46	-22	-17	20.5	-	126	-	283	secondary incl. on short plane, possibly necked down
IS89-70a(A5)	CQ	2	LVS	S	-46	-22	-17	20.5	-	126	-	283	same as above
IS89-70a(A5)	CQ	2	LVS	S	-46	-22	-17	20.5	-	129	-	283	same as above
IS89-70a(A5)	CQ	2	LVS	S	-46	-22	-17	20.5	234	126	234	283	homogenized into L by TdV without before decrep.
IS89-70a(A6)	CQ	1	LV	S	-53	-24	-17	20.5	-	-	-	183	aqueous lv-type incl. (~15 mic.) assoc. with one-phase CO2-rich
IS89-70a(A6)	CQ	1	LV	S	-53	-24	-17	20.5	288	-	288	-	inclusions on secondary planes (long), some have tiny H2O rims
IS89-70a(A7)	CQ	1	LV	S	-55	-24	-17	20.5	230	-	230	237	large (20 mic.) aqueous lv incl. assoc. with one-phase CO2 incl.'s
IS89-70a(A7)	CQ	1	LV	S	-55	-24	-17	20.5	182	-	182	-	on secondary planes; consistent l/v ratios
IS89-70a(A7)	CQ	1	LV	S	-55	-24	-17	20.5	267	-	267	-	same as above
IS89-70a(A8)	CQ	1	LV	S	-55	-23	-15.6	19.4	?	-	?		large lv incl on secondary plane
IS89-70a(A8)	CQ	1	LVS	S	-52	-23	-14.4	18.4	?	?	?		large lvs incl. assoc. with the above lv incl.
CORE SAMPLE- VEIN SET 1?													
S280-613(A1)	CQ	1	LV	S			-4	6.65	110		110		large aqueous inclusions associated with CH4-rich
S280-613(A1)	CQ	1	LV	S			-7.5	11.3	100		100		secondary inclusions, slightly necked down ?
S280-613(A1)	CQ	1	LV	S			-7.5	11.3	115		115		same as above
S280-613(A1)	CQ	1	LV	S			-5.6	8.87	112		112		same as above
S280-613(A1)	CQ	1	LVS	S			-7.5	11.3	300	215	300		possibly stretched due to its very high ThTOT
S280-613(A2)	CQ	1	LVS	S	-49	-24	-17	20.5	202	167	202	-	nahcolite-bearing lvs incl.'s on secondary planes
S280-613(A2)	CQ	1	LVS	S	-49	-24	-17	20.5	202	167	202	-	same as above
S280-613(A2)	CQ	1	LVS	S	-49	-24	-17	20.5	202	167	202	-	same as above
S280-613(A2)	CQ	1	LVS	S	-49	-24	-17	20.5	202	167	202	-	same as above
S280-613(A3)	CQ	1	LV	S	-51	-23	-17.5	20.9	184	-	184	-	aqueous lv incl. with consistent l/v ratio
S280-613(A3)	CQ	1	LV	S	-51	-23	-17.5	20.9	184	-	184	-	same as above
S280-613(A3)	CQ	1	LV	S	-51	-23	-17.5	20.9	184	-	184	-	same as above
S280-613(A3)	CQ	1	LV	S	-51	-23	-17.5	20.9	191	-	191	-	same as above

TABLE 2 (CONT'D)- SURLUGA MINE

SAMPLE	HTN	SET	TYPE	ORT	Tf	Te	TmICE	SAL	TdV	Tdds	Th	TD	COMMENTS
VEIN SET 2													
IS89-63(A1)	CQ	1	LV	S		-20	-10.4	14.6	135		135		Surluga mine vs2 (= pinto qtz); large
IS89-63(A1)	CQ	1	LVS	S		-22	-10.4	14.6	125	175	175		aqueous LV and LVS inclusions
IS89-63(A1)	CQ	1	LV	S			-10.6	14.8	100		100		consistent phase ratios
IS89-63(A1)	CQ	1	LVS	S		-21	-8.1	12	113		160		decrepitated at 150°C (TD)
IS89-63(A1)	CQ	1	LVS	S		-23	-8.1	12	100		167		decrepitated at 167°C (TD)
IS89-63(A1)	CQ	1	LVS	S		-23	-8	11.9	115	172	172		solid phase completely dissolved!
IS89-63(A1)	CQ	1	LVS	S			-8.3	12.2	125		176		decrepitated at 176°C (TD)
IS89-63(A1)	CQ	2	LVS	S		-20	-8	11.9	115	162	162		large (10-20μm) LVS type aqueous inclusions with
IS89-63(A1)	CQ	2	LVS	S		-15	-7.7	11.5	120	160	160		birefrengent prismatic solid (ds)
IS89-63(A1)	CQ	2	LVS	S		-24	-8.1	12	125	169	169		all homogenized into L by solid dissolution
IS89-63(A1)	CQ	2	LVS	S			-7.9	11.8	135	175	175		same as above
IS89-63(A1)	CQ	2	LVS	S			-8.2	12.1	142	210	210		same as above
IS89-63(A1)	CQ	3	LVS	S			-8.1	12	130	176	176		same as above
IS89-63(A1)	CQ	3	LVS	S			-8.1	12	135	154	154		same as above
IS89-63(A1)	CQ	3	LVS	S		-20	-8	11.9	130	165	165		same as above
IS89-63(A1)	CQ	3	LVS	S			-7.9	11.8	140	165	165		same as above
IS89-63(A1)	CQ	3	LVS	S			-8.1	12	131	181	181		same as above
IS89-63(A1)	CQ	3	LVS	S			-8.1	12	112	168	168		same as above
IS89-63(A1)	CQ	3	LVS	S			-8.1	12	115	171	171		same as above
IS89-63(A1)	CQ	3	LVS	S			-8.1	12	119	165	165		same as above
IS89-63(A1)	CQ	3	LVS	S			-8.1	12	134	163	163		same as above
IS89-63(A1)	CQ	3	LVS	S			-8.1	12	142	153	153		same as above
IS89-63(A1)	CQ	4	LV	S		-22	-13.4	17.5	114	-	114		aqueous LV inclusions with consistent phase ratios
IS89-63(A1)	CQ	4	LV	S		-23	-9.7	13.8	140	-	140		all homogenized into L
IS89-63(A1)	CQ	4	LV	S			-8.9	12.9	150	-	150		same as above
IS89-63(A1)	CQ	4	LV	S			-8.9	12.9	158	-	158		same as above
IS89-63(A1)	CQ	4	LV	S			-13.2	17.3	155	-	155		same as above
IS89-63(A2)	CQ	1	LVS	S		-20	-6.9	10.6	108	193	193		very large nahcolite-bearing aqueous inclusions
IS89-63(A2)	CQ	1	LVS	S		-20	-6.9	10.6	142	154	154		all homogenizations by solid dissolution
IS89-63(A2)	CQ	1	LVS	S		-20	-7.2	10.9	145	184	184		all homogenizations by solid dissolution
IS89-63(A2)	CQ	1	LVS	S		-20	-7.3	11	137	172	172		all homogenizations by solid dissolution
IS89-63(A2)	CQ	1	LVS	S		-20	-6.9	10.6	138	190	190		all homogenizations by solid dissolution
IS89-63(A2)	CQ	1	LVS	S		-20	-6.9	10.6	153	188	188		all homogenizations by solid dissolution
IS89-63(A2)	CQ	1	LVS	S		-20	-7	10.7	150	190	190		all homogenizations by solid dissolution

TABLE 2 (CONT'D)- SURLUGA MINE

SAMPLE	MIN	SET	TYPE	ORI	Tf	Te	TmICE	SAL	TdV	Tddm	Th	TD	COMMENTS
VEIN SET 2													
IS89-63(A2)	CQ	1	LVS	S		-20	-7.1	10.8	140	Decrep.			
IS89-63(A2)	CQ	1	LVS	S		-20	-6.9	10.6	135	185	185		all homogenizations by solid dissolution
IS89-63(A2)	CQ	1	LVS	S		-20	-6.9	10.6	157	200	200		all homogenizations by solid dissolution
IS89-63(A2)	CQ	1	LVS	S		-20	-7	10.7	160	206	206		all homogenizations by solid dissolution
IS89-63(A2)	CQ	1	LVS	S		-20	-6.9	10.6	138	180	180		all homogenizations by solid dissolution
IS89-63(A2)	CQ	1	LVS	S		-20	-7	10.7	135	172	172		all homogenizations by solid dissolution
IS89-63(A2)	CQ	1	LVS	S		-20	-6.9	10.6	140	175	175		all homogenizations by solid dissolution
IS89-63(A2)	CQ	1	LVS	S		-20	-7.1	10.8	136	175	175		all homogenizations by solid dissolution
IS89-63(A2)	CQ	1	LV	S		-19	-11.5	15.7	84		84		very large (>20μ) aqueous inclusions along a well-defined secondary
IS89-63(A2)	CQ	1	LV	S		-19	-11.5	15.7	92		92		plane (healed fracture), very consistent L/V ratios; all homogenized
IS89-63(A2)	CQ	1	LV	S		-19	-11.5	15.7	91		91		to liquid phase
IS89-63(A2)	CQ	1	LV	S		-19	-11.5	15.7	91		91		same as above
IS89-63(A2)	CQ	1	LV	S		-19	-11.5	15.7	108		108		same as above
IS89-63(A2)	CQ	1	LV	S		-19	-11.5	15.7	91		91		same as above
IS89-63(A2)	CQ	1	LV	S		-19	-11.5	15.7	92		92		same as above
IS89-63(A2)	CQ	1	LV	S		-19	-11.5	15.7	90		90		same as above
IS89-63(A2)	CQ	1	LV	S		-19	-11.5	15.7	91		91		same as above
IS89-63(A2)	CQ	1	LV	S		-19	-11.5	15.7	94		94		same as above
IS89-63(A2)	CQ	1	LV	S		-19	-11.5	15.7	102		102		same as above
IS89-63(A2)	CQ	1	LV	S		-19	-11.5	15.7	87		87		same as above
IS89-63(A5)	CQ	1	LVS	S		-24	-8.4	12.4		179	179		large aqueous LVS-type inclusions associated with
IS89-63(A5)	CQ	1	LVS	S			-8.4	12.4		179	179		mixed H2O-CO2 LVS inclusions in 3-D arrays?
IS89-63(A5)	CQ	1	LVS	S			-6.9	10.6	135	185	185		possibly some of them stretched
IS89-63(A5)	CQ	1	LVS	S			-8.4	12.4	125	180	180		
IS89-63(A6)	CQ	1	LVS	S		-20	-6.3	9.79	100	172	172		large inclusions with highly variable-sized biref.
IS89-63(A6)	CQ	1	LVS	S		-20	-6.3	9.79	104	190	190		solids suggesting their probable entrapment origin
IS89-63(A6)	CQ	1	LVS	S		-20	-6.3	9.79	155	172	172		but solids are highly soluble and regrow upon cooling
IS89-63(A6)	CQ	1	LVS	S		-20	-6.3	9.79	167	200	200		same as above
IS89-63(A6)	CQ	1	LVS	S		-20	-6.3	9.79	170	212	212		same as above
IS89-63(A6)	CQ	1	LVS	S		-20	-6.3	9.79	149	180	180		same as above
IS89-63(A6)	CQ	1	LVS	S		-20	-6.3	9.79	130	156	156		same as above
IS89-63(A6)	CQ	1	LVS	S		-20	-6.3	9.79	145	156	156		same as above
IS89-63(A6)	CQ	1	LVS	S		-20	-6.3	9.79	133	181	181		same as above

TABLE 2 (CONT'D)- SURLUGA MINE

SAMPLE	MIN	SET	TYPE	ORT	Tf	Te	TmICE	SAL	TdV	Tdom	Th	TD	COMMENTS
VEIN SET 2													
IS89-63(A6)	CQ	1	LVS	S		-20	-6.3	9.79	128	165	165		same as above
IS89-63(A6)	CQ	2	LVS	S			-5.8	9.14	149	200	200		same as above
IS89-63(A6)	CQ	2	LVS	S			-5.8	9.14	145	170	170		same as above
IS89-63(A6)	CQ	2	LVS	S			-5.8	9.14	134	181	181		same as above
IS89-63(A6)	CQ	2	LVS	S			-5.8	9.14	129	184	184		same as above
IS89-63(A7)	CQ	1	LV	S			-11.6	15.8	128		128		aqueous LV inclusions on secondary plane
IS89-63(A7)	CQ	1	LV	S			-11.6	15.8	128		128		aqueous LV inclusions on secondary plane
IS89-63(A7)	CQ	1	LV	S			-11.6	15.8	128		128		aqueous LV inclusions on secondary plane
IS89-63(A7)	CQ	1	LV	S			-11.6	15.8	128		128		aqueous LV inclusions on secondary plane
IS89-63(A7)	CQ	1	LV	S			-11.6	15.8	128		128		aqueous LV inclusions on secondary plane
IS89-63(A7)	CQ	2	LVS	S			-6.87	10.5	157	187	187		nahcolite-bearing inclusions on secondary plane
IS89-63(A7)	CQ	2	LVS	S			-6.87	10.5	157	187	187		nahcolite-bearing inclusions on secondary plane
IS89-63(A7)	CQ	2	LVS	S			-7.37	11.1	188	207	207		nahcolite-bearing inclusions on secondary plane
IS89-63(A7)	CQ	2	LVS	S			-7.37	11.1	177	212	212		nahcolite-bearing inclusions on secondary plane
IS89-63(A7)	CQ	2	LVS	S			-7.37	11.1	163	202	202		nahcolite-bearing inclusions on secondary plane
IS89-64(a1)	CQ	2	LV	S	-57	-29	-21	23.5	207	-	207		aqueous inclusion on long secondary plane
IS89-64(a1)	CQ	2	LV	S	-57	-29	-21	23.5	182	-	182		same as above
IS89-64(a1)	CQ	2	LV	S	-57		-20.5	23.1	187	-	187		same as above
IS89-64(a1)	CQ	2	LV	S	-57		-21	23.5	190	-	190		same as above
IS89-64(a1)	CQ	2	LV	S	-57		-21.5	23.8	197	-	197		same as above
IS89-64(a1)	CQ	4	LV	S	-69	-25	-18.5	21.7	166	-	166		same as above
IS89-64(a1)	CQ	4	LV	S	-69	-26	-16.5	20.1	180	-	180		same as above
IS89-64(a1)	CQ	4	LV	S	-69	-26	-18.5	21.7	192	-	192		same as above
IS89-64(a1)	CQ	4	LV	S	-69		-17.6	21	178	-	178		same as above
IS89-64(a1)	CQ	4	LV	S	-66		-18.5	21.7	169	-	169		same as above
IS89-64(a1)	CQ	4	LV	S	-63		-20.5	23.1	189	-	189		same as above
IS89-64(a1)	CQ	4	LV	S	-61		-17.5	20.9	187	-	187		same as above
IS89-64(a1)	CQ	4	LV	S	-61		-19.5	22.4	182	-	182		same as above
IS89-64(a2)	CQ	1	LV	S	-49	-22	-18.5	21.7	170	-	170		aqueous lv incl. on secondary trail,
IS89-64(a2)	CQ	1	LV	S	-49	-23	-17.7	21.1	171	-	171		consistent l/v ratio
IS89-64(a2)	CQ	1	LV	S	-49	-21	-19	22	171	-	171		same as above
IS89-64(a2)	CQ	1	LV	S	-53	-23	-19.5	22.4	166	-	166		same as above
IS89-64(a2)	CQ	1	LV	S	-50	-22	-17.5	20.9	166	-	166		same as above
IS89-64(a2)	CQ	1	LV	S	-49	-21	-18	21.3	169	-	169		same as above

TABLE 2 (CONT'D)- SURLUGA MINE

SAMPLE	MIN	SET	TYPE	ORT	Tf	Te	TmICE	SAL	TdV	Tddm	Th	TD	COMMENTS
VEIN SET 2													
IS89-64(a2)	CQ	1	LV	S	-51	-23	-19.5	22.4	166	-	166		same as above
IS89-64(a2)	CQ	1	LV	S	-50	-23	-19.5	22.4	169	-	169		same as above
IS89-64(a3)	CQ	1	LV	S	-37	-22	-14	18	187	-	187		aqueous lv incl. on short plane
IS89-64(a3)	CQ	1	LV	S	-37	-22	-14	18	189	-	189		same as above
IS89-64(a3)	CQ	1	LV	S	-37	-22	-14	18	194	-	194		same as above
IS89-64(a3)	CQ	1	LV	S	-37	-22	-14	18	194	-	194		same as above
IS89-64(a3)	CQ	2	LV	S	-43	-21	-16	19.7	192	-	192		aqueous lv incl. on secondary trail (short)
IS89-64(a3)	CQ	2	LV	S	-43	-21	-16	19.7	204	-	204		consistent l/v ratios
IS89-64(a3)	CQ	2	LV	S	-43	-21	-16	19.7	204	-	204		same as above
IS89-64(a3)	CQ	2	LV	S	-43	-21	-16	19.7	204	-	204		same as above
IS89-64(a3)	CQ	2	LV	S	-43	-21	-16	19.7	214	-	214		same as above
IS89-64(a3)	CQ	3	LV	S	-37	-21	-14.2	18.3	171	-	171		aqueous lv incl. with consistent l/v ratio
IS89-64(a3)	CQ	3	LV	S	-37	-21	-14.2	18.2	171	-	171		group of 2 inclusions
IS89-64(a3)	CQ	4	LV	S	-68	-31	-14.4	18.4	217	-	217		a group of 7 lv inclusions with consistent l/v ratios
IS89-64(a3)	CQ	4	LV	S	-73	-31	-14.4	18.4	214	-	214		same as above
IS89-64(a3)	CQ	4	LV	S			-16.5	20.1	198	-	198		same as above
IS89-64(a3)	CQ	4	LV	S			-14.4	18.4	171	-	171		same as above
IS89-64(a3)	CQ	4	LV	S			-16	19.7	207	-	207		same as above
IS89-64(a3)	CQ	4	LV	S			-15.5	19.3	207	-	207		same as above
IS89-64(a3)	CQ	4	LV	S			-14.4	18.4	198	-	198		same as above
IS89-64(a3)	CQ	5	LV	S	-63	-29	-13.4	17.5	195	-	195		a group of two large (~ 15 mic.) lv incl.'s
IS89-64(a3)	CQ	5	LV	S	-63	-29	-13.6	17.7	203	-	203		with consistent l/v ratios
IS89-64(a4)	CQ	1	LV	S		-26	-15	18.9	204		204		
IS89-64(a4)	CQ	1	LV	S		-26	-12.4	16.6	200		200		
IS89-64(a4)	CQ	1	LV	S		-26	-12.5	16.7	201		201		
IS89-64(a4)	CQ	1	LV	S		-26	-12.2	16.4	200		200		
IS89-64(A6)	CQ	1	LV	S		-23	-11.5	15.7	240		240		
IS89-64(a10)	CQ	2	LV	S		-21	-8.3	12.2	178		178		
IS89-64(a10)	CQ	2	LV	S		-21	-8.1	12	171		171		
IS89-64(a11)	CQ	3	LVS	S		-23	-8.2	12.1		138			

TABLE 2 (CONT'D)- SURLUGA MINE

SAMPLE	MIN	SET	TYPE	ORI	Tf	Te	TmICE	SAL	TdV	Tdcln	Th	TD	COMMENTS
VEIN SET 3													
IS89-69(A1)	CQ	1	LVS	P?			-6.8	10.4				143	large (>10 mic.), isolated aqueous inclusion with prism. biref. soli
IS89-69(A2)	CQ	1	LV	P?			-4.2	6.94	230		230		isolated group 3-D array? with consistent L/V ratios
IS89-69(A2)	CQ	1	LV	P?			-4.3	7.08	240		240		same as above
IS89-69(A2)	CQ	1	LV	P?			-4.5	7.37	235		235		same as above
IS89-69(A3)	CQ	1	LV	P	-41		-0.5	1.14	267		267		large, isolated inclusion, homo. into L
IS89-69(A3)	CQ	2	LV	P	-39		-0.81	1.65	262		262		large, isolated inclusion, homo. into L
IS89-69(A4)	CQ	1	LV	P	-32		0.104	0.08	227		227		large, isolated inclusion, homo. into L
IS89-69(A5)	CQ	1	LV	P	-39		-0.3	0.79	267		267		large, isolated inclusion, homo. into L
IS89-69(A5)	CQ	1	LV	P	-40		-0.4	0.96	262		262		large, isolated inclusion, homo. into L
IS89-69(A5)	CQ	2	LV	P	-41		0.003	0.26	222		222		large, isolated inclusion, homo. into L
IS89-69(A6)	CQ	1	LVS	PS	-40		-7.17	10.9	187		187		large, isolated incl. with trapped solid

MINTO A ZONE

TABLE 3. WAWA MICROTHERMOMETRY DATA FOR AQUEOUS INCLUSIONS
MINTO A ZONE

SAMPLE	MI	SET	TYP	ORT	Tf	Te	TmICE	SAL	TdV	TD	COMMENTS
VEIN SET 2											
IS89-54(B1)	FQ	1	LV	S	-55	-22	-13.3	17	229	-	aqueous inclusion on a secondary plane
IS89-54(B1)	FQ	1	LV	S	-56	-22	-12.5	17	175	-	aqueous inclusion on a secondary plane
IS89-54(B1)	FQ	1	LV	S	-56	-22	-13.2	17	193	-	aqueous inclusion on a secondary plane
IS89-54(B1)	FQ	1	LV	S	-57	-22	-12.7	17	194	-	aqueous inclusion on a secondary plane
IS89-54(B1)	FQ	1	LV	S	-56	-22	-12.4	17	195	-	aqueous inclusion on a secondary plane
IS89-54(B1)	FQ	1	LV	S	-55	-22	-13.5	18	197	-	aqueous inclusion on a secondary plane
IS89-54(B2)	FQ	2	LV	S	-48	-23	-13.1	17	188	-	aqueous inclusion on a secondary plane
IS89-54(B2)	FQ	2	LV	S	-48	-23	-12.4	17	184	-	same as above
IS89-54(B2)	FQ	2	LV	S	-49	-23	-13.2	17	180	-	same as above
IS89-54(B2)	FQ	2	LV	S	-50	-23	-12.8	17	200	-	same as above
IS89-54(B2)	FQ	2	LV	S	-49	-23	-12.4	17	196	-	same as above
IS89-54(B2)	FQ	2	LV	S	-50	-23	-13.5	18	200	-	same as above
IS89-54(B5)	FQ	3	LV	S	-46	-22	-14.1	18	185	-	aqueous inclusion on a secondary plane
IS89-54(B5)	FQ	3	LV	S	-47	-21	-14.2	18	187	-	same as above
IS89-54(B5)	FQ	3	LV	S	-46	-21	-13.5	18	170	-	same as above
IS89-54(B5)	FQ	3	LV	S	-48	-20	-13	17	200	-	same as above
IS89-54(B8)	FQ	4	LV	S	-45	-22	-13.3	17	210	-	aqueous inclusion on a secondary plane
IS89-54(B8)	FQ	4	LV	S	-46	-23	-12.5	17	178	-	same as above
IS89-54(B8)	FQ	4	LV	S	-47	-23	-13.8	18	198	-	same as above
IS89-54(B8)	FQ	4	LV	S	-45	-22	-12.7	17	205	-	same as above
IS89-54(B8)	FQ	4	LV	S	-45	-22	-12.1	16	197	-	same as above
IS89-54(B8)	FQ	4	LV	S	-45	-24	-13.5	18	199	-	same as above
IS89-54(B9)	FQ	5	LV	S	-43	-19	-12.9	17	213	-	aqueous inclusion on a secondary plane
IS89-54(B9)	FQ	5	LV	S	-43	-20	-13.2	17	230	-	same as above
IS89-54(B9)	FQ	5	LV	S	-42	-20	-13.6	18	197	-	same as above
IS89-54(B10)	FQ	6	LV	S	-45	-22	-13.3	17	210	-	aqueous inclusion on a secondary plane
IS89-54(B10)	FQ	6	LV	S	-46	-23	-12.7	17	179	-	same as above
IS89-54(B10)	FQ	6	LV	S	-47	-23	-13.8	18	200	-	same as above
IS89-54(B10)	FQ	6	LV	S	-45	-22	-14.2	18	205	-	same as above
IS89-54(B10)	FQ	6	LV	S	-45	-23	-12.3	16	190	-	same as above
IS89-54(B10)	FQ	6	LV	S	-45	-22	-13.5	18	199	-	same as above
IS89-54(B10)	FQ	6	LV	S	-45	-22	-13.5	18	190	-	same as above
IS89-54(B10)	FQ	6	LV	S	-45	-21	-13.5	18	202	-	same as above

TABLE 4. WAWA MICROTHERMOMETRY DATA FOR AQUEOUS INCLUSIONS
MINTO B ZONE

SAMPLE	MIN	SET	TYPE	OR	Tf	Te	TmICE	SAL	TdV	Tddn	ThTOT	TD	COMMENTS
VEIN SET 2													
IS90-43(B2)	FQ	1	LV	S	-53	-21	-7.6	11.4	153	-	153	-	large incl. on secondary plane; lots of necking
IS90-43(B2)	FQ	1	LV	S	-48	-21	-7.5	11.3	154	-	154	-	large incl. on secondary plane; lots of necking
IS90-43(B2)	FQ	1	LV	S	-45	-21	-7.7	11.5	135	-	135	-	large incl. on secondary plane; lots of necking
IS90-43(B2)	FQ	2	LV	S	-53	-20	-7.8	11.7	158	-	158	-	large incl. on secondary plane; lots of necking
IS90-43(B2)	FQ	2	LV	S	-50	-20	-8	11.9	155	-	155	-	large incl. on secondary plane; lots of necking
IS90-34(A1)	CQ	1	LVS	S	-		-	-	177	-	-	210	secondary incl. with a biref. solid

TABLE 5. WAWA MICROTHERMOMETRY DATA FOR AQUEOUS INCLUSIONS
MINTO E ZONE

SAMPLE	MIN	SET	TYPE	ORI	Tf	Te	TmICE	SAL	TdV	Tddm	ThTOT	TD	COMMENTS
MINTO E - AWAY FROM LAMPRO. DIKE													
1S90-53a(a1)	CQ	1	LVS	S		-44	-5.3	8.47	100	227	227		
1S90-53a(a1)	CQ	1	LVS	S		-43	-6.5	10					
1S90-53a(a1)	CQ	1	LVS	S		-36	-8.2	12.1	107				
1S90-53a(a1)	CQ	1	LVS	S		-39	-6.8	10.4	118	213	213		
1S90-53a(a1)	CQ	1	LVS	S		-30	-8.5	12.5	110	210	210		
1S90-53a(a1)	CQ	2	LV	S		-22	-7.5	11.3	280				
1S90-53a(a1)	CQ	2	LV	S		-20	-6.9	10.6	300				
1S90-53a(a1)	CQ	2	LV	S		-19	-8	11.9	250				
1S90-53a(a1)	CQ	2	LV	S		-20	-6.8	10.4	302				
1S90-53a(a1)	CQ	2	LV	S		-19	-9.2	13.3	264				
1S90-53a(a1)	CQ	2	LV	S		-21	-8.9	12.9	364				
1S90-53a(a1)	CQ	2	LV	S					305				
1S90-53a(a1)	CQ	2	LV	S					235				
1S90-53a(a1)	CQ	2	LV	S					292				
1S90-53a(a1)	CQ	2	LV	S					261				
1S90-53a(a1)	CQ	2	LV	S					195				
1S90-53a(a1)	CQ	2	LV	S					207				
1S90-53a(a1)	FQ	1	LVS	P?		-25	-5	8.06	178	195	195		
1S90-53a(a1)	FQ	1	LVS	P?		-28	-5.4	8.61	175	200	200		
1S90-53a(a1)	FQ	1	LVS	P?		-20	-7	10.7	150	212	212		total freezing at -65oC
1S90-53a(a1)	FQ	1	LVS	P?		-27	-6	9.4	145	206	206		solid completely dissolved
1S90-53a(a1)	FQ	1	LVS	P?			-5.5	8.74	120	150	150		solid completely dissolved
1S90-53a(a1)	FQ	2	LVS	P?		-26	-7	10.7	150	225	225		solid completely dissolved
1S90-53a(a1)	FQ	2	LS	S			-3	5.17		189	>189		decrepitated above 189oC
1S90-53a(a1)	FQ	2	LS	S		-28	-6.5	10					
1S90-53a(a1)	FQ	2	LS	S			-5.8	9.14	25	145	145		v.bubble upon ccoling; solid diss.
1S90-53a(a1)	FQ	3	L	S		-30	-9.6	13.7	25				upon cooling vapor bubble nucl.
1S90-53c(a1)	CQ	2	LVS	S			-5	8.06					
1S90-53c(a1)	CQ	2	LVS	S			-6.3	9.79					
1S90-53c(a1)	CQ	2	LVS	S		-28	-6.2	9.66					
1S90-53c(a1)	CQ	2	LVS	S			-4.8	7.78					
1S90-53c(a4)	CQ	2	LVS	S		-23	-6.5	10	187		193		decrep.as soon as solid dissolved

TABLE 5 (CONT'D)- HINTO E ZONE

SAMPLE	MIN	SET	TYPE	ORI	Tf	Te	TmICE	SAL	TdV	Tddm	ThTOT	TD	COMMENTS
ADJACENT TO LAMPRO. DIKE													
IS90-53b(a1)	CQ	1	LVS	S		-25	-7.6	11.4	95	161	161		solid completely dissolved
IS90-53b(a1)	CQ	1	LVS	S		-21	-7.6	11.4	110	185	185		solid completely dissolved
IS90-53b(a1)	CQ	1	LVS	S		-20	-7.6	11.4	105	180	180		decrepi. above 170oC
IS90-53b(a1)	CQ	1	LVS	S		-21	-7.6	11.4	115	170	170		solid completely dissolved
IS90-53b(a1)	CQ	1	LVS	S		-19	-7.7	11.5	100	165	165		solid completely dissolved
IS90-53b(a1)	CQ	1	LVS	S		-16	-7.7	11.5	135	178	178		solid completely dissolved
IS90-53b(a1)	CQ	1	LVS	S			-7.7	11.5	120	185	185		solid completely dissolved
IS90-53b(a1)	CQ	1	LVS	S		-16	-7.7	11.5	90	178	178		necked incl. TmICE:-7.7(LS)/-8.6(LV)
IS90-53b(a1)	CQ	1	LVS	S			-7.6	11.4	110	186	186		solid completely dissolved
IS90-53b(a1)	CQ	1	LVS	S			-7.4	11.2	125	190	190		solid completely dissolved
IS90-53b(a1)	CQ	1	LVS	S			-7.8	11.7	105	156	156		solid completely dissolved
IS90-53b(a2)	CQ	1	LVS	S		-31	-5.4	8.61	120	185	185		frozen at -57oC; solid dissol.
IS90-53b(a2)	CQ	1	LVS	S		-31	-6.8	10.4	120	185	185		solid completely dissolved
IS90-53b(a2)	CQ	1	LVS	S		-25	-7	10.7	105	170	170		solid completely dissolved
IS90-53b(a2)	CQ	1	LVS	S		-35	-3	5.17	130	189	189		solid completely dissolved
IS90-53b(a2)	CQ	1	LVS	S		-32	-6.9	10.6	140	189	189		solid completely dissolved
IS90-53b(a2)	CQ	1	LVS	S		-32	-7.3	11	115	176	176		solid completely dissolved
IS90-53b(a2)	CQ	1	LVS	S		-33	-8.4	12.4	140	189	189		solid completely dissolved
IS90-53b(a2)	CQ	1	LVS	S		-30	-8.9	12.9	125	185	185		solid completely dissolved
IS90-53b(a2)	CQ	1	LVS	S		-28	-6.5	10	134	180	180		
IS90-53b(a2)	CQ	1	LVS	S		-30	-8.2	12.1	155	199	199		solid diss.;rextall. upon cooling
IS90-53b(a2)	CQ	2	LV	S		-20	-4.5	7.37	175		175		
IS90-53b(a2)	CQ	2	LV	S		-32	-8.5	12.5	145		145		
IS90-53b(a3)	CQ	1	LVS	S		-35	-6.3	9.79	136	180	180		
IS90-53b(a3)	CQ	1	LVS	S		-30	-4	6.65					
IS90-53b(a3)	CQ	1	LVS	S		-33	-2	3.61					
IS90-53b(a3)	CQ	1	LVS	S		-35	-7	10.7	150	240	240		decrep. above 224o (=TD)
IS90-53b(a3)	CQ	1	LVS	S		-36	-8.5	12.5	145	221	221		solid completely dissolv.
IS90-53b(a3)	CQ	1	LS	S		-30	-7.3	11		215	215		solid completely dissolv.
IS90-53b(a3)	CQ	2	LV	PS?		-35	-6.3	9.79					contains CO2 phases
IS90-53b(a3)	CQ	3	L	S		-22	-5.4	8.61					possibly necked
IS90-53b(a6)	CQ	1	LVS	S		-16	-7	10.7					

TABLE 5 (CONT'D)- MINTO E ZONE

SAMPLE	MIN	SET	TYPE	ORI	Tf	Te	TmICE	SAL	TdV	Tddm	ThTOT	TD	COMMENTS
ADJACENT TO LAMPRO. DIKE													
IS90-53b(a6)	CQ	2	LVS	S		-17	-6.7	10.3					
IS90-53b(a6)	CQ	2	LVS	S		-17	-6.5	10					
IS90-53b(a6)	CQ	2	LVS	S		-17	-6.5	10					
IS90-53b(a6)	CQ	2	LVS	S		-17	-7	10.7					vapor bubble not disapp. upon freezing
IS90-53b(a8)	CQ	1	LV	S		-20	-7.5	11.3	131		131		homogenized to liquid
IS90-53b(a8)	CQ	1	LVS	S		-28	-8.1	12	104		178		hom. to liquid by dissol. of dm
IS90-53b(a8)	CQ	1	LVS	S			-7.7	11.5	175	220	>220		large (>10 mic.) LVS inclusions on long secondary planes
IS90-53b(a8)	CQ	2	LVS	S			-7.8	11.7	175	220	>220		of various orientations; consistent phase ratios;
IS90-53b(a8)	CQ	2	LVS	S			-7.8	11.7	175	220	>220		decrepitated above 220°C just after dissolution of the solid
IS90-53b(a8)	CQ	2	LVS	S			-7.8	11.7	175	220	>220		decrepitated above 220°C just after dissolution of the solid
IS90-53b(a8)	CQ	2	LVS	S			-7.8	11.7	175	220	>220		decrepitated above 220°C just after dissolution of the solid
IS90-53b(a8)	CQ	2	LVS	S			-7.8	11.7	175	220	>220		decrepitated above 220°C just after dissolution of the solid
IS90-53b(a8)	CQ	2	LVS	S			-7.8	11.7	175	220	>220		decrepitated above 220°C just after dissolution of the solid
IS90-53b(a8)	CQ	2	LVS	S			-7.8	11.7	175	220	>220		decrepitated above 220°C just after dissolution of the solid
IS90-53b(a8)	CQ	2	LVS	S			-7.8	11.7	175	220	>220		decrepitated above 220°C just after dissolution of the solid
IS90-53b(a8)	CQ	2	LVS	S			-7.8	11.7	175	220	>220		decrepitated above 220°C just after dissolution of the solid
IS90-53b(a8)	CQ	2	LVS	S			-7.8	11.7	175	220	>220		decrepitated above 220°C just after dissolution of the solid
IS90-53b(a8)	CQ	3	LVS	S			-9.4	13.5	175	220	>220		decrepitated above 220°C just after dissolution of the solid
IS90-53b(a8)	CQ	3	LVS	S			-9.4	13.5	175	220	>220		decrepitated above 220°C just after dissolution of the solid
IS90-53b(a8)	CQ	3	LVS	S			-9.4	13.5	175	220	>220		decrepitated above 220°C just after dissolution of the solid
IS90-53b(a8)	CQ	3	LVS	S			-9.4	13.5	175	220	>220		decrepitated above 220°C just after dissolution of the solid
IS90-53b(b3)	FQ	1	LVS	S		-15	-8.2	12.1					
IS90-53b(b3)	FQ	1	LVS	S		-16	-8.2	12.1					
IS90-53b(b4)	FQ	1	LVS	S		-29	-6.6	10.2	112		214		decrep. above 341oC (=TD)
IS90-53b(b4)	FQ	1	LVS	S		-27	-6.5	10	100		189		solid completely dissolv.
IS90-53b(b4)	FQ	1	LVS	S		-30	-2.2	3.93	85		165		solid completely dissolv.
IS90-53b(b4)	FQ	1	LVS	S		-30	-2.5	4.4	140		235		solid completely dissolv.
IS90-53b(b4)	FQ	1	LVS	S		-31	-8.4	12.4					
IS90-53b(b4)	FQ	1	LVS	S		-32	-9.4	13.5					
IS90-50C(A1)	CQ	1	LVS	S		-24	-8.6	12.6	155	150	155		Minto E vsl; large LVS aqueous secondary incl.
IS90-50C(A1)	CQ	1	LVS	S			-8.2	12.1	165	145	165		with large biref. solid; mostly planes
IS90-50C(A1)	CQ	1	LVS	S			-8.1	12	156	146	156		solid completely dissolved upon heating
IS90-50C(A1)	CQ	1	LVS	S		-28	-8.4	12.4	160	150	160		

PART II: MICROTHERMOMETRY DATA FOR MIXED AQUEOUS-CARBONIC FLUID INCLUSIONS

FAT VEIN ZONE

TABLE 6. WAWA MICROTHERMOMETRY DATA FOR MIXED AQUEOUS-CARBONIC INCLUSIONS
FAT VEIN ZONE salinity formula from Bozzo et al. (1974)

SAMPLE	MIN	SET	TYPE	OR	Te	TmCO2	TmCLATH	ThC	TmICE	SAL	ThTOT	TD	COMMENTS
VEIN SET 1													
IS90-4(A1)	CO	1	LL	S	-	-58.4	5.4	7.9	-	8.5	250	-	isolated group of 3 inclusions with consistent phase ratios
IS90-4(A1)	CO	1	LL	S	-	-58.3	6	8.2	-	7.5	260	-	vb nucleated upon cooling
IS90-4(A1)	CO	1	LL	S	-	-58.4	5.8	8.1	-	7.8	269	-	same as above
IS90-4(A1)	CO	1	LL	S	-	-	-	-	-	-	180	-	relatively small inclusions on secondary planes
IS90-4(A1)	CO	2	LL	S	-	-	-	-	-	-	185	-	CO2/H2O phase ratios somewhat variable
IS90-4(A1)	CO	2	LL	S	-	-	-	-	-	-	235	-	dissolving in the aqueous phase
IS90-4(A1)	CO	2	LL	S	-	-	-	-	-	-	280	-	same as above
IS90-4(A1)	CO	2	LL	S	-	-	-	-	-	-	280	-	same as above
VEIN SET 3 "JUBILEE BX"													
IS90-100(A1)	CO	1	LL	P	-	-58.1	8.7	9.6	-	2.6	195	-	relatively small (≈10μ) inclusions with consistent
IS90-100(A1)	CO	1	LL	P	-	-57.8	9	9.4	-	2	195	-	CO2/H2O phase ratios; could be on secondary plane?;
IS90-100(A1)	CO	1	LL	P	-	-57.8	8.9	9.2	-	2.2	195	-	look like aqueous LV incl.'s but upon cooling
IS90-100(A1)	CO	1	LL	P	-	-58.2	9	16	-	2	193	-	a vb nucleates within CO2 phase; in some inclusions
IS90-100(A1)	CO	1	LL	P	-	-58	8.5	8.8	-	3		274	CO2 phase disappears upon freezing; possibly decrepitated
IS90-100(A1)	CO	1	LL	P	-	-57.9	9.1	9.5	-	1.8	-	-	at the indicated temperatures by CO2 phase rather
IS90-100(A1)	CO	1	LL	P	-	-57.8	9.2	6.9	-	1.6	-	-	suddenly filling up the entire inclusion
IS90-100(A1)	CO	1	LL	P	-	-58		2.6	-	-	-	-	same as above
IS90-100(A1)	CO	2	LLV	P	-	-57.7	9	31.1	-	2		265	one large isolated inclusion from the same fragment
IS90-100(A1)	CO	1	LL	P	-	-59.1	4.5	3.9	-	9.8	185	-	large (>10μ) isolated inclusion; vb nucleates upon cooling
IS90-100(A2)	CO	1	LL	P	-	-57.8	7.4	8.1	-	5.1	-	-	isolated group with consistent phase ratios
IS90-100(A3)	CO	1	LL	P	-	-57.8	7.4	9.8	-	5.1	-	-	look like aqueous LV inclusions but upon cooling vb
IS90-100(A3)	CO	1	LL	P	-	-57.8	7.4	9.4	-	5.1	-	-	nucleates within CO2 part
IS90-100(A3)	CO	1	LL	P	-	-57.8	7.4	8.5	-	5.1	-	-	same as above
IS90-100(A3)	CO	1	LL	P	-	-57.8	7.4	8.1	-	5.1	-	-	same as above
IS90-100(A4)	CO	1	LL	P	-	-58	9	-8.6	-	2	-	-	rather small (<10μ) inclusions with variable phase
IS90-100(A4)	CO	1	LL	P	-	-58	9	-8.6	-	2	-	-	ratios probably due to necking down?
IS90-100(A4)	CO	1	LL	P	-	-58	9	-8.6	-	2	-	-	ThCO2 in the presence of clath.= +5.0°C
IS90-100(A4)	CO	1	LL	P	-	-58	9	-8.6	-	2	-	-	same as above
IS90-100(A4)	CO	1	LL	P	-	-58	9	-8.6	-	2	-	-	same as above
IS90-100(A6)	CO	1	LL	P	-	-58.2	8	2.3	-	3.9		150	relatively small group with rather consistent
IS90-100(A6)	CO	1	LL	P	-	-58.2	8	2	-	3.9	180	-	phase ratios; vb nucleated upon cooling
IS90-100(A6)	CO	1	LL	P	-	-58.2	8	2.1	-	3.9	185	-	large one decrepitated at 150°C smaller ones
IS90-100(A6)	CO	1	LL	P	-	-58.2	8	2.2	-	3.9	180	-	homogenized by the dissolution of CO2 within
IS90-100(A6)	CO	1	LL	P	-	-58.2	8	2.3	-	3.9	135	-	aqueous phase
IS90-100(A6)	CO	1	LL	P	-	-58.2	8	3	-	3.9	192	-	same as above
IS90-100(A6)	CO	1	LL	P	-	-58.2	8	2.6	-	3.9	187	-	same as above

TABLE 7. WAWA MICROTHERMOMETRY DATA FOR MIXED AQUEOUS-CARBONIC INCLUSIONS
SURLUGA MINE

SAMPLE	MIN	SET	TYPE	OR	YTC	Te	YmCO2	TmCLATH	ThC	YTH	YmICE	SAL	Tdis	ThTOT	TD	COMMENTS
VEIN SET 1 "AU-QTZ"																
IS89-70A(A4)	CQ	1	LV	S			-58.3	5.6	28.2	-	-	8.13	-	365	-	Surluga mine vs1 Au-qtz
IS89-70A(A4)	CQ	1	LV	S			-58.5	5.4	28	-	-	8.45	-	365	-	
IS89-70A(A4)	CQ	1	LV	S			-58.3	5.8	28.4	-	-	7.81	-	370	-	
IS89-70A(A4)	CQ	1	LL	S			-58.5	5.6	27.9	-	-	8.13	-	360	-	
IS89-70A(A5)	CQ	2	LL	S			-62.3	-	-23.3	-	-	15.5	-	325	-	vapour bubble nucleated within CO2 part upon cooling down to 13°C
IS89-70A(A5)	CQ	2	LL	S			-61.5	6.5	-20.1	-	-	6.63	-	256	-	vapour bubble nucleated within CO2 part upon cooling down to 13°C
IS89-70A(A5)	CQ	2	LL	S			-65.3	-	-19.3	-	-	15.5	-	278	-	same as above
IS89-70A(A5)	CQ	3	LL	S			-65.2	-	-17.3	-	-	15.5	-	-	256	same as above
IS89-70A(A5)	CQ	3	LL	S			-60.3	7.2	-21.2	-	-	5.41	-	-	235	same as above
IS89-70A(A5)	CQ	3	LL	S			-62.3	8.3	-23.5	-	-	3.38	-	-	267	vapour bubble nucleated within CO2 part upon cooling down to -3°C
IS89-70A(A6)	CQ	2	LL	S			-63.6	-	-15.2	-	-	15.5	-	-	234	same as above
IS89-70A(A6)	CQ	2	LL	S			-62.1	7.1	-12.4	-	-	5.59	-	-	225	consistent group along secondary planes in quartz
IS89-70A(A6)	CQ	2	LL	S			-62.1	5.6	-23.5	-	-	8.13	-	-	265	same as above
IS89-70A(A6)	CQ	2	LL	S			-61.3	-	-22.2	-	-	15.5	-	-	231	same as above
VEIN SET 2 "PINTO QTZ"																
IS89-63(A1)	CQ	1	LLVS	S	-98		-59.9	4.2	20.8	-45	-12.1	10.3	-	-	200	Surluga mine vs2=pinto qtz; large (=20 mic.) isolated group ?
IS89-63(A1)	CQ	1	LLVS	S	-98		-59.3	4.2	25.9	-45	-11.8	10.3	-	-	200	contains large biref. solid; assoc. with aqueous LVS incl.'s
IS89-63(A1)	CQ	2	LLVS	S	-89		-60.8	6.5	14.9	-50	-11.5	6.63	-	?	?	Surluga mine vs2=pinto qtz; large (=20 mic.) isolated group ?
IS89-63(A1)	CQ	2	LLVS	S	-85		-60.8	6.3	15.3	-50	n.v	6.97	-	?	?	Surluga mine vs2=pinto qtz; large (=20 mic.) isolated group ?
IS89-63(A1)	CQ	2	LLVS	S	-99		-60.6	6.6	20.3	-48	n.v	6.46	-	?	?	Surluga mine vs2=pinto qtz; large (=20 mic.) isolated group ?
IS89-63(A3)	CQ	1	LL	S			-58.5	6	14.7		-9.7	7.48	-	170		could be TD as well but CO2 liquid filled up
IS89-63(A3)	CQ	1	LL	S			-58.6	5	10.9		-9.7	9.08	-	175		the entire inclusion
IS89-63(A3)	CQ	1	LL	S			-58.6	6	16.6		-9.7	7.48	-			
IS89-63(A3)	CQ	1	LLVS	S			-58.4		15			15.5	182	224		could be TD as well though carbonic liquid
IS89-63(A5)	CQ	1	LLVS	PS			-59.3	4	23.5		-13.5	10.6		190		large mixed H2O-CO2 inclusions (LVS-type)
IS89-63(A5)	CQ	1	LLVS	PS			-59.3	4	18.7		-13.3	10.6	200	239		in 3-D arrays? Thtot values could be TDt
IS89-63(A5)	CQ	1	LLVS	PS			-59.3	4	22.4		-13.4	10.6		200		TDT CO2(L) phase filled up the entire inclusion
IS89-63(A5)	CQ	1	LLVS	PS			-58.4	4.5	26.5		-12.5	9.84	170	280		could be decrepitated before final homo.

TABLE 7 (CONT'D)- SURLUGA MINE

SAMPLE	MIN	SET	TYPE	OR	TfC	Te	TmCO2	TmCLATH	ThC	TfH	TmICE	SAL	Tdclm	ThTOT	TD	COMMENTS
VEIN SET 2																
IS89-64(A3)	CQ	1	LLV	S	-100		-58.4	6.7	31.0	-42	n.v.	6.3	?			secondary plane, consistent l/v ratios
IS89-64(A3)	CQ	1	LLV	S	-99		-58.6	6.7	31.0	-43	-8.4	6.3	?			same as above
IS89-64(A3)	CQ	1	LLV	S	-100		-58.5	6.6	31.0	-42	n.v.	6.5	?			same as above
IS89-64(A3)	CQ	1	LLV	S	-99		-58.5	6.7	31.0	-43	n.v.	6.3	?			same as above
IS89-64(A4)	CQ	1	LV	S?		-69	-59.7		31.0		-8.4	15.5				probably stretched because of anomalous TdV
IS89-64(A4)	CQ	2	LL	S			-58.4	2.4	24.6		-	12.8		-	303	inclusions with slightly variable H2O/CO2 phase ratios occuring
IS89-64(A4)	CQ	2	LLV	S			-58.4	2.7	24.6		-	12.4		243	-	on variously oriented secondary planes, consistent HT results
IS89-64(A4)	CQ	2	LLV	S			-58.4	2.6	25.0		-	12.5		265	-	few aqueous LV-type inclusions (5) with TmICE = -9.8 consistently
IS89-64(A4)	CQ	2	LLV	S			-58.9	3.0	25.2		-	12.0		250	-	
IS89-64(A4)	CQ	2	LLV	S			-58.8	2.9	24.8		-	12.1		245	-	
IS89-64(A4)	CQ	2	LLV	S			-58.7	2.8	26.0		-	12.2		-	255	decrepitated
IS89-64(A4)	CQ	2	LLV	S			-59	3.1	25.4		-	11.8		249	-	homogenized into L
IS89-64(A4)	CQ	2	LLV	S			-59	3.1	25.4		-	11.8		250	-	homogenized into L
VEINSET 3																
IS89-69(A3)	CQ	1	LLS	P?	-99		-58.7	3.1	4.5	-46	-6.2	11.8	?	?	?	a group of 3 inclusions with variably-sized
IS89-69(A3)	CQ	1	LLS	P?	-99		-58.7	3.3	-	-46	-	11.6	?	?	?	biref. solid (a trapped phase?)
IS89-69(A3)	CQ	1	LLS	P?	-99		-58.7	3.1	4.2	-47	-	11.8	?	?	?	same as above
IS89-69(A2)	CQ	1	LLV	P	-96		-58.4	3.9	27.5	-49	-	10.7		?	?	a group of 3 inclusions in a 3-D array
IS89-69(A2)	CQ	1	LLV	P	-96		-58.5	3.9	27.5	-49	-	10.7		?	?	one of them has no vb in carbonic part
IS89-69(A2)	CQ	1	LLV	P	-96		-58.4	4.2	24.4	-46	-	10.2		?	?	

TABLE 8. WAVA MICROTHERMOMETRY DATA FOR MIXED AQUEOUS-CARBONIC INCLUSIONS
MINTO A ZONE

SAMPLE	MIN	SE	TYPE	ORIG	TFC	Te	TmCO2	TmCLATH	ThC	TfH	TmICE	SAL	TdDH	ThTOT	TD	COMMENTS
VEIN SET 2 (PINTO VEIN)																
IS89-19(A1)	CQ	1	LLV	S	-95		-59.7	3.8	30	-42	-12.8	10.9	-	305	305?	mixed incl. on a steep (vertical) secondary plane
IS89-19(A1)	CQ	1	LLV	S	-98		-59.7	3.8	30.4	-45	-12.5	10.9	-	305	305?	could be TD
IS89-19(A1)	CQ	2	LLV	S	-100		-59.7	4	28	-50	-12.6	10.6	-	-	212	decrep.
IS89-19(A1)	CQ	2	LLV	S	-98		-59.9	3.8	26	-48	-12.8	10.9	-	-	245	decrep.
IS89-19(A1)	CQ	2	LLV	S	-90		-59.9	4.1	26	-50		10.4	-	-	223	no observation on homo.
IS89-19(A2)	CQ	1	LLV	S	-100		-59.4	4	31.1	-37	-10.5	10.6	-	295	-	mixed incl. on a steep secondary plane
IS89-19(A2)	CQ	1	LLV	S	-100		-59.4	4	30.5	-37	-10.5	10.6	-	283	-	mixed incl. on a steep secondary plane
IS89-19(A2)	CQ	1	LLV	S	-100		-59.4	4	30	-37	-10.5	10.6	-	300	-	mixed incl. on a steep secondary plane
IS89-19(A2)	CQ	1	LLV	S	-100		-59.4	4	30.2	-37	-10.5	10.6	-	305	-	mixed incl. on a steep secondary plane
IS89-19(A2)	CQ	2	LLV	S	-100		-59.4	4	26.5	-37	-10.5	10.6	-	300	-	mixed incl. on a steep secondary plane
IS89-19(A2)	CQ	2	LLV	S	-100		-59.4	4	28	-37	-10.5	10.6	-	286	-	mixed incl. on a steep secondary plane
IS89-19(A2)	CQ	2	LLV	S	-100		-59.4	4	26.7	-37	-10.5	10.6	-	281	-	mixed incl. on a steep secondary plane
IS89-19(A2)	CQ	2	LLV	S	-100		-59.4	4	27.9	-37	-10.5	10.6	-	290	-	mixed incl. on a steep secondary plane
IS89-21(A2)	CQ	1	LLV	S	-95		-58.0	5.3	29.6	-46	n.v.	8.7	-	-	223	mixed 3-phase inclusions on a secondary plane
IS89-21(A2)	CQ	1	LLV	S	-97		-57.9	4.8	29.4	-47	n.v.	9.5	-	-	245	consistent l/v phase ratios; 5-10μ in size
IS89-21(A2)	CQ	1	LLV	S	-96		-57.8	4.5	29.5	-46	n.v.	9.8	-	-	167	same as above; decrepitated
IS89-21(A2)	CQ	1	LLV	S	-96		-58.0	4.5	29.2	-47	-12.4	9.8	-	-	189	same as above; decrepitated
IS89-21(A2)	CQ	1	LLV	S	-96		-58.0	4.5	29.2	-47	n.v.	9.8	-	-	167	same as above; decrepitated
IS89-21(A2)	CQ	1	LLV	S	-96		-58.2	4.8	29.3	-47	n.v.	9.5	-	-	187	same as above; decrepitated
IS89-21(A2)	CQ	1	LLV	S	-95		-58.1	4.5	29.5	-47	n.v.	9.8	-	-	189	same as above; decrepitated
IS89-21(A2)	CQ	1	LLV	S	-96		-58.0	4.7	29.3	-47	n.v.	9.5	-	-	213	same as above; decrepitated
IS89-21(A2)	CQ	2	LLV	S	-98		-57.9	4.8	30.7	-46	n.v.	9.5	-	-	200	mixed 3-phase inclusions with consistent l/v ratios
IS89-21(A2)	CQ	2	LLVS	S	-99		-57.9	5.0	30.7	-44	n.v.	9.2	139	-	223	some contain small biref. solids
IS89-21(A2)	CQ	2	LLV	S	-94		-58.0	5.3	30.1	-51	-11.4	8.7	-	-	221	liv-type; decrepitated
IS89-21(A2)	CQ	2	LLV	S	-96		-58.0	5.3	30.1	-50	-10.4	8.6	-	-	189	liv-type; decrepitated
IS89-21(A2)	CQ	3	LLV	S	-96		-58.0	5.3	29.8	-48	n.v.	8.7	-	-	167	liv-type; decrepitated
IS89-21(A2)	CQ	3	LLVS	S	-97		-58.2	5.1	29.7	-46	n.v.	8.9	125	-	197	contains birefrengent solid; decrepitated
IS89-21(A2)	CQ	3	LLVS	S	-96		-58.2	5.0	29.8	-48	n.v.	9.1	137	-	234	contains birefrengent solid; decrepitated
IS89-21(A2)	CQ	3	LLV	S	-95		-57.9	5.2	29.9	-48	n.v.	8.8	-	-	234	liv-type; decrepitated
IS89-21(A2)	CQ	3	LLV	S	-96		-58.0	5.0	29.4	-46	n.v.	9.1	-	-	256	liv-type; decrepitated

TABLE 8 (CONT'D)- MINTO A ZONE

SAMPLE	MIN	SE	TYPE	ORIG	TfC	Te	TmCO2	TmCLATH	ThC	TfH	TmICE	SAL	TdDH	ThTOT	TD	COMMENTS
VEIN f.r 2 (PINTO VEIN)																
IS89-21(A3)	CQ	4	LLVS	S	-99		-58.3	3.2	20.1	-49	n.v.	11.7	142	-	267	mixed 3-phase inclusions on long secondary planes
IS89-21(A3)	CQ	4	LLV	S	-99		-58.1	3.7	20.3	-47	-13.4	11.0	-	-	258	some contain small biref. solids
IS89-21(A3)	CQ	4	LLV	S	-98		-58.3	3.7	20.4	-48	n.v.	11.0	-	-	272	liv-type; decrepitated
IS89-21(A3)	CQ	4	LLV	S	-97		-58.1	3.9	20.2	-48	n.v	10.7	-	-	252	liv-type; decrepitated
IS89-21(A3)	CQ	4	LLV	S	-96		-58.2	3.7	20.3	-48	n.v.	11.0	-	-	275	liv-type; decrepitated
IS89-21(A3)	CQ	4	LLV	S	-97		-58.2	3.9	20.1	-47	n.v.	10.7	-	-	272	liv-type; decrepitated
IS89-21(A3)	CQ	5	LLV	S	-96		-58.0	5.8	28.8	-63	-11.4	7.9	-	-	242	large (>20µ) liv-type secondary incl.; decrepitated
IS89-21(A3)	CQ	5	LLV	S	-99		-57.9	5.6	29.4	-66	-13.4	8.2	-	-	223	large (>20µ) liv-type secondary incl.; decrepitated
IS89-21(A4)	CQ	1	LLVS	S	-96		-57.8	5.0	30.4	-61	-13.4	9.2	135	-	224	large (>10µ) 3-phase incl. with biref. prism. solid
IS89-21(A4)	CQ	1	LLV	S	-96		-57.8	5.2	30.3	-59	n.v.	8.8	-	-	224	secondary plane (short)
VEINSET 3 (QUARTZ-BIOTITE VEIN)																
IS90-10(A2)	CQ	1	LL	S	-100		-59.0	8.4	2.2	-43	n.v.	3.2	-	-	210	large mixed incl. with a large vb=CO2 phase; v phase
IS90-10(A2)	CQ	1	LL	S	-100		-59.2	7.8	3.1	-44	n.v.	4.4	-	-	186	nucleated within this part at -4.2°C upon cooling
IS90-10(A2)	CQ	1	LL	S	-98		-58.9	8.2	4.5	-45	n.v	3.6	-	-	178	same as above;decrepitated
IS90-10(A3)	CQ	2	LL	S	-98		-57.6	7.2	8.1	-46	n.v	5.4	-	-	167	same as above;decrepitated
IS90-10(A3)	CQ	2	LL	S	-101		-57.4	6.3	6.1	-38	n.v	7.0	-	-	213	same as above;decrepitated
IS90-10(A3)	CQ	2	LL	S	-89		-58.1	6.8	4.8	-43	n.v	6.1	-	-	187	same as above;decrepitated

TABLE 9. WAWA MICROTHERMOMETRY DATA FOR MIXED AQUEOUS-CARBONIC INCLUSIONS
MINTO B ZONE

SAMPLE	MIN	SET	TYPE	ORIG	Tfc	Te	TmCO2	TmCLATH	ThC	Tfh	TmICE	SAL	ThTO	TD	COMMENTS
VEIN SET 2 (PINTO VEIN)															
IS90-43(F1)	FQ	1	LLV	S	-100		-59.3	1.7	30.8	-55	n.v	13.63	189	-	three-phase inclusion on a short plane
IS90-43(F1)	FQ	1	LLV	S	-100		-59.3	1.7	30.8	-55	n.v	13.63	-	198	three-phase inclusion on a short plane
IS90-43(F1)	FQ	1	LLV	S	-100		-59.3	1.7	30.8	-55	n.v	13.63	192	-	three-phase inclusion on a short plane
IS90-43(F1)	FQ	1	LLV	S	-100		-59.3	1.7	30.8	-55	n.v	13.63	-	223	three-phase inclusion on a short plane
IS90-43(F1)	FQ	1	LLV	S	-100		-59.3	1.7	30.8	-55	n.v	13.63	-	156	three-phase inclusion on a short plane
IS90-43(F3)	FQ	1	LLV	S	-100		-59.1	2.4	28.8	-53	n.v	12.76	-	174	three-phase inclusion on a short plane
IS90-43(F3)	FQ	1	LLV	S	-100		-59.1	2.4	30	-53	n.v	12.76	182	-	three-phase inclusion on a short plane
IS90-43(F3)	FQ	1	LLV	S	-100		-59.1	2.4	30	-53	n.v	12.76	213	-	three-phase inclusion on a short plane
IS90-43(F3)	FQ	1	LLV	S	-100		-59.1	2.4	30	-53	n.v	12.76	-	167	three-phase inclusion on a short plane
IS90-43(F3)	FQ	1	LLV	S	-100		-59.1	2.4	26.5	-53	n.v	12.76	200	-	three-phase inclusion on a short plane

TABLE 10. WAWA MICROTHERMOMETRY DATA FOR MIXED AQUEOUS-CARBONIC INCLUSIONS
MINTO E ZONE

SAMPLE	MIN	SET	TYPE	ORT	YTC	Te	YmCO2	YmCLATH	ThC	TfH	YmICE	SAL	YdV	Ydcm	YhTO	TD	COMMENTS
ADJACENT TO LAMPRO. DIKE																	
IS90-53B(A3)	CQ	1	LLVS	S			-59.3	-7.1	28.8	-46	-6.3	20.12	0	123	n.d	186	decrepitated
IS90-53B(A6)	CQ	1	LLS	S			-59.1	-5	22.8	-		19.32	n.d	n.d	n.d	n.d	vapor bubble nucl. upon cooling to 17oC
IS90-53B(A6)	CQ	1	LLVS	S			-59.1	-7.4	22.8	-39	-6.6	20.2	n.d	145	n.d	n.d	no vCO2 at room T, bubble nucl. upon cool.
IS90-53B(A6)	CQ	1	LLVS	S			-59.1	-7.4	22.5	-	-6.5	20.2	n.d	n.d	n.d	n.d	min.T=-111oC
IS90-53B(A6)	CQ	1	LLV	S			-59.1	-7.4	26.6	-	-7	20.2	n.d	153	n.d	187	
IS90-53B(A6)	CQ	1	LLVS	S			-59.2	-7	27	-	-6.6	20.09	n.d	145	n.d	168	
IS90-53B(B3)	FQ	1	LLVS	S			-59	-7.2	28.1	-43	-10.5	20.15	n.d	151	n.d	n.d	min T of cooling =-105°C
IS90-53B(B3)	FQ	1	LLVS	S			-59.2	-7	28.7	-	-8.7	20.09	n.d	128	n.d	213	decrepitated
IS90-53B(B3)	FQ	1	LLVS	S			-59	-7.4	22.5	-	-9.6	20.2	n.d	n.d	n.d	198	decrepitated
AWAY FROM LAMPRO. DIKE																	
IS90-53C(A1)	CQ	1	LV	S			-59.1	-7.2	22	-48	-12	15.52 20.15					
IS90-53C(A1)	CQ	1	LV	S			-58.9	-6.9	21	-	-12	20.07					
IS90-53C(A1)	CQ	1	LVS	S			-59.1	-7.2	24.1	-36	-8.5	20.15					
IS90-53C(A1)	CQ	1	L	S			-59.3	-7	15	-	-5.3	20.09					large L-L mixed H2-CO2 incl., VCO2 nucl. 6oC

PART III: MICROTHERMOMETRY DATA FOR CARBONIC FLUID INCLUSIONS SURLUGA MINE

TABLE 11. WAWA MICROTHERMOMETRY DATA FOR CARBONIC INCLUSIONS
SURLUGA MINE

SAMPLE #	MIN	SET	TYPE	ORIG	Tf	Te	Tm.CO2	Thc	COMMENTS
CORE SAMPLE- VEIN SET 1									
S280-613(A1)	CQ	1	V	S				-87	large (>20 microns) V CH4-rich inclusion with minor CO2
S280-613(A1)	CQ	1	V	S				-88	large, one-phase CH4-rich inclusions on a secondary plane
VEIN SET 1 (NO GOLD)									
IS89-708(A1)	CQ	1	L	S	-96		-59.2	1.2	long secondary planes transecting grain boundaries
IS89-708(A1)	CQ	1	L	S	-96		-59.3	-1.1	homogenized to L phase
IS89-708(A1)	CQ	1	L	S	-96		-59.2	1.5	vsl with no v.g. from Surluga mine; one-phase
IS89-708(A1)	CQ	1	L	S	-96		-59.4	5	dense L CO2-rich inclusions (>15µm in size)
IS89-708(A1)	CQ	2	L	S	-96	-65	-58.9	-0.1	dense (L) one-phase inclusions along a well-defined
IS89-708(A1)	CQ	2	L	S	-96	-65	-58.9	1.7	secondary plane; very large in size (>20µ)
IS89-708(A1)	CQ	2	L	S	-96	-65	-58.9	3.8	vb nucleated upon cooling; homo. into L
IS89-708(A1)	CQ	2	L	S	-96	-65	-58.9	13.5	same as above; Raman file #: Wawa57.asc
IS89-708(A1)	CQ	3	L	S			-59.3	0.9	a differently-oriented secondary plane
IS89-708(A1)	CQ	3	L	S			-59.3	1.4	with the same type of inclusions as above
IS89-708(A1)	CQ	3	L	S			-59.3	1.6	same as above; Raman file #: Wawa57.asc
IS89-708(A1)	CQ	3	L	S			-59.3	1.4	same as above
IS89-708(A2)	CQ	1	L	S	-99		-57.8	6.5	isolated group of 15 one-phase high-density inclusions
IS89-708(A2)	CQ	1	L	S	-99		-57.8	6.5	same as above
IS89-708(A2)	CQ	1	L	S	-99		-57.8	6.5	same as above
IS89-708(A2)	CQ	1	L	S	-99		-57.8	6.5	same as above
IS89-708(A2)	CQ	1	L	S	-99		-57.8	8	same as above
IS89-708(A2)	CQ	1	L	S	-99		-57.8	8	same as above
IS89-708(A2)	CQ	1	L	S	-99		-57.8	8	same as above
IS89-708(A2)	CQ	1	L	S	-99		-57.8	8	same as above
IS89-708(A2)	CQ	1	L	S	-99		-57.8	8	same as above
IS89-708(A2)	CQ	1	L	S	-99		-57.8	8	same as above
IS89-708(A2)	CQ	1	L	S	-99		-57.8	8	same as above
IS89-708(A2)	CQ	1	L	S	-99		-57.8	8	same as above

TABLE 11 (CONT'D)- SURLUGA MINE

SAMPLE #	MIN	SET	TYPE	ORIG	Tf	Te	TmCO2	Thc	COMMENTS
VEIN SET 1 (NO GOLD)									
IS89-70B(A2)	CQ	1	L	S	-99		-57.8	8	same as abcve
IS89-70B(A2)	CQ	2	L	S			-57.8	4.6	same as above
IS89-70B(A2)	CQ	2	L	S			-57.8	4.2	same as above
IS89-70B(A2)	CQ	2	L	S			-57.8	5.9	same as above
IS89-70B(A2)	CQ	2	L	S			-57.8	6.8	same as above
IS89-70B(A2)	CQ	2	L	S			-57.8	7.1	same as above
IS89-70B(A2)	CQ	2	L	S			-57.8	4.5	same as above
IS89-70B(A2)	CQ	2	L	S			-57.8	5.6	same as above
IS89-70B(A2)	CQ	2	L	S	-93		-57.8	6.5	same as above
IS89-70B(A2)	CQ	3	L	S	-93		-59.1	2.7	same as above
IS89-70B(A2)	CQ	3	L	S	-93	-64	-59.1	3.8	same as above
IS89-70B(A2)	CQ	3	L	S	-93		-59.1	4.2	same as above
IS89-70B(A2)	CQ	3	L	S	-93		-59.1	4.2	same as above
IS89-70B(A2)	CQ	3	L	S	-93		-59.1	4.2	same as above
IS89-70B(A2)	CQ	3	L	S	-93		-59.1	4.2	same as above
IS89-70B(A3)	CQ	1	L	S	-96		-58.3	2.7	a group of 10 inclusions with sizes ranging from
IS89-70B(A3)	CQ	1	L	S	-96		-58.3	2.7	5 to >20μ; one-phase; occuring on secondary planes
IS89-70B(A3)	CQ	1	L	S	-96		-58.3	2.7	same as above
IS89-70B(A3)	CQ	1	L	S	-96		-58.3	2.7	same as above
IS89-70B(A3)	CQ	1	L	S	-96	-66	-58.3	2.7	same as above
IS89-70B(A3)	CQ	1	L	S	-96		-58.3	2.7	same as above
IS89-70B(A3)	CQ	1	L	S	-96		-58.3	2.7	same as above
IS89-70B(A3)	CQ	1	L	S	-96		-58.3	2.7	same as above
IS89-70B(A3)	CQ	1	L	S	-96		-58.3	2.7	same as above
IS89-70B(A3)	CQ	1	L	S	-96		-58.3	2.7	same as above
IS89-70B(A3)	CQ	2	L	S	-91		-57.6	3.1	same as above
IS89-70B(A3)	CQ	2	L	S	-91		-57.6	3.1	same as above
IS89-70B(A3)	CQ	2	L	S	-91	-67	-57.6	3.1	same as above
VEIN SET 1 (AU-BEARING SAMPLE)									
IS89-70A(A1)	CQ	1	LV	S	-111		-65	-20	
IS89-70A(A1)	CQ	1	LV	S	-106		-65.1	-20	
IS89-70A(A1)	CQ	1	LV	S	-109		-65	-22	
IS89-70A(A1)	CQ	1	LV	S	-109		-65	-19	

TABLE 11 (CONT'D)- SURLUGA MINE

SAMPLE #	MIN	SET	TYPE	ORIG	Tf	Te	TmCO2	ThC	COMMENTS
VEIN SET 1 (AU-BEARING SAMPLE)									
IS89-70A(A1)	CQ	1	LV	S	-109		-65	-20	
IS89-70A(A1)	CQ	1	LV	S	-109		-65.3	-21	
IS89-70A(A1)	CQ	1	LV	S	-109		-65	-20	
IS89-70A(A1)	CQ	2	L	S	-106		-66	-55	vb nucleated at -59°C upon cooling
IS89-70A(A1)	CQ	2	L	S	-106		-66	-55	same as above
IS89-70A(A1)	CQ	3	L	S	-106		-67	-20	vb nucleated at -25°C; large (>10 mic.) one-phase inclusions
IS89-70A(A1)	CQ	3	L	S	-106		-67	-21	same as above
IS89-70A(A1)	CQ	3	L	S	-106		-67	-20	same as above
IS89-70A(A1)	CQ	3	L	S	-106		-67	-20	same as above
IS89-70A(A1)	CQ	3	L	S	-116		-67	-20	same as above
IS89-70A(A1)	CQ	3	L	S	-116		-67	-20	same as above
IS89-70A(A1)	CQ	3	L	S	-116		-67	-20	same as above
IS89-70A(A1)	CQ	3	L	S	-116		-67	-20	same as above
IS89-70A(A1)	CQ	4	L	S	-116		-65	-20	a group of 7 one-phase inclusions on secondary planes
IS89-70A(A1)	CQ	4	L	S	-116		-64.7	-25	same as above
IS89-70A(A1)	CQ	4	L	S	-116		-64.5	-25	same as above
IS89-70A(A1)	CQ	4	L	S	-116		-65	-19	same as above
IS89-70A(A1)	CQ	4	L	S	-116		-65	-20	same as above
IS89-70A(A1)	CQ	4	L	S	-116		-65	-19	same as above
IS89-70A(A1)	CQ	4	L	S	-116		-65	-20	same as above
IS89-70A(A2)	CQ	1	L	S	-116		-65	-20	a group of 10 one-phase inclusions on long, secondary trails
IS89-70A(A2)	CQ	1	L	S	-116		-65	-20	vb nucleated at -25°C; consistent MT for the group
IS89-70A(A2)	CQ	1	L	S	-116		-65	-20	same as above
IS89-70A(A2)	CQ	1	L	S	-116		-65	-20	same as above
IS89-70A(A2)	CQ	1	L	S	-116		-65	-20	same as above
IS89-70A(A2)	CQ	1	L	S	-116		-65	-20	same as above
IS89-70A(A2)	CQ	1	L	S	-116		-65	-20	same as above
IS89-70A(A2)	CQ	1	L	S	-116		-65	-20	same as above
IS89-70A(A2)	CQ	1	L	S	-116		-65	-20	same as above
IS89-70A(A2)	CQ	2	L	S	-111		-65.2	-11	CO2 inclusions associated with aqueous LVS/LV
IS89-70A(A2)	CQ	2	L	S	-111		-65.2	-11	inclusions on secondary plane
IS89-70A(A2)	CQ	2	L	S	-111		-65.1	-11	some have a small rim of aqueous liquid

TABLE 11 (CONT'D)- SURLUGA MINE

SAMPLE #	MIN	SET	TYPE	ORIG	Tf	Te	TmCO2	ThC	COMMENTS
VEIN SET 1 (AU-BEARING SAMPLE)									
IS89-70A(A3)	CQ	1	L	S	-106		-67	-55	one-phase inclusions on a secondary trail
IS89-70A(A3)	CQ	1	L	S	-106		-67	-55	assoc. with aqueous lv-type incl.'s
IS89-70A(A3)	CQ	1	L	S	-106		-67	-55	same as above
IS89-70A(A3)	CQ	1	L	S	-106		-67	-53	same as above
IS89-70A(A3)	CQ	1	L	S	-106		-67	-53	same as above
IS89-70A(A3)	CQ	1	L	S	-106		-67	-53	same as above
IS89-70A(A4)	CQ	1	L	S	-106		-66	-26	one-phase inclusions (>15 microns) assoc. with
IS89-70A(A4)	CQ	1	L	S	-106		-66	-26	two-types of mixed incl.'s: one with a low TmCO2
IS89-70A(A4)	CQ	1	L	S	-106		-66	-26	other with a very high TmCO2
IS89-70A(A4)	CQ	1	L	S	-106		-66	-26	same as above
IS89-70A(A4)	CQ	1	L	S	-106		-66	-26	same as above
IS89-70A(A4)	CQ	1	L	S	-106		-66	-26	same as above
VEIN SET 2 "PINTO QTZ"									
IS89-63(A2)	CQ	1	L	S			-57.4	10.4	Surluga mine vs2 (= pinto qtz);
IS89-63(A2)	CQ	1	L	S			-57.4	10.9	dense one-phase L CO2 inclusions on
IS89-63(A2)	CQ	1	L	S			-57.4	11.5	dense secondary planes; various sizes (1-15μm)
IS89-63(A2)	CQ	1	L	S			-57.4	10.7	very consistent TmCO2 values
IS89-63(A2)	CQ	1	L	S			-57.4	13.3	on secondary planes
IS89-64(A1)	CQ	1	LV	S	-99		-58.6	27	two-phase(LV) inclusions on secondary planes
IS89-64(A1)	CQ	1	LV	S	-99		-58.6	27	assoc. with large lvs-type (nahco.) and lv-type incl.'s
IS89-64(A1)	CQ	1	LV	S	-99		-58.6	27	very consistent MT data
IS89-64(A1)	CQ	1	LV	S	-99		-58.6	27	size variable: 5-10 microns on the average
IS89-64(A1)	CQ	1	LV	S	-99		-58.6	27	same as above
IS89-64(A1)	CQ	1	LV	S	-99		-58.6	27	same as above
IS89-64(A10)	CQ	1	LV	S			-58.4	28	two-phase incl. on secondary plane
IS89-64(A10)	CQ	1	LV	S			-58.4	29	same as above
IS89-64(A10)	CQ	1	LV	S			-58.4	29	same as above
IS89-64(A10)	CQ	1	LV	S			-58.4	29	same as above
IS89-64(A11)	CQ	1	LV	S			-58	25.8	same as above
IS89-64(A11)	CQ	2	VL	S			-57.9	27	homogenized into V
IS89-64(A11)	CQ	2	VL	S			-57.8	27	homogenized into V
IS89-64(A11)	CQ	3	LV	S			-57.7	23.5	same as above
IS89-64(A11)	CQ	3	LV	S			-57.7	23.5	same as above
IS89-64(A11)	CQ	3	LV	S			-57.7	27	same as above
IS89-64(A11)	CQ	3	LV	S			-57.8	27.7	same as above

MINTO B ZONE

TABLE 12. WAWA MICROTHERMOMETRY DATA FOR CARBONIC INCLUSIONS
MINTO B ZONE

SAMPLE #	MIN	SET	TYPE	ORIG	Tf	Te	TmCO2	ThC	COMMENTS
VEIN SET 2									
IS90-43(A1)	FQ	1	L	S	-75		-58.4	12	one-phase inclusion occuring on a secondary plane
IS90-43(A1)	FQ	1	L	S	-75		-58.4	12	along with mixed type inclusions with same TmCO2
IS90-43(A1)	FQ	1	L	S	-75		-58.4	12	vb nucleated upon cooling; homogen. into L
IS90-43(A1)	FQ	1	L	S	-75		-58.5	16.4	same as above

MINTO E ZONE

TABLE 13. WAWA MICROTHERMOMETRY DATA FOR CARBONIC INCLUSIONS
MINTO E ZONE

SAMPLE #	MIN	SET	TYPE	ORIG	TfCO2	Te	TmCO2	ThC	COMMENTS
ADJACENT TO LAMPRO. DIKE									
IS90-53b(A5)	CQ	1	LVS	S	-98	-	-58	29.8	trapped solid; Raman:wawa25
IS90-53b(A6)	CQ	1	LVS	S	-100	-	-58.3	28.1	solid phase trapped
IS90-53b(A6)	CQ	1	LV	S	-98	-	-58.2	28.1	
IS90-53b(A7)	CQ	1	LVS	S	-97	-	-59	28.4	
IS90-53b(A7)	CQ	1	LV	S	-98	-	-59	28.3	
IS90-53b(A9)	CQ	1	L	S	-91	-	-58.3	16.6	large one-phase LCO2 incl.
IS90-53b(A9)	CQ	1	L	S	-92	-	-58.3	18	vapor bubble nucl. at -1oC
IS90-53b(A9)	CQ	1	L	S	-95	-	-58.3	16.1	
IS90-53b(A9)	CQ	1	L	S	-94	-	-58.3	17.3	max. TdV=19.5
IS90-53b(A9)	CQ	1	L	S	-91	-	-59.2	14.1	
IS90-53b(A9)	CQ	1	L	S	-93	-	-58.8	11	
IS90-53b(A9)	CQ	1	L	S	-92	-	-58.8	14.8	
IS90-53b(A9)	CQ	2	L	S	-98.3	-	-58.5	12.1	one-phase inclusions on long, secondary planes
IS90-53b(A9)	CQ	2	L	S	-98.3	-	-58.5	14.3	vb nucleated at ~12oC upon cooling
IS90-53b(A9)	CQ	2	L	S	-98.3	-	-58.5	14.3	various sizes: 5-30 microns
IS90-53b(A9)	CQ	2	L	S	-98.3	-	-58.5	14.3	same as above
IS90-53b(A9)	CQ	2	L	S	-98.3	-	-58.5	14.3	same as above
IS90-53b(A9)	CQ	2	L	S	-98.3	-	-58.5	15.2	same as above
IS90-53b(A9)	CQ	2	L	S	-98.3	-	-58.5	15.2	same as above
IS90-53b(A9)	CQ	2	L	S	-98.3	-	-58.5	15.2	same as above
IS90-53b(A9)	CQ	2	L	S	-98.3	-	-58.5	15.2	same as above
IS90-53b(A9)	CQ	3	L	S	-99.3	-	-58.6	17.9	same as above
IS90-53b(A9)	CQ	3	L	S	-99.3	-	-58.6	17.9	same as above
IS90-53b(A9)	CQ	3	L	S	-99.3	-	-58.6	17.9	same as above
IS90-53b(A9)	CQ	3	L	S	-99.3	-	-58.6	17.9	same as above
IS90-53b(A9)	CQ	3	L	S	-99.3	-	-58.6	17.9	same as above
IS90-53b(A9)	CQ	3	L	S	-99.3	-	-58.6	17.9	same as above
IS90-53b(A9)	CQ	3	L	S	-99.3	-	-58.6	17.9	same as above
IS90-53b(A9)	CQ	3	L	S	-99.3	-	-58.6	17.9	same as above
IS90-53b(A9)	CQ	3	L	S	-99.3	-	-58.6	17.9	same as above
IS90-53b(A9)	CQ	4	L	S	-98.3	-	-58.4	19.9	one-phase inclusions assoc. with mixed incl.
IS90-53b(A9)	CQ	4	L	S	-98.3	-	-58.4	19.9	same as above
IS90-53b(A9)	CQ	4	L	S	-98.3	-	-58.4	19.9	same as above
AWAY FROM LAMPRO. DIKE									
IS90-53c(A4)	CQ	1	L	S		-	-58.4	7.6	v bubble nucl. at -21oC
IS90-53c(A4)	CQ	1	L	S		-	-58.4	7.5	one-phase LCO2 incl.
IS90-53c(A6)	CQ	1	L	S		-	-60.2	1	large one-phase LCO2 incl., v bubble nucl. -15oC
IS90-53c(A6)	CQ	1	L	S		-	-60.2	4.3	very consistent TmCO2 values for cluster of 8 incl.,

VITA AUCTORIS

PERSONAL DATA

Name:	Bulent Bas
Place of Birth:	Kirsehir, Turkey
Date of Birth:	August 20, 1962

EDUCATION

Kirsehir High School, Turkey
1977-1980

Middle East Technical University
Ankara, Turkey
1982-1987 B.Sc. (Honours Geology)

University of Windsor, Windsor, Ontario
1989-1992 M.Sc. (Geology)

WORK HISTORY

Sept. 1990-May 1991, Sept. 1989-May 1990
University of Windsor, Windsor, Ontario
Graduate Assistant

May 1990-Aug. 1990, May 1991-Aug. 1991
University of Windsor, Windsor, Ontario
Research Assistant

May 1989-August 1989
Department of Natural Resources & Energy, Fredericton, N.B.
Geologist

March 1988-March 1989
University of New Brunswick, Fredericton, N.B.
Graduate Teaching and Research Assistant

July 1987-Dec. 1987
Greenwich Resources PLC, SW Turkey
Geologist

THESES

Geology of the Alci Area, S.W. Ankara, Turkey (B.Sc.)

Hydrothermal Alteration and Fluid Inclusion Geochemistry of Auriferous Deformation Zones and Vein Systems, S.W. Michipicoten Greenstone Belt, Ontario (M.Sc.)